THE CHEMICAL STABILITY OF CARBON FIBRES AND THEIR COMPOSITES

A Study of Carbon Fibre Chemical Reactivity and its Relationship to Fibre Microstructure and Corrosive Mechanisms in Composites.

by

Gerald L. Hart, B.Sc., A.R.I.C., Ch C.

A thesis submitted for the degree of Doctor of Philosophy of the Council for National Academic Awards.

December, 1975.

The following figures have been omitted on request of the University –

Fig. 2	pg. 4
Fig. 8	pg. 21
Fig. 9	pg. 21
Fig. 10	pg. 21
Fig. 13	pg. 29
Fig. 14	pg. 29
Fig. 15	pg. 30
Fig. 18	pg. 49

SUMMARY.

Degradative chemical processes in carbon fibre reinforced resins receive little attention compared to the purely mechanical failure mechanisms. The need to assess the chemical reactivity of these composites and identify stability levels, led to the present work being undertaken.

A knowledge of fibre chemical reactivity was considered essential for discreet processes of composite degradation to be identified. Only limited information was available in the literature and expanding this, therefore, became the first practical aim of the programme.

Young's modulus and the ultimate tensile stress were considered to be good indicators of mechanical damage in carbon and graphite fibres exposed to several fluid environments at different temperatures. Apparently anomalous modulus increases were examined in more detail using polarised light spectroscopy; electrical resistivity; specific gravity; electron diffraction and transmission microscopy; elemental analysis; and oxidation rate measurements.

Changes in short beam shear strength; flexural strength and modulus; shear and loss modulus; and fibre-resin adhesion, were measured as indications of mechanical damage in carbon fibre composites after exposure to several fluid environments at different temperatures.

Appraisals of general damage by microscopical (both optical and electron scanning) and dimensional changes were made throughout the work.

Oxidising agents have a deleterious effect on the mechanical properties of the least graphitised fibre type (Type 111), causing less apparent damage in the more highly graphitised fibres (Types 11 and 1).

This particular property is not reflected in the chemical stability of phenolic composites made from the three fibre types. The degree of attack by oxidative reagents on composites is greatest for highly graphitised (Type 1) fibres. A mechanism is proposed which cites the poor fibre-resin adhesion in Type 1 graphite fibre composites as the key to this reversal. Poor fibre-resin contact presents additional surface at which the resin, and to a lesser extent, the fibres, can be oxidised.

Matrix swelling and matrix solution are two more degradative mechanisms proposed for several of the reagents used. In all exposures the phenolic resin matrices were far more susceptible to attack than the reinforcing carbon fibre.

Reagents which intercalate graphite fibres produce fairly oxidation resistant composites by a mechanism thought to involve fibre swelling in the regions of composite-reagent contact. The highly graphitised fibre (Type 1) benefits most from this mechanism by hindering the access of reagent to the composite interior.

Type 11 graphite fibres undergo an interaction with nitrogen dioxide which is extremely temperature and pressure sensitive. The results of this interaction are increases in Young's modulus; diameter reductions; and surface smoothing.

Preferential removal of non-graphitic carbon occurs to a fixed depth below the fibre surface. The depth and extent of carbon removal are governed by temperature, pressure and time.

Graphitic rearrangements occur, both in the stacking sequences and ribbon conformations. These are best induced by insertion and removal of an intercalating species, which is most probably NO_3^+.

ACKNOWLEDGEMENTS.

The author wishes to thank the following people and organisations for their assistance in enabling the work described here to be carried out.

The Courtaulds Educational Trust Fund, who provided a studentship from September, 1970, to September, 1973, and the Courtauld's staff, particularly Mr D.R. Chapman and Mr L.S. Evans;

Dr G. Pritchard, who supervised the work and gave considerable encouragement by his interest and guidance;

The staff of Kingston Polytechnic for their constant support;

Albright and Wilson (Midland Silicones), B.X.L., and Shell for supplying resins and useful discussion about their properties and constitution;

Mr. W. Watt, Mr. W. Johnson, and Mr. N.C.W. Judd of the Royal Aircraft Establishment, Farnborough, for invaluable discussions and suggestions;

Dr. D.J. Johnson of Leeds University for electron transmission and diffraction studies and their interpretation;

Sussex University, Unilever Research Ltd., National Physical Laboratory and the Royal Aircraft Establishment for giving time on various equipment.

CONTENTS

List of Plates

List of Figures.

Fig. No.

Results Section.

List of Tables.

Result Section

Table No.

THE PROBLEM.

Since the discovery of the R.A.E. Process for the manufacture of high strength carbon fibres from polyacrylonitrile, the fabrication and mechanical properties of carbon fibre reinforced plastics (C.F.R.P.) have received the closest attention of researchers in this field. Certain properties, however, have received little or almost no attention. The self-lubricating nature of composite surfaces; electrical conductivity; and possible corrosion resistance, are three examples of neglected fields.

It was decided that a thorough examination should be made of the chemical stability of carbon fibres and their resin composites.

One would anticipate from the inert nature of graphite to all but intercalating and oxidising media that carbon fibres would make a first-class reinforcing material in plastics intended for service in corrosive environments. Unlike glass, the surface of graphite is not hydrophilic, which leads one to conclude that carbon fibre composites might exhibit better resistance to aqueous reagents.

Although the behaviour of bulk graphite in chemical reagents and gases is well documented, several factors may cause significant departures from the results expected when substituting carbon fibres in these media. Traces of impurities, imperfections in fibre surfaces, the degree of amorphous carbon in the outer regions, and the accessibility of pores and central regions to attacking reagents may be governing factors in their chemical reactivity. It would seem likely, therefore, that carbon fibre microstructure has an important part to play. Although considerable attention has been paid to carbon fibre morphology, the radial structure is still the subject of much debate.

Carbon fibre composites have not received a comprehensive examination of performance in corrosive environments. It is doubtful whether a simple relationship between fibre chemical reactivity and composite

chemical resistance can be assumed.

The problems are, therefore, to examine the chemical reactivities of three types of carbon fibre, with varying degrees of graphitisation, and to test the compatibility of these results with present theories of radial structure

Secondly, the chemical reactivities of the fibres should be related to composite performances in corrosive media in an attempt to discover what failure mechanisms operate

Technological Significance. Carbon fibres, in their composite form, are only cost-effective for a very few applications utilising their mechanical properties alone. They will not find widespread usage unless their cost becomes competitive with more conventional materials.

It is hoped that the attempted work programme will serve to supply useful information to technologists. Applications utilising not only the stiffness and lightness of carbon fibre composites, but also their chemical stability, may lead to wider economic usage.

CHAPTER ONE

-INTRODUCTORY SURVEY-

1.1 INTRODUCTION.

Carbon fibres and filaments have been known and used for at least a century, but highly graphitised fibres are a more recent discovery. The principles used by Edison in 1880 are still fundamentally employed today. He obtained carbon filaments by pyrolysing natural cellulose fibres, the long carbon backbones remaining to ensure its fibrous nature Modern carbon fibres are mainly the product of pyrolysing synthetic fibres such as acrylic or rayon based textiles.

Interest in stiff, light materials was roused in the 1950's in the search for suitable materials to fill applications in aerospace The good ablative properties of carbon fibre reinforced plastics gave an excellent bonus. It can be seen from Fig. 1 [1] that graphite fibre reinforced epoxy-resin composites were amongst the first of a new generation of materials with exceptional specific modulus of elasticity.

FIG. 1. Specific Stiffness of Some Materials.

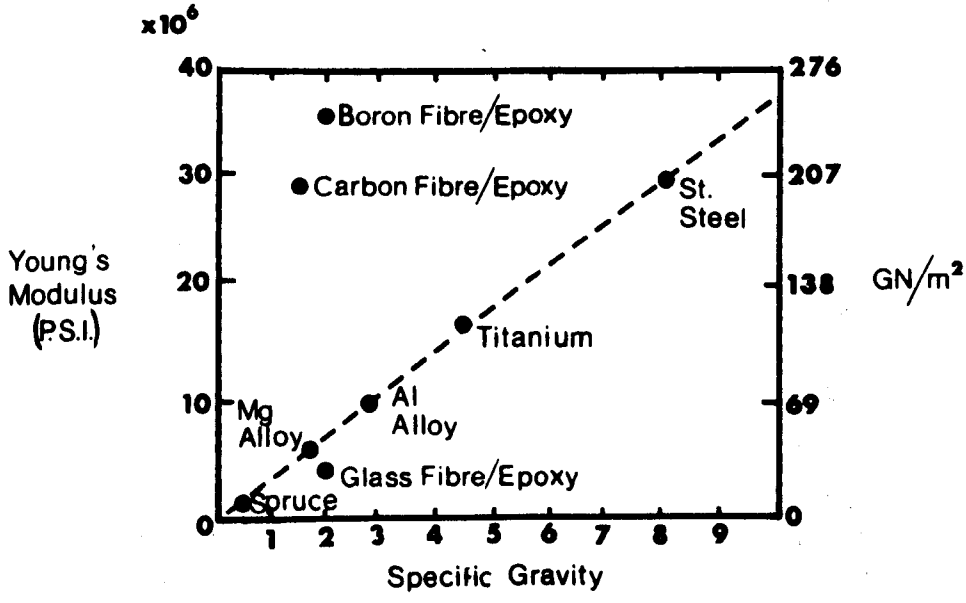

The discovery of carbon fibres was made independently in the years 1960-5 by W. Watt, A. Shindo and R. Bacon. The process of W. Watt, using a polyacrylonitrile (PAN) precursor, is widely adopted (R.A.E. Process), but it is interesting to note that regardless of starting material the final fibres are all structurally similar.[2]

During the planning and expansion of the work programme, it became clear that a detailed knowledge of bulk graphite and carbon and graphite fibre microstructures was essential. The physical properties and structure of carbon and graphite fibres are, therefore, reviewed in detail (1.2). Their chemical reactivity (1.3) and the chemical reactivity of the resins used in the study (1.4) also receive close attention.

The information contained in these sections is referred to in the discussion (chapter 4) without detailed recitation.

1.1.1 Manufacture.

This introduction will be limited to the production of carbon and graphite fibres from a P.A.N. homopolymer precursor. Four stages can be identified in the conversion of a P.A.N. precursor to graphite fibres by the R.A.E. process:

(a) Oxidation of P.A.N. fibre.

(b) Pyrolysis.

(c) Heat treatment.

and possibly (d) Stress graphitisation.

Although the heat treatment largely determines the extent of graphitisation, the radial structure is determined at the oxidation stage.

(a) Oxidation.

The precursor is stabilised by heating in air with shrinkage restraint, in the temperature range 490-540K. This may be regarded as uptake of oxygen to about 10% by weight.

The extent and rate of oxidation can have marked effects on final fibre properties. Too little oxidation fails to give cross-links and core fusion occurs during pyrolysis [3]. Too much oxidation leads to large drops in carbon yield [13] Slow rates of incubation during oxidation and pyrolysis (carbonising) lead to retrograde core formation [114]. Layden [114] reported that with these conditions a 'soft core' develops which is eventually bound only weakly to the carbonised fibre 'rim' (See Fig. 2).

Grassie [4] draws attention to the importance of comonomers in commercial P.A.N. fibres. The highly exothermic processes occuring

around 490K., which can be detrimental to gross fibre structure, are considerably reduced by the presence of comonomers. For example, 4 per cent concentration of vinyl chloride reduces the exotherm temperature by 80%, spreading it over a longer period as a consequence.

The chemistry of the oxidation process is uncertain. In general, however, a laddered polymer modified by the presence of oxygen is usually envisaged as based on the condensed naphthyridene model of Grassie, consisting of a conjugated $- \overset{|}{C} = N - \overset{|}{C} = N -$ chain forming a series of fused rings [5] (See Fig. 3).

FIG. 3. The Naphthyridene Model [5].

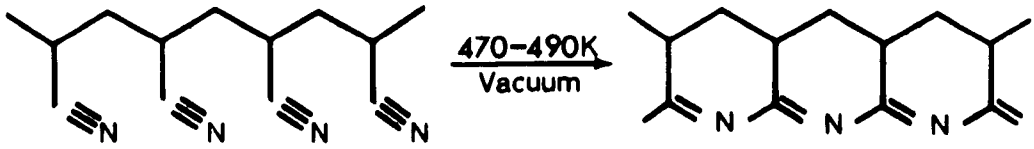

The production of a conjugated ladder polymer by heating polyacrylonitrile in vacuum.

Three current theories on the oxidation mechanism are given below:

(i) Watt, W. [13] - Oxidation of -CH - to C = O in the carbon backbone after ladder polymer formation with more ladder polymer formation promoted by -COOH.

(ii) Clarke, A.J. and Bailey, J. [6] - Dehydrogenation and oxidation of the carbon backbone to give hydroxyl groups which mainly promote ladder formation.

(iii) Potter, W.D. and Scott, G. [7] - Initiation of ladder polymer by cyanide anion to give a structure of condensed 1-4 dihydro-pyridene, 4 pyridone and fully aromatic pyridene rings.

(b) Pyrolysis.

During this stage, the preoxidised fibres are heated to about 1270K. in vacuo or an inert atmosphere. This is essentially a carbonising period where extensive crosslinking and ladder growth occur [8, 9, 13].

(c) Heat Treatment (Carbonisation and Graphitisation).

It is important to distinguish between carbonisation and graphitisation processes and their products. Pyrolysis of the precursor fibres up to a temperature of 1470K. results in a fibre without detectable graphitic material present according to Bacon [19]. Non-carbonaceous material is found as inclusions and extensive graphitic regions only develop above 2270K. It has been suggested more recently [20], however, that the graphitised structure is already developing at 1370K. and is well advanced by 1970K. Unfortunately, the experimental method of investigation (boiling in nitric acid) may itself introduce a certain degree of ordering into the structure [22]. Graphite fibres contain very little three-dimensional material with ABABA....stacking, as found in bulk graphite, but a considerable amount of turbostratic arrangement.

Pyrolysis below 1470K. shall be termed carbonisation and heat treatment temperatures above 1470K. as graphitisation. The three main classes of fibre are those obtained at 1470K., 2000K., and 2770K. which shall be referred to as Type 111 carbon fibres, Type 11 graphite fibres, and Type 1 graphite fibres respectively.

Young's modulus increases almost linearly with heat treatment temperature (H.T.T.) (Fig. 4) [23-4] which is consistent with increasing the degree of graphitisation and orientation during this process. The ultimate tensile strength (U.T.S.), however, reaches a maximum and then declines. This phenomenon has been attributed to Mrozowski cracking [25-7], large internal voids [28] and surface defects [29]. Surface defects have recently been reported [18, 30] as arising from surface deposits occuring during processing. Experiments with production under ultra-clean conditions [31] have shown improvements in U.T.S. for higher H.T.T.

FIG. 4. Development of Mechanical Properties During Heat Treatment.

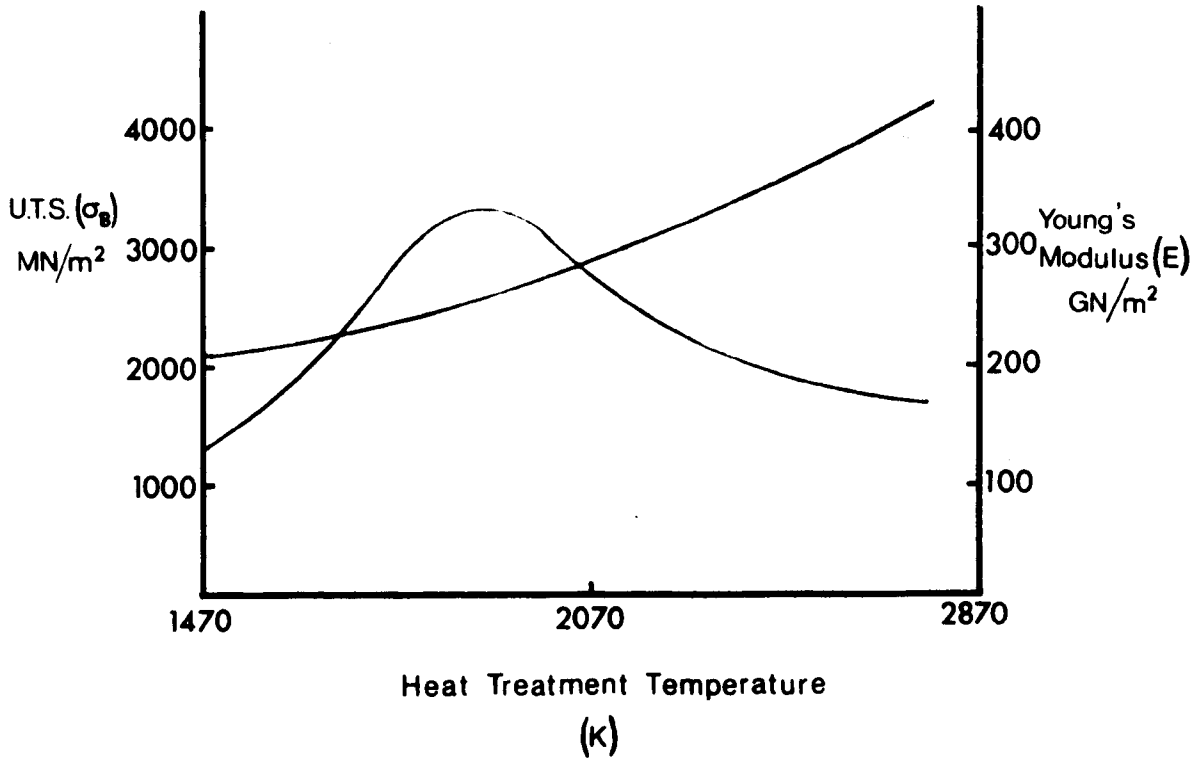

(d) Stress Graphitisation.

The processes for rayon-based and P.A.N.-based fibres differ in that they are stressed during graphitisation [16] and preoxidation respectively [14, 17]. Both methods lead to high degrees of orientation with graphite basal planes parallel to the fibre axis [16-18].

Stretching fibres by up to 28% at 3070K. however, yields fibres with increased stiffness and tensile strength [10].

1.1.2 Applications for Carbon Fibre Reinforced Plastics.(C.F.R.P.).

Fibres alone would have few uses, if any, which utilise their tensile modulus and strength. A matrix of much lower Young's modulus and strength is needed to bind the fibres together, the most convenient being a thermoplastic or thermosetting resin. The functions of the matrix [32] are to protect the fibre from mechanical and chemical attack; provide the means whereby the load is applied to the fibres and to separate them, thereby ensuring reasonable work of fracture and insensitivity to composite surface irregularities.

The mechanical requirements for a fibre reinforced composite material are that the fibre is relatively brittle in a weak (low yield stress) matrix of much smaller elastic modulus than the fibre but with much greater elongation to failure. The fibre-resin bond must be sufficiently strong to transfer load from matrix to fibre. If the bond is too strong, however, the work of fracture is reduced and brittle failure can result.

Properties of C.F.R.P. which have not been exploited fully, perhaps through lack of data, are chemical resistance; friction and wear; electrical conductivity and thermal stability. Based on the excellent chemical resistance of massive graphite to all but intercalating and oxidising agents, some data has been published on the corrosion resistance of carbon fibre and carbon fibre composites [1, 33, 34]. Suggestions have been made to incorporate C.F.R.P. in chemical plant process equipment [35-8].

The friction and wear properties of carbon fibre composites have been reported [39] and the self-lubricating nature of composite/metal surfaces in sliding contact give excellent performances which show no dependence on fibre orientation. Applications here are for bearings

[40] and gears [41].

The electrical resistivity of carbon fibre has received considerable coverage as a function of graphitisation [42-55] and recently attention has been paid to the possibility of using composites as heating elements [56]. Unidirectional composites exhibit good electrical conductivity, but an inherent feature is the temperature gradient in the direction of fibre orientation. This arises from the difficulty in making contact with all the fibre ends.

Matrices have not yet been found which will utilise the excellent thermal stability of carbon fibres when protected from oxidising media. Polyimides, polyphenylenes and Friedel-Crafts type phenolics will operate in the 520 - 570K. temperature range, but their cost and the processing difficulties make them economically unviable for all but the most specialised applications.

It is envisaged that economical applications exist where more than one of the properties exhibited by carbon fibre composites is employed.

1.2 MICRO-STRUCTURE OF CARBON AND GRAPHITE FIBRES.

1.2.1 Structure of Bulk Graphite.

When carbon with a high level of purity shows a well-developed layer structure in which the atoms are arranged in open hexagons and the basal planes show some order in stacking sequence, the material is called a graphite.

The interatomic distance in the hexagons is 1.415Å [57] and the interlayer spacing (c-axis) of synthetic graphites has not been observed below 3.3528 ± 0.0002Å [58-9]. The structure is under compression to obtain this spacing and upon removal of the external forces the distance expands to c=3.3544Å. It is generally accepted that the c-axis spacing for the crystallographic cell is 3.3539±0.0001Å [60]. This arrangement gives a theoretical density of 2.265 g/ml.

1.2.2 Cell Structure.

Several forms of graphite exist, of which the hexagonal unit cell crystal structure is the commonest and the inter-layer spacing has already been given. This is the accepted closest-packed system but a recent discovery [61] in the Reiss Crater indicated that another form based on a primitive hexagonal lattice may exist. This new form has a larger unit cell, a theoretical density of 3.43 g/ml., and no apparent anisotropy. Only small samples have been reported (thin lamellae 3 to 15 μm wide) making comment on isotropy extremely tenuous.

The hexagonal unit cell is shown in Fig. 5 . Each layer in the lattice can be superimposed with the layer one plane removed, thus making an ABAB.... stacking system.

A form commonly found in natural graphites, but which has never been isolated, has an ABCABC.... stacking arrangement [62-3]. This form occurs in small quantities associated with the hexagonal material and

FIG. 5. The Hexagonal Unit Cell of Graphite.

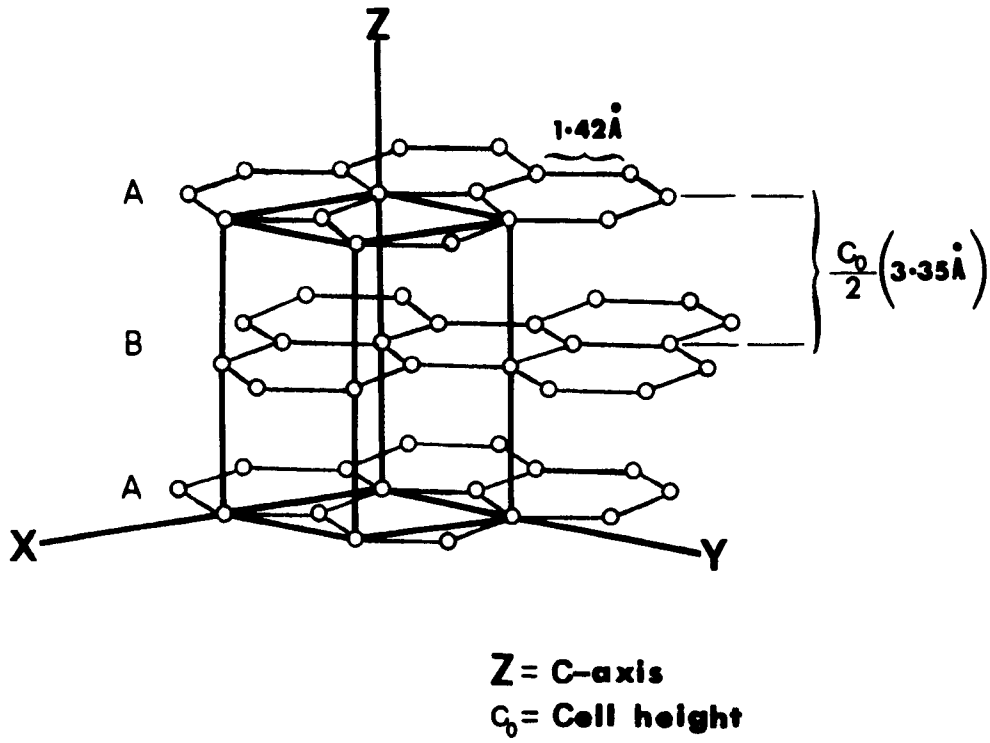

has a rhombohedral unit cell structure with c-axis spacing identical to the former.

A third type has a completely randomised stacking sequence of parallel planes and is called turbostratic (Turbulent = disturbed; Stratify = to form in layers). The interlayer spacing is 3.44Å [65-8]. There is no three-dimensional order in this system, unlike the other two.

1.2.3 Crystallite Structural Defects.

The fact that perfect graphite crystals exhibiting the theoretical density conferred by the hexagonal lattice structure do not exist shows that imperfections are difficult to minimise and impossible to eliminate totally. Basically the defects encountered may be concerned with layer stacking or the basal plane network.

(i) Defects in layer stacking.

During the process of graphitisation, the layer spacing in a 'graphitising' carbon will fall from 3.44Å to give apparent spacings of 3.38 - 3.36Å. It is thought that the graphite is heterogeneous and that the final product is a mixture of turbostratic and hexagonal crystallites. Bacon [65] produced a graph which related the apparent inter-layer spacing to the proportion of disorientated layers. He denoted the proportion of disorientated layers as 'p' (p = 0 = hexagonal p = 1 = turbostratic). Ruland [69] prefers a notation $|q|$, such that $|q| = 0$ is a random structure

$|q| = 1$ means complete order.

The notation of Ruland avoids defining the random material and includes turbostratic graphite in the ordered category. Random structure is considered to be amorphous carbon.

The low energy of stacking fault formation can lead to several defects arising naturally or mechanically from the interaction between layers of defects in basal planes and partial dislocations. Partial slippage on a glide plane can result in a plane edge forming and an ABAB sequence may transform to an ABCABC system. This is a well known phenomenon associated with grinding graphite and is analogous to 'mechanical twinning' [70].

(ii) Defects in the hexagonal bond network.

Hole defects [71] in the layer planes can result in bulging and buckling. Repulsion between corner atoms can lead to plane separation (See Fig.6.) and unpaired electrons in the system affect the spatial relationships of atoms.

Co-operative network defects (twinned material), in the form of screw dislocations, are believed to occur on the same basal plane. The twin matrix boundary was thought by Freise and Kelly [72] to be the source

FIG. 6. Layer Plane Dislocation.

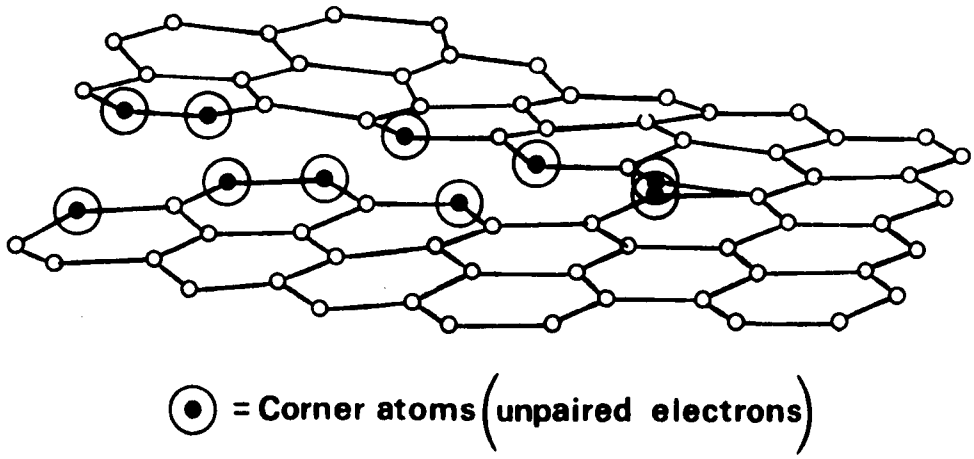

of rhombohedral graphite during grinding. A shear stress parallel to a twin-matrix boundary leads to a large volume of rhombohedral material by the motion of very few dislocations.

Screw dislocations may start at hole defects or other buckling mechanisms (foreign groups). The result is a hexagonal layer growth [73] which may be significant in various chemical reactions of graphite and act as stress concentrators in mechanical appraisals.

Amelinckx et al [74] comprehensively discuss various combinations of partial dislocations in terms of single plane and multiple layer interactions.

1.2.4 Crystallite Size and Gross Defects.

The layer structure considered above has been assumed infinite. Graphite is composed, however, of relatively small crystallites with poorly defined boundaries in most cases. The crystallite sizes can be determined from x-ray diffraction [75] and have the dimensions La (diameter of unperturbed layers in the a-axis directions) and Lc (thickness in the c-axis direction). The proportion of graphitic to turbostratic structure is equivalent to Bacon's 'p' value. For a good commercial graphite the p-value is 0.2.

Gross defects such as pores and cracks are easily observed using

modern scanning electron microscope (S.E.M.) techniques. Pores occur in all graphites as the result of 'crystallites' being joined together inadequately and may lead to bulk densities far below that of ideal graphite. Not all the pores are accessible to even helium and it is thought [76] that carbon atoms blocking these pores are more reactive than those in more perfectly graphitised regions. A short oxidative treatment soon 'opens up' the pore system with only a 3% loss of mass. The pore characteristics of carbons have received considerable investigation, the most comprehensive modern coverage being completed by Turkdogan [77].

Mrozowski cracks [25-7] are visualised as basal plane faults formed during cooling from heat treatment graphitisation. Angular and shear stresses are induced in carbon and graphite structures through the anisotropic thermal contraction of the crystallites and this results in separation, particularly between crystallites. Rapid cooling is to be avoided if extensive crack systems, with individual cracks 1-10μm long, are not acceptable.

Submicroscopic voids have been observed in synthetic carbons from organic polymers [78]. These take the form of oblate ellipsoids with radius of gyration approximately 10.5Å and a ratio of the axis of revolution to the perpendicular axis of 0.36. The surface area of these voids was not in exact agreement with Porod's law [79] of heterogeneity and thus their real shape only approximates to that shown in Fig. 7 . 3.6 to 10 x 10^{18} voids cm^{-3} were calculated as present in commercial samples.

The process of graphitisation is generally accepted as being a physical reformation, although recent discoveries add weight to the theory that a process of chemical graphitisation may occur (See Sect. 1.3). The theories of graphitisation by heat treatment cannot be

FIG. 7 Submicroscopic Void - Oblate Ellipsoid.

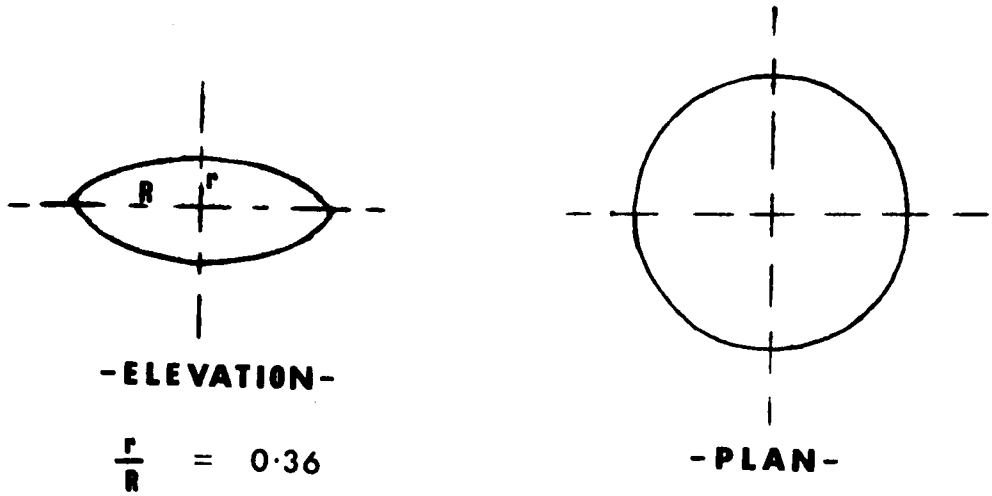

generally applied. The terms 'soft' and 'hard' carbons have been introduced to describe those which graphitise between 2270K and 2770K. and those which remain turbostratic (ungraphitisable) at these temperatures. Comparative mobility of individual layers plays a part but graphitisation is essentially a mutual orientation of neighbouring layers by a local discontinuous transformation [80]. The rate of graphitisation increases with temperature but the degree of graphitisation is independent of the time during which the temperature is maintained constant.

Franklin [66-7] proposed that strong crosslinks between ordered material prevented graphitisation in 'hard' carbons. This idea finds support in the structures found by Noda et al [81] in 'glassy' carbons, which were described as comprising tetrahedrally bonded carbon atoms in an amorphous phase which linked graphite-like layers in a random way.

Graphitisation by a screw dislocation mechanism was proposed by Frank [82]. This theory attempted to explain the growth spirals observed in natural and synthetic graphites. He proposed that they result from

crystal growth based on a screw dislocation process involving scores of unit dislocations at the crystal centre. The crystallite can only grow larger in this case by incorporating additional sites, associated with larger heats of activation. This is where Franks' theory explains why complete graphitisation is not possible at any one intermediate temperature. Franklin's theory would call for variable bond strengths to explain this phenomenon.

The work on carbon migration [83-4] by using labelled isotopic C^{14} diffusion in graphite indicates that such a mechanism must not be ruled out in graphitisation. The migration of carbon atoms has been interpreted in terms of combined grain boundary and network diffusion, but recent work [85] indicates that this may be an over-simplification.

The process may be summarised as a general increase in (a) order of stacking; and (b) size of carbon hexagonal networks.

1.2.5 Structure of Carbon and Graphite Fibres.

If the structure of a graphitised fibre comprises a prefect ABAB.... hexagonal close-packing, then we can expect a density of 2.265 g/ml and interlayer spacings of 3.35Å. If the basal planes all lie parallel to the fibre axis, the values for tensile modulus and strength may be anticipated as being 900 GN/m^2 and 90 GN/m^2 respectively (values for the basal plane). The actual maximum values for stiffness and strength in graphite fibres are, however, 500 GN/m^2 and 3.2 GN/m^2, respectively.

Without considering the average density of 1.9 g/ml and the average interlayer spacing of 3.4Å, it is clear that the carbon atoms in carbon and graphite fibres are arranged in a structure far removed from an ideal hexagonal system.

For a perfect solid, tensile strength is theoretically about one-tenth of Young's modulus [32]. The values given above indicate that the fibres do not even obey the law of mixtures in one direction.

N.B. Although general characteristics have been found by researchers, the variation of properties of single filaments taken from one batch may be so large that there is no certainty of finding a feature peculiar to that type in any one filament.

1.2.6 Basal Plane Stacking.

A turbostratic arrangement of basal planes was first reported by Watt and Johnson [86] and later by Badami et al [87]. No three-dimensional ordering in the graphite crystallites was noticed and the interlayer spacing was reported separately as being 3.42Å and 3.39Å for a P.A.N. precursor. The basal planes of the turbostratic layers lie approximately parallel to the fibre axis. Soon after a turbostratic graphite structure was accepted, doubt about the validity of applying

the term 'graphitisation' to these fibres during heat treatment arose. Fourdeux et al 291 defined graphitisation as heating above 2270K. in an inert atmosphere, but drew attention to the difference between turbostratic graphite and the generally accepted meaning of the term graphite, which is crystallographic hexagonal graphite. Bacon [19] suggested heating above 2770K to 99% purity was the correct definition of graphitisation, but neither interpretation really compromises the hitherto accepted terminology of 'hard' (ungraphitisable) carbons from synthetic polymers.

A three-dimensional ordered stacking arrangement was first observed in fibres recrystallised from nickel by Jackson and Marjoram [88]. The accomplishment of three-dimensional order during the recrystallisation was assumed to be the result of a solvent transport mechanism moving carbon atoms from short-order systems to fill vacancies in more extensive layer stacks.

Other workers [89-91] have repeated similar experiments to find that the three-dimensional phase often orientates itself randomly. Johnson,D.J. and Tyson [90] identified a small amount of three-dimensional graphite by x-ray diffraction in commercial fibres heated above 3070K., which has been substantiated by further observations using E.S.R. [92], electron diffraction and high resolution electron microscopy [93]. Johnson, D.J. et al [93] identified three distinct phases in commercial P.A.N. based fibres heat treated above 3070K. They designated a poorly-ordered turbostratic phase, T11; a well-ordered turbostratic phase, T1; and the small amount of three-dimensional ordering, G. Unfortunately, the specimen preparation of grinding the fibres before observation prevented the identification of the origin of each phase within the fibre.

A phase commonly found in carbons derived from an organic polymer consists of tetrahedrally bonded carbon atoms in an amorphous region

which links graphite-like crystallites in a random manner [81]. This is a major feature of all 'non-graphitising' carbons. The strong binding force between crystallites in graphite fibres suggests that a similar phase may exist in them. Hérinckx et al [94] have shown, however, that potassium intercalates the fibres to an extent comparable to ideal graphite systems. This is not possible with the amorphous phase described above present. Its absence from graphite fibres is only explicable by consideration of the high degree of orientation already to be found in the precursor [95].

During graphitisation, the layer spacing gets smaller, which may be the result of impurities volatilising in the 1470K. - 1570K. temperature range [96] or general ordering by heat treatment. Layer spacings for P.A.N.-based Type 1 fibres are 3.35 - 3.40Å and layer spacings for P.A.N.-based Type 111 fibres are 3.41 - 3.44Å. A predominance of smaller layer spacings at the surface of fibres has been reported [97].

The layer stacking can show all the defects of bulk graphite with an additional property that the a-axis of the hexagonal two-dimensional lattice has no correlation with the borders of the ribbons of which it is part [2].

1.2.7 Crystallites, Ribbons, Micro-Fibrils and Fibrils.

It is generally thought [289] that ribbons of crystallites, with their basal planes parallel to the longest side of the ribbons, run together to form micro-fibrils. Ribbons crossing between parallel micro-fibrils result in bundles of micro-fibrils forming a fibril.

(a) Crystallites and Ribbons.

Two schools of thought dispute the existence of discrete crystallite structure within ribbons. Johnson, W. and Watt [86] first proposed that

the microstructure comprised small crystallites which they concluded from high electrical resistivity measurements. Later [51-2] this finding was confirmed and an associated electrical 'noise' was attributed to a system similar to that found in hard-packed carbon granules.

Johnson, D.J. and Tyson [90] using x-ray diffraction and electron microscopy suggested that misorientated turbostratic crystals were stacked end to end with sub-grain twist and tilt boundaries between them. These crystallites have the average dimensions of 70Å x 70Å in the basal plane and 65Å in the c-axis direction.

The basal plane layers have a general orientation parallel to the ribbon boundaries but the a-axes of Type 1 P.A.N.-based fibres show preferred orientation parallel to the fibre axis with a standard deviation of 26°. Previous work [99-100] found a-axis orientation only in strain-graphitised fibres.

Contrary to the findings of Johnson, D.J. and Tyson, work by Hugo et al [97] suggests that no transverse grain boundaries exist. Using an ingenious technique of high resolution phase contrast electron microscopy through 'flutes' on the fibre surface several features were observed. Graphite crystallites have their basal planes with preferred orientation parallel to the fibre surface, and these continue over long distances despite sharp bends in individual packets of planes. This is in opposition to earlier findings. Ruland et al [2] reported a similar finding, and attributed the structures of Johnson, D.J. and Tyson to a misinterpretation of light and dark portions on ribbons as tilted faces when they were really ribbons crossing one another. Schematic diagrams of both structures are shown in Figs. 8,9 and an intermediate structure in Fig. 10 [29]. Ribbon widths of about 60Å have been recorded [87], with lengths ranging from several thousand angstroms up to one micrometre.

PAGES
NOT SCANNED
AT THE REQUEST OF
THE UNIVERSITY

SEE ORIGINAL COPY
OF THE THESIS FOR
THIS MATERIAL

There is general agreement that many voids occur between crystallites These voids are elongated in the direction of the fibre-axis, and are of the order 200 to 300Å long by 10Å wide. It is not possible to say whether the voids are needle or penny-shaped, but the latter would seem to be more likely if they are voids between stacks of graphite layer planes. (Fig. 8 and 9).

Recent work by Johnson, D.J. 101 suggests the original representation (Fig. 8) may be over-simplified but maintains that sub-grain transverse boundaries do exist. Workers favouring the Johnson model would quote La as the dimension of the crystallites in the direction of the ribbon axis. Workers favouring the Hugo and Ruland models quote La as the dimension of straight portions of the ribbons.

(b) Micro-Fibrils and Fibrils.

Bacon and Tang [102] were the first workers to observe a fibrillar structure in cellulose-based graphite fibres. This structure comprising aligned crystallites in ribbon formation bunching into micro-fibrils and fibrils has been observed many times since [87, 2, 103-108, 93, 98]. Fibrillar structure has been cited [51] as the cause of lower electrical resistivity in tensioned fibres. Better contact between fibrils in the tensioned case would lower the inter-fibrillar resistance and this may occur in a similar manner to tensioning a bundle of loosely woven wires. Bacon et al [103] claim that the failure of inter-fibrillar bonds is the cause of the grainy appearance of transverse fracture surface.

Wicks [109] claims that the fibrillar structure observed by Bacon, Tang and subsequent workers is an artefact of the specimen preparation. Flame polishing is suggested as a less damaging technique to the micro-structure than microtoming. A ribbon structure enclosing a network of extended pores was reported with platelets of more ideal graphite present, probably as the result of catalysis by impurities. The observation of

transverse tilt or bend plane boundaries between crystallites were observed, adding support for Johnson's 'discrete crystal' structure for ribbons.

Most workers use the term 'fibrils' to describe the bundles of ribbons observed in fibres. This term may be inaccurate, especially in the sense used by Badami et al [87], who observed separate and grouped fibrils with diameters in the range 250 - 1000Å. Support for these observations has been reported by Watt and Johnson, J.W. who found fibril units 800 - 1000Å units across and running the length of sections without termination. A clearer description of this structure was given by Barnet and Norr [108] where ribbons run parallel in bundles to form micro-fibrils, and groups of these run parallel in bundles to form fibrils. It is envisaged that some ribbons interconnect adjacent micro-fibrils [2].

Hence, a fibril is a bundle of non-planar turbostratic layers has a preferred orientation parallel to the fibre axis, but discrete from neighbouring fibrils. This cannot be said of micro-fibrils which have the general orienation of the fibril of which they are a part (±20°).

(c) Effect of Heat Treatment.

Although it is generally accepted that heat treatment increases both the axial orientation of crystallite basal planes and the length of crystallite regions, Johnson and Ruland present different mechanisms which apply to their 'discrete crystallite' and 'wrinkled ribbon' structures respectively.

Johnson, D.J. [110] proposes that heat treatment generally straightens up the crystallite stacks by decreasing the twist, tilt and void space between them. Ruland [2] suggests that wrinkled ribbons at low H.T.T. lie poorly stacked in the micro-fibrils with various extents of basal planes in the direction of fibril width. During heat treatment, atoms diffuse

FIG. 11. Schematic Recrystallisation Process.

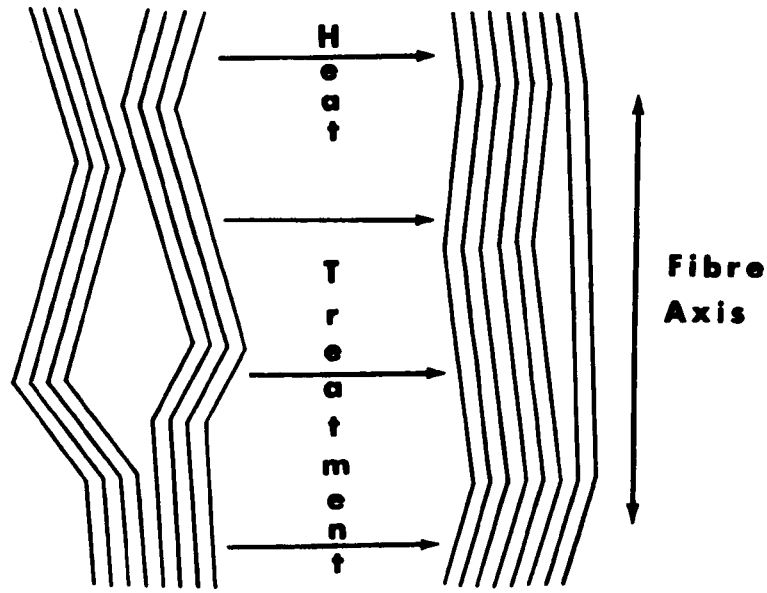

inwards from the ribbon boundaries, thus smoothing and matching up ribbon contours. This he terms an 'elastic unwrinkling' (Fig. 11). Both mechanisms explain the mechanical, electrical, x-ray and electron-microscopical findings.

1.2.8 Gross Fibre Defects and Their Mechanical Consequences.

(a) Micropores and Voids.

Both Johnson, D.J. [110] and Ruland [2] associate micro-voids at the crystallite boundaries with their interpretations of micro-fibrillar structure. These micro-voids have been referred to as a closed micro-pore network [109]. Most evidence points to sharp-edged, disc-shaped voids rather than needle-shaped voids. The dimensions of the micro-voids have been presented by several workers as having widths of 10 - 20Å and lengths 100 - 300Å [90, 108, 2, 110, 106].

The degree of porosity depends upon the preoxidation of the precursor fibre [111] and the H.T.T. it has experienced [110]. During heat treatment, the interconnected pores grow smoother and larger with fewer branches. There are, of course, fewer of these larger pores [110] (See Table 1).

TABLE 1.

H.T.T.(K)	Volume of Voids	Sp. Internal Surfaces m^2/cm^3
1270 (PAN)	1 - 3%	50 - 100
2270 (PAN)	18 - 25%	700 - 900
3170 (PAN)	15 - 33%	200 - 700
2770 - (cellulose) [94]	27%	500

(b) Surface and Internal Flaws.

Inhomogeneities and impurities in the precursor fibres [112, 108, 113, 18, 28], damage during spinning [108], retrograde core formation [91, 114] and Mrozowski cracking [93, 115] have all been cited as causes of flaws in carbon and graphite fibres. Discrete organic and inorganic

impurities in the precursor fibres manifest themselves as inclusions and small cylindrical or irregular shaped voids at H.T.T.'s of about 1480K. At H.T.T.'s of 2000K and above, some organic inclusions grow into elongated cavities of between 1 and 3 μm in length as they decompose generating expanding gases. These cavities have a frequency of 0.03 to 2.3 flaws/mm.

Surface flaws are largely the product of damage to the precursor during spinning. Moreton[18] showed that surface dirt on carbonised fibres was a source of weakness when heat-treated. Experiments using clean processing conditions have achieved increases in strength[31] which, however, do not approach a tenth of the modulus.

If the rate of carbonisation of the oxidised P.A.N. precursor is too rapid, the exothermic reaction melts the core and forms longitudinal cracks on the fibre axis. Incomplete oxidation, however, is thought to generate continuous cylindrical holes along the fibre axis.

Mrozowski cracking occurs particularly in fibres with high H.T.T. and arises from a mechanism similar to that found in bulk graphite. It can be minimised by long cooling down periods[290].

(c) Mechanical Consequences.

Moreton[116, 117] realised that tensile strength was a function of specimen gauge length. Shorter gauge lengths had a lower probability of including major flaws. He went on to show that by keeping the surface flaws to a minimum the U.T.S. improved.

Thorne[113] and others[14, 118], by the examination of fracture surfaces, were able to conclude that when surface flaws were removed by etching, the incidence of failure at an internal flaw rose. A mechanism was proposed by Johnson, J.W. et al[91] which cited small cracks associated with internal gross defects (≈3 μm diam. and frequency ≈ 1/mm). Major defects show larger layerstacks of possible three-dimensional

graphite on their surfaces[109]. Johnson suggested that these lamellae of thickness 0.1 - 0.3 μm correspond well with the crack lengths required to satisfy a Griffiths relationship which would account for the observed strengths. Incipient cracks in these lamellae perpendicular to the fibre axis would act as stress concentrators causing premature failure.

Cooper et al[119] and Ruland et al[2] see the poor U.T.S. of highly graphitised fibres as the result of intercrystallite shear failure. Larger, smoother (unwrinkled) crystallites allow larger local stress raising and easier shear separation. Mrozowski cracking will obviously contribute to this mechanism.

1.2.9 Radial Structure.

Badami et al[87] first reported that a radial inhomogeneity may exist when they observed that certain parts of the fibre were more ordered than others. Diefendorf and Butler[120] were more precise and stated that crystallites closer to the surface were larger and better aligned. In the same year, Johnson, D.J. and Tyson[90] discovered three-dimensional graphite was present in commercial fibres, which, after ion-etching, they concluded was not exclusive to the surface.

Watt[14] reports his earlier findings of an annular ring of oxidised material in the stereoscan observations of transverse sections cut from partly oxidised fibres. The existence of two zones offered a convenient explanation of a fibre diameter/modulus relationship found by Perry et al[121, 118] and Jones et al[115, 25] in graphitised fibres. These workers assumed that the well oxidised regions became the most highly graphitised after heat treatment. Since the extent of oxidation is diffusion controlled, it was reasonable to argue that 'fatter' precursor fibres would have proportionately smaller volumes of graphitic material than thin ones after graphitisation. Observation showed that

thinner fibres did have higher Young's modulus than fat ones, a fact particularly noticeable in Type 1 fibres (Fig. 12).

FIG. 12. Diameter/Modulus Relationship for Type 1 Graphite Fibres. [25]

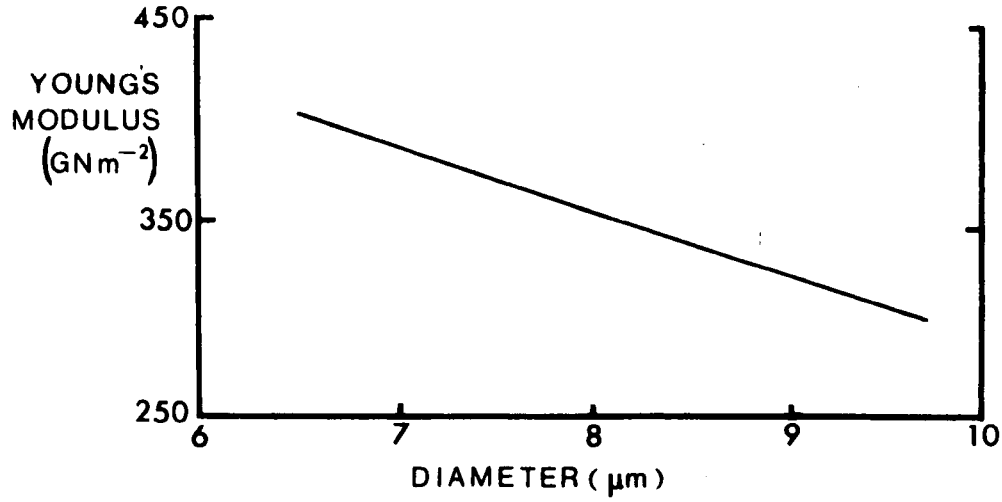

A similar dependence of U.T.S. on diameter was reported separately by Jones and Perry. Subsequent refinements in diameter measurement, however, have led Perry [118] to conclude that such a relationship does not exist.

Many workers [47, 122, 120, 123, 97, 108] have observed that basal planes have preferred circumferential orientation in a sheath region with radial orientation in the core. Knibbs [357-8] using polarised light microscopy and Barnet [108] using plasma oxidation have been more explicit in this matter. Knibbs reports a dependence of structure on the extent of oxidation in the precursor. Less than two hours' oxidation leads to very little preferred orientation in the sheath with a central amorphous core. Three hours' oxidation gives radially orientated basal planes in the core with an external layer of circumferentially orientated sheath. Twenty-eight hours oxidation gives only circumferential orientation. Rayon-based fibres appear to always have a random core. Butler and Diefendorf [120, 123] refer to the circum-

PAGES
NOT SCANNED
AT THE REQUEST OF
THE UNIVERSITY

SEE ORIGINAL COPY
OF THE THESIS FOR
THIS MATERIAL

The existence of these two regions has become known as the 'Sheath and Core Theory'. The crystallite phases of Johnson, D.J. et al[93] seem to fit the theory, although no direct knowledge of the location of phases is claimed by these workers. The G-phase, it is suggested, exists interleaved between layers of turbostratic graphite. It seems more likely[114, 91], however, that highly graphitic lamellar sheets occur around internal voids and cavities or in the very centre of the fibre as a result of core collapse at H.T.T.s in excess of 2770K. This latter phenomenon is thought to arise from incomplete precursor oxidation.

1.3 CHEMICAL REACTIVITY OF CARBON AND GRAPHITE FIBRES.

1.3.1 Chemical Reactivity of Bulk Graphite.

The chemical reactions of graphite fall into two main classes; intercalation and oxidation. Both are powerful disruptive forces to the mechanical integrity of graphitic material.

1.3.2 Intercalation.

Ubbelohde and Lewis [126] define intercalation as the insertion of additive atoms or groups of atoms between the carbon hexagon networks, whose aromatic character and planarity appear to be preserved. Considerable swelling is usually produced in the graphite body, but the original structure can be recovered by subsequent treatment. Caution must be employed when interpreting data on 'condensed' systems as opposed to 'intercalated' systems. Chlorine has been reported [127-9] as intercalating to a C_8Cl ratio at 195K. Hooley [130] recently reversed this conclusion following a detailed investigation of the mass and rate of adsorption and the adsorption isotherms between 148K and 293K. He reported that the system behaved characteristically for condensation in a porous structure. This view is now widely held.

Many different kinds of additives have been studied at various times, but the detailed physical properties have not been established in many cases. Amongst the most interesting are the alkali metal compounds, which can be prepared by vapour diffusion. This applies to potassium, rubidium and caesium [131], but not to lithium or sodium. The ability of soot (amorphous carbon) to combine extensively with sodium [132] gives some indication of the type of bonding present in intercalated systems. Sodium is unable to enter a graphitic network to form metastable compounds but quite capable of forming bonds with small aromatic molecules.

The intercalated ion may be complex, as in the formation of graphite bisulphate by warming with a strong mixture of sulphuric and nitric acids. The nitrate, phosphate and other compounds are also known. Simple non-metals also form intercalation compounds, primarily graphite-halogen combinations.

Apart from acid-ion compounds, metal-graphite compounds and graphite-halogens, graphite absorbs metal halides[133-5]and metal oxides and sulphides[135].

Most of the intercalated compounds are unstable in air, especially if heated. Any intercalating atoms remaining, even after vigorous attempts to remove them, are thought to be located at crystal defects and give the name 'residual compound' to intercalated graphite behaving in this way.

The electrical properties are the most widely investigated, and it appears to be broadly true that both donor and acceptor type additives decrease the electrical resistivity by increasing the carrier concentration in either the upper or the lower π-bands respectively. Recent examinations of the electrical properties of bromine/graphite compounds are reviewed in Sect. 1.3.4..

An important phenomenon accompanying intercalation is the rearrangement of graphite layers by successive formation and decomposition. Treatment of natural graphite with hot strong acids tends to rearrange successive layers in such a way that extensive sequences of ABCABC..... are suppressed, giving way to ABAB.... stacking[22]. The apparent mobility of carbon networks in the strong acid has been explained by the formation of an acid salt with slippage to new positions. As the lamellar compound decomposes, the new network positions are 'frozen' into the structure. Similar restructuring has been observed with bromine[136]and ferric chloride.

Intercalation occurs much more readily into graphitic regions than amorphous [137-9], the reason being that cross-linking of the graphite planes is assumed to block the diffusion of entering atoms. Where resistance to corrosion by compounds known to intercalate graphite is required, therefore, some form of cross-linking between hexagonal networks is needed otherwise local swelling and cracking will lead to structural failure.

1.3.3 Oxidation.

Three important reactions are considered under this heading:-

$$C(s) + O_2 \longrightarrow CO_2$$

$$C(s) + CO_2 \longrightarrow 2CO$$

$$C(s) + H_2O \longrightarrow CO + H_2$$

Each is a surface reaction which will initially open up the pore system. This factor, along with diffusion limitations caused by gaseous products, makes the reaction rates complex at the threshold temperatures for activation. Hewitt [140] concluded that diffusion limits the air oxidation rate of graphite blocks even below 770K. Reaction with CO_2 is not diffusion controlled until much higher temperatures are reached.

Oxidation depends upon surface structure, gas pressure and absorbed gas population. In air it is measurable at 570K., but needs to be subjected to 1070K to obtain appreciable rates.

The mechanism of oxidation is thought to involve a succession of steps repeated many times. The first stage is to form a 'surface oxide' which at a sufficiently high temperature breaks down to give a gaseous molecule and a fresh site. The procedure repeats itself but it is noteworthy that the easiest point of attack on the graphite will be at basal plane edges or at sites of catalytic chemical impurities [141-2].

Preferred removal of defective regions has led to important analytical work on defects in graphitic materials as these are placed in relief by controlled oxidation[143-4].

The introduction of defects in the basal planes has led to significant drops in activation energies from the values obtained for natural graphites (48.8 Kcal/mole) to those for irradiated specimens (37 Kcal/mole)[145]. This supports the 'Succession Steps' theory above, but Watt and Franklin[142] using ozonised oxygen in an attempt to detect a lamellar intermediate during oxidation noted that the most vulnerable parts are those which exist as simple hexagon networks, not parallel networks. These authors concluded that sorption of oxygen on both sided of a network leads to instability and readily disrupts into oxides of carbon.

The surface oxides on graphite have been excellently reviewed by Boehm[146] and later by Boehm and Voll[147]. Typical active groupings are carboxylic, phenolic hydroxyl, carbonyl and lactonic. In a later paper, Epstein et al[148] suggest that in an electrochemically alternate oxidising-reducing environment, a reproducible surface functionality exists. This is suggested to be a quinone-hydroquinone system.

Fluid oxidation is catalysed by many metal impurities, especially the oxides of copper, lead, vanadium, and the transition metals [149]. The catalytic effects of these impurities fall into two classes. When copper oxide is placed on the basal-plane surface of graphite and heated in oxygen to between 570 and 970K. the formation of a network of shallow irregular channels is observed[150]. This is the result of rapid movement of the catalyst particles on the graphite surface. Other catalysts do not show the same reluctance to catalyse oxidation in the c-axis direction. Traces of lead, manganese, and molybdenum oxides lead to rapid pitting of the graphite surfaces in the c-axis

direction at temperatures considerably below those required for uncatalysed oxidation.

1.3.4 Bromination.

The lamellar compounds of bromine with graphite have received more chemical and physical attention than any other intercalating system. Reported examinations of this system serve to illustrate the extent and the uncertainty of the field. Although intercalation is the subject of most investigation, it must be remembered that as a mild oxidant, bromine attacks non-graphitic regions as well.

Marie and Mering[151] have discussed the use of bromine as an intercalation material in nearly perfect graphites, the extent of bromine uptake being a measure of the degree of graphitisation. Near perfect graphite crystals will intercalate bromine to form a material C_8Br which has a discrete x-ray diffraction pattern. The layer plane separation increases from 3.35Å to 7.05Å during this process [152]. The enveloping C-atom hexagon planes were found by Heerschap et al [153] and Eeles and Turnbull [154] to be in A - A register. On removal of most of the bromine, a 'residue compound' remains with the approximate formula $C_{28}Br$. This compound is thought to constitute bromine bound to crystal imperfections and can only be removed by heating which causes exfoliation of the crystals.

Brocklehurst et al [155-6] suggested that C_8Br has a definite structure with one bromine layer every second carbon layer. Thus, the chief dimensional effect on the crystallite is a considerable growth in the c-axis direction. This results in a steady closure of the porosity as the proportion of bromine in the compound is increased. However, the dimensions of polycrystalline materials increase by factors between 1.4 and 2.2, whereas the factor for a single crystallite is about 1.55.

This is, therefore, evidence that, at least under extreme conditions, there is a considerable generation of new porosity. The whole process is assumed to encompass crack and pore closure at moderate intercalation, increases in layer separation and finally the development of porosity in extreme conditions.

A simple theory of thermal expansion was based on these and other observations [157] which considered the bromine layer to be a gaseous bubble between carbon layers forming a potential crack. At certain temperatures, characteristic of the bromine concentration, a greatly enhanced thermal expansion in the c-axis direction was the result of the pressure bubble causing neighbouring flaws to separate. At 570K., for example, a 'breakaway' expansion occurs in residual bromine/graphite compounds.

A clearer understanding of the processes outlined above can be given by resistivity measurements over a range of temperatures for the graphite/bromine compound. Koichi et al [45] and Miyauchi et al [54] describe the high temperature electrical resistivity of graphite/bromine residual compounds in terms of x-ray diffraction studies. At room temperature, a considerable fraction of bromine molecules are located between graphite layers causing an increase in c-spacing and a decrease in electrical resistivity. The molecules become thermodynamically unstable above 600K. and migrate to crystal imperfections, grain boundaries or closed micropores. Thus the resistivity returns to a value comparable to ordinary graphite at this temperature. Above 600K. the gaseous phase causes macroscopic expansion (exfoliation) as described by Ubbelohde [126]. Upon cooling from 600K., the resistivity measurements indicated a reversible process with limited hysteresis.

The electrical resistivity of graphite bromide was studied by

Blackman et al [158] who reported a decrease in both a-axis and c-axis directions at high bromine concentrations. These effects he attributed to trapping of electrons from the conduction bands by the bromine atoms, since it is known that the Hall effect tends from negative to positive [127], and also thermo-electric power tends from negative to positive as the bromine is taken up.

An increase in modulus by introducing higher internal frictional forces has been reported by Tsuzuku and Saito [159]. These authors propose that clustered bromine atoms at dislocations 'pin' the fault to prevent slippage, a mechanism of considerable importance if valid.

1.3.5 Reduction.

The reaction:-

$$xC + \frac{y}{2}H_2 \longrightarrow C_xH_y$$

has received very little attention for near-ideal graphite crystals. When heated in flowing hydrogen gas at 990K., no observable changes in surface structure are shown after eight hours exposure [162]. If the graphite is first activated and mixed with one of several transition metal catalysts it is possible to hydrogenate at temperatures as low as 810K. [163]. McCarroll and McKee identified the process as dependent upon active species or sites [164]. They discuss the free energy changes involved with the formation of hydrides and nitrides over a range of temperatures up to 1410K.

1.3.6 Chemical Reactivity of Carbon and Graphite Fibres.

1.3.7 Intercalation.

The graphite/bromine system has received the closest attention of workers [160-1], but intercalation of potassium has also been reported [165].

Herinckx et al [165] conclude from the uptake of potassium vapour in Type 1 fibres that, unlike glassy carbons generally, the interstitial compounds correspond to those obtained in near-ideal graphite. The K/C ratio in these fibres was 0.16 which is remarkably higher than for ideal graphite (0.125 [166]). This was attibuted to adsorption in the extensive pore system. This factor, combined with the reactivity of potassium with amorphous carbon, places some doubt on the validity of the conclusions reached.

Deitz and Vaughan [160] suggest that graphite fibres are more difficult to intercalate than block graphite. A suggestion is made that the bromine only intercalates turbostratic and not amorphous regions, which is in contention with the findings of Herinckx et al. Contrary to the behaviour of bulk graphite, which exfoliates when heated under vacuum [42], the graphite fibre/bromine compounds decompose at moderate temperatures and the fibre returns to its original dimensions [161].

The graphite fibre/bromine system has shown some interesting features. A certain degree of plane movement can occur during the process of repeated intercalation and degasification. This rearrangement has been likened to a 'chemical working' [160] of the fibre microstructure and manifests itself by giving higher works of fracture and continuous increases in modulus from initial strain to failure. The mechanism making plane movements possible in brominated graphites is easily understood, but what actually motivates them to rearrange requires further study. Mrozowski [167] estimated that during cooling from heat

treatment temperatures, enormous stresses are 'frozen' into bulk graphite by contraction. Similar frozen-in stresses may occur in graphite fibres and it is envisaged that bromine intercalation gives the opportunity for these stresses to resolve themselves by plane movement, especially at flaw locations.

In a similar manner, Warner et al[161] 'froze' induced stresses into the graphite fibre/bromine system. By brominating graphite fibres, a degree of plasticization is conferred on them. If these fibres are held crimped during debromination, the induced stresses remain and the fibre tow retains a portion of the crimping imparted to them.

1.3.8 Oxidation and Oxidative Surface Treatments.

Experiments on the extensive oxidation of carbon and graphite fibres have not been numerous. Most treatments have been limited to the surface regions in efforts to improve fibre-resin adhesion. Some of the work on extensive oxidation has led to important knowledge of fibre structure.

(i) Extensive Oxidation.

Thorne and Price[168] showed that while commencing the oxidation of graphite fibres with carbon dioxide at 970K., an opening up of porosity leads to little overall removal of carbon and hence a small initial oxidation rate. The fact must not be forgotten, therefore, that although oxidation is a surface phenomenon it does not exclude internal surface.

Byrne and Jeffries[169] used a wet oxidation technique (potassium dichromate in either orthophosphoric acid or sulphuric acid) to determine the degree of graphitisation in carbon and graphite fibres. This wet oxidation usually oxidised graphitised fibres much faster than carbonised fibres according to the results presented. This throws doubt on a purely oxidising mechanism, and suggests that an ion inter-

calation may be involved as disrupting influence in graphite sequences.

Mimeault [170] oxidised commercially available fibres equivalent to Types 1 and 111 in 60% nitric acid at 391K for different periods of time. The weight loss of Type 1 fibres was independent of time after 4% weight loss, but Type 111 fibres lost 50% of their weight in 72 hours. Oxidation removed the flutings which appear on the fibres and left minute etch-pits on the surface (0.1 μm).

Air oxidation has received slightly more attention [171-4]. Johnson, J.W. et al [171], by oxidising in air at 720K, removed fibre flutings and gross surface flaws, hence achieving uniform surface smoothing. McKee and Mimeault [172] reported similar findings of a uniform fibre topography after 70% weight loss. The etch-pits are produced only in the early stages of oxidation and no trace of them is found in fibres reduced from diameters of 8 μm to 6 μm. Galasso and Pinto [173] heated various commercial fibres in air between 470K.and 870K. Oxidation was rapid for all types above 770K., but rayon-based fibres oxidised at slower rates than their P.A.N.-based counterparts. Low modulus fibres (Type 111) oxidised more rapidly than high modulus fibres (Type 1).

Murphy and Jones [174] discovered that vigorous oxidation of Type 1 fibres in air at 950K. leads to severe pitting of the surface. Circumferential flaws are credited to oxidation of surface deposits arising from precursor fibres sticking together or droplets of P.A.N. These surface deposits are claimed to be amorphous after carbonisation and act as regions of preferential attack.

Barnet and Norr [108] plasma oxidised fibres and claim that the etch-patterns produced are a reflection of the radial distribution of graphitic and amorphous regions. Insufficient evidence is produced to eliminate the possibility that these patterns are artefacts of the

experimental technique used.

(ii) Oxidative Surface Treatments.

As the degree of graphitisation increases in carbon fibres, it is accompanied by a decrease in the inter-laminar shear strength of composites made from them. This was first reported by Simon et al [175] after the original work of Phillips and Wadsworth (1966). Mild surface oxidations were found to increase the inter-laminar shear strength although some controversy exists over the precise reason for this.

The most common oxidative surface-treatment methods used in the past are listed in Table 2 [172].

Table 2. Oxidative Surface Treatments.

Wet Methods	Dry Methods
Boiling nitric acid	Vacuum desorption
Permanganate-sulphuric acid	Air
Chromic acid	Oxygen
Hypochlorous acid	Ozone
Sodium hypochlorite	Catalytic oxidation

Wet and dry methods of surface oxidative etching lead to general removal of gross surface roughness, but an increase in surface area. The latter result is probably caused by the formation of micro-etch pits [176-8] or the exposure of hitherto inaccessible pores [179].

Butler et al [180], using dark field microscopy, estimated that Type 1 P.A.N.-based fibres offered 60% basal plane and 40% basal plane edge at their surfaces. Lower modulus fibres had substantially less basal surface. Mild oxidation serves to increase the proportion of basal plane

edge in the fibre surface.

Johnson, J.W. [181] concludes that an important effect of mild air oxidation is to remove structural flaws and cavities that are partly responsible for tensile failure in untreated fibres. Inspite of these improvements, the conditions used in air oxidation are critical and slight deviations in temperature and pressure lead to marked pitting and low tensile strengths in the resulting composite [182].

Oxidation by oxygen, ozone and catalytic intermediates has received little attention. Bobka and Lowell [183] reported unfavourable non-uniform etching of graphitic yarn in oxygen, but Goan and Prosen [184], working with a rayon-based fibre, achieved surface etching similar to that found with air oxidation. These workers used an oxygen/ozone mixture and the generally better resistance to oxidation of rayon-based fibres may have contributed to their success.

Catalytic oxidation using lead and copper oxides has been reported by McKee and Mimeault [172]. Type 1 fibres were heated in air between 670K. and 770K. for 10-30 minutes after first coating them with lead or copper acetates. Surface topography changes were not presented, but if it can be assumed that channelling occurs [150] then an interesting surface roughening treatment has been introduced that does not produce adverse etch-pits.

The surface groups introduced by oxidation have been suggested by Herrick [179] to be carboxyl, phenolic hydroxyl, quinone and lactone, after the work by Boehm [146-7]. The significance of surface area, surface functionality and proportion of basal plane surface in the adhesion of fibres to resins will be discussed in Section 1.5.1. In all cases of surface treatment, it has been recommended by Wadsworth and Watt [185] that to minimise adverse pitting, the weight loss during oxidation

should not exceed 6 wt %.

1.3.9 Reduction.

At temperatures exceeding 970K., McKee and Mimeault [172] report a gradual loss in weight of Type 11 P.A.N.-based fibres in flowing hydrogen. At 1270K. this amounts to a loss of 2.3 wt %hr., as determined by isothermal thermogravimetry. A uniform decrease in fibre diameter is claimed, accompanied by a general smoothing of the fibre surface.

1.4 CHEMICAL AND THERMAL STABILITY OF PHENOLIC AND FRIEDEL-CRAFTS' RESIN MATRICES.

1.4.1 Novolak phenolic resins have been known and utilised for over 60 years. They are prepared by reacting phenol with formaldehyde in a molar ratio of approximately 1:0.8 under acidic conditions [186]. The addition products of o- and p- methylol phenols condense with more phenol to give dihydroxydiphenyl methane (d.p.m.) (eg. Fig. 16).

FIG. 16.

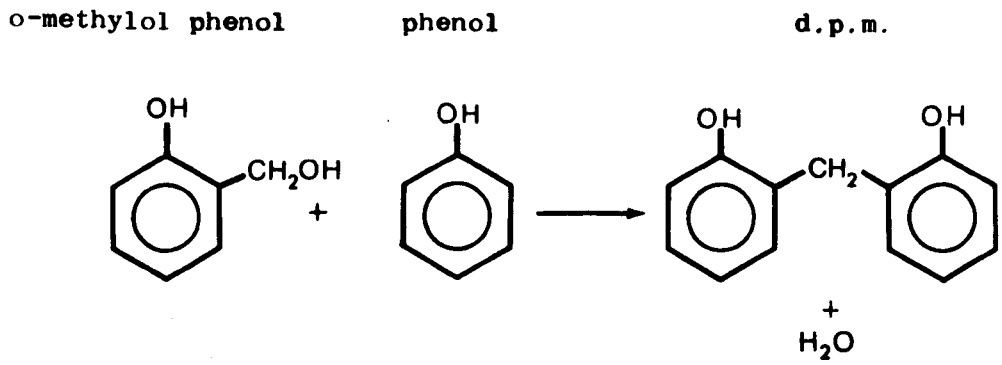

This product reacts with more formaldehyde, then phenol, etc., until molecules containing five or six benzene rings are obtained. The novolak resins contain no reactive methylol groups and need to be mixed with compounds capable of forming methylene bridges before a satisfactory 'thermoset' structure can be achieved. Hexamethylene tetramine is an example of a compound capable of cross-linking in the novolak system upon heating.

Conventional phenolic resins show poor alkali resistance as a result of the hydroxyl group adjacent to the methylene bridge. substituting xylenols for the phenols used in novolak production improves this property but often at the cost of lower mechanical strength and speed of cure.

The same relative positioning of hydroxyl and methylene groups leads to thermal instability in the polymer chain. The electron withdrawing nature of the hydroxyl group activates the methylene bridge making it susceptible to thermal bond scission.

However, highly interlocked, cross-linked, phenolic mouldings show good resistance to most acids, unless they are oxidising, and are thermally stable up to 470K.

1.4.2 The Friedel-Crafts reaction was first employed in a polymerisation reaction in 1885[187] and has since received considerable attention in this respect. It was not until recently[188-91] that the mechanical properties of Friedel-Crafts resins, although still poor, were of a standard considered to be worthy of development for use with present filler and reinforcing systems.

Aromatic compounds were chloromethylated to give di- and tri-substituted products, which were then either subjected to self-condensation or used as agents for coupling other classes of aromatic compounds to give polymers. Hydrogen chloride is given off as a condensation product. The evolution of this corrosive gas is not desirable during processing and an alternative linking reagent was sought.

In 1964, alternative coupling agents were found which gave alcohols as byproducts of the Friedel-Crafts condensation. Phillips[192] and Harris[193] independently discovered that aralkyl ethers would condense with unsubstituted aromatic ring systems eliminating simple alcohols. The condensation, using a moderate catalyst (stannic chloride), is allowed to proceed until the prepolymer has attained a suitable application viscosity. The final cure is preferably achieved with a stronger Friedel-Crafts catalyst such as ferric chloride [194].

Resins prepared by a mechanism relying solely on a Friedel-Crafts

type condensation have poor mechanical properties and are slow curing. Harris [195] has compromised the excellent thermal stability of Friedel-Crafts type resins with the strength and processability of the phenolic resins. By condensing aralkyl halides or ethers with phenols and subsequently cross-linking the pre-polymer with hexamethylene tetramine, cured resin specimens are obtained which exhibit better chemical and thermal stability than their counterparts (See Fig. 17).

FIG. 17.

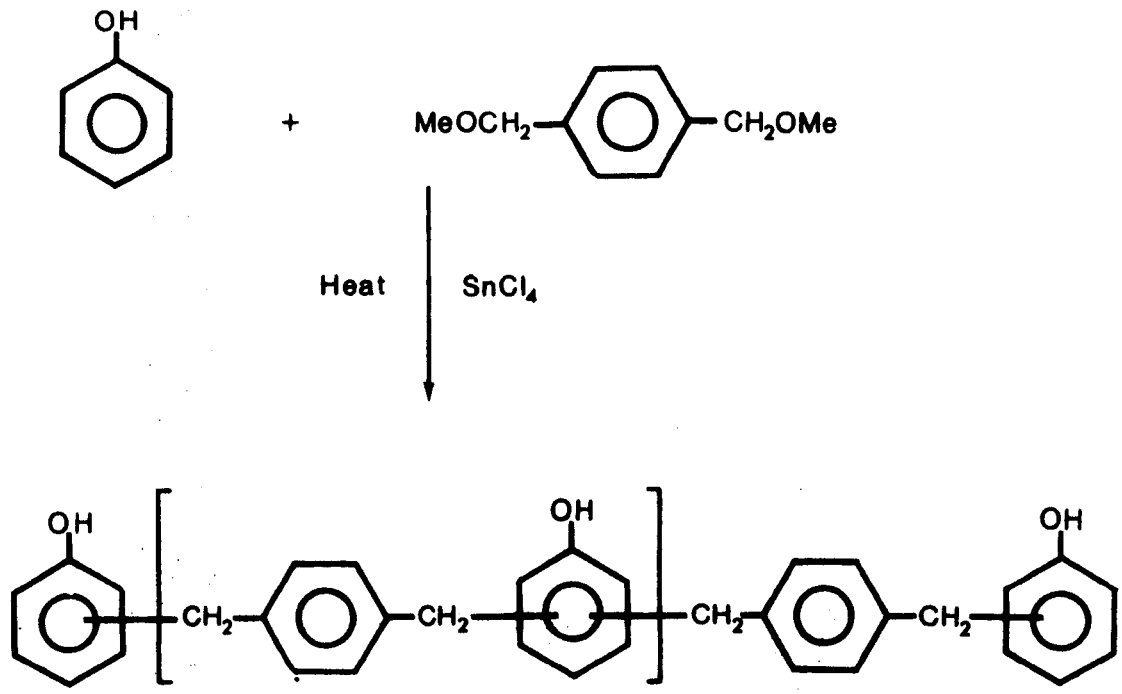

Pre polymer + (2n + 2)MeOH

$\xrightarrow[\text{Heat}]{\text{Hexamine}}$ Hard intractable resin + NH_3

The hydroxyl groups confer a susceptibility to attack by alkalis and strong acids. These resins are thermally stable to 520K.

1.5 PHYSICAL AND CHEMICAL PROPERTIES OF CARBON FIBRE COMPOSITES.

The requirements and functions of matrix and reinforcement have been outlined in Section 1.14. Both the physical and chemical properties of composites will reflect those of the fibre and matrix. Deviations in results anticipated from fibre and resin physics must be attributed to interaction at the interface between fibre and matrix. The role of the interface is well documented for the mechanical properties of reinforced plastics [195-204, 184]. Although a strong adhesive bond is not always desirable, a compromise is generally sought between requirements of impact, uniaxial tensile strength and modulus, and chemical stability.

1.5.1 The Nature of the Resin-Fibre Interface.

It has already been mentioned (Section 1.3.8) that fibres produced at higher heat treatment temperatures show a poorer adhesion to resins. Mild oxidative surface treatments have been found to improve this property, although the exact mechanism for this has been the subject of much debate.

Herrick [173, 205] attributes the improvement of resin-fibre adhesion, after mild nitric acid oxidation, to an increase of the surface functionality. He reached this conclusion by observing that as the number of chemical groups on the surface (surface functionality) increased with oxidation, so also did the shear strength of composites made from such treated fibres. During the oxidative process, however, the fibre surface areas also increased. Herrick dismissed the possibility of a surface area contribution by reducing the surface chemical groups in a hydrogen furnace at 770K. Composites made using these reduced fibres showed shear strengths barely comparable to virgin fibres. It is important to note that although a weakness of carbon composites

(ie. shear strength) had been improved, one of the fibres' main properties (ie. tensile strength) had suffered from etch-pitting in the process. In carbon fibre-epoxy composites, 60% increases in inter-laminar shear strength (I.L.S.S.) were obtained only at the cost of a 45% loss in longitudinal tensile strength.

In contradiction to Herrick, more recently, Scola and Brooks [206] pointed out that as the surface area is increased, the carboxyl group concentration per unit area may only increase slightly or even decrease. Upon hydrogen treatment of oxidised fibres, they reported an increase in surface area and no decreases in shear strength. The importance of a dependence on surface area found by Scola and Brooks reflects the findings two years earlier of Ergun [107].

In defence of Herrick, the increases in surface area upon hydrogenation found by Scola and Brooks are not consistent with fibre reactivity (Section 1.3.9), although similar increases have been reported [199] after degasification. Surface area measurements, although critical to the arguments and largely ignored by Herrick, are also a source of error. It is quite likely that the pores exposed by oxidative treatment are small enough to exclude resin molecules while admitting the nitrogen or krypton used in surface-area determinations.

Mimeault [170] finds a lack of correlation in P.A.N.-based fibres between composite shear strengths, surface area and functionality changes resulting from oxidative treatments. He suggests that chemical treatments may merely remove defects in the fibre surface which act as local points of weakness.

Butler et al [180] observed that since the basal surface of graphite has a low surface energy, it exhibits poorer wetting characteristics than edge planes (See Fig. 18).

Wetting and adhesion of an epoxy to a fibre surface, therefore, becomes poorer with increasing fibre modulus. The presence of chemical groups on the fibre's surface which are compatible with the resin matrix will also aid wetting. This approach to the problem explains why micro-etch-pit formation increases resin-fibre adhesion. The pits expose more basal plane edge and at the same time it is well known that chemical groups will concentrate themselves at these edges. From a simple 'wetting' stand point it also becomes clear why oxidative treatments improve Type 1 fibre composite shear properties more than Type 111. Type 111 fibres are not so deficient in basal plane edges in their surfaces even before oxidative treatment.

If 'wetting' is accepted as governing adhesion between fibre and resin, then the observations of previous workers may be compromised to fit the suggestions of Butler et al.

If increases in surface area are the result of basal-plane edge exposure (micro-pit formation) then surface area will be a factor in the shear properties of composites.

Increases in surface functionality will accompany basal-plane edge exposure and enhance increases of the shear strength of composites.

Thus the proportion of basal-plane edge in the surface and the concentration of chemical groupings are complementary. The former is able to stand alone in the improvement of shear properties of composites, but together they are termed 'active sites' for the improvement of resin-fibre adhesion.

Apart from oxidative treatments to improve resin-fibre adhesion, several types of coating have been applied. Polymers[184, 207,] pyrolytic graphite, nitrides and carbides[208,] silica, silicon[184, 205,] silicon carbide[196] and a variety of electrochemically deposited metal coatings[205] have been examined. Application of silane coatings to fibres in a fashion comparable to that used for glass showed little improvement in resin adhesion[184, 209-10.]

Generally speaking, the application of surface coatings does little to improve composite shear strengths, but do serve to reduce the susceptibility of fibres to oxidation. The exception is the deposition of silicon carbide 'whiskers' on the fibre surface, perpendicular to the fibre axis. 'Whiskerising' leads to a five-fold increase in shear strength for P.A.N.-based fibre composites. The improvement in mechanical properties is probably the result of the three-dimensional network of whiskers, the strong bonding of these to the graphite

substrate and the enormously increased interfacial area, rather than any increase in bonding strength between fibre and resin [172].

1.5.2 Mechanical Properties of Carbon Fibre Composites Influenced by the Resin-Fibre Interface.

This section has been introduced because many of the weakening mechanisms found in fibre reinforced plastics have been identified as interfacial phenomena.

As already mentioned, the many aspects of interfacial failure in reinforced plastics materials have received close attention in recent years. A host of new developments have been made in the theories of fracture mechanics, which would otherwise have stood unaltered for the established structural materials.

Properties of filamentary composites that are influenced strongly by the fibre-matrix interface are the tensile and flexural strengths [202], inter-laminar shear strengths and modes of failure [184, 211], and fracture energy (toughness) [197-8, 203, 200].

Poor interfacial bond strengths invariably lead to low values for the first three properties listed above. Associated with these values are shear failures along the composite axis (parallel to fibre orientation) and compressive failure on the concave surfaces of flexed test-bars [198, 200, 212-3]. An important fact emerges from I.L.S.S. failures which is that the tensile strength of carbon fibre composites is greater than the compressive strength, particularly where poor resin-fibre adhesion is present.

Fracture toughness (fracture energy) has always been of interest to workers examining filamentary composites. The simple 'law of mixtures' does not apply to this property. Outwater and Murphy [197] estimated that by a mixture-rule, the toughness of C.F.R.P. should be 100 Jm^{-2}.

The experimental value is, however, 33 KJm^{-2} for untreated Type 1 P.A.N.-based fibres in polyester resin. Many theories of crack propagation in composite materials have been put forward to replace the classical Griffith's [214] idea that all fracture energy is dissipated in the creation of new crack surface. By combining and modifying the popular theories of crack propagation, a general assessment of fracture toughness may be reached.

Kelly [32] supports a theory that fibre pull-out makes the major contribution to fracture energy. In this general theory he assumes that the original shear strength of the filament/matrix bond is maintained during pull-out. This is not valid for carbon fibres.

Outwater and Murphy [197] attribute the work of fracture to filament debonding. This is acceptable with a system such as glass fibre/epoxy where the fracture strain of the reinforcement is somewhat greater than that of the matrix. With carbon and graphite fibres, however, the strain that would be experienced by the fibres as a matrix crack passes around them far exceeds the fracture strain. Cook and Gordon [216] modified the Outwater-Murphy theory by postulating an interfacial bond failure occurring before the crack gets to the filament or passes it. Their explanation, therefore, applied to systems where the filament fracture strain is less than, or approximately equal to, the matrix fracture strain.

Pigott [217] and Fitz-Randolph [218] suggest that the energy-dissipating mechanism is the redistribution of strain energy from the fibre to the matrix after a filament breaks.

It is now generally accepted that composite toughness may be attributed to all these factors. Energy is absorbed by debonding of the fibre, matrix-fibre friction during pull-out and ultimate fibre failure [219].

Marston et al [203] presented a new theory encompassing most previous suggestions, but reverting to a Griffith's model. None of the theories above successfully predicted the toughness of more than one composite system. In Marston's theory it is suggested that toughness is achieved by the work done in creating new surfaces during composite fracture. Three types of surfaces are generated, namely: (i) filament cross-sectional surfaces after fracture; (ii) matrix cross-sectional surfaces after passage of the crack; (iii) cylindrical surfaces created between filament and matrix (debonded surface).

Unlike the cases for tensile, flexural and inter-laminar shear strengths, the interfacial bond does not need to be as strong as possible for good composite toughness. Indeed, the best values are obtained where considerable debonding may occur before the ultimate tensile strength of the fibres are exceeded. The involvement of large frictional forces during fibre pull-out is also important. Harris et al [198] estimated that in composites made with surface treated Type 1 graphite fibres, the fibre pull-out contributed only $2KJm^{-2}$ to the overall value of $9KJm^{-2}$ for the work of fracture. In the case of untreated fibres, however, 26 KJm^{-2} are contributed by frictional work.

Since the importance of fibre-resin adhesion has become apparent, several techniques have been tested to measure the strength of the interfacial bond. Single filament castings of various shapes have been suggested by Broutman [220], McGarry [221], Outwater [197] and Favre [222]. Two modified composite shear tests are described by Prosen et al [184] in an appraisal of fibre surface treatments in which conventional short-beam inter-laminar shear testing was also reported.

1.5.3 Chemical Stability of the Resin-Fibre Interface.

The exact role of the interface in terms of the chemical stability

of C.F.R.P. has not been reported in detail by any author. Wyatt [223] and Judd [224] have reported fibre debonding and loss of mechanical strength after boiling composites in water. Harris et al [198] exposed composites containing fibres with different surface treatments to steam at 370K. for one week. Composites containing acid-etched fibres exhibited greater weight increases than was the case for other surface treatments. The authors conclude that this may have been the result of increased fibre surface area, but it seems more likely to be the introduction of more polar groups on the fibre surface that governs the moisture uptake, if this is indeed an interfacial phenomenon.

Harris continued by showing that good resin-fibre adhesion in composites leads to low values for works of fracture. He recommends surface treatments which maintain composite work of fracture after exposure to steam suggesting that this is a sign of retaining mechanical integrity. In fact, this latter suggestion is not acceptable for the data presented. Loss of work of fracture on exposure to steam should be interpreted as better resin-fibre bonding, if judged purely on the premises used for unexposed composites. The reason that works of fracture drop, however, is because of fibre-resin separation as the matrix swells, which serves to lower the frictional contribution of fibre pull-out. No clear mechanism for bond failure was put forward, but drawing-in of moisture along the interface was suggested as a possible cause of this.

The Influence of Defective Laminating on Fibre Composites.

1.5.4 Voids.

Voids are impossible to eliminate wholly from a composite, particularly in cases where the resin gives off volatile products during the curing cycle. Walters [225] has shown that the inter-laminar

shear strength decreases with increasing void content, with about 9% voids required to reduce the I.L.S.S. by 25%. Modern ultrasonic techniques for estimating void contents are described by Stone [226] who suggests that if fabrication procedures are optimised and strictly adhered to, void contents of less than one per cent are obtainable with most commercial resin systems.

Voids may act as stress raisers in tensile and flexural loadings, particularly when they are associated with misaligned fibres [227]. These will bring about premature failure, and offer no compensating advantages.

1.5.5. Delamination

A similar defect may arise which is the result of delamination of fibre from resin. This may occur between laminates in cross-plied structures or locally around fibre bundles. Deposits on the fibres or pre-impregnated fibre tows may contribute to this, but Chamis and co-workers [228] suggest that differences in thermal behaviour of resin and fibre may play an important role. Resin shrinkage during cure, and subsequent contraction as ambient temperatures are reached, serves to place compressive radial and shear axial stresses on the fibre-resin interface. Considering these contractions with the negative value for the axial coefficient of thermal expansion for graphite fibres, the shear stress at the resin-fibre interface may exceed the shear strength of the bond. Kalnin [229] has observed that this mechanism will certainly prevail in composites fabricated with highly 'graphitised' Type 1 fibres which have the largest negative coefficients of axial expansion.

In corrosive environments, composites generally absorb larger quantities of reagents after immersion than the resin alone. Judd [230]

associates this phenomenon with the void and defect contents of the composite. For this reason, he draws attention to the need for care in the fabrication of composites which will experience service in corrosive fluids, even if mechanical strength is not being utilised.

Some of the most successful fabricating techniques have been assessed for void contents by Fairbairn et al [227]. Void contents of less that 2 per cent have been measured by these authors on composites using a pneumatic bag, restricted bleed method.

1.5.6 Fibre Volume Fraction and Alignment.

Theoretically, with perfect packing, 91 per cent fibre by volume may be contained in a composite. In practice, however, the limit is about 70 per cent unless special precautions are taken.

Properties dependent largely on the interfacial bond between fibre and matrix will deteriorate with increasing graphite fibre volume fractions. Properties gaining from increased fibre volume fractions will be those depending upon stress redistribution at fibre-resin interfaces. Other properties, which have values governed largely by the 'law of mixtures', may deviate from this law with high fibre loadings if defects in individual fibres or resin matrix are present.

Heaton [215] presented a theoretical curve for composite shear modulus versus volume percent. fibres. This he derived for a square array of fibres in a matrix with a fibre to matrix shear modulus ratio of 12.1. Hancox [231] found good agreement between his experimental results and the predictions of Heaton for changes in composite shear modulus with various fibre volume fractions. In these results, all types of carbon and graphite fibres, regardless of surface treatment, gave increases in composite shear modulus for increasing fibre volume fraction. Torsional shear strengths decrease, however, except for surface treated Type 11

fibres which confer maximum shear strength at 50% fibre volume loading.

Hancox also reports that it is quite sufficient to estimate fibre loadings by simply comparing the volume of fibre used in preparation and the final volume of the composite. The accuracy of this method he confirmed by acid-peroxide digestion of the matrix, leaving only the fibres, and found values to within ±1.5% of the rough estimate.

The alignment of fibres in unidirectional fibre reinforced composites plays an important role in their mechanical properties. Dimmock et al [232] reported on the necessity for misalignment to be minimised if standards of mechanical strength and modulus are to be maintained. Fig. 19 illustrates the dependence of tensile strength on the angle that the fibres make with the composite axis.

FIG. 19.

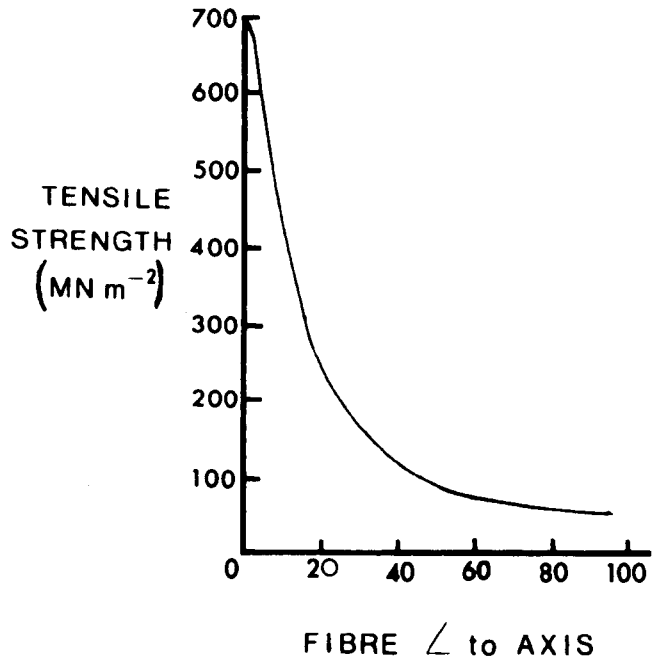

CHAPTER TWO

-METHODS & RESULTS-

2 EXPERIMENTAL METHODS, MATERIALS AND RESULTS.

The work falls into three sequential studies:-

2.1. The chemical reactivity of carbon and graphite fibres and its relationships with

2.2. Carbon fibre composite chemical stability and

2.3. Carbon fibre microstructure.

The following properties were measured as indications of physical changes in each study.

2.1

.1 Diameter

.2 Young's Modulus

Ultimate Tensile Strength (U.T.S.)

.3 Surface Topography

2.2

.1 Weights and Dimensions

.2 Short Beam Shear Strength

.3 Flexural Strength and Modulus

.4 Shear Modulus

Loss Modulus

.5 Surface Topography

.6 Fibre-Resin Adhesion

2.3

.1 Diameter

.2 Young's Modulus

Ultimate Tensile Strength

.3 Surface Topography (Including Transverse Fracture Contours)

.4 Polarised Light Spectroscopy

.5 Electrical Resistivity

.6 Specific Gravity

.7 Degree of Crystallinity (Electron Diffraction and Transmission)

.8 Chemical Constitution

.9 Oxidation Rate (T.G.A.)

Oxidation Rate (Diam v's Time)

2.1 THE CHEMICAL REACTIVITY OF CARBON AND GRAPHITE FIBRES.

In this work, three types of fibre were taken from normal production batches (ex Courtaulds Ltd., England). They were designated as follows:-

TABLE 3.

Fibre	Nominal Modulus GN/m^2	Nominal Tensile Strength MN/m^2	Heat Treatment Temperature
Grafil HM (Type 1)	350-410	1700-2200	High
Grafil HT (Type 2)	240-290	2400-3200	Intermediate
Grafil A (Type 3)	190-240	1900-2600	Low

The fibres received no surface treatment and were produced from acrylic precursor fibres.

180mm lengths of 10,000 filament tows of each fibre type were immersed in 12 liquid and 9 gaseous reagents in closed ampoules. With exceptions (indicated in the tabulated results), these were held at 293K.,323K. and 360K. for 100 days in thermostatted baths. Reagents were selected which were known to attack either the fibres or the resins to be used in subsequent exposures. Hence, gaseous and liquid oxidising agents and intercalating agents were included for attack on the fibres, whereas swelling agents and solvents were expected to attack composites. In addition, several reagents experienced frequently by materials in chemical plant were included, aqueous acid and alkali being in this category.

Assessment of these fibres before and after immersion was designed to appraise gross structural changes by mechanical testing; extensive

surface attack by optical and electron microscopy.

All observations were made on sets of fifteen fibres chosen from the tows after immersion. Fifty fibres were tested for control values.

2.1.1 Diameter Changes.

Accurate determination of fibre diameter is essential for the computation of filament tensile strengths and modulus.

Many workers [232-5] have used a laser-beam diffraction method. The most sophisticated of these methods was described by Gauville et al [233] which enabled ellipticity to be recorded by continuous measurements during filament rotation. The principle involved is the measurement of the distance, e, between the two dark zones in the diffraction pattern nearest to the focus. (See Fig. 20).

FIG. 20.

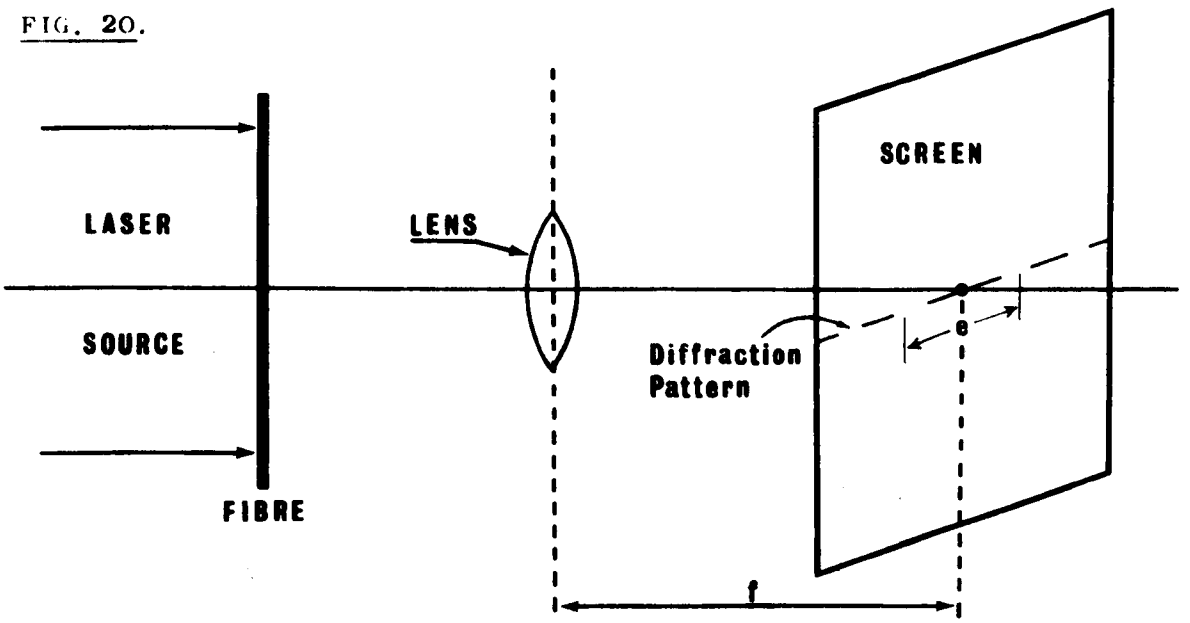

If 'λ' is the wavelength of the monochromatic light from a gas (He/Ne) laser source and 'd' is the diameter of the filament, then $e = \frac{2\lambda f}{d}$. An accuracy of ± 0.1 μm in the range of filament diameters 3-20 μm is claimed.

A direct optical method using transmitted light may suffer from error by edge diffraction, but has been accepted as standard technique. In the absence of a laser facility, optical and electron microscopical methods have been adopted in this work with considerable attention being paid to their accuracy and operator sensitivity.

The first method used was the direct measurement of fibre diameter from the screen of a Union Optical projection microscope with a micrometer gauge. The screen dimensions were initially calibrated by projecting a Perkin Elmer infrared spectrophotometric diffraction grating of known lines per inch. This method proved satisfactory for the detection of atypical bulges, which could then be avoided, but was prone to be sensitive to the operators' judgement, either from day to day, or from one operator to another.

This method was replaced by the one recommended in 'Grafil Test Methods' [236]. An eyepiece was removed from the microscope and a Watson Image Shearing Eyepiece replaced it.

With the filament mounted perpendicularly to the transmitted light, the split images may be moved by adjustment of the knob on the eyepiece fitted with a scale and vernier. Readings are taken for the cases when the images are superimposed and just touching without overlap (See Fig.21). The arbitrary reading of diameter from the eyepiece scale is converted to micrometres by reference to a calibration graph obtained using standard diameter tungsten wires (ex R.A.E. Farnborough). The diameter of these wires were calculated from consideration of length, density and uniformity.

As a check on the accuracy of this optical method, some fibres were mounted adjacent to the tungsten wires in a Cambridge 600 Stereoscan Electron Microscope. The agreement between optical and electron microscopical measurements was acceptable.

The method using an image splitting eyepiece cut down operator sensitivity to a negligible level and was considered a reliable route to the determination of cross-sectional areas if the fibres were circular in transverse section. This is fortunately the case with

British P.A.N.-based fibres. Ultimate tensile strengths were calculated using the smallest of ten diameter readings made at separate places along the fibre. The modulus was calculated using the arithmetic mean of these readings.

FIG. 21. Operation of the Image Shearing Eyepiece, Showing Superimposed, Overlapping, Touching and Separated Images.

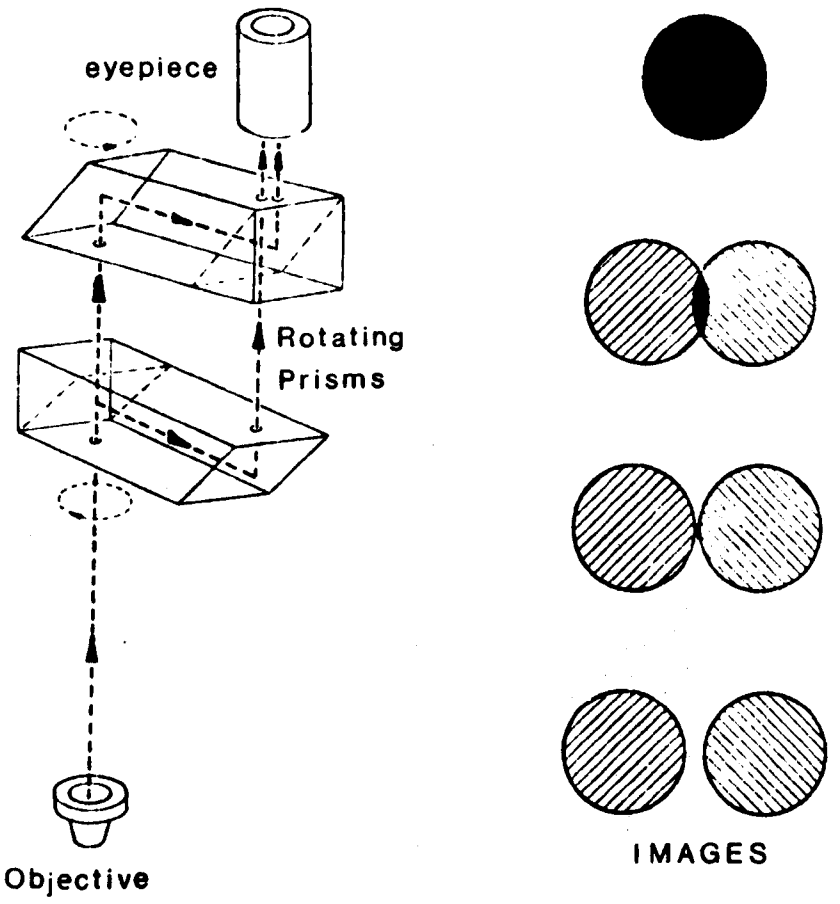

2.1.2 Filament Tensile Strengths and Modulus.

The original work on the determination of tensile strength and modulus was carried out by Watt, Phillips and Johnson [237] using a simple dead-weight procedure. Weights were added one gram at a time until failure occured. The load-extension graph gives an absolute measurement of Young's Modulus. This is very useful for high modulus materials where machine 'softness' may become significant.

In the present work it was considered too time consuming to test each filament by a manual loading method and so the standard method outlined in the Grafil Test Method [236] and described in detail by Gill [238] was used. This method involves mounting each filament on a card (See Fig. 22) and securing it with Durofix cement in four places.

FIG. 22.

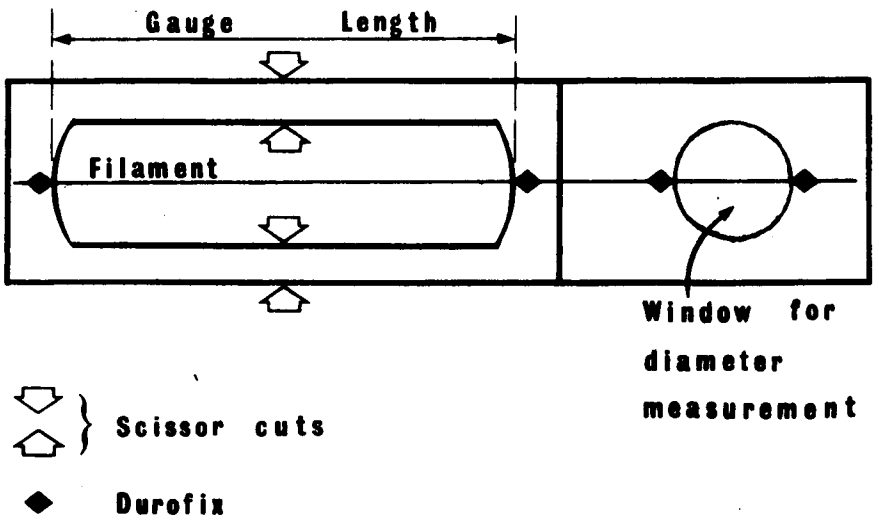

The card is mounted in the grips of an Instron TM-M machine, fitted with a Type A load cell, where it is cut through to leave the fibre in place. The highly-graphitised (H.M.) fibres did not adhere to Durofix very well and an epoxy resin system was successfully substituted.

It was necessary to decide upon a convenient gauge length. Moreton [239], Thorne [240] and Gill [238] draw attention to the fact that a whole

range of fibre defects exist, the full complement of which may spread over more than 0.2 m. These flaws will affect the ultimate tensile strength (U.T.S.) of the fibre under test by acting as stress concentrators to initiate premature failure. (See Fig. 23 [238]).

FIG. 23. The Effect of Flaws on Filament Tensile Strength.

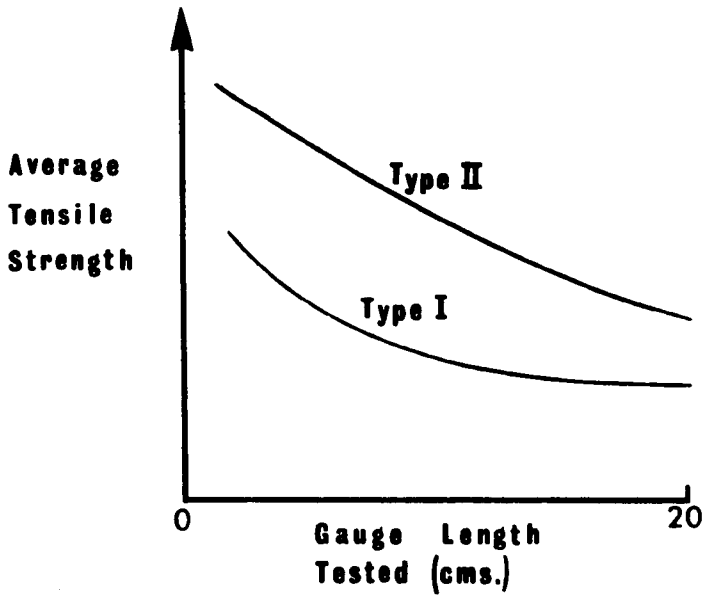

To measure the U.T.S. of a fibre accurately, it is, therefore, necessary to take very short gauge lengths ($\leq$ 0.01 m). Using such short gauge lengths, however, introduces error in the modulus measurement. The small extension experienced with short gauge lengths make the machine 'softness' highly significant.

Because the effect of certain reagents on fibre surfaces was of interest, it was decided to compromise the measurement of tensile strength and modulus by using a 0.05 m. gauge length. This made the 3 μm/g correction for the deflection of the load cell and the Instron less significant with the extensions obtained.

The strain-rate for the tests was fixed at 8% per minute, the chart speed at 0.1 m/min and the full scale load deflection at 20 grms.

The filament ultimate tensile strength (σ_{uT}) is calculated from the breaking load (P) read directly from the Instron chart and the filament diameter (d)

$$\sigma_{uT} = \frac{4P}{\pi d^2}$$

The filament modulus is calculated as

$$E = \frac{\text{load/unit extension}}{\text{cross sectional area}}$$

The load per unit extension may be obtained directly from the Instron chart after correcting for the extension of the machine (softness) and load cell and compensating for the gauge length. The mean modulus and tensile strength of fifteen filaments are taken as the average properties of the tow under test.

2.1.3 Surface Topography.

All microscopical observations of fibre surfaces were carried out on a Cambridge Stereoscan Model 600. The fibres were not coated with a conducting film as their intrinsic conducting properties were sufficient to prevent local charging of the samples.

The techniques involved and operation of electron microscopes have been well documented elsewhere [279].

2.2 CARBON FIBRE COMPOSITE CHEMICAL STABILITY.

In this work, limited experiments were carried out on two fibre types in addition to those used in the fibre exposures of Section 2.1. These were surface treated Types HM and HT and will be designated HM-S and HT-S respectively. It was considered unnecessary to include these in the preliminary study on fibre chemical reactivities because their graphite structure will not differ from their counterparts which have not received surface treatments.

The carbon and graphite fibres were taken from the same batches as those for Section 2.1. and laminated using two phenolic resins chosen for their chemical and thermal stability. One resin was a commercially available Friedel-Crafts phenolic resin, and is described in Section 1.4.2. The other was an experimental resin, VW 61933, from the BXL Company.

Composite test bars were exposed to liquid and gaseous reagents at various temperatures and changes in their mechanical properties were measured by the methods described in this section.

The changes in mechanical properties of composites in certain environments were monitored to assess the rate of chemical attack. Care was taken to ensure that the test bars were in excess reagent and that they were frequently agitated.

Preparation of Composite Test Bars.

Unidirectional composites were moulded using the resins above in a ratio of 1:1 by weight of fibre to resin. A matched-metal mould was constructed which had a 300 mm. x 85 mm. moulding area.

The first stage in the fabrication of these phenolic composites was to preimpregnate the fibres with the correct amount of resin. This was achieved by adjusting the viscosity of the resin system with a solvent

and pouring the mixture over the fibres arranged unidirectionally in an aluminium boat. Resin uptake was checked after driving off all solvent under vacuum at 350K. for two hours.

The stiff 'pre-preg' was trimmed to fit the mould and cured in a press for 45 minutes at 450K. and 19.3 Mn/m^2. Enough 'pre-preg' was used to give panels 2.5 mm. thick. Care was taken during the curing stage that the press-plates were frequently parted to allow the volatiles produced by the curing mechanism to escape. This 'breathing' of the press was essential to prevent high void contents in the composites and blistering during post-cure. The panels were post-cured next. This was carried out with the panels still in the mould but under no pressure The temperature was allowed to rise slowly over a period of 8 hours to 480K. in the case of the experimental resin and 510K. in the case of the Friedel-Crafts resin. (See Fig. 44).

Test bars were cut from the moulded panel using a circular saw fitted with a special blade designed for brittle plastics. The dimensions of these test strips were 150 mm. x 12 mm. x 2.5 mm., the fibre orientation being parallel to the greatest dimension.

In an attempt to produce the test bars more quickly, a larger matched-metal mould was tried for one pressing. This mould had dimensions of 650 mm. x 300 mm. The negative coefficient of expansion of graphite in the basal plane direction from 0 - 670K 245 gave a large discrepancy in the natural length of the mould at 290K after cooling from 520K and the laminate. Whereas the mould had contracted on cooling, the composite had expanded and buckled upon opening the mould. In the case of the smaller mould these strains were clearly not large enough to cause the buckling stress to be exceeded for the laminate's particular length to thickness ratio.

The flexural modulus of one moulding was monitored during post-cure to see how effective this was in the press. (See Fig.44).

The results of the work indicated that further examination of the role of the fibre-resin interface would be informative. It was decided to set up a model system which is described in Section 2.2.6.

Choice of Tests to Appraise Damage in Exposed Composite Bars.

Bearing in mind that as many tests as possible should characterise a single specimen, it was decided to minimise destructive testing. It was not forgotten, however, that the tests should be meaningful in their assessment of damage to the composites.

Simple non-destructive assessment of the degree of chemical attack was carried out by visual examination, weighing and measuring. More complicated techniques include stress wave emission (acoustic emission) [248, 218, 226], ultrasonics,[226, 246, 247], torsional shear modulus measurement[231, 204, 249-52]and flexural modulus measurement[236, 253] [254](both at small strains). Only the ultrasonic technique is strictly non-destructive but the other three can be measured with very little overall damage. The analysis of acoustic emission spectra from composites experiencing small strains is complicated[248]and was felt to be too difficult and unreliable as a technique for this work. Ultrasonic equipment was not available and so measurement of shear modulus and loss modulus was chosen as a reliable non-destructive technique to assess both the degradation in fibre-resin adhesion and plasticisation of the resin matrix. Flexural modulus measurements were not used as a measure of mechanical change in exposed composite bars because they would need to be at least 25 centimetres long to facilitate accurate values being obtained. The 100:1 span to depth ratio used in the three-point bending method for flexural modulus is essential if the penetration of the

loading nose between the supports is to be ignored.

An additional non-destructive test commonly used with plastics is the measurement of surface hardness. This test is not reliable for use with reinforced systems, especially in this work where each component is attacked to a different degree.

Tensile testing was not considered to be sensitive enough or reliable in the cases of Young's modulus and ultimate strength measurements respectively. The tensile modulus of a composite (E_c) in the direction of fibre orientation shows only small departures from values predicted by the law of mixtures [255] :-

$$E_c = E_f V_f + E_m V_m$$

where E_f = fibre modulus
V_f = fibre volume fraction
E_m = matrix modulus
V_m = matrix volume fraction

If $\frac{E_f}{E_m}$ is taken as approximately 100 and volume fraction of fibre as 0·6, then it is clear that even drastic changes in matrix modulus will have little effect on the composite modulus.

Measurement of the ultimate tensile strength of a unidirectional composite is neither simple nor particularly informative with regard to the present work. The method generally used [236] requires waisting of the specimen to reduce its width and thickness. Although this ensures failure of the specimen at a point away from the grips, it may still suffer from premature failure by imperfections acting as stress concentrators. Voids are impossible to wholly eliminate and these must result in scatter of data. The main argument against this test, however, is that whereas it should yield information relevant to the loss of composite mechanical integrity, it is insensitive to small changes in the matrix properties. In a case where fibre failure strain is significantly smaller than matrix yield strain, any changes in matrix

properties will not reflect significantly in the value of composite failure stress.

The remaining mechanical parameters involved in the choice were the energy and work of fracture, flexural strength, compressive strength and short-beam shear strength (inter-laminar shear strength, I.L.S.S.).

It was decided to use the short-beam shear test not only because it is the most widely accepted measure of mechanical degradation, but also because it could be performed on very short sections of specimen. Including this test allowed one more long beam destructive test to be chosen. The reason for choosing a flexural strength test was partly because of the success of Judd [230] in a similar programme, and partly because of the continuing arguments concerning fracture mechanisms [197, 349, 218, 203]. None of the current toughness theories completely predict the work of fracture for all fibre reinforced matrices. The theories of fibre pull-out, debonding, stress redistribution and work to create new surfaces are still debated and this must exclude measurement of fracture work from this programme.

Although the transverse compressive behaviour would have yielded useful information [256], it was not chosen because the specimen geometry did not conform to the others in the programme.

All composite tabulated results represent average values of four determinations, unless otherwise stated.

2.2.1 Weight and Dimensional Changes.

Samples withdrawn from liquids were carefully dried with filter papers to remove excess moisture and weighed immediately. Dimensional changes were measured by a micrometer screw gauge capable of reading to an accuracy of $\pm 2 \times 10^{-5}$ metres. When free fibres were found on the surface of exposed bars, they were not removed.

2.2.2 Short-Beam Shear Strength.

This test is usually referred to as an inter-laminar shear strength (I.L.S.S.) test. For reasons outlined below, shear is not the only possible mode of failure and reference to this parameter should be made with reservation.

The theory involves many approximations [212], but it gives a parameter which is best called the apparent short beam (horizontal) shear strength (S_H).

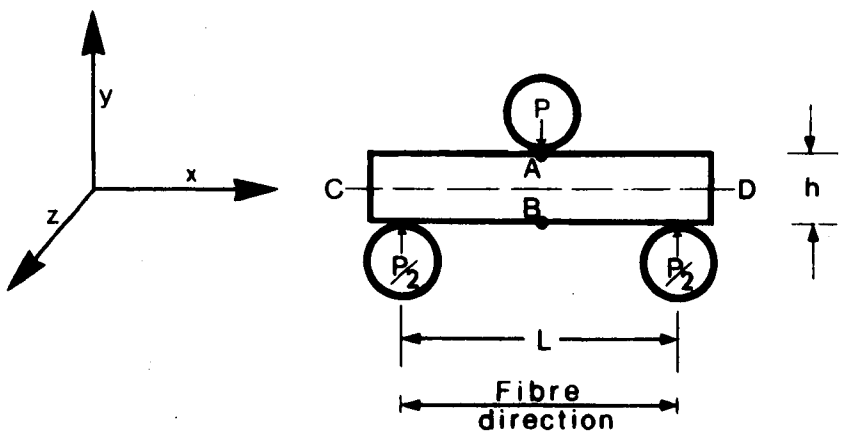

FIG. 24. The Geometry of the Short Beam Shear Test.

In Fig. 24 the stress has two major components: the normal stress (σ_x) and the longitudinal shearing stress (τ_{xy}). For a transversely isotropic material, the normal stress will have a maximum tensile value at A and a compressive stress of equal magnitude at B. The maximum stress value of σ_x is

$$\sigma_x = \frac{3PL}{2bh^2}$$

where
P = applied force
L = distance between reaction noses
b = breadth of specimen
h = depth of specimen

The longitudinal shearing component (τ_{xy}) has a maximum value in the plane CD, with the condition that transverse isotropy exists.

$$\tau_{xy\,max} \simeq S_H = \frac{3P}{4bh}$$

According to these two equations, the beam will fail in shear if

$$\sigma_{x\,max} > \frac{2S_H L}{h}$$

For graphite fibre/epoxy composites, good agreement between theoretical and experimental $\frac{L}{h}$ ratios have been found [213]. These materials show a change from tensile to shear failure at span to depth ratios of approximately 4.

Goan and Prosen [184] have shown that deviations from the theory become highly significant using surface treated or 'whiskerised' fibres. Specimens in short beam tests fractured as brittle isotropic materials with a tensile mode of failure. The true shear strength was eventually measured using a technique (See Fig. 25) developed by the University of Virginia [257].

FIG. 25.

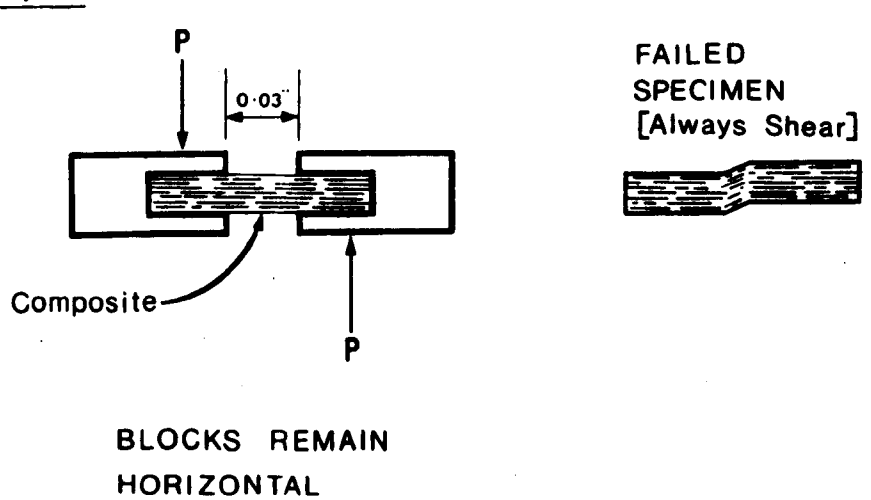

Agreement between short beam shear results and this method was acceptable for untreated fibres but showed diverging values for surface oxidised and 'whiskered' fibres.

In the present work, the existence of errors in the measurement of fundamental longitudinal shear properties is acknowledged. The nature of the assessment before and after chemical attack does facilitate changes in properties to be recorded, however, which do not necessarily need to be discrete parameters.

The short-beam shear test was carried out on a Howden compression rig using a 5:1 span to depth ratio. The apparatus was hand-cranked but every effort was made to ensure the smooth application of load. The loading nose and supports had diameters of 6 mm. The load at which failure occured was recorded and the mode of failure noted.

2.2.3 Flexural Strength and Modulus.

As outlined in Section 2.2.2, the maximum tensile and compressive stresses in a flexed bar normal to the applied force are:-

$$\sigma_{x\,max} = \frac{3PL}{2bh^2}$$

and tensile or compressive failures occur when:-

$$\sigma_{x\,max} < \frac{2S_H L}{h}$$

By making $\frac{L}{h}$ large, the cross breaking strength (flexural strength) is obtained.

Once again the Howden machine was used, but this time the support noses were moved out to give a span/depth of 40:1.

The flexural modulus measurements mentioned in the introduction to Section 2.2. were carried out on 300 mm. x 12 mm. x 2.5 mm. test bars using a span/depth ratio of 100:1. The penetration of the loading nose between the supports is less significant at this ratio and the modulus is calculated from:-

$$E = \frac{L^3}{4bh^3} \cdot \frac{P}{\delta}$$ where δ = deflection of beam

2.2.4 Torsional Shear Modulus and Loss Modulus.

A choice of test method was available in the investigation of torque-torsion relationships. Hancox[231, 204], described an applied stress technique where torque was applied and the resulting torsion measured until failure occured. In this work it was felt that damping (stress relaxation) was an important indication of internal weakening and this was better measured by an oscillatory technique in a natural mode.

A torsional pendulum was available which would measure the shear (or storage) modulus at frequencies of 0.2 ⟶ 10 Hz.

This equipment was capable of applying a pure shear stress to a specimen. The shear storage modulus (G′) in a specimen which is not highly damped is calculated from [258]

$$G' = \frac{64\pi^2 I L f^2}{\mu b h}$$

where
- L = length of specimen between grips
- I = moment of inertia of the inertia beam
- f = frequency of oscillation
- μ = shape factor

The shape factor, μ, was obtained from tables[258]. The logarithmic decrement of decay, Δ, is defined as

$$\Delta = \ln \frac{A_n}{A_{n+1}} = \frac{1}{k} \ln \frac{A_n}{A_{n+k}}$$

where
- A_n = amplitude at nth swing
- A_{n+k} = amplitude at n+k th swing

This relationship was shown by Nielson[259] to link the shear modulus, G′, which is strictly the dynamic storage modulus, with the loss modulus (G″) :-

$$G'' = \frac{G'\Delta}{\pi} - G'\Delta^2$$

The loss modulus is a parameter related to the quantity of energy lost as heat during motion. McCrum [260] favoured the rectangular cross-section specimen geometry for torsional tests because it had a larger surface area/volume ratio than a rod shaped specimen. Not only does it give good heat exchange, but lower torsional rigidity.

The storage and loss moduli are related in the equation to the complex modulus (G^*) thus:-

$$G^* = G' + iG''$$

The torsional pendulum apparatus has been described in detail by Learmonth et al [261] and is based on the design of a commercial instrument made by Nonius (Delft, Holland) (See Fig. 26).

The inertia bar and weights are balanced by a counter-weight to avoid tensile or compressive stresses being imposed on the test specimen. Once a specimen is clamped into position, the inertia bar is released from its locked position and a small angular displacement applied manually. Only shear components of stress are present in the specimen and measurement of the period of oscillation and decay of the amplitude were made. Several methods were available to make this measurement which are reviewed by Pritchard [262]. The most convenient method was by direct observation using a light-beam, scale and electronic stop-clock. The scale was placed at a distance great enough for its' lack of curvature to have negligible effect on the accuracy of amplitude measurements.

It was decided to test all specimens at a frequency of 0.5 ⟶ 1.0 Hz. This was achieved by placing the inertia weights in the outermost of the three possible positions on the inertia beam. Measurements were made at ambient temperatures (293-297K.), although the effect of temperature on the shear storage modulus was measured (See Fig. 65).

Fig. 26. The Nonius Torsional Pendulum.

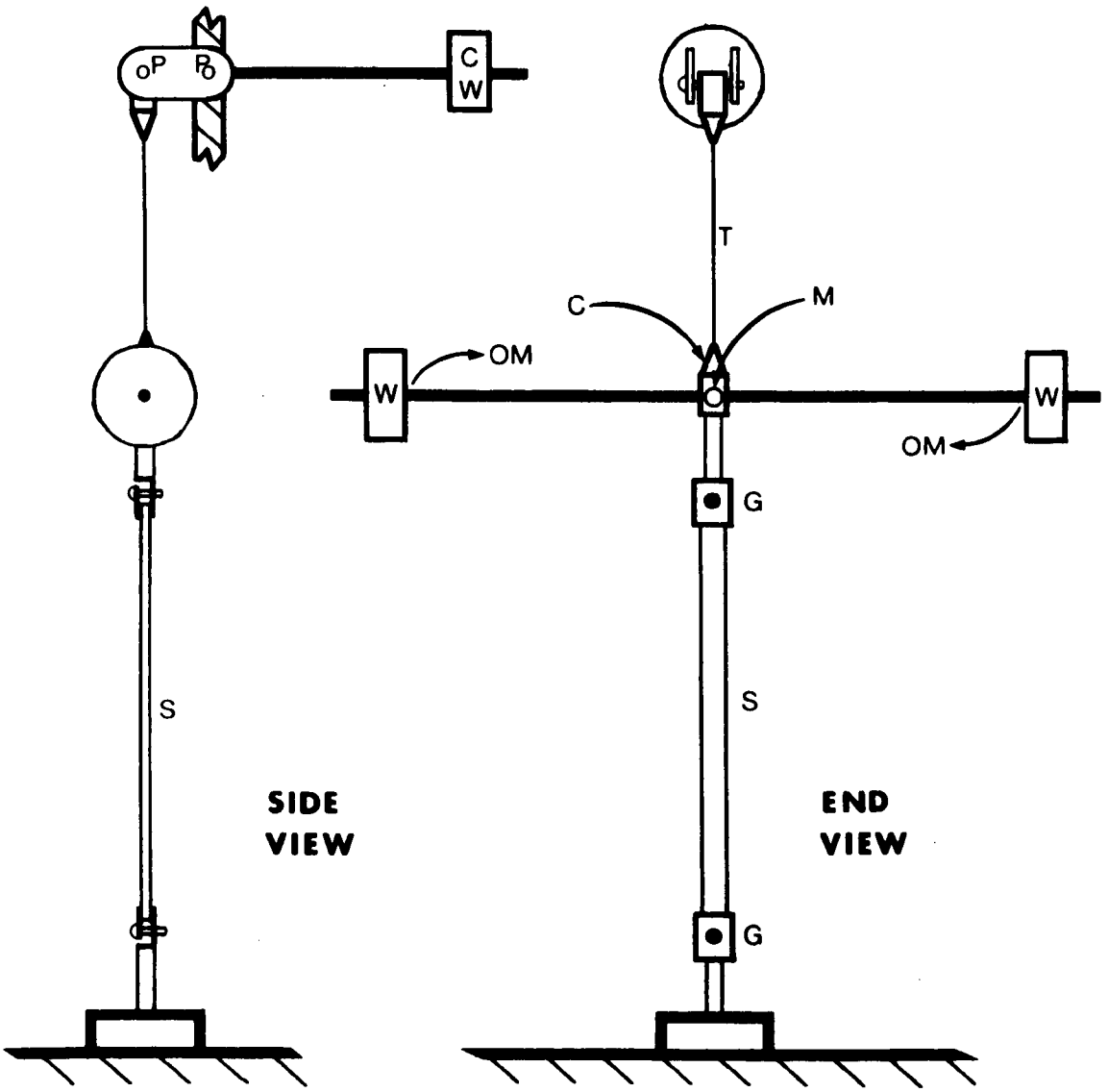

T = Torque Wire

C = Chuck Grips

M = Mirror for Lamp and Scale

W = Inertia Weights

OM = Oscillating Mode

G = Grips

S = Specimen

P = Pivots

CW = Counter Weight

= Supports

2.2.5 Surface Topography.

Optical and electron microscopy were used to examine the degree and nature of chemical attack on the exposed composite specimens. Composite surfaces required coating with a conducting deposit to avoid charge build-up during electron microscopy.

In certain cases the test bars were sectioned and their cross-sections examined at low magnifications.

2.2.6 Fibre-Resin Adhesion.

The strength of the fibre-resin adhesion can be characterised by two parameters, namely the shear strength (τ_{fm}) and the tensile strength (σ_{fm}). These will act in line and at right angles with the interface, respectively.

They have been related to overall composite failure criteria by Puck and Schneider [263] using the following unidirectionally reinforced model :-

FIG. 27.

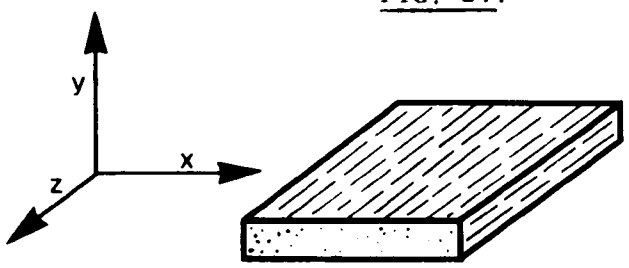

For adhesive failure at the interface

$$\frac{\sigma_x}{\sigma_{fm}} + \left(\frac{\tau_{xz}}{\tau_{fm}}\right)^2 = 1$$

This failure is not always the prime fracture mechanism involved and the other possibilities should be included here:-

For fibre failure

$$\frac{\sigma_z}{\sigma_{uT}} = 1$$

and for matrix failure

$$\left(\frac{\sigma_z^2+\sigma_x^2}{\sigma_m^2}\right) + \left(\frac{\tau_{xz}}{\tau_m}\right)^2 = 1$$

where σ_m = matrix failure stress
τ_m = matrix shear failure stress

Simple fibre pull-out tests have been tried [201-2, 222, 264] without much success for treated carbon fibres. The maximum embedded length of

fibre (t) is governed by the shear strength of the interface (τ_{fm}) and the ultimate tensile strength of the fibre (σ_{uT}). In the limiting case for fibre pull-out:-

$$t \leq \frac{\sigma_{uT}\, d}{4\tau_{fm}}$$

where d = fibre diameter

Clearly for small values of 'd' and large values of τ_{fm}, the length of embedded fibre must be very small. Favre and Perrin [222] have overcome this problem of specimen preparation by an ingenious method involving the casting of a fine pastille of resin on a mercury meniscus.

The average shear strength of the interface is given by

$$\tau_{fm} = \frac{P_{max}}{\pi d\, t}$$

The most popular methods for characterising fibre-resin adhesion are those described by Broutman [265, 201] and McGarry [266].

Two specimen shapes are recommended, each with a single fibre embedded in resin subject to a compressive load applied parallel to the filament (See Figs. 28 and 29).

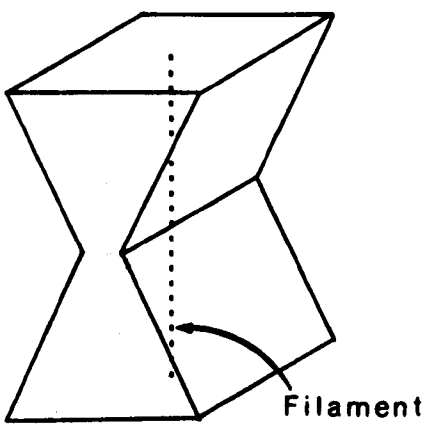

Double
Trapezoidal
-SHEAR-

FIG. 28.

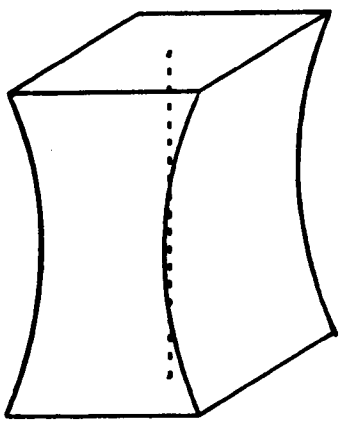

Curved
Neck
-TENSILE-

FIG. 29.

The trapezoidal specimen produces a sharply changing axial stress as the result of the sloping sides. This continuous change of axial stress results in a large shear component of stress at the interface.

The curved neck specimen under compressive axial load undergoes a radial expansion at its narrowest point, which is governed by the Poisson's ratio of the matrix. Since Poisson's ratios of polymers are greater than those for fibrous reinforcements, the matrix will expand transversely more than the fibre, and an interfacial tensile stress is created.

Although these specimens have been used for glass fibres in epoxy resin systems and the computation of results is simple from a knowledge of the load at debonding, certain difficulties are encountered if graphite fibres are used. With glass, the transparent nature of the glass-resin interface is used to advantage to detect debonding of the filament [267]. When the filament debonds, it is possible to get internal reflectance and a dark outline appears at the interface. For graphite fibres, however, a convenient method has not previously been described as these are opaque.

The preparation and detection of carbon fibre-epoxy resin debonding in the curved necked specimen by an acoustic emission technique has been the sole subject of a thesis by Arrington [268] and is reported briefly elsewhere [269]. Many problems were encountered which included the 'noise' of the specimen shape and premature debonding of the filament from the specimen ends. An examination of the former problem gave results which showed high 'noise emission' even for necked castings without filaments embedded.

One criterium for a single filament test in this work was that the effect of chemical reagents on the interfacial bond should be examined.

None of the specimens described so far gave direct access of reagent to the interface under test.

Outwater and Murphy [197, 270], however, describe a specimen which, although not imposing pure shear or tensile interfacial stresses, does allow a complex interfacial failure mode to be measured. The sample shape is shown in Fig. 30 and the drill-hole, which acts as an artificial crack, allows direct access of fluids to the fibre-resin crack interface.

FIG. 30.

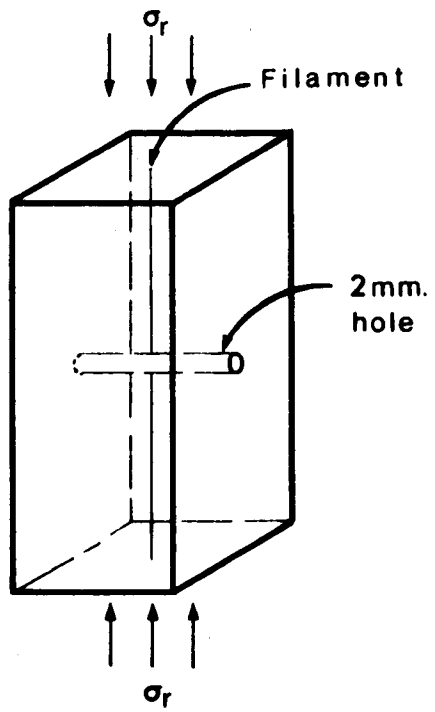

In this method, the specimens are loaded in compression along their longest axis and a complex stress pattern builds up which is primarily tensile with respect to the fibre-resin interface. A shear component is also present and the two result from transverse expansion of the specimen around the crack and the difference between matrix and fibre compressive moduli.

The parameter measured in this test is the strain energy released (G_{11}) during fibre debonding. This is a measure of both the interfacial bond strength and subsequent fibre-resin friction (τ_d) after

debonding.

Outwater derived an equation for the energy required to debond a length, x, of a fibre:-

$$G_{11} = \left[\left(\frac{\sigma_r E_f}{E_m}\right)^2 - \left(\frac{4\tau_d x}{d}\right)^2\right]\frac{d}{8E_f}$$

where E_f = fibre compressive modulus
E_m = matrix compressive modulus

He found τ_d to be negligible for glass, and it would seem fairly safe to assume a similar case for graphite. Hence,

$$G_{11} = \frac{\sigma_r^2 E_f d}{8E_m^2}$$

Test specimens were prepared using an epoxide resin with an amine hardener in a specially constructed mould (See Fig. 31).

FIG. 31.

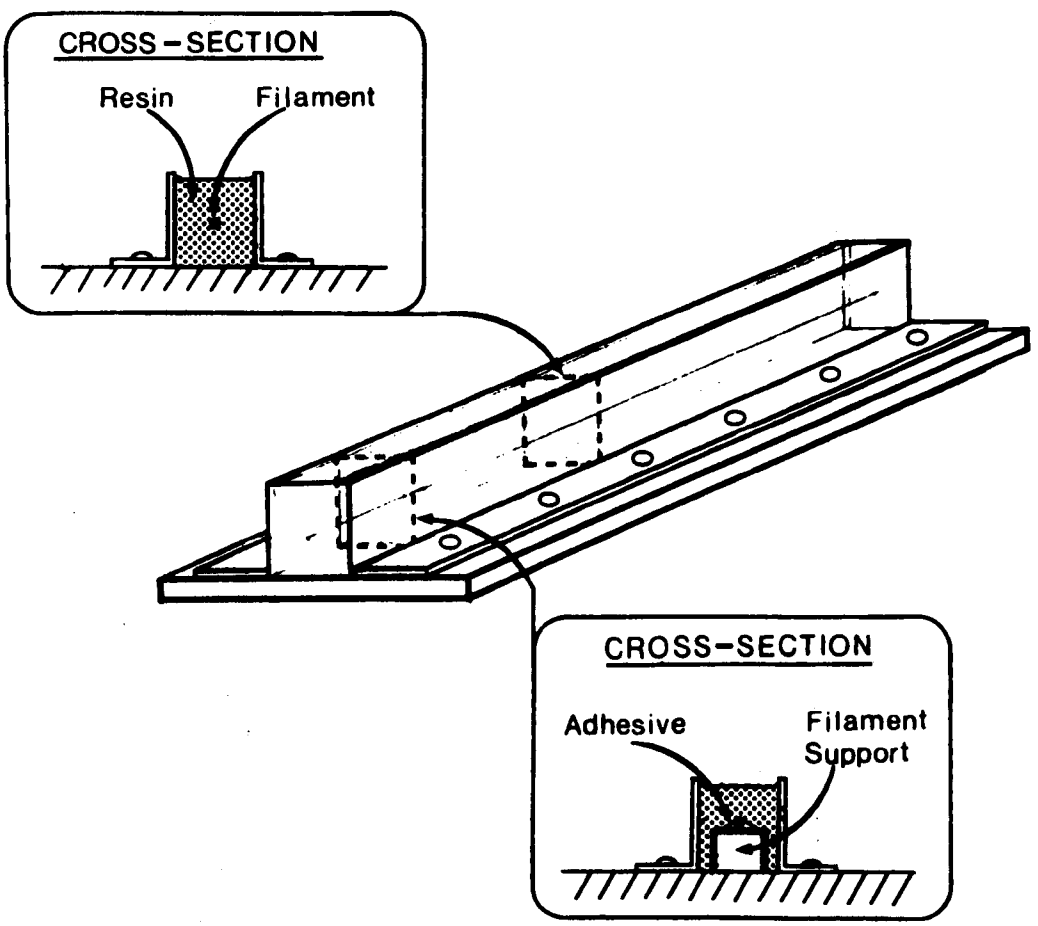

Approximately fifteen void free specimens could be made using a single long filament in one casting. Specimens of all five types of carbon and graphite fibres were used and each one was machined to the shape shown in Fig. 30 (35 mm. x 14 mm. x 14 mm.) and polished.

The specimens were compressed at a rate of 0·5 mm. min^{-1} in a cage fitted to an Instron Type 1114 tensile testing machine. Outwater used observed changes in the stress pattern, as viewed in polarised light, to detect the initial debonding of fibre from resin. This was tried but a sharp pattern change was not detectable, so a different method of detection was sought.

Using the Outwater shaped specimens in the apparatus of Arrington [269] for acoustic emission detection (See Fig. 32), it was possible to correlate the visual debonding with the actual event.

FIG. 32. Detection of Fibre Debonding by Acoustic Emission 269 .

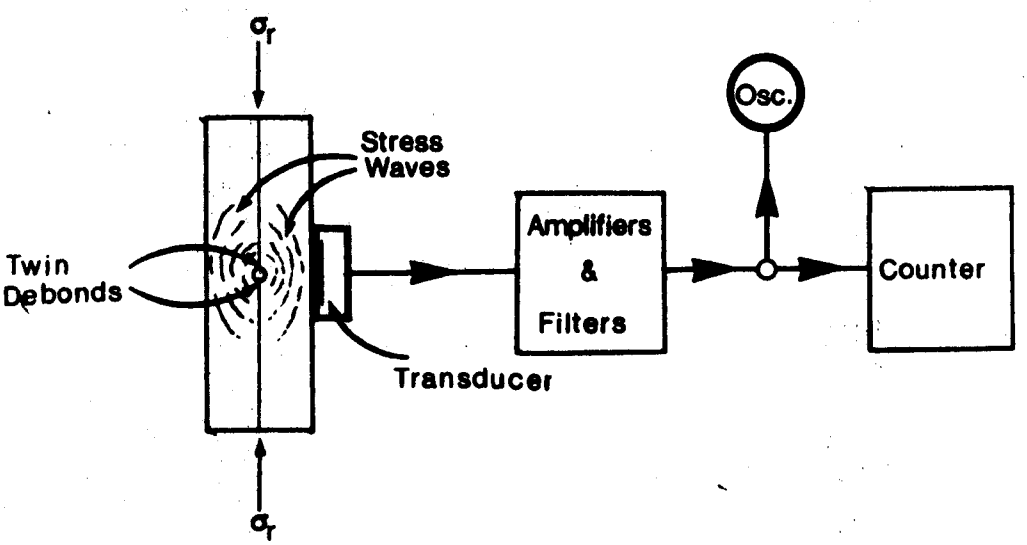

The debonding phenomenon could be seen when a correctly positioned light source was shone obliquely into the specimen and the fibre-resin-crack area was observed closely with a low powered binocular microscope (See Figs. 33 and 35).

FIG. 33. Positioning of Light Source for the Observation of Fibre Debonding.

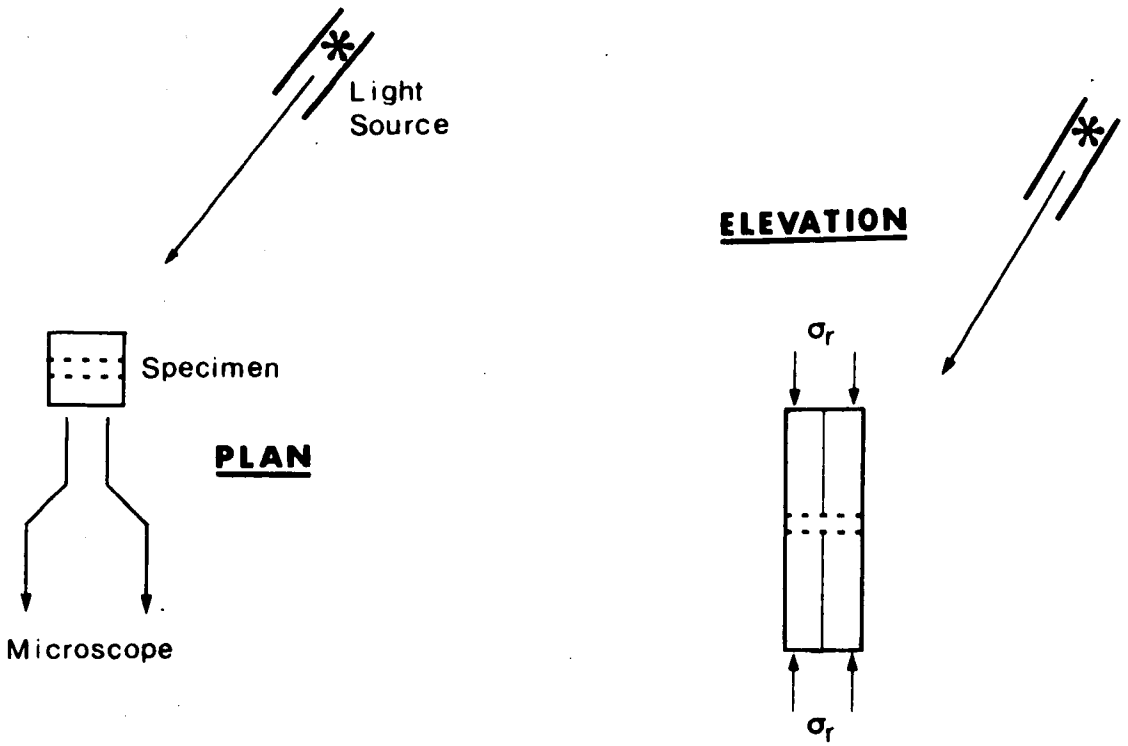

The observed light portion of the fibre denoting fibre-resin debonding is the result of refraction and reflection around the internal surface of the resin (Fig. 34).

The matrix stress (σ_r) at the point of fibre-resin debonding were recorded.

Specimens were also tested after one hour in boiling water.

FIG. 34. Light Paths for Incidence on Bonded and Debonded Fibres.

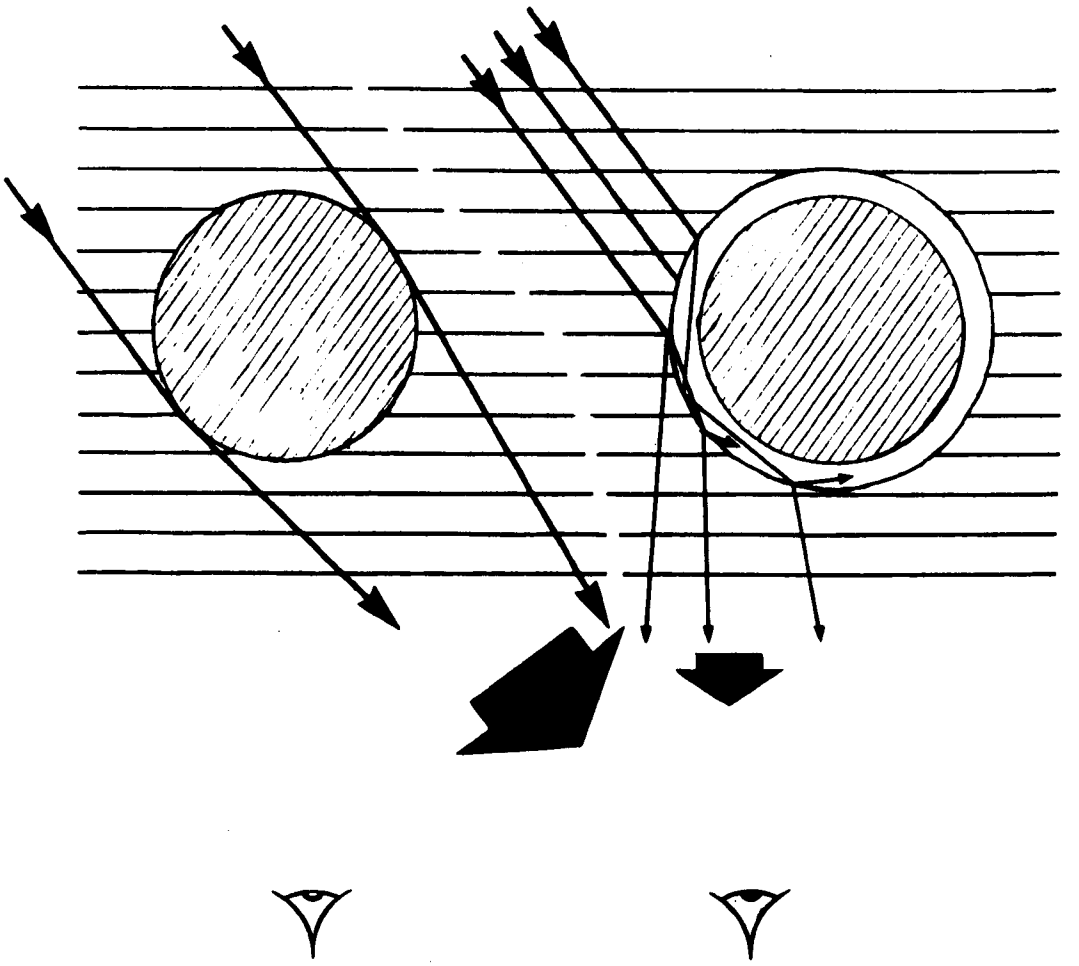

1 Bonded

Light diffracted.

2 Debonded

Light refracted and internally reflected.

FIG. 35

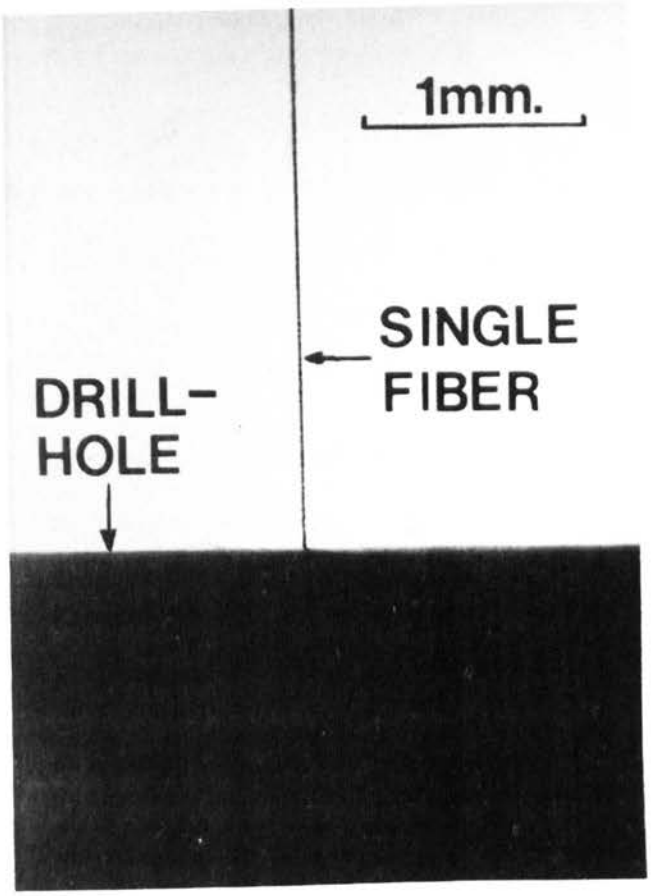

The matrix-fibre-crack interface before debonding.

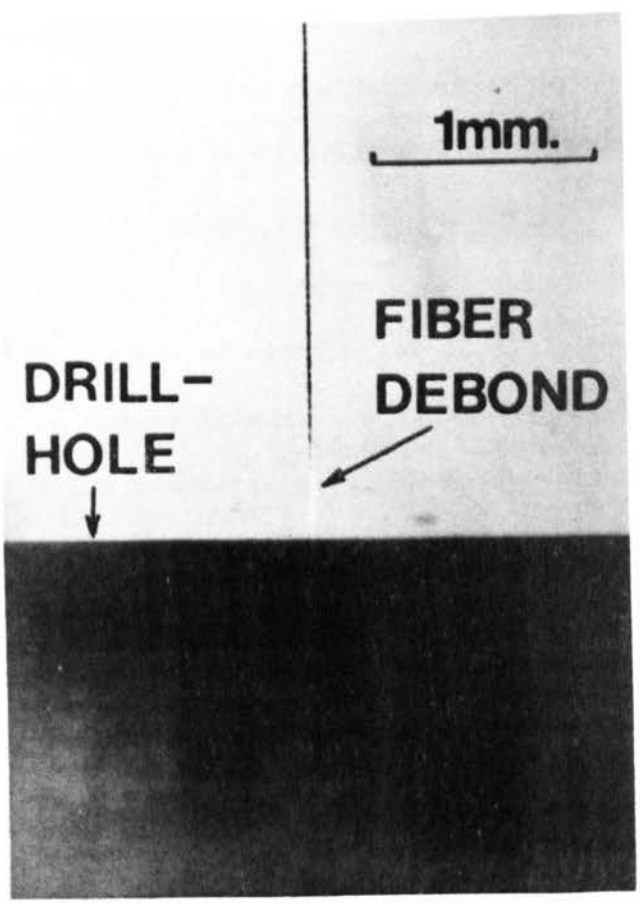

The matrix-fibre-crack interface after debonding.

2.3 CHANGES CONFERRED ON THE MICROSTRUCTURE OF CARBON AND GRAPHITE FIBRES BY CHEMICAL TREATMENT.

The decision to study fibre microstructure by the measurement of changes in physical and mechanical properties after chemical attack was the direct consequence of anomalies appearing in the results of work in Section 2.1.

By the measurement of changes in fibre properties after chemical attack, it was anticipated that the location and extent of graphitic regions would be indicated. At the same time, it was hoped to give some insight into their crystallite perfection.

Attention centred on the nitrogen dioxide oxidising system unless otherwise stated in the methods.

At first, three fibre types were exposed as tows in sealed ampoules with excess nitrogen dioxide for up to 24 hours at 420K. and 12 atmospheres pressure. These preliminary experiments suffered from a nitrogen dioxide concentration gradient forming through the tow to give inhomogeneity of treatment. The overall effect was to 'burn off' the fibres on the perimeter of the tow and progress inwards, with the result that only a small percentage of the tow was effectively treated. Consequently, a technique of exposing single filaments was adhered to for most of the work. After unsuccessful attempts to use adhesives, the filaments were tied individually to the lugs on a glass tube (See Fig. 36) with P.T.F.E. tape.

This was then placed in a glass ampoule and sealed up with the required amount of nitrogen dioxide.

This method was superceded by a less exacting one. Filaments were laid across the sticky sides of two strips of sellotape a set distance

FIG. 36. First Method of Filament Exposure.

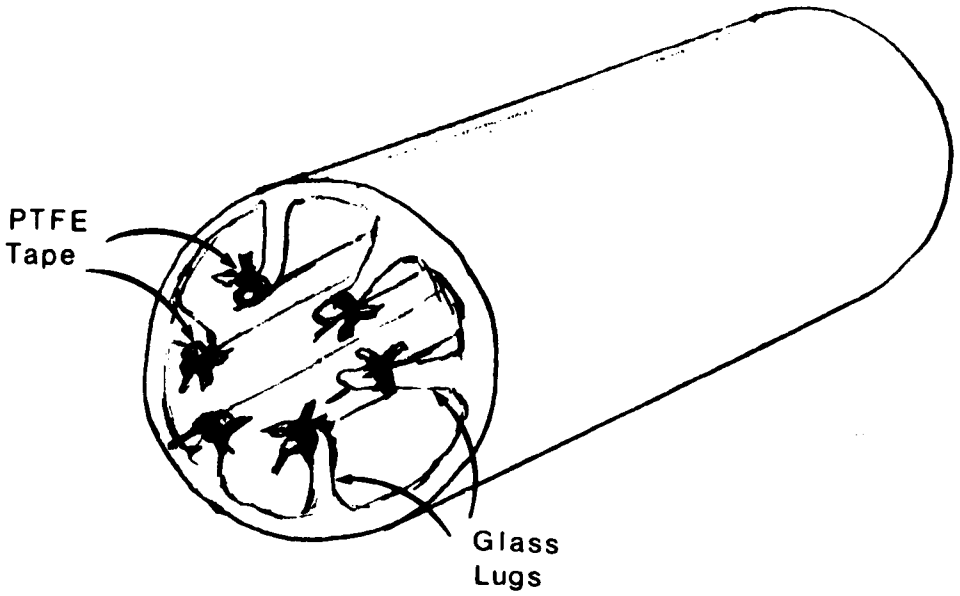

apart (See Fig. 37). This distance corresponds to approximately two centimetres less than the length of the former on which they will be rolled.

After the glass dumb-bell-shaped former has been rolled in the direction indicated, a single P.T.F.E. strip is tied tightly around the fibres alone (see inset) to secure them. The sellotape is then cut away and the former placed in a test-tube before putting both into an ampoule.

By this method it was not only possible to obtain better reproducibility, but other advantages:-

(a) If adjacent portions of the same filament were kept as controls, the central portion could be treated and appraised. This cut down scatter in results.

(b) As many as twenty fibres could be mounted and treated at one time.

It was possible to say that without doubt these had all received identical treatments.

FIG. 37. Technique of Securing Filaments to Glass Former.

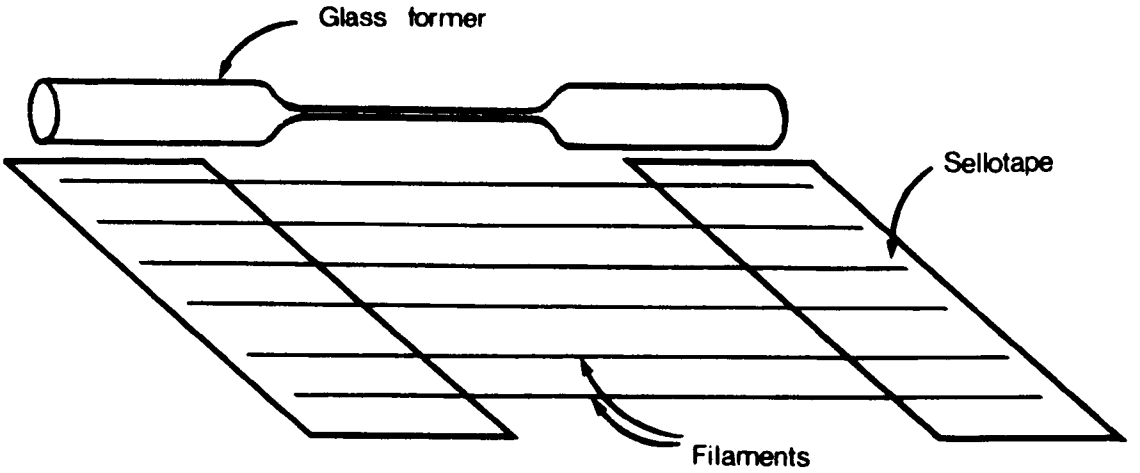

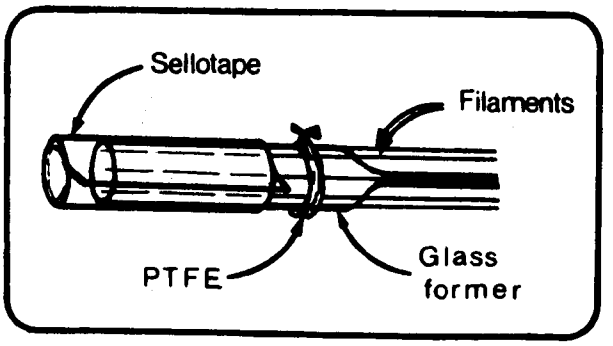

Many oxidations with nitrogen dioxide were carried out for periods from 5 minutes to 100 days at temperatures from 320K. to 520K.

A few experiments were carried out on fibres that had been oxidised in air at atmospheric pressure and temperatures from 570K. to 870K.

2.3.1 Diameter Measurement.

2.3.2 Young's Modulus and Ultimate Tensile Strength.

The methods used here were the same as for Sections 2.1.1. and 2.1.2 with minor alterations.

Because of the difficulty in obtaining lengths greater than 1-2 cms. without breaking the specimen during handling, it was necessary to reduce the test gauge length to 1 cm.

The fibre diameter measurements became critical at the small values of 2.5-1.5 μm. An error of 0.1 μm has larger significance in these fibres than for a fibre of diameter 8 μm, say, when used to compute modulus and strength values.

Apart from using the scanning electron microscope to check the diameters, the thin fibre diameters were measured on three separate image-shearing eyepieces, fitted to three different microscopes by three experienced operators using the calibration graphs for each system. Agreement to within 0.01μm was achieved. This remarkable agreement may be a result of the uniformity in diameter found with NO_2 etched fibres.

2.3.3 Surface Topography.

Photographs were taken on a Cambridge Stereoscan 600 of fibre surfaces after a variety of treatments.

Photographs showing end-on views of transverse fracture surfaces were taken on the same instrument.

2.3.4 Polarised Light Spectroscopy.

Knibbs [124-5] used polarised light to examine radial structure in polished transverse sections of various fibre types.

Woodrow, Mott and Haines [271] have outlined the basic theory and analysis of polarised light reflected from absorbing materials at normal incidence. Briefly, for polarised light with incidence normal to the basal plane of graphite, the reflectivities and phase shifts parallel and perpendicular to the plane of polarisation are equal and complete extinction is obtained. For polarised light, incident normal to the c-axis, the reflected ray suffers different amounts of absorption and phase shift along the two principal directions of the crystal. Woodrow et al showed that, under crossed Nicols (a) the maximum intensity occured when the plane of polarisation was parallel to either of the principal axes and (b) that the minimum intensity, on rotation of the sample, was zero.

Carbon and graphite samples were imbedded in an epoxy resin using the following casting technique (See Fig. 38).

FIG. 38.

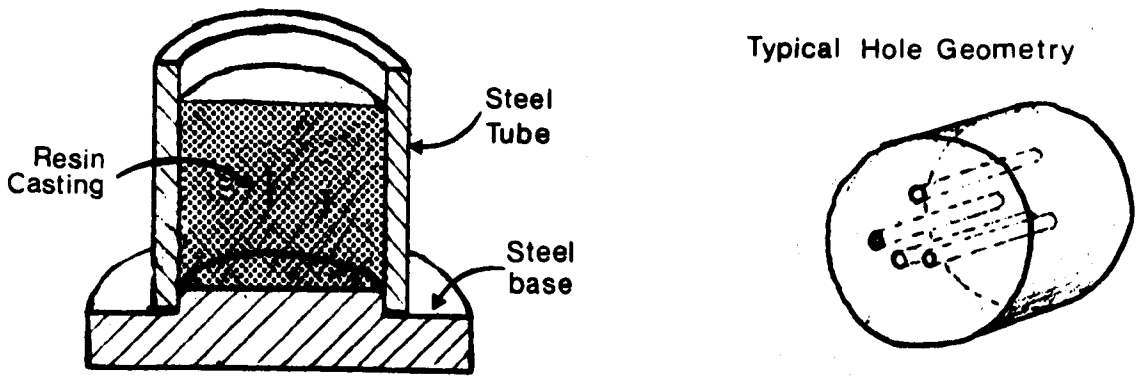

(a) A 20 mm. diameter casting was made in the mould.

(b) 2 mm. holes were drilled through with identifiable geometry.

(c) A little uncured resin was placed in the empty mould and forced up through the drill-holes as the casting was replaced.

(d) Fibres were inserted into the holes and the resin cured.

Specimens were polished on a Buehler vibrating polishing machine - model AB - Vibromet (8"). The final polishing compound was 0.25 μm diamond powder in water as lubricant. Specimens were obtained with flat cross-sections, but without fibre-resin relief or fragmentation.

Samples were examined using polarised light incident normal to the polished surface, with the Nicols in the crossed position.

2.3.5 Electrical Resistivity.

The measurement of the electrical resistivity of single carbon and graphite filaments has been carried out by many workers [46-8, 50-2,] [86-94, 272-4]. Attempts have been made to correlate crystallite size and heat-treatment temperature with electrical resistivity. These will be discussed later.

A simple test-rig was made to enable the resistance of fibres approximately 90 mm. long to be measured (See Fig. 39).

FIG. 39.

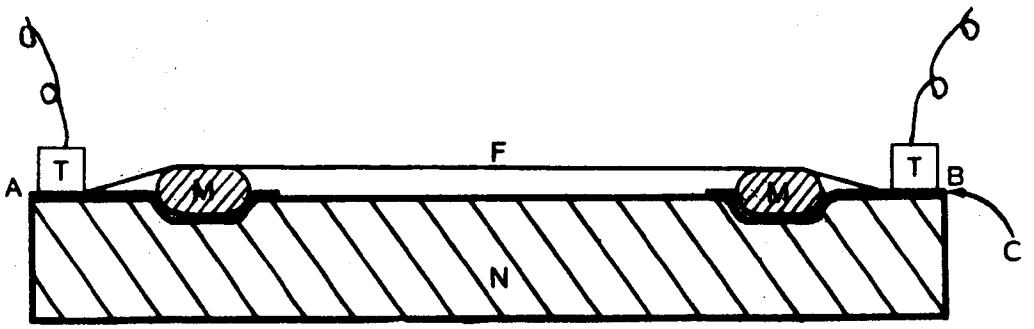

F - Filament
T - Terminal
M - Mercury
N - Non-conducting base
C - Conducting strip

This was included in a circuit as one arm of a Wheatstone bridge (See Fig. 40).

FIG. 40.

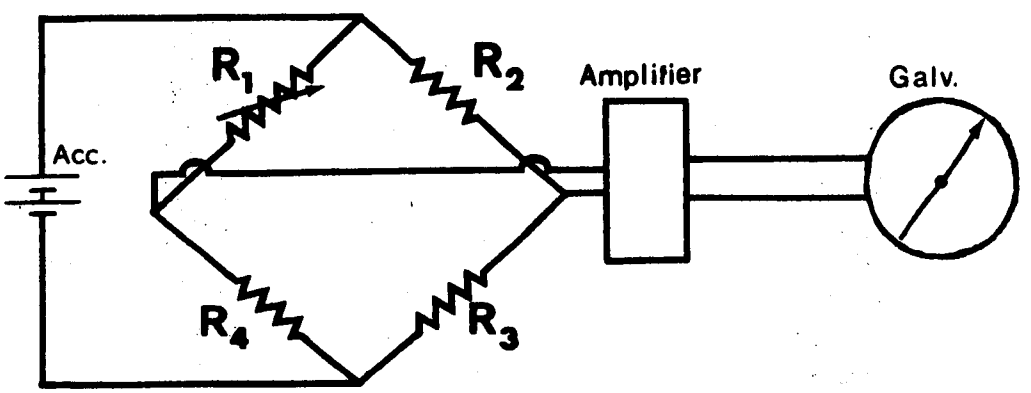

A voltage generator delivered a potential of 10 volts to a Wheatstone Bridge having $R_2 = 100\Omega$ and $R_3 = 10\Omega$. R_1 was a variable resistor capable of balancing the bridge and the null detection was by means of an amplifier and digital galvanometer.

Fibres were mounted securely across the mercury terminals by adhesive tape at A and B. The length of the specimen between contacts (L) was measured by a travelling microscope and its diameter by the image-splitting eyepiece method. Now, at balance:

$$R_F = \frac{R_3 R_1}{R_2} - r_c$$

$$\text{and } \rho \text{ (electrical resistivity)} = \frac{R_F \pi d^2}{4L}$$

Fuse-wire was substituted for the graphite fibre to measure the resistance of the mercury contacts. Several lengths of wire were used and the resistance of the contacts (r_c) obtained by plotting R_F against L and extrapolating to L = 0 (See Fig. 41).

FIG. 41.

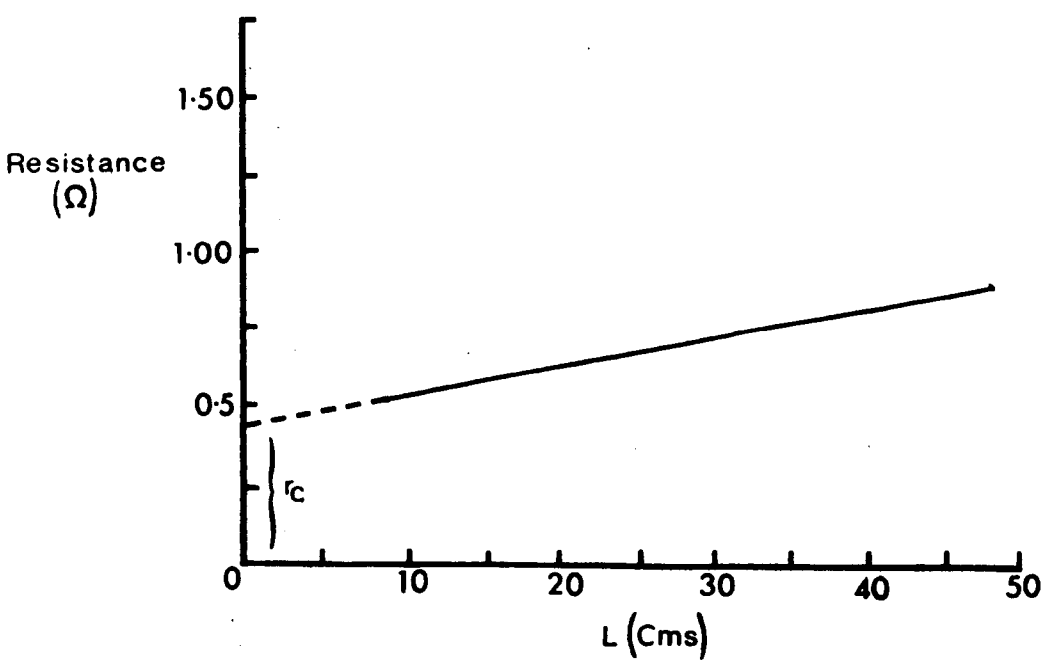

2.3.6 Specific Gravity.

Accurate determinations of single-filament densities have not previously been made. The problem with this work, however, lay in the fact that very few individually treated fibres were obtainable anyway.

The method used by Watt [86] for small amounts of fibre was adopted. This involved taking a liquid of slightly lower density than the fibres and shaking them up in it, periodically adding small portions of a denser liquid. Eventually the fibres neither sink nor rise in the mixed liquids after shaking, and at this point the density of the liquid is measured in a specific gravity bottle. This is the density of the fibres.

Limited experiments were carried out on treated single filaments but the bulk of the work was on treated portions of tows.

Positive changes in density after treatment were recorded by floating treated fibres in a liquid in which untreated fibres sank.

The liquids used for these determinations were di-iodomethane (S.G.3.325) and di-chloromethane (S.G.1.335).

2.3.7 Degree of Crystallinity (High Resolution Transmission Electron Microscopy and Electron Diffraction).

The last ten years have seen rapid developments in electron optics and also in the understandings of interactions between an electron beam and either crystalline or poorly ordered material[275]. The design and performance of modern electron microscopes approaches the theoretical requirements set out by Haine[276], Heidenreich[273], and Van Dorsten[278].

The preparation of specimens, operation of the microscope and interpretation of micrographs are described elsewhere in convenient detail[279].

The microscope used in this study was a Phillips EM 300. The work was kindly carried out by Johnson, D.J. and Bennett at Leeds University. Most specimens were ground-up before being viewed in transmission, but a few were carefully sectioned enabling electron diffraction patterns to be obtained.

The object of this study was to discover if any changes in crystallinity had occured in fibres oxidised to approximately 20% of their original diameters. For this reason, it was felt that treatments of single filaments were not necessary and bulk tows were oxidised. These were the main subject for examination but control fibres and some oxidised single filaments were also examined.

The results of other workers have been commented upon in Section 1.2.5, but it is significant that attempts to locate specific graphitic ordering have largely met with failure. It was not essential in this work to locate graphitic areas, but to ascertain if the general degree of graphitisation had increased.

2.3.8 Chemical Constitution.

Quantitative elemental analysis of combustable material is conveniently carried out in a micro-combustion furnace assembly. The equipment used in this work was a Type 10-A micro-combustion furnace supplied by S.J. Murray Ltd. (See Fig. 42).

FIG. 42.

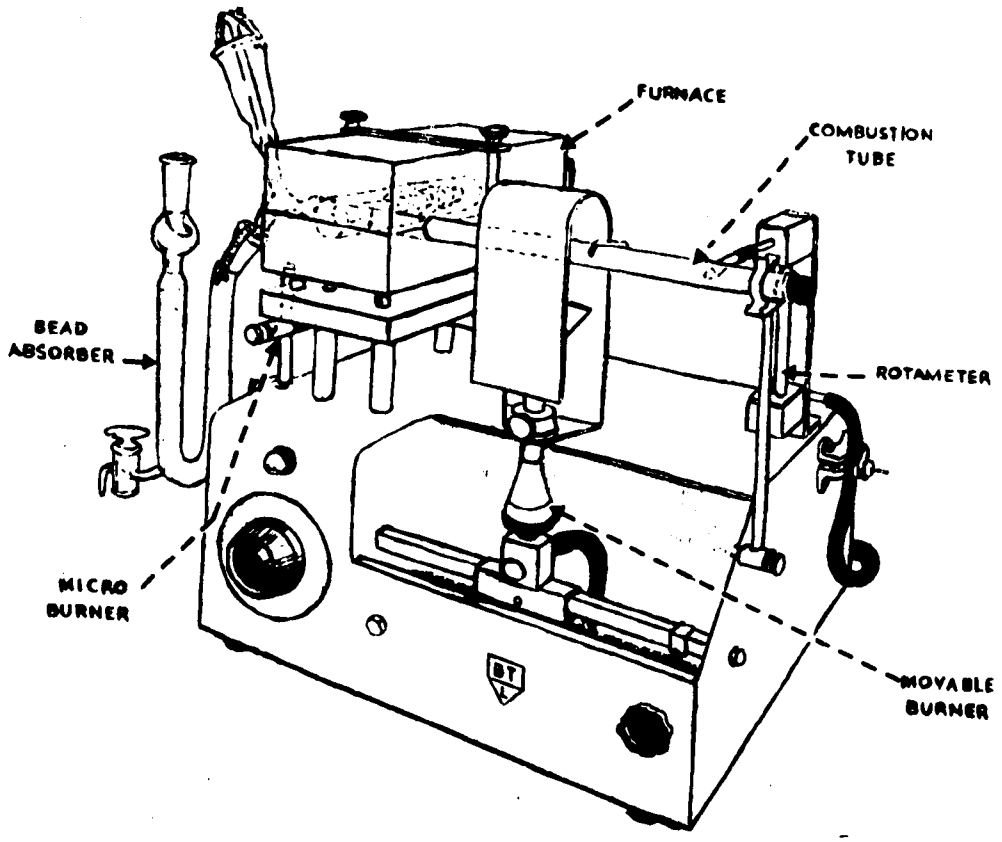

The estimation of hydrogen, carbon and nitrogen was carried out by the absorption of their highest oxides by 'Anhydrone' (magnesium perchlorate), soda-asbestos (NaOH on asbestos) and manganese dioxide, respectively. Halogen and sulphur oxidation products are retained by a heated (970K.) roll of silver gauze in the exit portion of the combustion tube.

The elemental analyses were repeated by the Analytical Services Division at the National Physical Laboratory, Teddington.

2.3.9 Oxidation Rate.

Thermal Gravimetric Analysis (T.G.A.).

A Stanton Thermobalance, Model HT-D, was used, with linear temperature rise and constant temperature programmes. The failure of this method to identify small changes in oxidation rates in air led to the adoption of microscopical technique.

Diameter v's Time at Constant Temperature.

Diameters were monitored during air oxidation on a Union Optical Hot Stage (Type HHS-3) fitted to a Union Optical projection microscope. Temperatures were measured with a 30% platinum-rhodium thermocouple and the current regulated accordingly. (See Fig. 43) . The close proximity of the detecting thermocouple and fibre are essential in the large temperature gradient experienced in the furnace. It was experimentally impossible to reduce fibre diameters below 2-3 μm by this method without their fracture.

FIG. 43

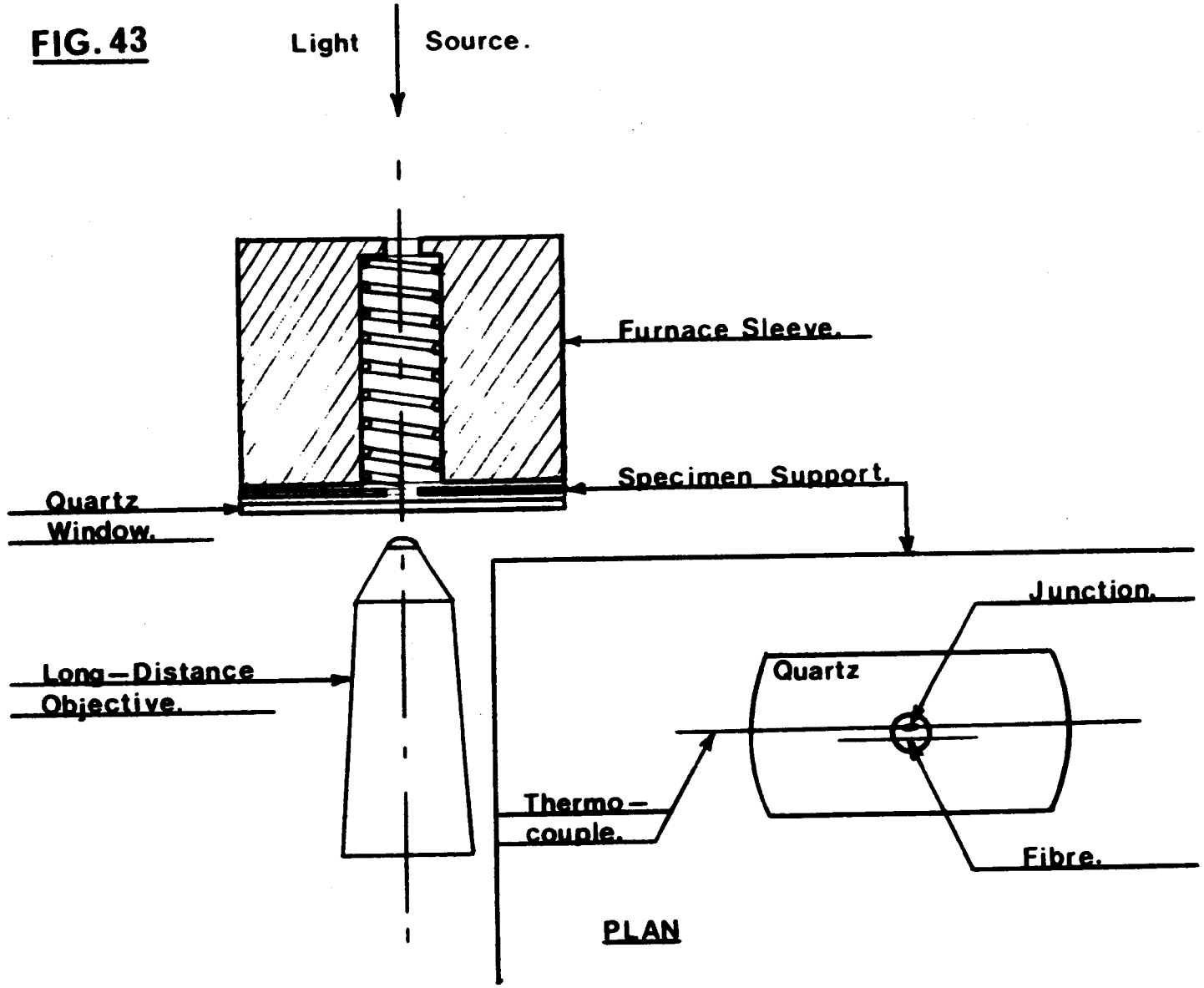
Light
Source.
Furnace Sleeve.
Specimen Support.
Quartz
Window.
Long—Distance
Objective.
Junction.
Quartz
Thermo—
couple.
Fibre.
PLAN

RESULTS

TABLE 4

Retention of Properties of Type 1 Filaments at 296K.

Reagent	Diameter (micrometres)	Young's Modulus GN/m^2	Tensile Strength MN/m^2
Control	8.1	380 ± 8	2010 ± 80
5% Ferric chloride	8.3	350	1886
30% Sodium Hydroxide	8.3	398	1990
Distilled Water	8.1	390	2100
14% Sodium Hypo-chlorite	6.8	410 ± 20	2280 ± 175
Conc. Nitric Acid (s.g. 1.42)	8.5	370	1843
Glacial Acetic Acid	7.6	402 ± 16	2110 ± 120
Carbon Tetrachloride	8.6	400	2108
Methyl Ethyl Ketone	8.5	392	2042
Methanol	7.9	392	2068

TABLE 5

Retention of Properties of Type 11 Filaments at 296K.

Reagent	Diameter (micrometres)	Young's Modulus GN/m^2	Tensile Strength MN/m^2
Control	8.5	220 ± 6	2382 ± 60
5% Ferric chloride	8.7	200	1936
30% Sodium Hydroxide	8.5	235	2246
Distilled Water	8.7	232	2340
14% Sodium Hypo-chlorite	7.3	254 ± 18	2521 ± 110
Conc. Nitric Acid (Sp. Gr. 1.42)	7.7	230 ± 12	1758 ± 170
Glacial Acetic Acid	8.1	230	2241
Carbon Tetrachloride	9.2	230	2320
Methyl Ethyl Ketone	8.7	230	2188
Methanol	8.5	225	2256

TABLE 6

Retention of Properties of Type 111 Filaments at 296K.

Reagent	Diameter (micrometres)	Young's Modulus GN/m^2	Tensile Strength MN/m^2
CONTROL	9.0	190 ± 6	1736 ± 50
5% Ferric Chloride	9.1	147 ± 14	1420 ± 120
30% Sodium Hydroxide	9.1	187 ± 14	1685 ± 105
Distilled Water	8.7	190 ± 12	1790 ± 95
14% Sodium Hypo-chlorite	8.8	141 ± 15	1527 ± 90
Conc. Nitric Acid (Sp. Gr. 1.42)	9.7	140 ± 14	1340 ± 110
Glacial Acetic Acid	9.1	195	1700
Carbon Tetrachloride	9.4	190	1726
Methyl Ethyl Ketone	8.0	190	1657
Methanol	9.1	190	1710

TABLE 7

Retention of Properties of Type 1 Filaments at 323K.

Reagent	Diameter (micrometre)	Young's Modulus GN/m^2	Tensile Strength MN/m^2
CONTROL	8.1	380 ± 8	2010 ± 80
5% Ferric Chloride	8.6	315 ± 15	1360 ± 95
30% Sodium Hydroxide	8.0	385	2000
Distilled Water	8.3	392	1980
Glacial Acetic Acid	8.1	395	2005
Carbon Tetrachloride	8.5	405 ± 18	2260 ± 105
Nitric Acid (Sp. Gr. 1.21)	7.4	340 ± 15	1715 ± 120
5% Sulphuric Acid	8.4	337 ± 14	2450 ± 145
Methyl Ethyl Ketone	8.4.	390	2120
Methanol	7.7	394	2018
Oxygen	8.3	391	2090
Acetylene	9.0	365 ± 15	2113 ± 115
Ethylene	7.8	400	2086
Propylene	8.5	388	2181
Sulphur Dioxide	8.1	425	2179
Nitrogen Dioxide	8.1	380	2160
Bromine	8.4	395	2054
Ammonia	8.1	410	2196
Chlorine	8.9	400 ± 14	2343 ± 125

TABLE 8

Retention of Properties of Type 11 Filaments at 323K

Reagent	Diameter (micrometres)	Young's Modulus GN/m^2	Tensile Strength MN/m^2
Control	8.5	220 ± 6	2282 ± 60
5% Ferric chloride	9.8	180 ± 18	1360 ± 135
30% Sodium Hydroxide	8.3	230	2000
Distilled Water	7.9	234	1980
Glacial Acetic Acid	9.1	228	2005
Carbon Tetrachloride	9.1	230	2260
Nitric Acid (Sp.Gr. 1.21)	7.9	215	1715
5% Sulphuric Acid	8.5	208 ± 12	2450 ± 115
Methyl Ethyl Ketone	8.8	230	2120
Methanol	8.2	230	2018
Oxygen	8.5	234	2300
Acetylene	9.2	220	2317
Ethylene	8.3	235	2273
Propylene	8.2	249 ± 16	2415 ± 85
Sulphur Dioxide	8.6	235	2276
Nitrogen Dioxide	8.3	265 ± 14	2980 ± 105
Bromine	8.5	250 ± 15	2503 ± 115
Ammonia	7.0	235	2270
Chlorine	8.4	255 ± 15	2771 ± 120

TABLE 9

Retention of Properties of Type 111 Filaments at 323K.

Reagent	Diameter (micrometre)	Young's Modulus GN/m^2	Tensile Strength MN/m^2
Control	9.0	190 ± 6	1736 ± 50
5% Ferric chloride	10.4	162 ± 12	1390 ± 100
30% Sodium Hydroxide	9.3	195	1720
Distilled Water	8.5	192	1825
Glacial Acetic Acid	9.1	190	1730
Carbon Tetrachloride	9.7	187	1750
Nitric acid (sp.gr.1.21)	9.3	147 ± 14	1731 ± 90
5% Sulphuric acid	9.1	190	1771
Methyl ethyl ketone	9.8	185	1595
Methanol	9.4	192	1750
Oxygen	9.1	195	1740
Acetylene	9.1	195	1775
Ethylene	8.7	193	1740
Propylene	8.4	193 ± 13	2178 ± 105
Sulphur Dioxide	9.5	195	1680
Nitrogen Dioxide	9.2	185 ± 12	1969 ± 90
Bromine	9.3	188 ± 12	1604 ± 95
Ammonia	9.0	190 ± 14	1600 ± 120
Chlorine	9.1	155 ± 16	2020 ± 110

TABLE 10

Retention of Properties of Type 1 Filaments at 363K.

Reagent	Diameter (micrometres)	Young's Modulus GN/m^2	Tensile Strength MN/m^2
Control	8.1	380 ± 8	2010 ± 80
5% Ferric chloride	8.9	320 ± 14	2115 ± 120
30% Sodium Hydroxide	7.9	401	1953
Distilled Water	8.0	392	1990
Conc. Nitric Acid (sp.gr.1.42)	8.8	312 ± 12	1750 ± 70
Nitric Acid (sp.gr.1.21)	8.8	298 ± 14	1976 ± 90
Mineral Oil	7.7	405 ± 26	2070 ± 130

TABLE 11

Retention of Properties of Type 11 Filaments at 363K.

Reagent	Diameter (micrometres)	Young's Modulus GN/m^2	Tensile Strength MN/m^2
Control	8.5	220 ± 6	2282 ± 60
5% Ferric chloride	8.2	227 ± 12	1626 ± 85
30% Sodium hydroxide	8.6	230	2197
Distilled Water	8.2	230	2320
Conc. Nitric Acid (sp.gr. 1.42)	7.1	210 ± 11	1503 ± 50
Nitric Acid (sp.gr. 1.21)	7.2	210 ± 12	1720 ± 80
Mineral Oil	8.5	230	2302

TABLE 12

Retention of Properties of Type 111 Filaments at 363K.

Reagent	Diameter (micrometres)	Young's Modulus GN/m^2	Tensile Strength MN/m^2
Control	9.0	190 ± 6	1736 ± 50
5% Ferric chloride	8.3	158 ± 14	1920 ± 95
30% Sodium hydroxide	8.7	195	1700
Distilled Water	8.9	190	1758
Conc. Nitric Acid (sp.gr. 1.42)	← Filaments disintegrated →		
Nitric acid (sp.gr. 1.21)	← Filaments disintegrated →		
Mineral oil	9.2	192	1694

TABLE 13

Effect on Filament Properties of Heat Ageing in Air for 100 Days

	Diameter (micrometres)	Young's Modulus GN/m^2	Tensile Strength MN/m^2
TYPE 1 Control	8.1	380 ± 8	2010 ± 80
323K	8.4	327 ± 28	2223 ± 135
523K	8.5	370	2010
573K	8.5	370	1957
TYPE II Control	8.5	220 ± 6	2282 ± 60
323K	8.2	230	2222
523K	8.5	250 ± 32	2806 ± 165
573K	6.8	325 ± 45	2658 ± 180
TYPE III Control	9.0	190 ± 6	1736 ± 50
323K	9.1	166	1977
523K	9.0	138 ± 40	1483 ± 185
573K	destroyed leaving sodium carbonate residue		

(a) Type I (HM)
Carbon Fibre
x 5,500

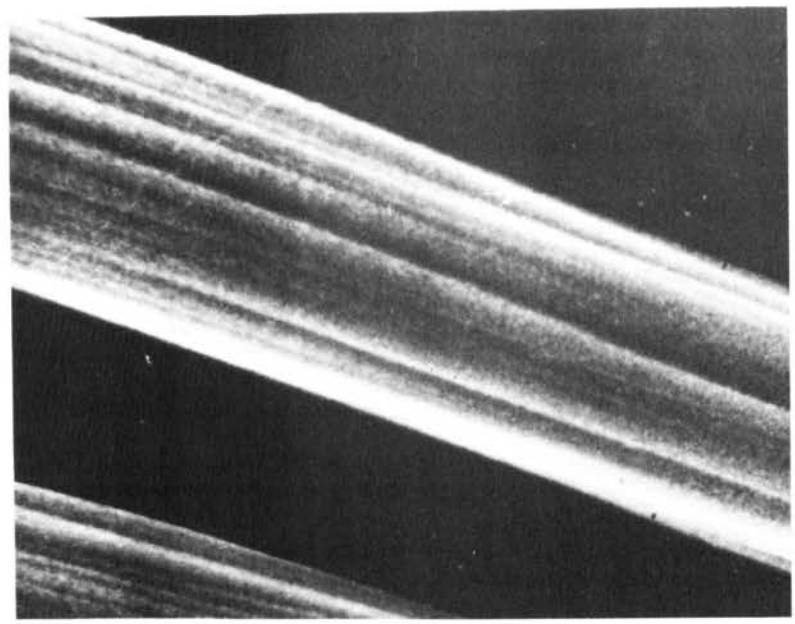

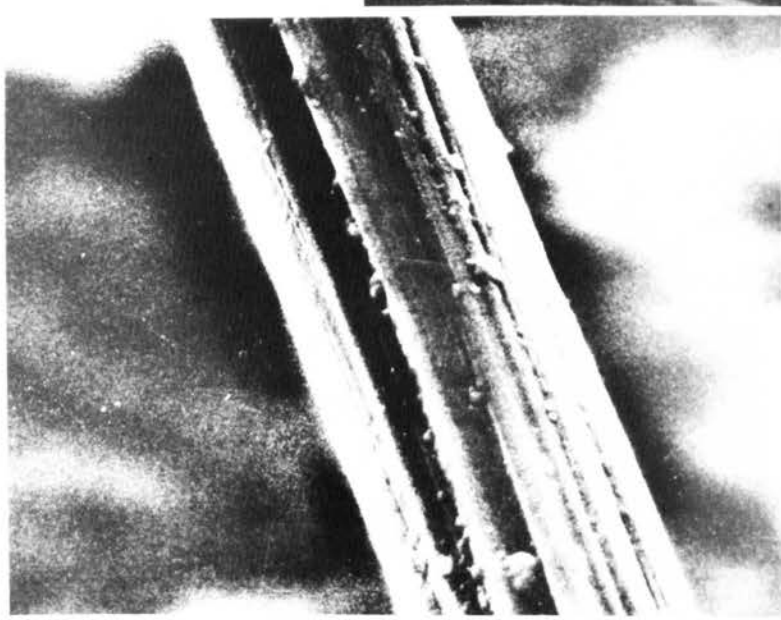

(b) Type I (HM)
Nitric Acid
(S.G. 1.21)
323K
100 Days
x 5,000

(c) Type I (HM)
Nitric Acid
(S.G. 1.42)
363K
100 Days
x 3,000

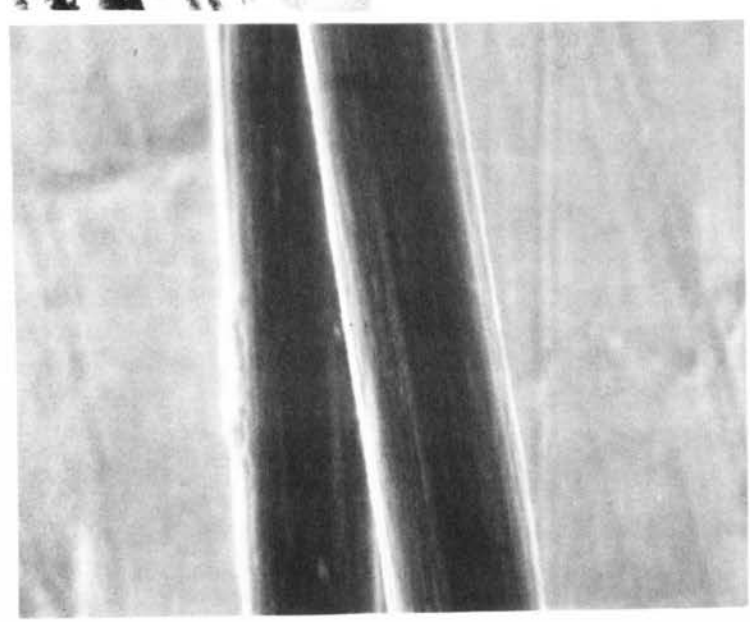

PLATE I

(a) Type II (HT)
Carbon Fibre
x 6,000

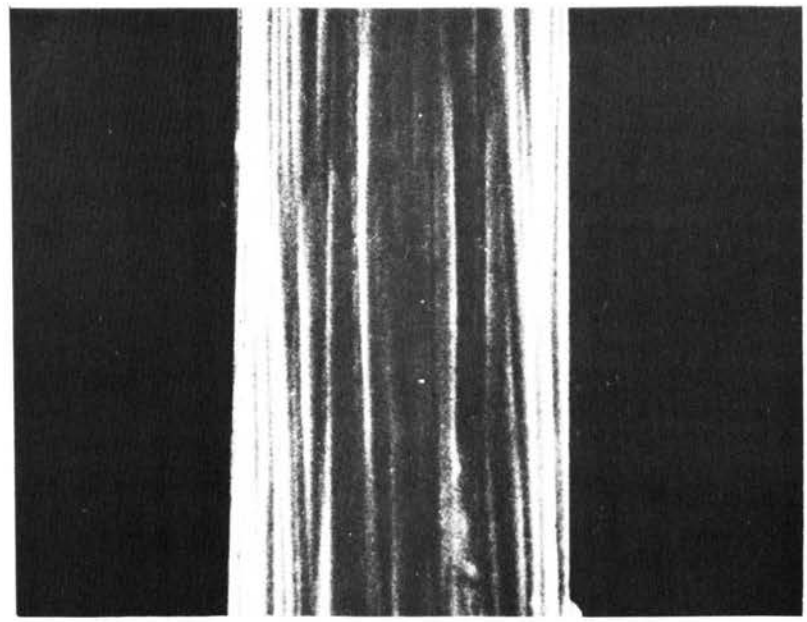

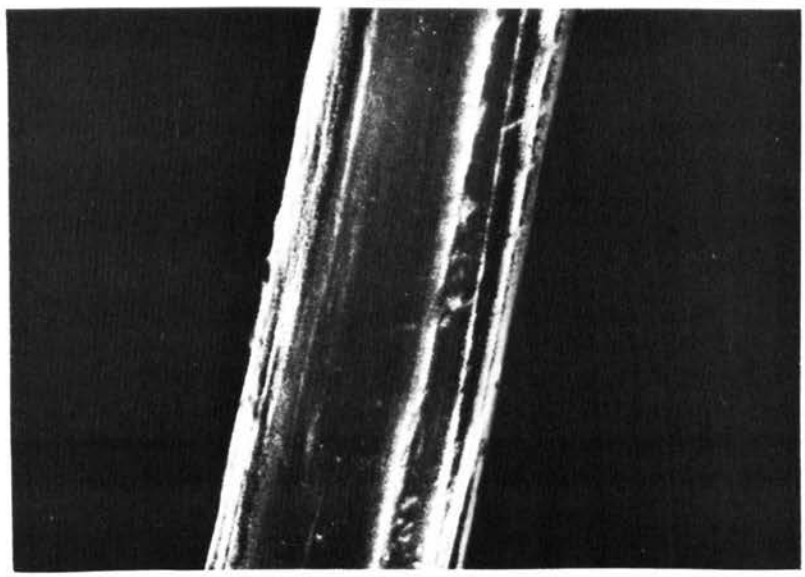

(b) Type II (HT)
Nitric Acid
(S.G. 1.21)
323K
100 Days
x 5,000

(c) Type II (HT)
Nitric Acid
(S.G. 1.42)
363K
100 Days
x 5,000

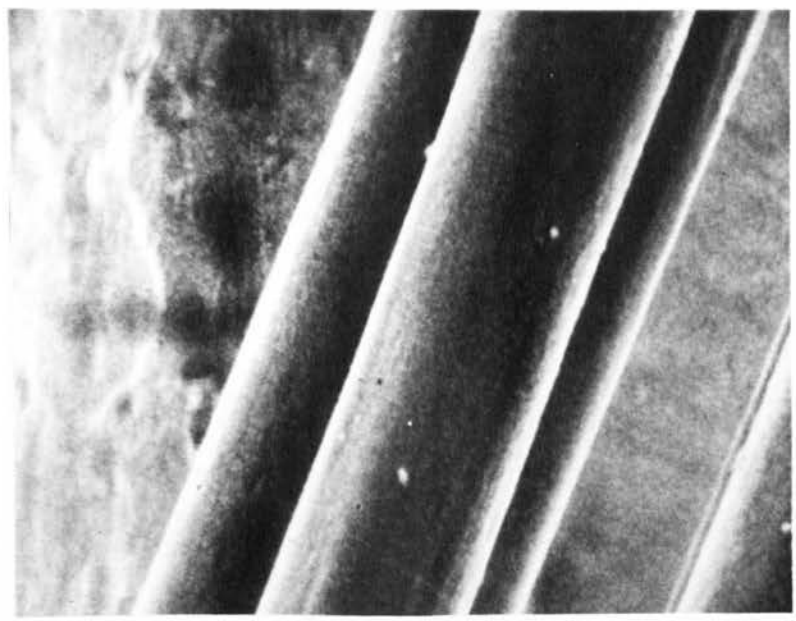

PLATE II

(a) Type III (A)
Carbon Fibre
x 6,000

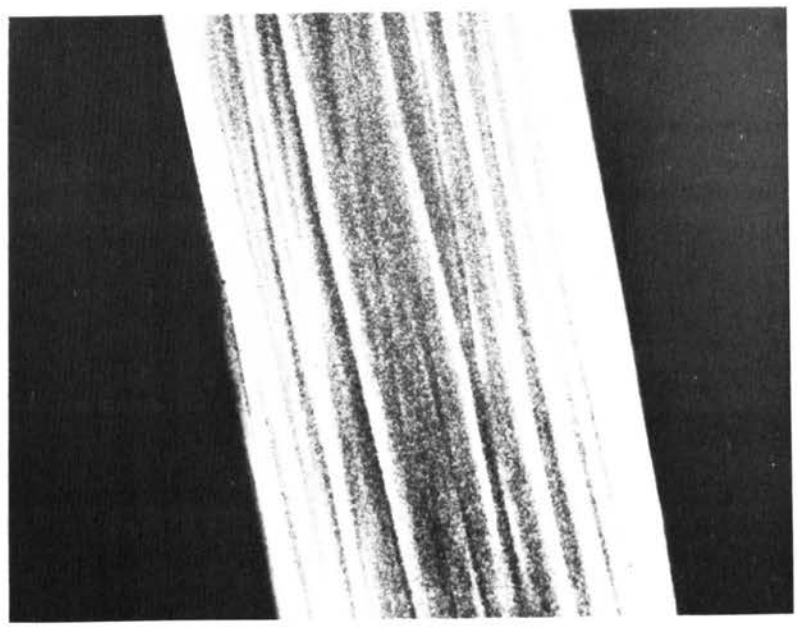

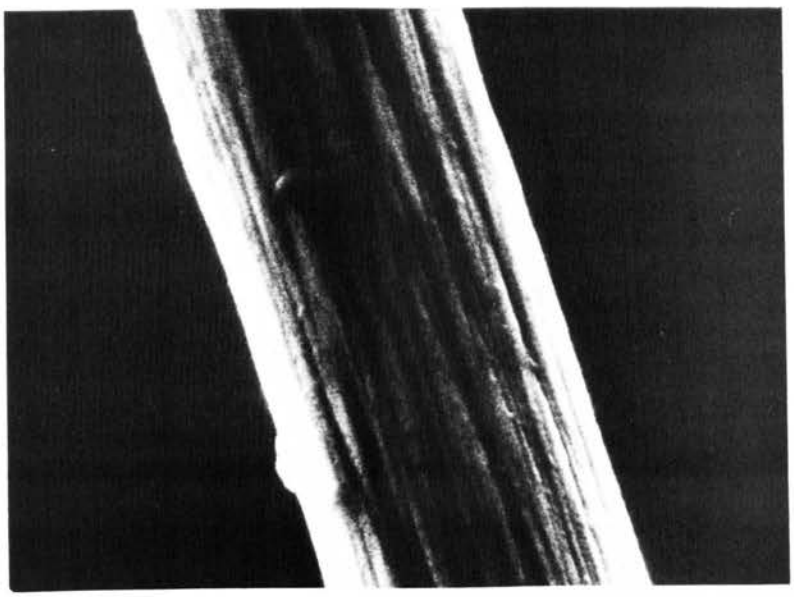

(b) Type III (A)
Nitric Acid
(S.G. 1.21)
323K
100 Days
x 5,000

(c) Type III (A)
5% Ferric
Chloride
Solution
363K
100 Days
x 8,000

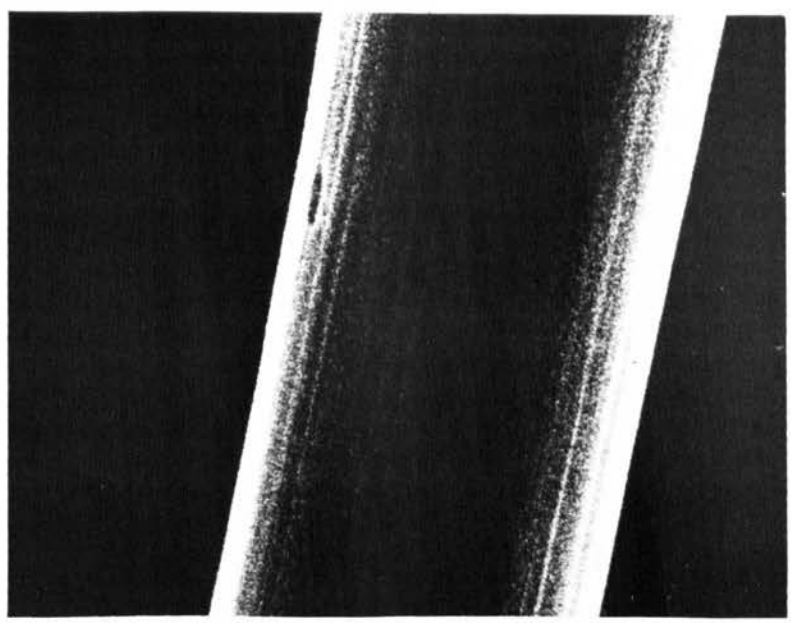

PLATE III

(a) Type III (A)
Air
573K
14 Days
x 5,000

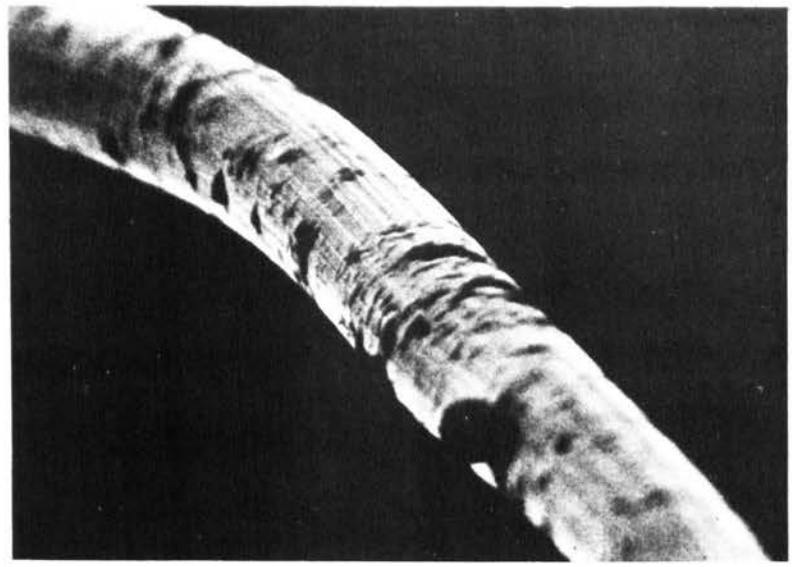

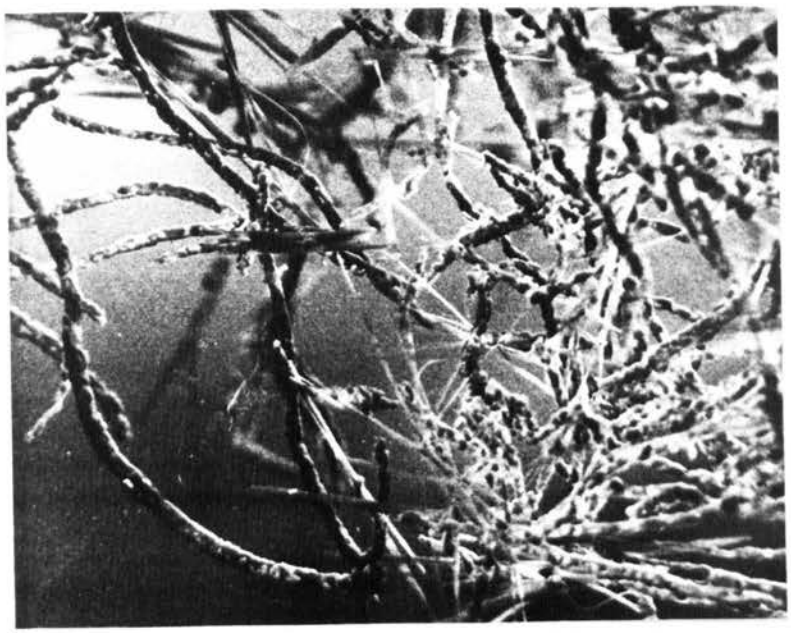

(b) Type III (A)
Air
573K
28 Days
x 800

(c) Type III (A)
Air
573K
x 1.5 - 2.0

PLATE IV

FIG. 44. Development of Flexural Modulus during Post-Cure (Measured at Room Temperature)

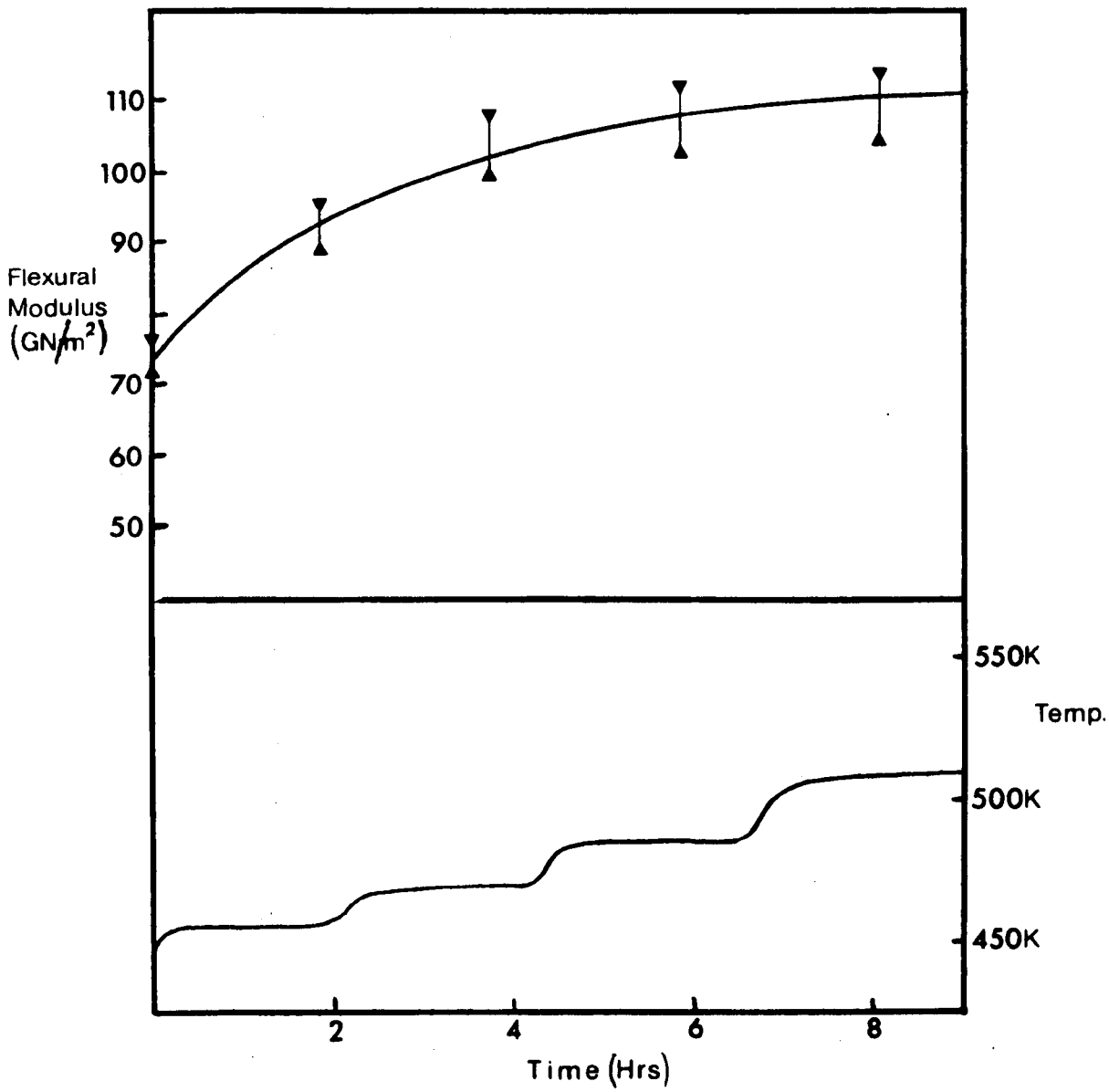

TABLE 14.

Changes in Weight and Volume after Exposure.

RESIN TYPE: Xylok

FIBRE TYPE: I

REAGENT	TEMP.	% INCREASE IN WEIGHT	% INCREASE IN VOLUME
NaOCl	296K	-10%	- 6%
HNO_3 (S.G. 1.21)	"	+ 6%	0
M.E.K.	"	+ 6%	+ 8%
10% H_2SO_4	"	0	0
CH_3COOH (Glacial)	"	0	0
HNO_3 (S.G. 1.21)	320K	-32%	Not Measurable
5% $FeCl_3$	"	+10%	0
10% H_2SO_4	"	0	0
30% NaOH	"	+ 6%	+ 8%
CH_3COOH (Glacial)	"	0	0
5% $FeCl_3$ (20 days)	360K	0	0
30% NaOH	"	+10%	+ 8%
Air (50 days)	500K	- 3%	+ 1%
Steam (50 days)	"	- 1%	+ 1%

TABLE 15.

Changes in Weight and Volume after Exposure.

RESIN TYPE: Xylok

FIBRE TYPE: II

REAGENT	TEMP.	% INCREASE IN WEIGHT	% INCREASE IN VOLUME
NaOCl	296K	- 6%	- 4%
HNO_3 (S.G. 1.21)	"	+ 4%	0
M.E.K.	"	+ 6%	+ 8%
CH_3COOH (Glacial)	"	0	0
10% H_2SO_4		0	0
HNO_3 (S.G. 1.21)	320K	-40%	Not Measurable
5% $FeCl_3$	"	0	0
10% H_2SO_4	"	0	0
30% NaOH	"	+10%	+ 6%
CH_3COOH (Glacial)	"	+ 3%	+ 5%
5% $FeCl_3$ (20 days)	360K	0	0
30% NaOH	"	+16%	+17%
Air (50 days)	500K	- 4%	- 3%
Steam (50 days)	"	- 2%	0

TABLE 16.

Changes in Weight and Volume after Exposure.

RESIN TYPE: Xylok FIBRE TYPE: 111

REAGENT	TEMP	% INCREASE IN WEIGHT	% INCREASE IN VOLUME
Na OCl	296K	- 7%	- 2%
HNO_3 (S.G. 1.21)	"	0	0
5% $FeCl_3$	"	0	0
10% H_2SO_4	"	0	0
M.E.K.	"	+ 4%	+ 6%
CH_3COOH (Glac.)	"	0	0
HNO_3 (S.G. 1.21)	320K	- 9%	+ 4%
5% $FeCl_3$	"	+ 1%	0
10% H_2SO_3	"	0	0
30% NaOH	"	+18%	+16%
CH_3COOH (Glacial)	"	+ 9%	+16%
NH_3	"	+ 1%	0
Cl_2	"	+ 2%	0
CCl_4	"	0	0
5% $FeCl_3$	360K	0	0
30% NaOH	"	+18%	+18%
Air (50 days)	500K	- 2%	- 4%
Steam (50 days)	"	0	+ 3%

TABLE 17.

Changes in Weight and Volume after Exposure.

RESIN TYPE: V.W. Phenolic FIBRE TYPE: I

REAGENT	TEMP.	% INCREASE IN WEIGHT	% INCREASE IN VOLUME
NaOCl	296K	- 2%	- 5%
HNO_3 (S.G. 1.42)	"	-	-
10% H_2SO_4	"	0	0
IND. METHS	"	0	0
CH_3COOH (Glacial)	"	0	0
HNO_3 (S.G. 1.21)	320K	-	-
5% $FeCl_3$	"	0	0
10% H_2SO_4	"	0	0
30% NaOH	"	to +55%	+300%
CH_3COOH (Glacial)	"	0	0

TABLE 18.

RESIN TYPE: V.W. Phenolic FIBRE TYPE: II

REAGENT	TEMP.	% INCREASE IN WEIGHT	% INCREASE IN VOLUME
NaOCl	296K	0	0
HNO_3(S.G. 1.42)	"	-	-
10% H_2SO_4	"	0	0
IND. METHS	"	0	0
CH_3COOH (Glacial)	"	0	0
HNO_3 (S.G. 1.21)	320K	-	-
5% FeCl	"	0	0
10% H_2SO_4	"	0	0
30% NaOH	"	+60%	+300%
CH_3COOH (Glacial)	"	0	0

TABLE 19.

Changes in Weight and Volume after Exposure.

RESIN TYPE: V.W. Phenolic

FIBRE TYPE: III

REAGENT	TEMP.	% INCREASE IN WEIGHT	% INCREASE IN VOLUME
NaOCl	296K	- 9%	approx. - 10%
HNO_3 (S.G. 1.42)	"	-	-
5% $FeCl_3$	"	- 2%	0
IND. METHS	"	0	0
CH_3COOH (Glacial)	"	0	0
10% H_2SO_4	"	0	0
HNO_3 (S.G. 1.21)	320K	-	-
5% $FeCl_3$	"	0	0
10% H_2SO_4	"	0	0
30% NaOH	"	to +60%	+300%
CH_3COOH (Glacial)	"	0	0
5% $FeCl_3$	360K	- 2%	- 1%

TABLE 20.

Percentage Retention of Inter-Laminar Shear Strength.

RESIN TYPE: Xylok.

		Fibre Type	III	II	I	HT-S	HM-S
		Control ILSS (MN/m^2)	45-50	35-40	25-30	60-65	45-50
REAGENT	Temp(K)		% retention of I.L.S.S.				
NaOCl	296		100	96	80	-	-
HNO_3(1.21)	"		98	84	70	96	90
5% $FeCl_3$	"		100	-	-	-	-
10% H_2SO_4	"		100	100	100	-	-
M.E.K.	"		75	88	92	-	-
CH_3COOH(Glac.)	"		100	100	100	100	100
HNO_3 (1.21)	320		68	4	7	60	42
5% $FeCl_3$	"		85	100	80	-	-
10% H_2SO_4	"		100	100	100	-	-
30% NaOH			71	77	82	57	69
CH_3COOH(Glac.)	"		53	60	64	-	-
NH_3	"		96	-	-	-	-
Cl_2	"		83	-	-	-	-
5% $FeCl_3$	360		80	100	100	-	-
30% NaOH	"		67	69	72	54	60
Air (50 days)	500		100	64	62	96	91
Steam (50 days)	"		90	84	82	-	-

TABLE 21.

Percentage Retention of Inter-Laminar Shear Strength.

RESIN TYPE: V.W. Phenolic.

		Fibre Type	III	II	I
		Control ILSS (MN/m)	45-50	40-45	30-35
Reagent	Temp(K)		% Retention of ILSS		
NaOCl	296		95	94	89
HNO_3 (1.42)	"		X	X	X
5% $FeCl_3$	"		100	-	-
IND. METHS	"		95	100	100
CH_3COOH (Glac.)	"		95	100	100
10% H_2SO_4	"		100	100	100
HNO_3 (1.21)	320		X	X	X
5% $FeCl_3$	"		85	100	92
10% H_2SO_4	"		100	100	100
30% NaOH	"		X	X	X
CH_3COOH (Glac.)	"		88	97	100
5% $FeCl_3$	360		86	-	-

X = Measurement impossible

TABLE 22

Modes of Failure in I.L.S.S. Test

DISCREET SHEAR	TENSILE	HOMOGENEOUS SHEAR	COMPRESSIVE
NaOCl (296K)			
HNO_3 (1.21) "	Air (500K)	30% NaOH (320K)	M.E.K. (296K)
5% $FeCl_3$		CH_3COOH (320K)	
10% H_2SO_4 "		30% NaOH (360K)	IND. METHS (290K)
CH_3COOH "			Steam (500K)
5% $FeCl_3$ (320K)			
10% H_2SO_4 "			
NH_3 "			
Cl_3 "			
5% $FeCl_3$ (360K)			

TABLE 23.

Percentage Retention of Flexural Strength.

RESIN TYPE: Xylok.

Reagent	Temp(K)	Fibre Type	III	II	I	HT-S	HM-S
		Control Flex. Str. (MN/m^2)	$0.6x10^3$	$0.6x10^3$	$0.5x10^3$	$1.0x10^3$	$0.8x10^3$
			% Retention of Flex. Str.				
NaOCl	296		94	92	85	-	-
HNO_3 (1.21	"		94	80	82	96	90
5% $FeCl_3$	"		96	-	-	-	-
10% H_2SO_4			100	100	100	-	-
M.E.K.	"		81	89	88	-	-
CH_3COOH(Glac.)	"		100	100	100	100	100
HNO_3 (1.21)	320		55	X	X	63	28
5% $FeCl_3$	"		84	85	82	-	-
10% H_2SO_4	"		100	100	100	-	-
30% NaOH			48	55	59	40	45
CH_3COOH(Glac.)	"		36	46	50	-	-
-	-	-	-	-	-	-	-
-	-	-	-	-	-	-	-
Air	500		68	40	37	70	62
Steam	"		64	44	41	-	-

X = Measurement Impossible.

TABLE 24

Progressive Changes in I.L.S.S. and Flexural Modulus

RESIN TYPE: Xylok.

TYPE I	AIR (498K)		STEAM (498K)	
TIME (days)	I.L.S.S. (MN/m^2)	FLEX.MOD (GN/m^2)	I.L.S.S. (MN/m^2)	FLEX.MOD (GN/m^2)
0	28.2	132	29.1	128
4	25.4	131	27.9	NO SIGNIFICANT CHANGES
7	23.2	129	27.2	
10	21.8	129	26.5	
25	13.7	126	24.2	
35	8.7	123	21.9	
50	4.2	119	19.6	
TYPE II				
TIME (days)				
0	36.7	112	36.4	104
4	34.0	110	36.1	NO SIGNIFICANT CHANGES
7	32.4	110	35.9	
10	31.1	109	35.8	
25	27.0	104	34.0	
35	24.3	98	32.8	
50	20.7	92	31.6	
TYPE III				
TIME (days)				
0	46.2	98	48.5	100
4	45.8	96	48.2	NO SIGNIFICANT CHANGES
7	45.6	97	48.1	
10	45.9	95	47.9	
25	45.7	92	46.1	
35	46.0	89	44.9	
50	46.0	86	43.7	

TABLE 25

Retention of I.L.S.S. at 323K.

RESIN TYPE: Xylok.

Reagent	HNO_3	NaOH	CH_3COOH
TYPE I			
TIME (days)			
0	100%	100%	100%
10	76%	92%	96%
26	48%	87%	90%
56	14%	84%	80%
100	7%	82%	64%
TYPE II			
TIME (days)			
0	100%	100%	100%
10	77%	90%	96%
26	44%	86%	87%
56	8%	82%	74%
100	4%	77%	60%
TYPE III			
TIME (days)			
0	100%	100%	100%
10	97%	87%	91%
26	92%	82%	80%
56	84%	79%	67%
100	68%	71%	53%

TABLE 26.

Changes in Torsional Storage Modulus with Temperature.

RESIN TYPE: Xylok. FIBRE TYPE: 111.

TEMP.	SHEAR MODULUS
290K	3.20 GN/m^2
326K	3.10 "
345K	3.03 "
358K	2.94 "
383K	2.84 "
403K	2.70 "
431K	2.35 "
465K	1.60 "
483K	0.72 "

TABLE 27.

Torsional Results.

RESIN TYPE: Xylok.

		TYPE III			TYPE II			TYPE I		
		G' (GN/m^2)	Δ	G^* (MN/m^2)	G' (GN/m^2)	Δ	G^* (MN/m^2)	G' (GN/m^2)	Δ	G'' (MN/m^2)
296K	CONTROL	3.20	0.04	40.74	2.40	0.09	68.75	1.95	0.14	86.89
	NaOCl	-	-	-	2.35	0.09	68.1	1.50	0.168	80.2
	HNO_3(S.G.1.21)	3.20	0.045	45.8	2.02	0.098	63.0	0.94	0.276	82.6
	5% $FeCl_3$	-	-	-	-	-	-	1.79	0.162	93.9
	Butanone	1.47	0.183	85.6	1.07	0.212	72.2	0.97	0.231	71.3
	CH_3COOH(Glac.)	2.8	0.084	74.9	2.25	0.117	83.8	1.90	0.195	117.9
323K	HNO_3(S.G.1.21)	0.85	0.202	54.6	-	-	-	-	-	-
	5% $FeCl_3$	3.15	0.014	41.1	2.25	0.103	73.7	1.42	0.162	73.2
	10% H_2SO_4	3.20	0.045	45.8	-	-	-	-	-	-
	30% NaOH	1.20	0.160	61.1	0.86	0.271	74.2	0.82	0.294	76.7
	CH_3COOH(Glac.)	0.60	0.221	59.8	0.60	0.223	61.7	0.5	0.356	56.7
	NH_3	3.20	0.047	47.8	-	-	-	-	-	-
	Cl_2	3.20	0.045	45.8	-	-	-	-	-	-
	CCl_4	3.10	0.047	46.4	-	-	-	-	-	-
363K	5% $FeCl_3$	3.10	0.035	34.5	2.05	0.095	62.0	1.85	0.167	77.1
	30% NaOH	1.02	0.141	45.8	0.74	0.156	36.7	0.75	0.183	43.7
500K	Air	-	-	-	1.73	0.128	70.3	1.24	0.164	64.7
	Steam	2.85	0.062	56.2	2.02	0.140	90.0	1.65	0.172	88.1

Fig. 45

V.W. Phenolic/Type II Composite after 30% NaOH at 323K for 100 days

x 15

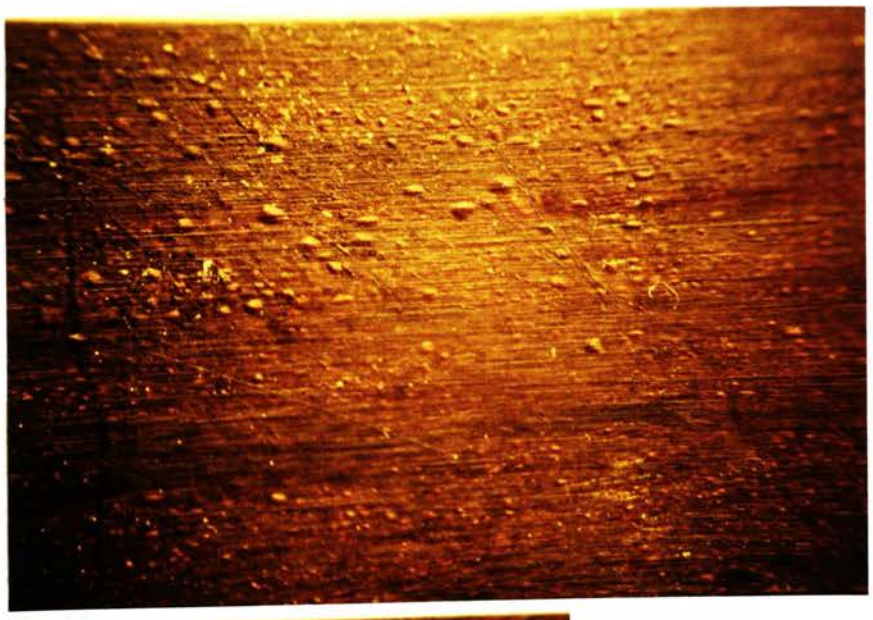

Fig. 46

V.W. Phenolic/Type I Composite after Glacial CH_3COOH at 323K for 100 days

x 8

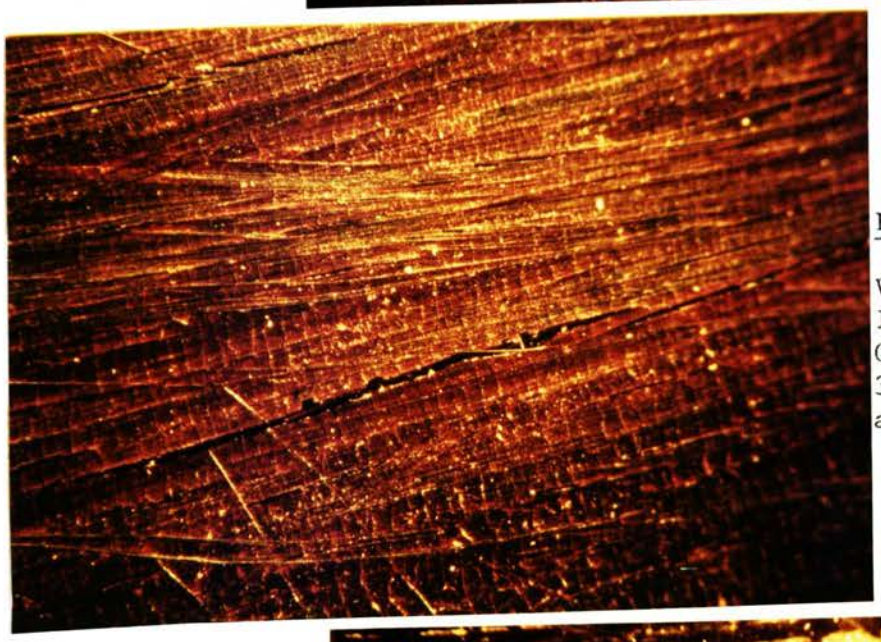

Fig. 47

V.W. Phenolic/Type III Composite after Glacial CH_3COOH at 323K for 100 days and drying

x8

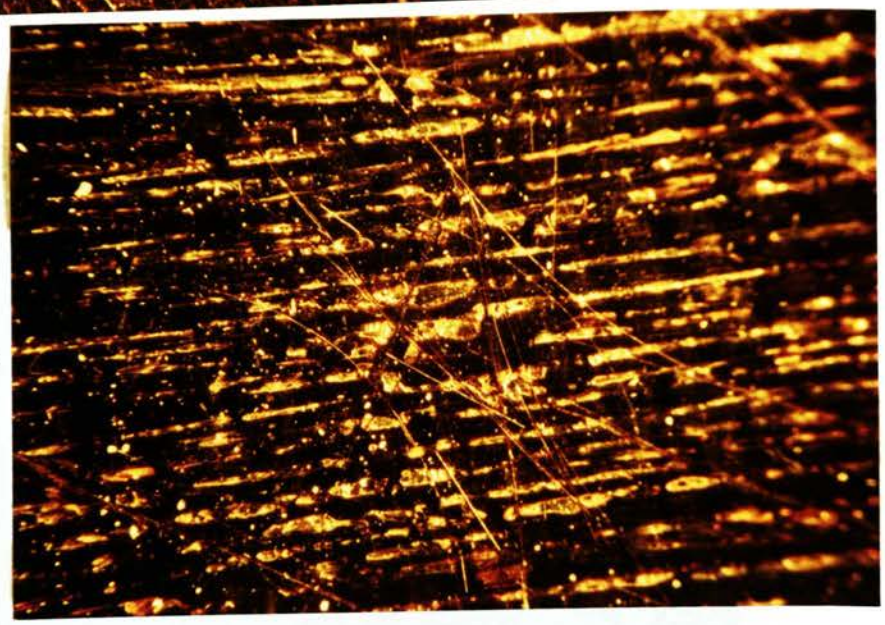

Fig. 48

Xylok Phenolic/ Type III Composite after Glacial CH_3COOH at 323K for 100 days

x 20

Fig. 49

Xylok Phenolic/
Type III Composite
after Butanone at
296K for 100 days
x 8

Fig. 50

V.W. Phenolic/Type
III Composite
after Ind. Meths.
at 296K for 100
days.
x8

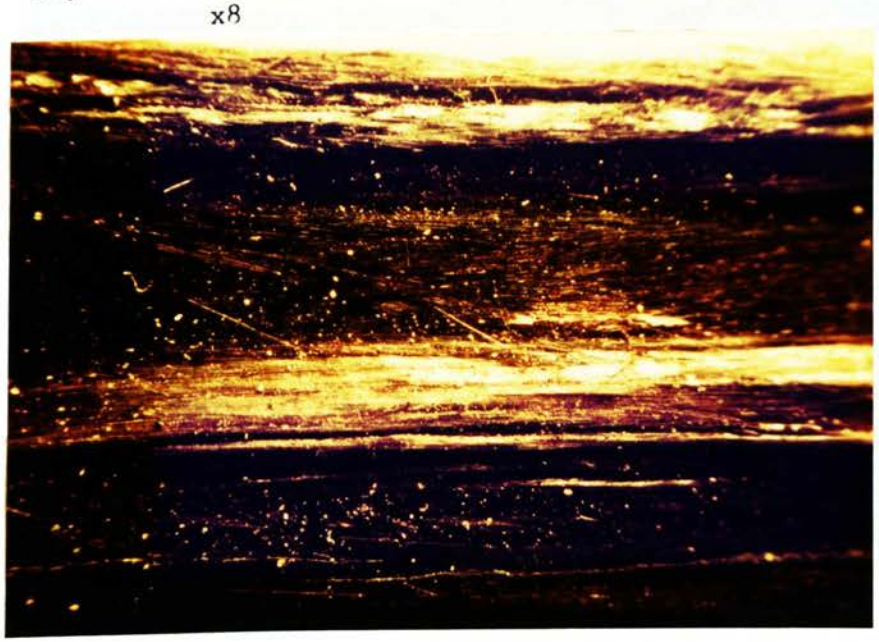

Fig. 51

Xylok Phenolic/
Type II Composite
after HNO_3 (S.G.
1.21) at 296K for
100 days.
x 10

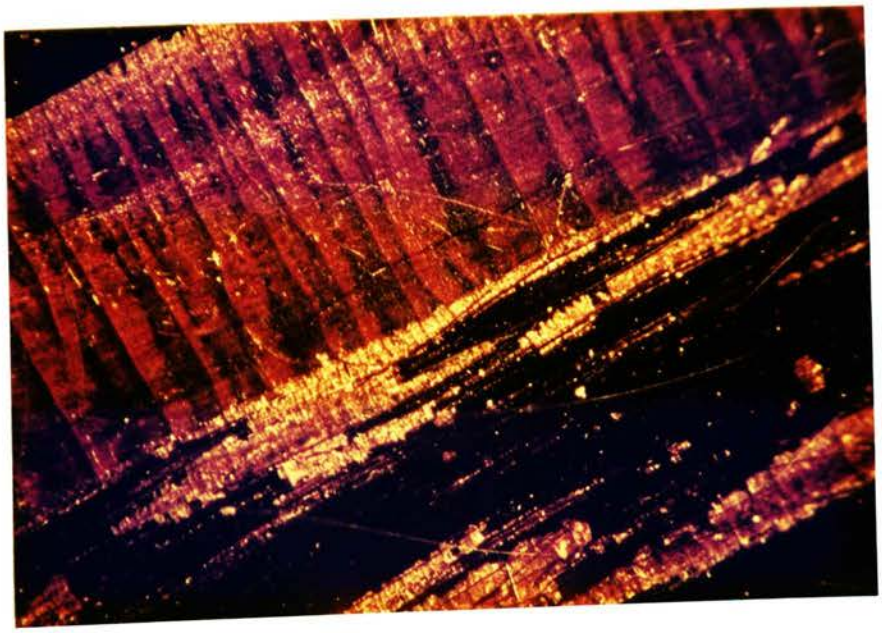

Fig. 52

Xylok Phenolic/
Type I Composite
after 5% $FeCl_3$ at
320K for 100 days.
x 10

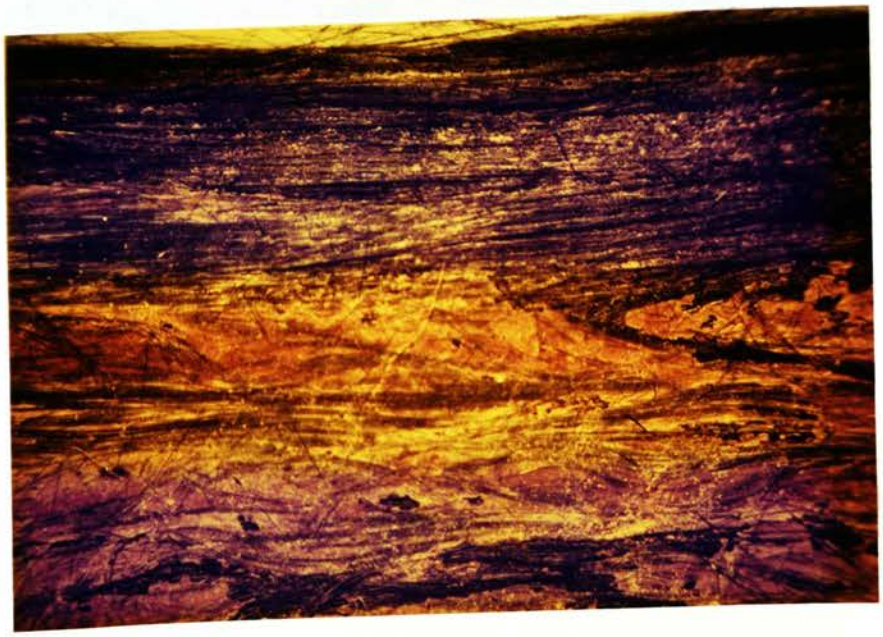

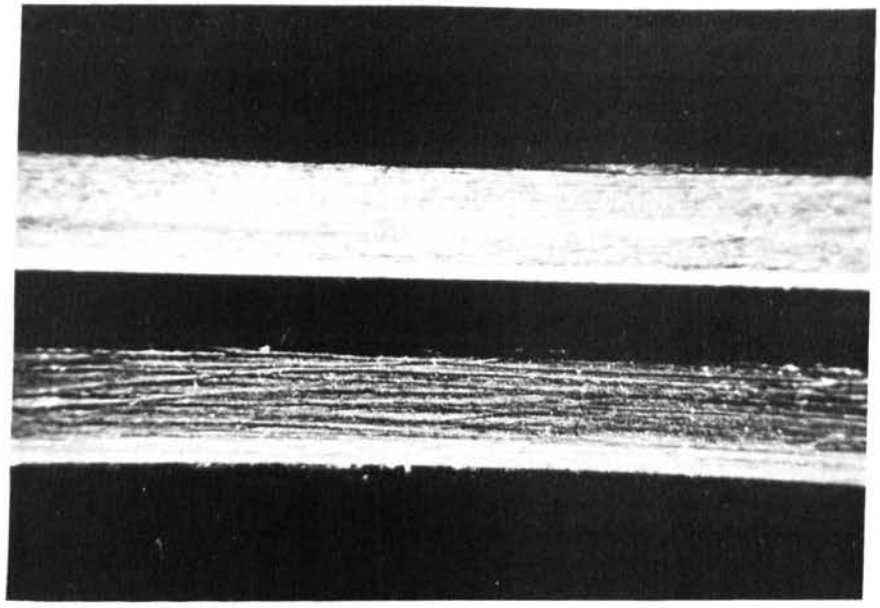

(a) Phenolic/Type III (A) Composites. Control above and Air at 498K for 50 days below. x6

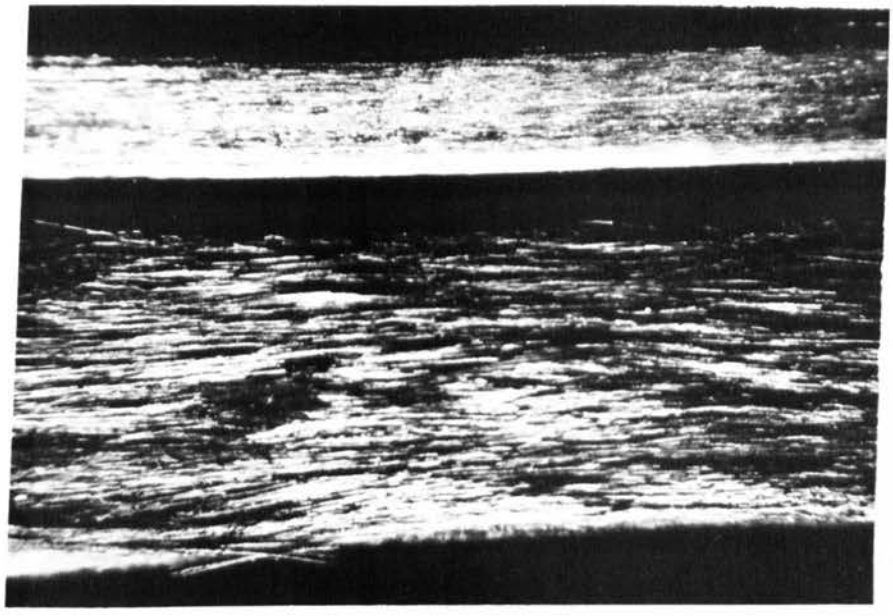

(b) Phenolic/Type III (A) Composites. Control above and 30% sodium hydroxide solution at 323K for 100 days. x6

(a) Micro-cracking of a phenolic/type III (A) Composite. Sodium hypochlorite solution (14% w/v available chlorine) at 298K for 30 days.
x 500

(b) Micrograph of moderately oxidised composite.
x 8

(c) Micrograph of composite extensively surface oxidised. Type III (A)
x 8

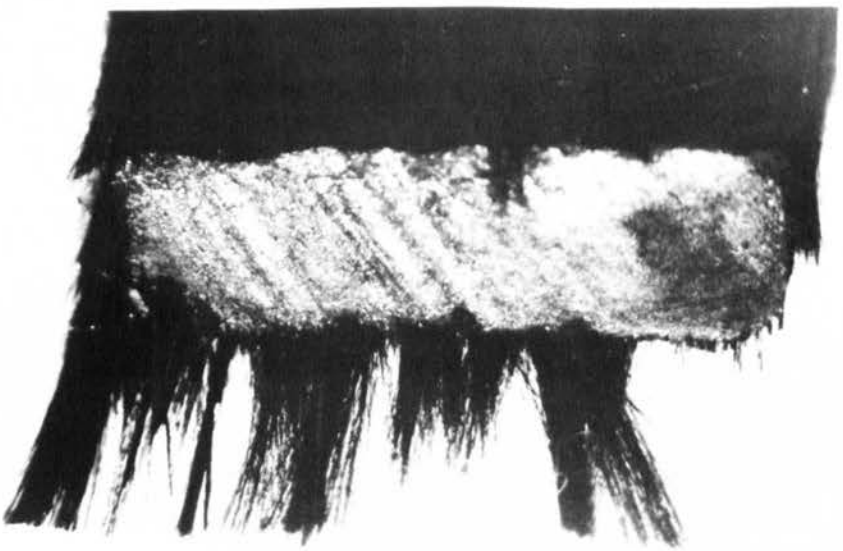

PLATE VI

Machine cut cross-sections of:-

(a) Control phenolic/Type II composite.

(b) Phenolic/Type II composite after 30% sodium hydroxide at 323K for 100 days.

Both x 300

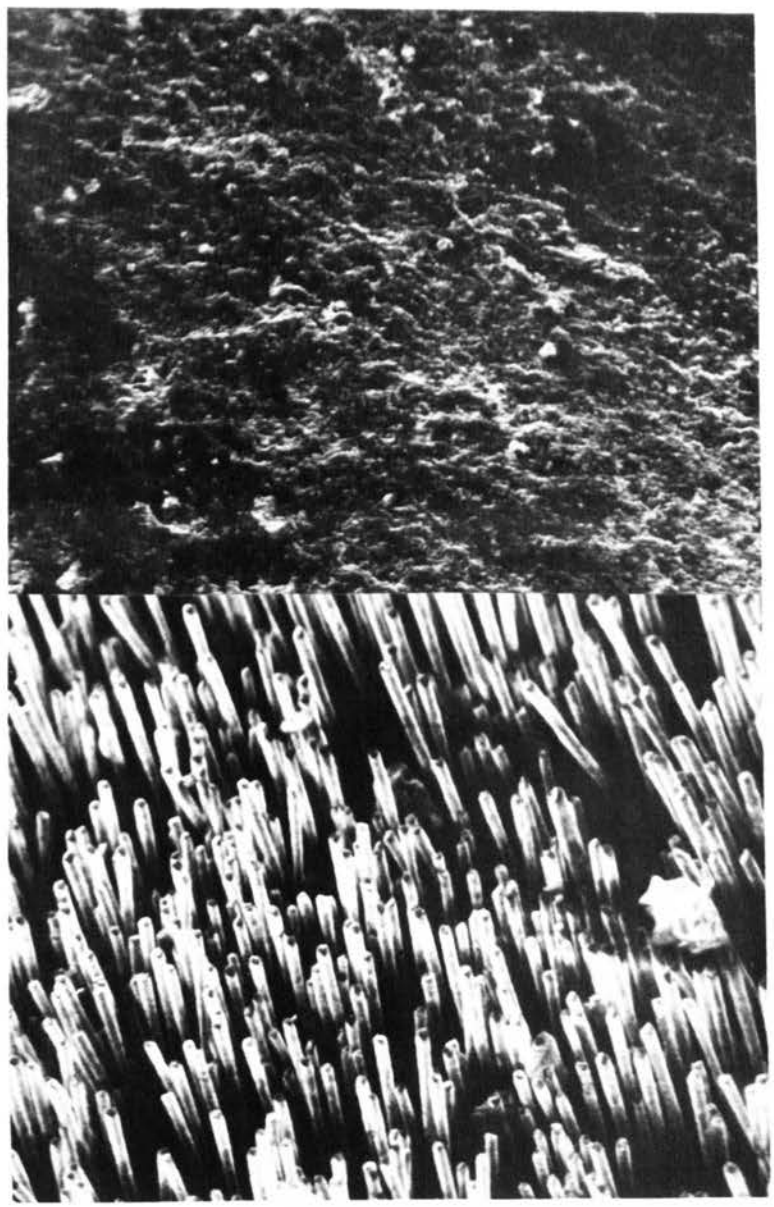

PLATE VII

TABLE 28.

Axial Loads Causing Fibre-Resin Debonding.

	Axial Load (MN/m^2)			
Fibre Type	III	II	HT-S	I
Control	*	135	*	95
Water Boil	-	-	-	-

* = Matrix Failure.

Fig. 53

Stress pattern of
Single Filament
Specimen Under
Axial Loading

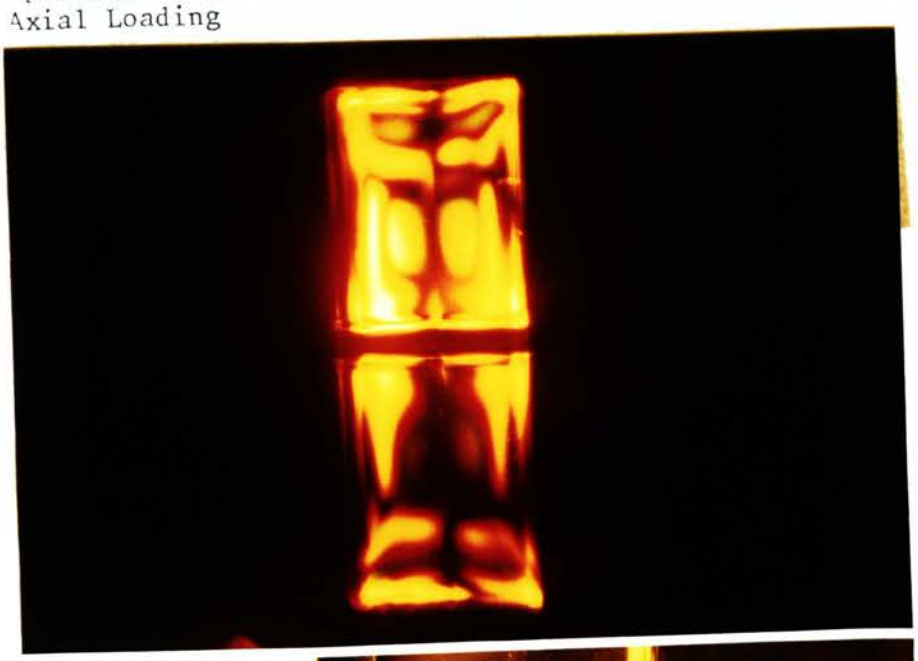

Fig. 54

The Region Around
the Artificial Crack
After Failure
x5

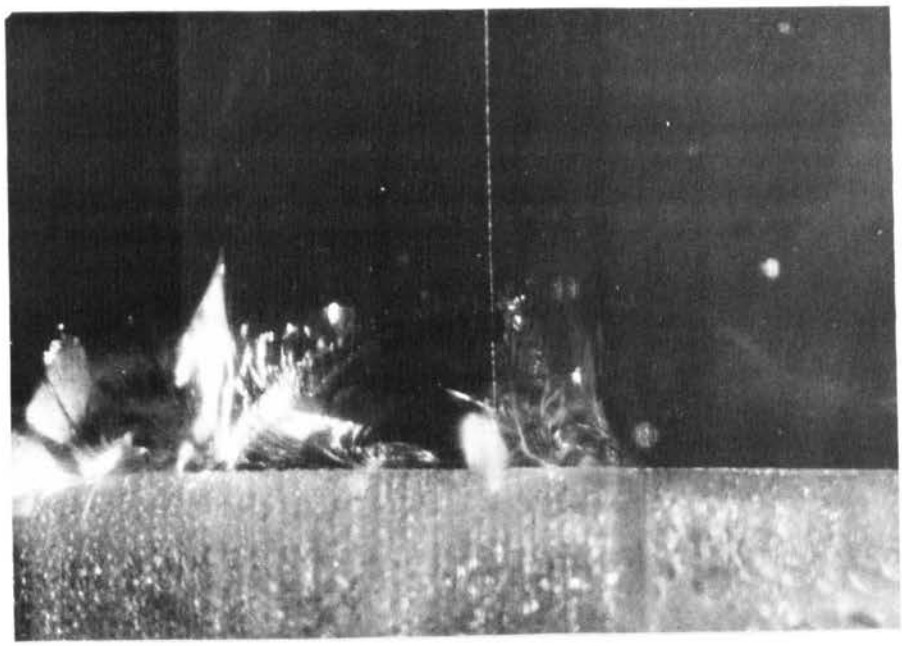

(a) Crack propagating vertically from horizontal drill-hole immediately before total failure. Note: vertical totally debonded carbon fibre.

(b) Totally failed single-fibre/resin block specimen

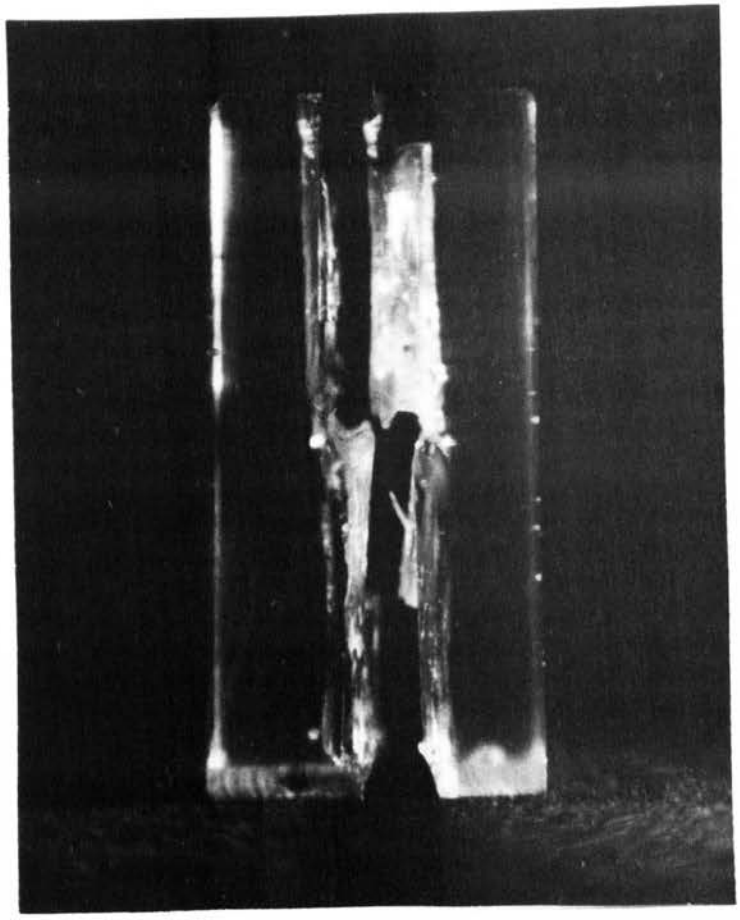

PLATE VIII

TABLE 29.

Diameter/Modulus Values for Type 11 Fibres (as received).

DIAMETER (Micrometres)	YOUNG'S MODULUS (GN/m^2)	DIAMETER (Micrometres)	YOUNG'S MODULUS (GN/m^2)
6.54	317	8.27	2.70
6.65	311	8.32	263
6.73	312	8.33	270
6.90	302	8.39	268
7.00	300	8.45	260
7.03	298	8.47	266
7.10	298	8.54	264
7.17	294	8.61	268
7.25	292	8.63	262
7.38	288	8.70	263
7.45	288	8.71	258
7.51	284	8.75	267
7.62	284	8.78	264
7.77	279	8.82	266
7.85	278	8.89	259
7.90	275	8.91	265
7.90	282	8.97	254
8.01	274	8.99	260
8.04	273	9.10	258
8.10	272	9.13	252
8.14	271	9.30	257
8.18	279	9.43	256
8.20	268		

TABLE 30. Diameter/Modulus Values along Filaments with NO_2 (423K., 90mins.) Treated Centre Portions.

FIBRE TYPE: 11.

	Diam (μm) Mod (GN/m^2)	Control Left	Treated Left-Centre	Treated Centre	Treated Right-Centre	Control Right
1	Diam	8.56	8.00	8.15	8.15	8.35
	Mod	254	292	277	286	260
2	Diam	8.70	8.37	8.40	8.55	8.65
	Mod	268	295	290	277	270
3	Diam	7.93	7.57	7.59	7.57	7.87
	Mod	277	290	288	290	252
4	Diam	5.93	5.90	5.85	5.80	5.94
	Mod	327	327	3.46	3.49	3.42
5	Diam	7.45	7.14	7.14	7.10	7.37
	Mod	285	312	300	302	277

TABLE 30. (Continued)

	Diam. (μm) M d. (GN/m^2)	Control Left	Treated Left-Centre	Treated Centre	Treated Right-Centre	Control Right
6	Diam.	8.68	8.22	8.20	8.30	8.58
	M d.	258	295	290	286	264
7	Diam.	8.55	8.20	8.13	8.20	8.35
	M d.	258	281	284	281	270
8	Diam.	7.13	7.02	7.00	7.01	7.12
	M d.	312	323	312	316	308
9	Diam.	7.65	7.5	7.45	7.40	7.60
	M d.	286	297	297	295	292
10	Diam.	7.30	7.04	7.00	7.01	7.22
	M d.	297	324	320	328	310

TABLE 31.

Diameter/Modulus Values for Various NO_2 Treatments on Type 11 Fibres.

Temperature (K)	523		523		523	
Time (mins)	90		120		150	
	Diam (μm)	Modulus (GN/m^2)	Diam (μm)	Modulus (GN/m^2)	Diam (μm)	Modulus (GN/m^2)
	7.70	304	6.22	282	5.80	318
	7.50	297	6.22	294	5.38	297
	7.40	291	5.96	286	3.22	348
	7.34	299	5.72	290	3.07	352
	7.33	282	4.96	290	3.02	440
	7.17	298	4.10	292	2.84	398
	7.08	332	4.50	300	2.40	525
	7.05	291	4.05	294	2.32	480
	7.01	292	3.95	320	2.30	420
	6.92	277	3.80	324	2.20	430
	6.85	294	2.32	358	2.18	450
	6.75	302			2.02	427
	6.62	297			1.98	463
	6.60	290			1.95	485
	6.57	280			1.95	518
	6.50	294			1.80	562
	6.48	291			1.45	552
	6.37	291				
	6.20	275				
	6.16	288				
	6.12	260				
	5.30	272				
	5.08	280				

FIG. 55. Typical TGA Trace for a Tow of Type 11 Fibres at 813K.

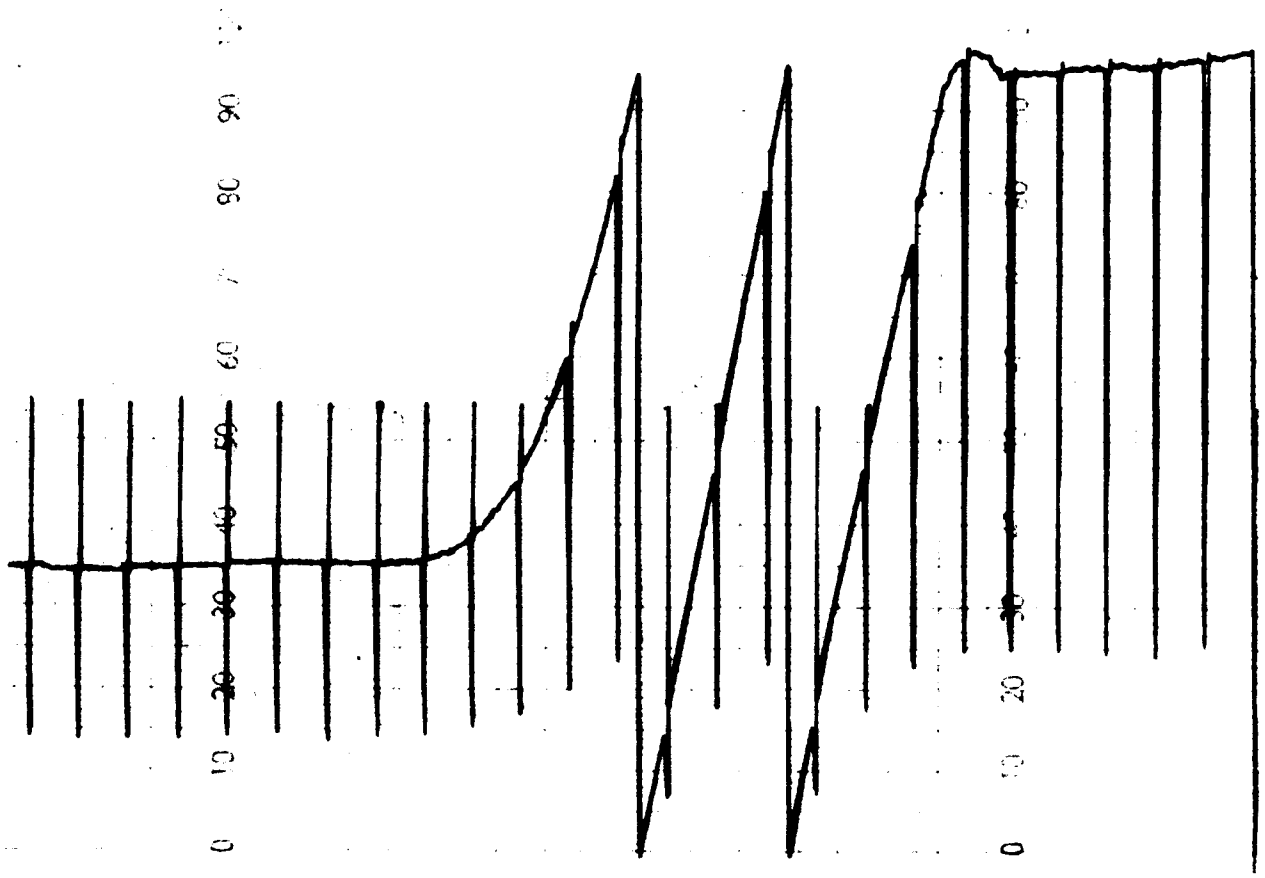

TABLE 32.

Percentage Retention of Diameter During Air Oxidation.

Fibre Type I					
Time (mins) \ Temp. (K)	793	813	833	853	873
10	99%	99%	98%	97%	80%
20	99%	98%	95%	86%	55%
40	98%	94%	75%	58%	31%
60	98%	88%	60%	36%	-
80	97%	81%	48%	27%	-
100	96%	74%	38%	-	-
140	94%	61%	-	-	-

TABLE 33.

Fibre Type II					
Time (mins) \ Temp. (K)	793	813	833	853	873
10	99%	99%	96%	78%	20%
20	98%	96%	80%	25%	-
40	96%	84%	56%	-	-
60	94%	73%	45%	-	-
80	92%	67%	36%	-	-
100	89%	61%	28%	-	-
140	85%	50%	-	-	-

TABLE 34.

Percentage Retention of Diameter During Air Oxidation.

Fibre Type III				
Time (mins) \ Temp (K)	703	783	763	793
10	97%	95%	92%	57%
20	95%	90%	83%	32%
40	90%	82%	67%	-
60	85%	73%	56%	-
80	81%	67%	48%	-
100	78%	62%	42%	-
140	71%	53%	33%	-

Tables 32-4 are the average values for three determinations.

TABLE 35.

Electrical Resistivity Measurements on NO_2 Treated Type 11 Fibres.

Type 11 Fibres	R (Ω)	L (cms)	d(μm)	(10^{-3} Ωcm)
Untreated	26,630	10.8	8.12	1.27
	25,240	10.5	8.36	1.32
	23,880	10.5	8.60	1.32
	25,420	10.1	8.45	1.31
	26,210	10.5	8.02	1.26
Treated NO_2 423K. 12 atmos. 120 mins.	28,310	10.4	7.80	1.29
	28,620	10.7	7.32	1.12
	28,510	10.6	7.95	1.31
	30,220	10.4	6.84	1.06
	29,770	10.7	7.55	1.24
	33,680	10.6	5.72	1.03
	31.100	10.5	5 90	1.04

TABLE 36.

Specific Gravity Measurements on NO_2 Treated Type 11 Fibres.

	Specific Gravity	% Change
Untreated	2.17	—
Treated	2.25	3.7

In liquids close to their densities, NO_2-treated Type II fibres consistently rose, whilst untreated Type II fibres sank.

TABLE 37.

Elemental Analysis of Carbon Fibres - NO_2 Treatment is at 523K for 120 mins.

	C%	H%	N%
Type II Control	97.93	0.15	1.57
" " "	97.87	0.17	1.42
Type II - NO_2 Treated	98.71	0.11	1.06
" " "	98.75	0.12	1.01

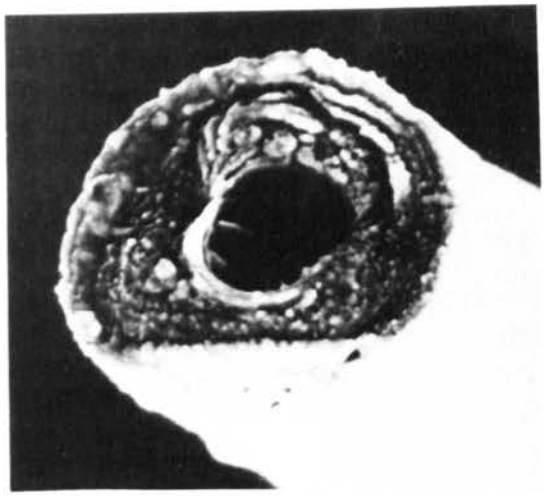

(a) Internal cavity
Type I fibre

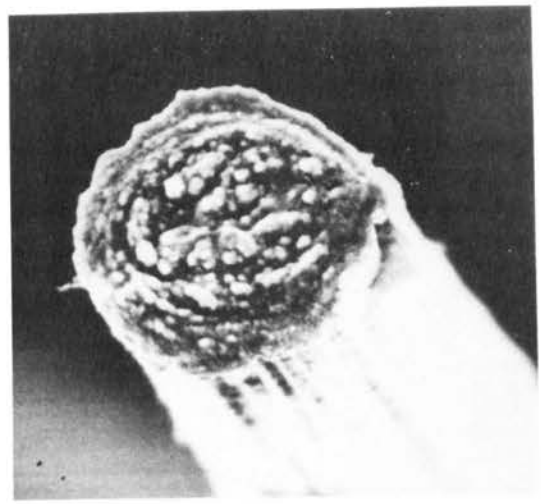

(b) Type I fibre

(c) Type II fibre

TRANSVERSE
FRACTURES
× 6,000

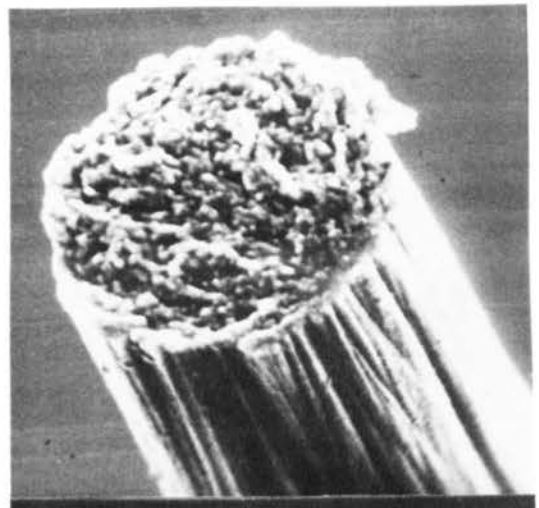

(d) Type III (A)
fibre

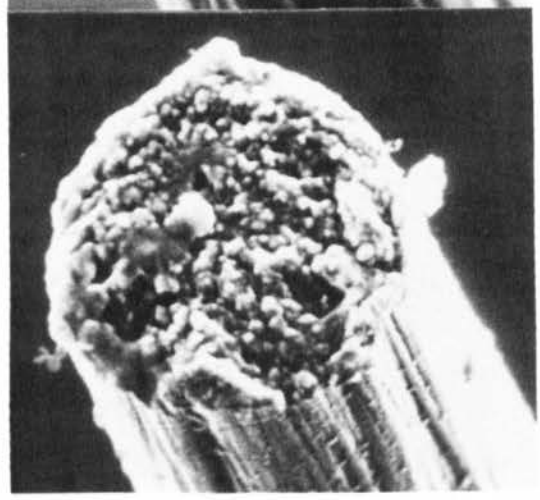

PLATE IX

(a) Rapid short-term oxidation. Air 873K 10 mins Type II fibres × 7,500

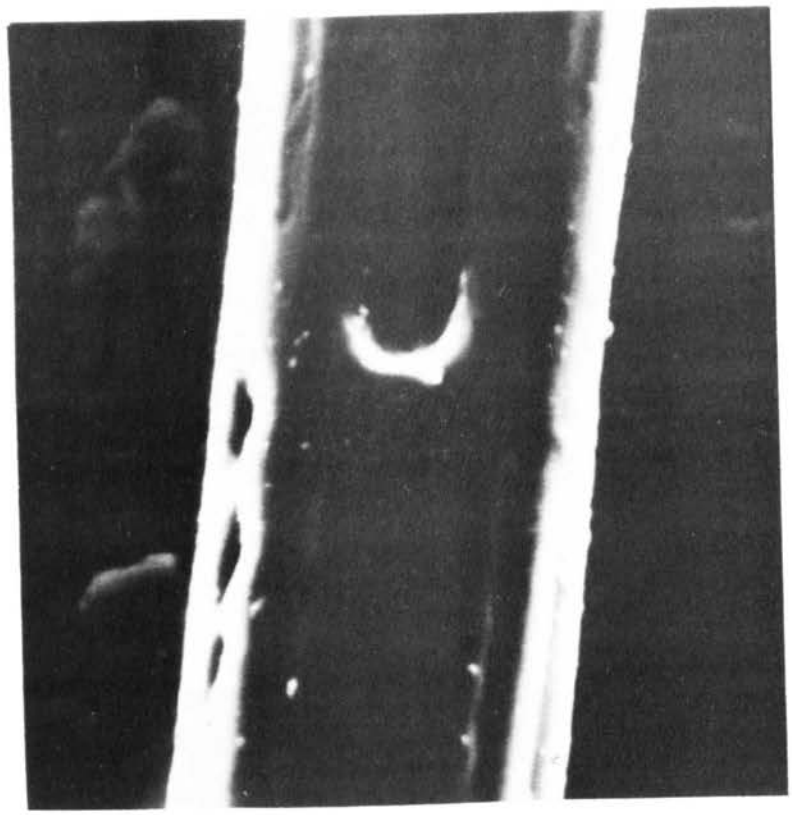

(b) As above

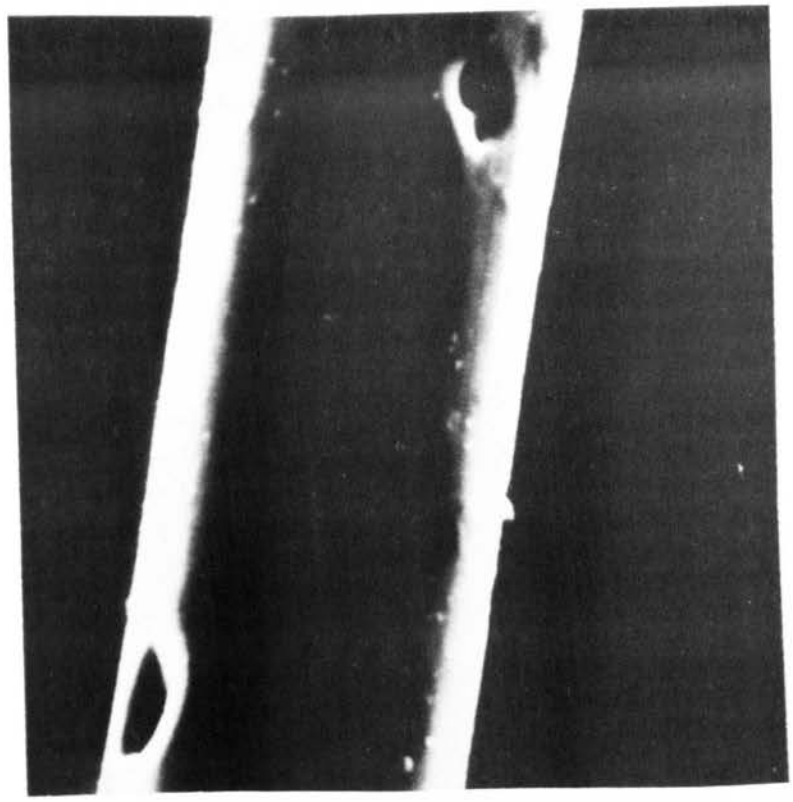

PLATE X

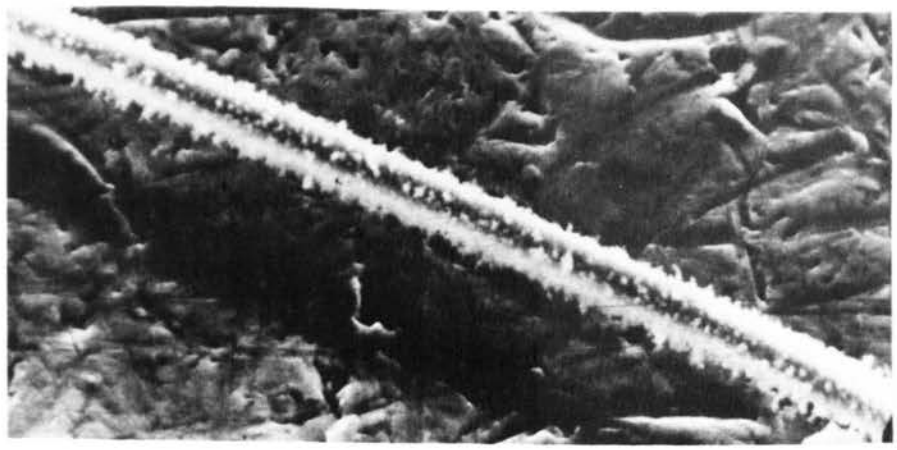

(a) Deposit during nitrogen dioxide oxidation using silicone based adhesive in aluminium.

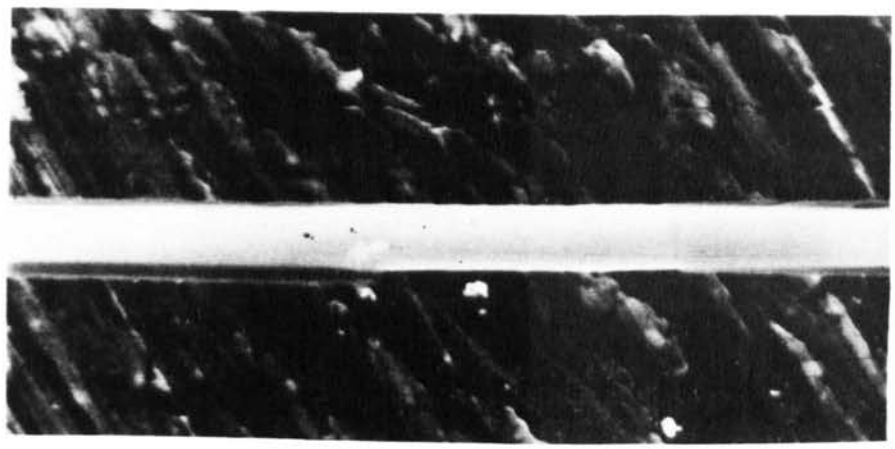

(b) Deposit giving apparent sheath during oxidation in air using silicone based adhesive.

(c) Rapid extensive oxidation of Type II fibres in air at 873K x 3,000

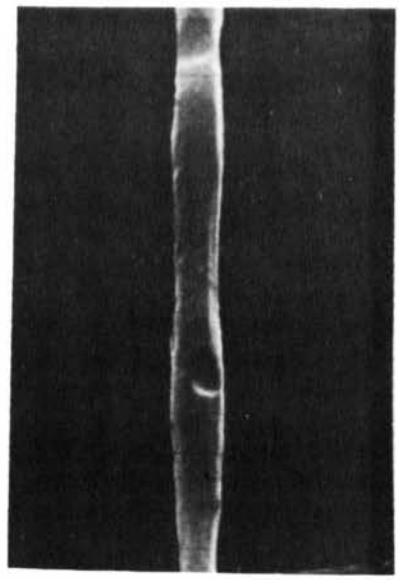

(a) Bundle of Type II fibres oxidised in nitrogen dioxide.
$2\frac{1}{2}$ hours
503K
x 3,000

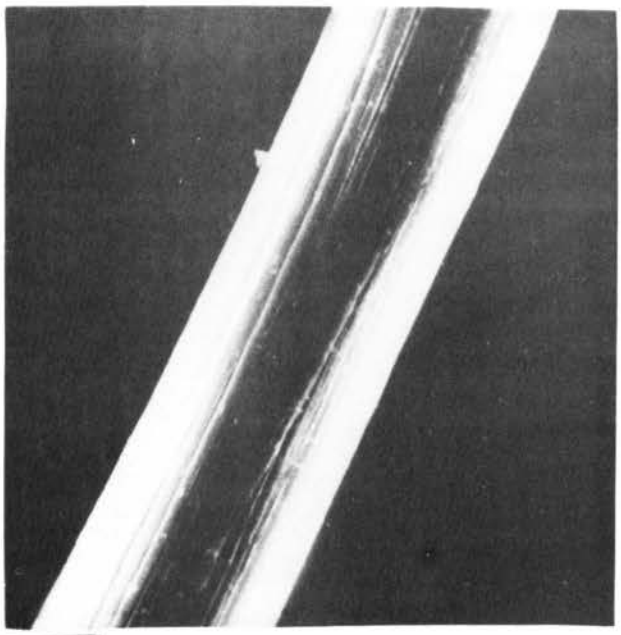

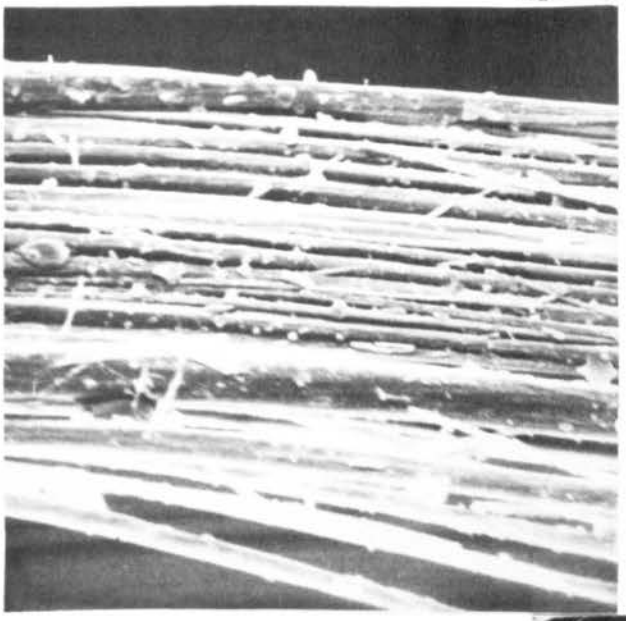

(b) Bundle splitting into individual filaments.
x 6,500

(c) As for (b)
x 9,000

PLATE XII

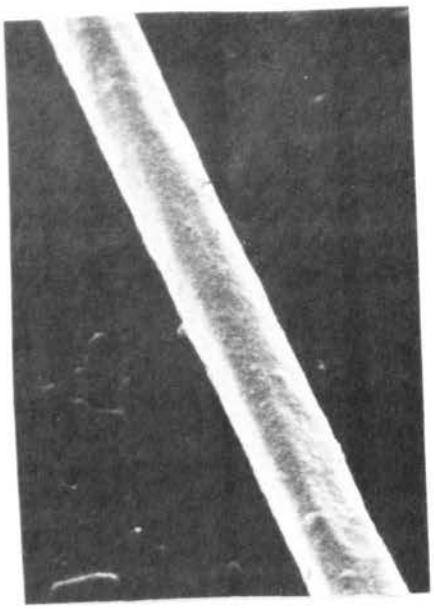

(a) Type II Nitrogen dioxide
523K 2 hours

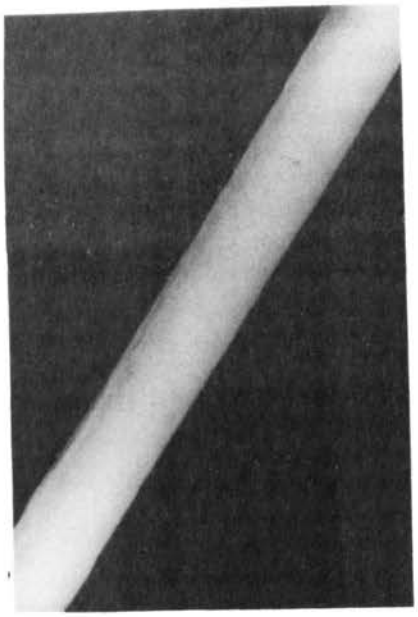

(b) Type II Nitrogen dioxide
503K $2\frac{1}{2}$ hours

(a), (b) and (c) X 6000

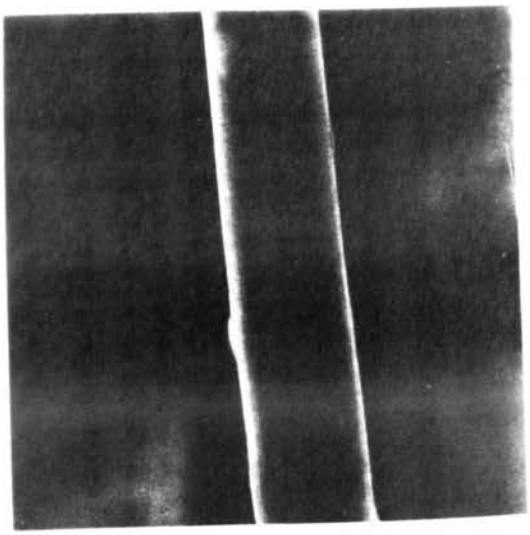

(c) Type II Nitrogen dioxide
498K $2\frac{1}{2}$ hours

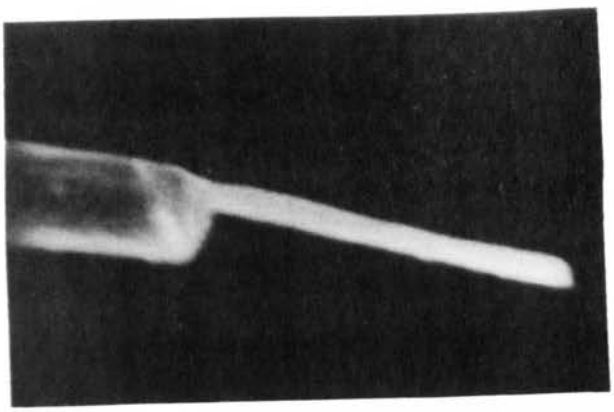

(d) As for (a) x 12,000

PLATE XIII

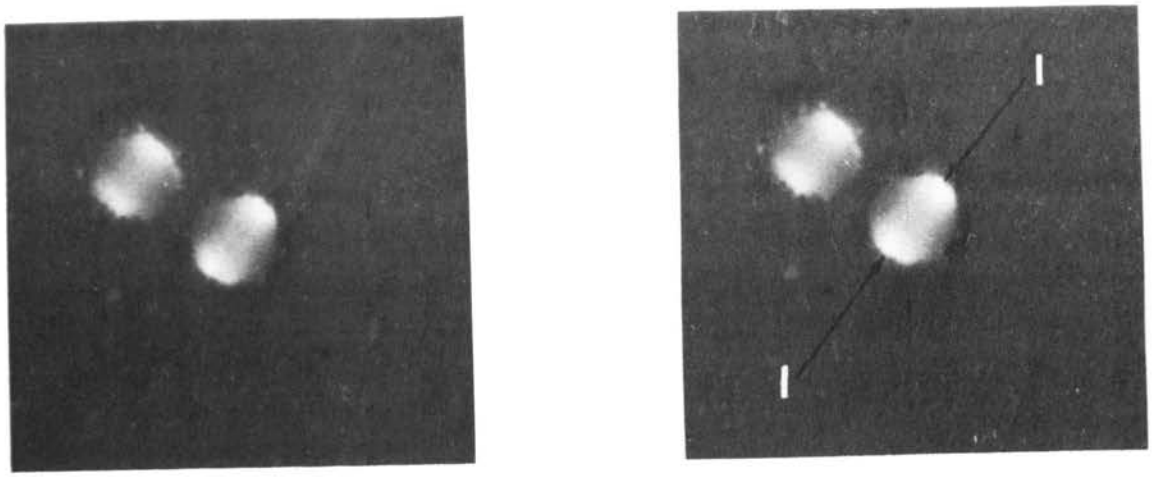

(a) Polarised light micrographs of Type I fibres.

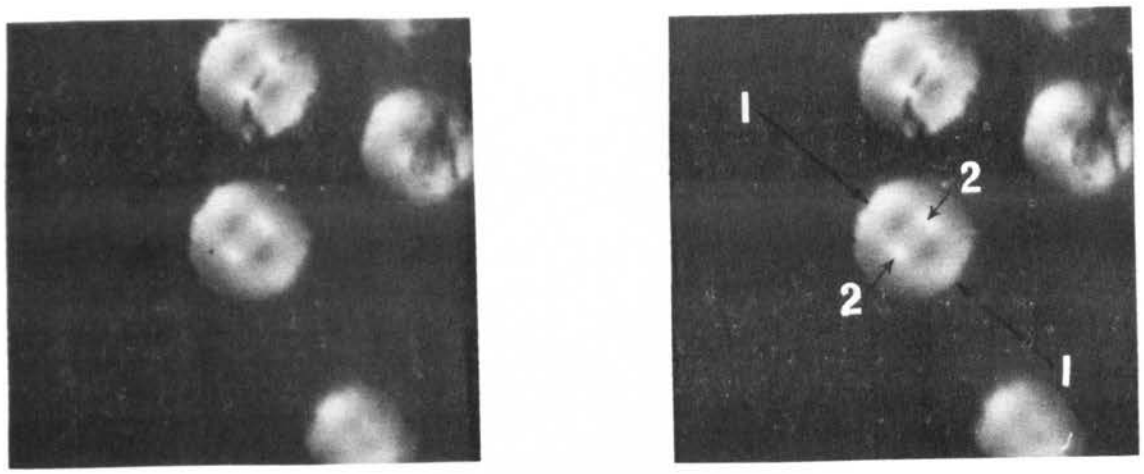

(b) Polarised light micrographs of Type II fibres.

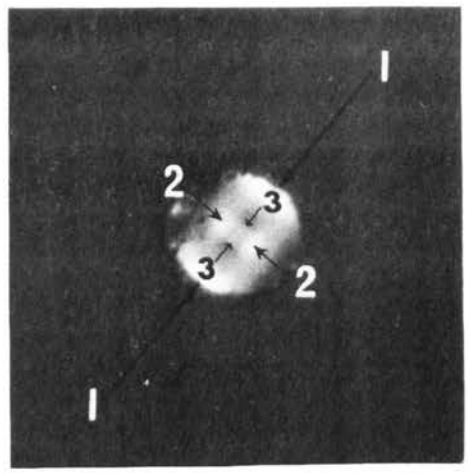

(c) Polarised light micrographs of Type III (A) fibres.

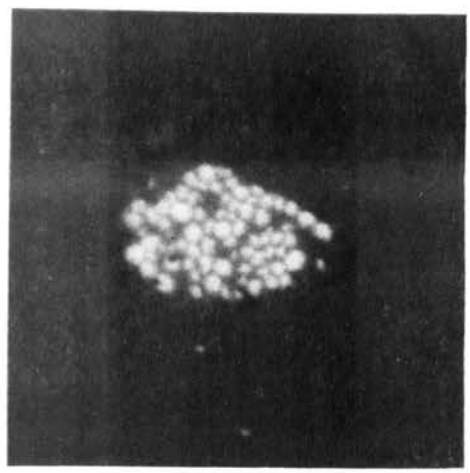

(d) Polarised light micrographs of Type II fibres treated in nitrogen dioxide at 523K for 2 hours. × 1,700

CAPTIONS FOR PLATES XVI – XIX.

PLATE XVI

Transmission micrograph showing a typical example of order in a Type II fibre.

x 2,000,000

PLATE XVII

PLATE XIX (a)

Transmission micrographs of well graphitised phases found in powdered fibres after NO_2 treatment (Single filaments exposed at 523K and 20 atmos. pressure for 150 mins.).

x 2,000,000
and x 1,500,000
respectively.

PLATE XVIII

Transmission micrograph of polygonal crystallites showing considerable interlinking. (NO_2 treated).

x 2,000,000

PLATE XIX (b)

Electron diffraction pattern for NO_2 treated Type II fibre tow.

PLATE XIX (c)

Transmission micrograph of a section of an NO_2 treated Type II fibre tow.

x 200,000

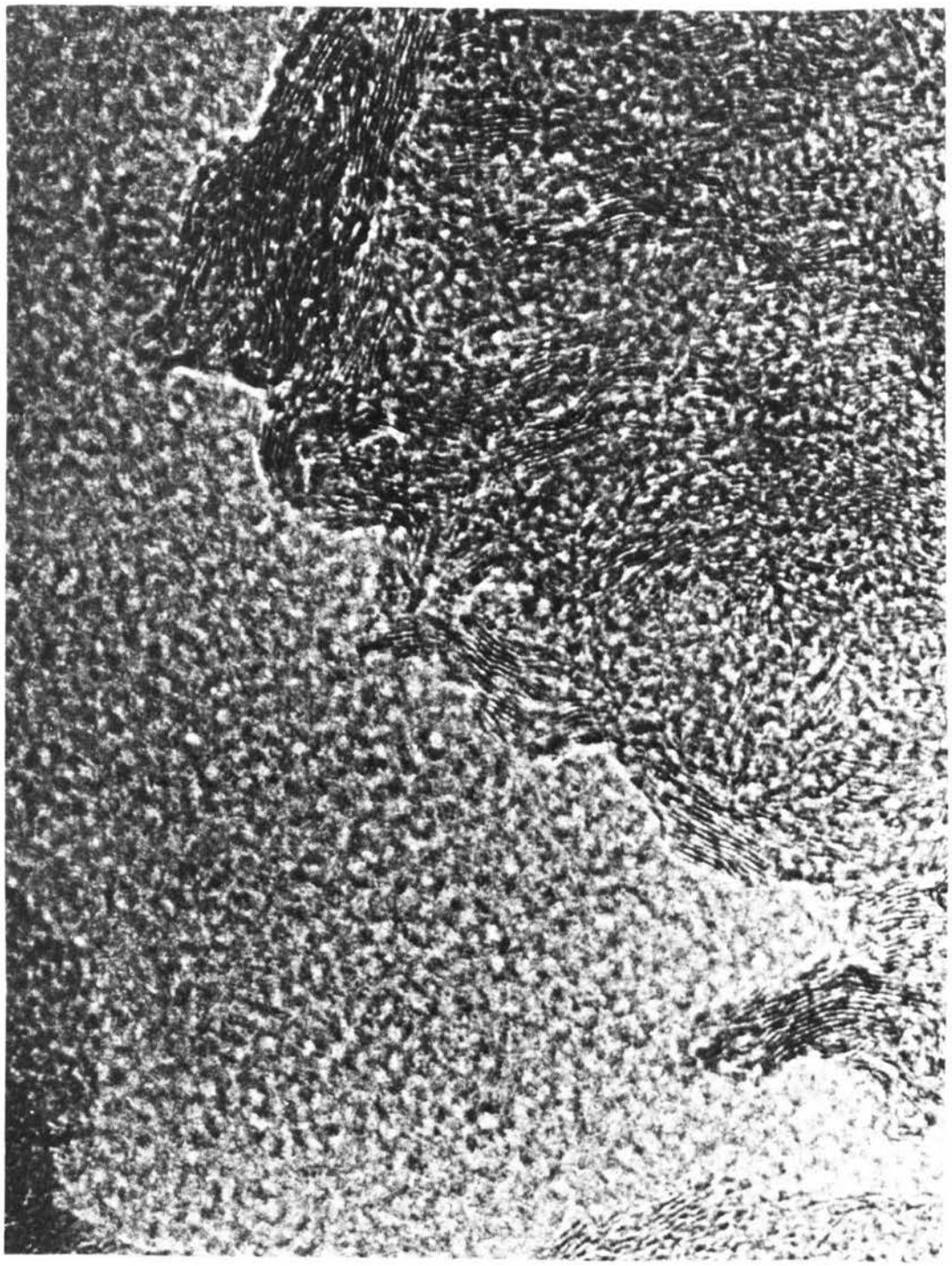

PLATE XVI

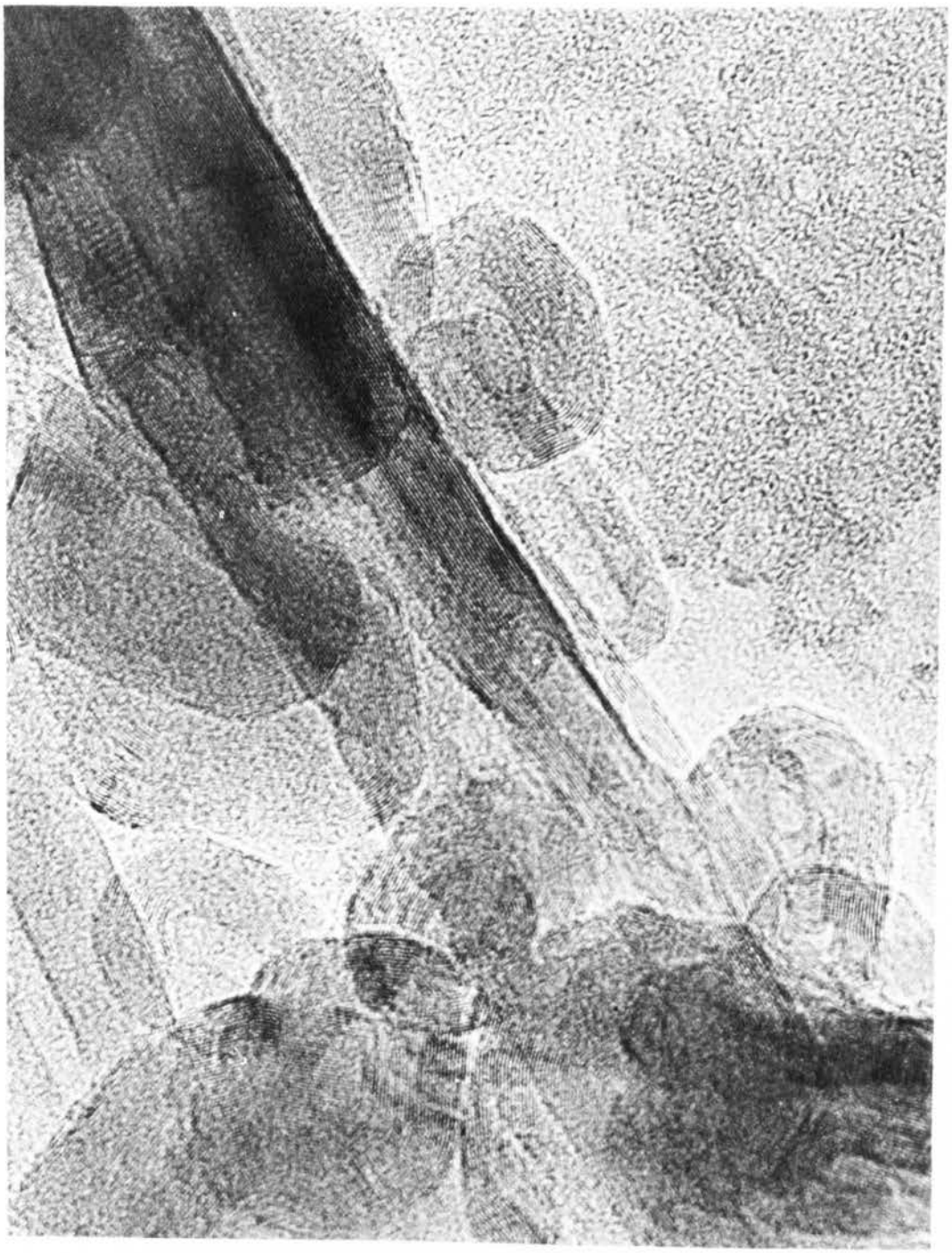

PLATE XVII

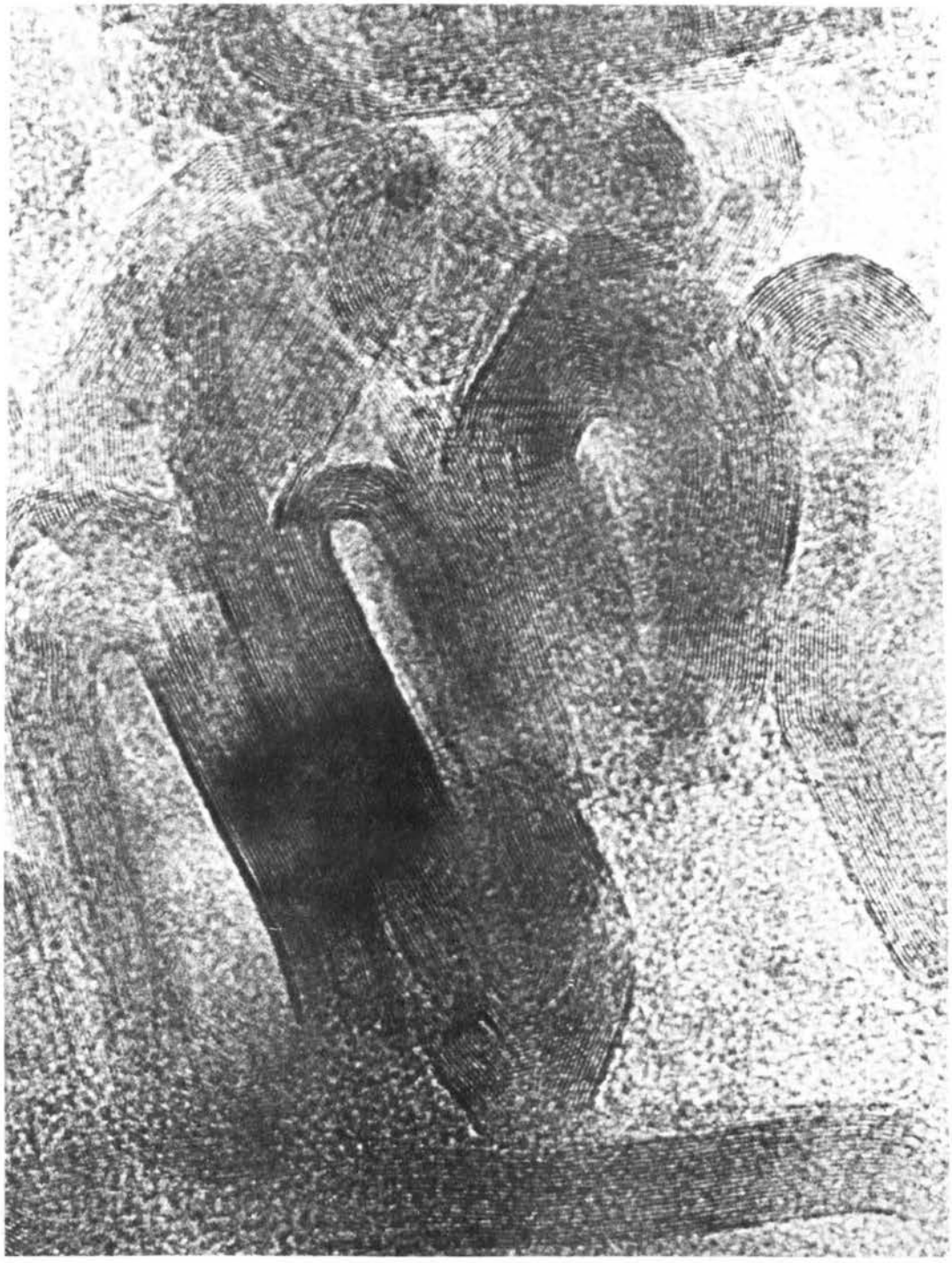

PLATE XVIII

(a)

(b)

(c)

PLATE XIX

CHAPTER THREE

-A CRITIQUE-

3 A CRITIQUE OF THE METHODS, MATERIALS AND RESULTS.

It is intended to examine critically the methods used and to point out the experimental limitations of interpretations discussed in Chapter 4. This will be ordered in the sequence of methods laid down at the beginning of Chapter 2.

3.1 CHEMICAL REACTIVITY OF CARBON AND GRAPHITE FIBRES.

The methods used in this section on fibre exposures are well tried and generally adopted techniques. Diameter measurements using an image-shearing eyepiece are accepted as giving a sensitivity of ±0.05μm. Errors introduced of this order may lead to inaccuracies in tensile strength and modulus of 2-5% in an 8 μm fibre. Machine softness, test gauge length and adhesive have already been discussed which leaves the sampling procedure to be examined.

Statistical analysis of results (See Appendix 1) shows that the least possible sample from a tow giving acceptable variance in U.T.S. at the 95% confidence level is 12 for early batches of fibres. This is illustrated by the plot of confidence limits against sample size for untreated control fibres (Type 111)(Fig. 56).

FIG. 56. 95% Confidence Limits on the Mean Versus Sample Size.

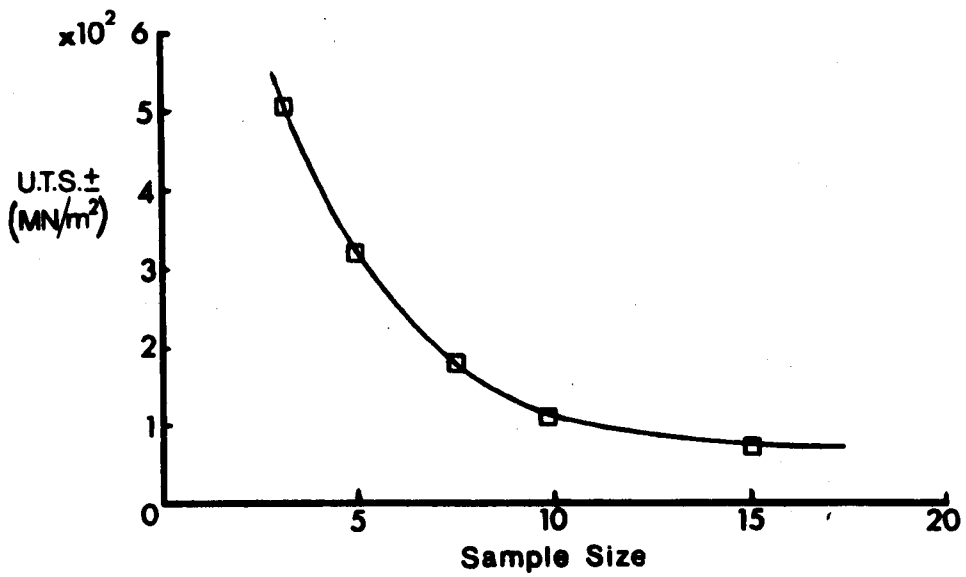

Assuming circular x-sections, it was considered prudent to take a sample of 15 for each fibre treatment.

3.2 CARBON FIBRE COMPOSITE CHEMICAL STABILITY.

(A) No attempt has been made to draw strict parallels between I.L.S.S. and the true shear strength. This is because the compressional and tensile properties of C.F.R.P. differ to give a neutral shear plane in flexure that is not central.

The location of the neutral plane (plane of zero bending stress, Fig. 57) is given by

$$\frac{h_t}{h_b} = \left(\frac{E_T}{E_C}\right)^{1/2}$$

where h_t = dist. from top side
h_b = dist. from bottom side

FIG. 57. Location of Neutral Shear Plane. [212]

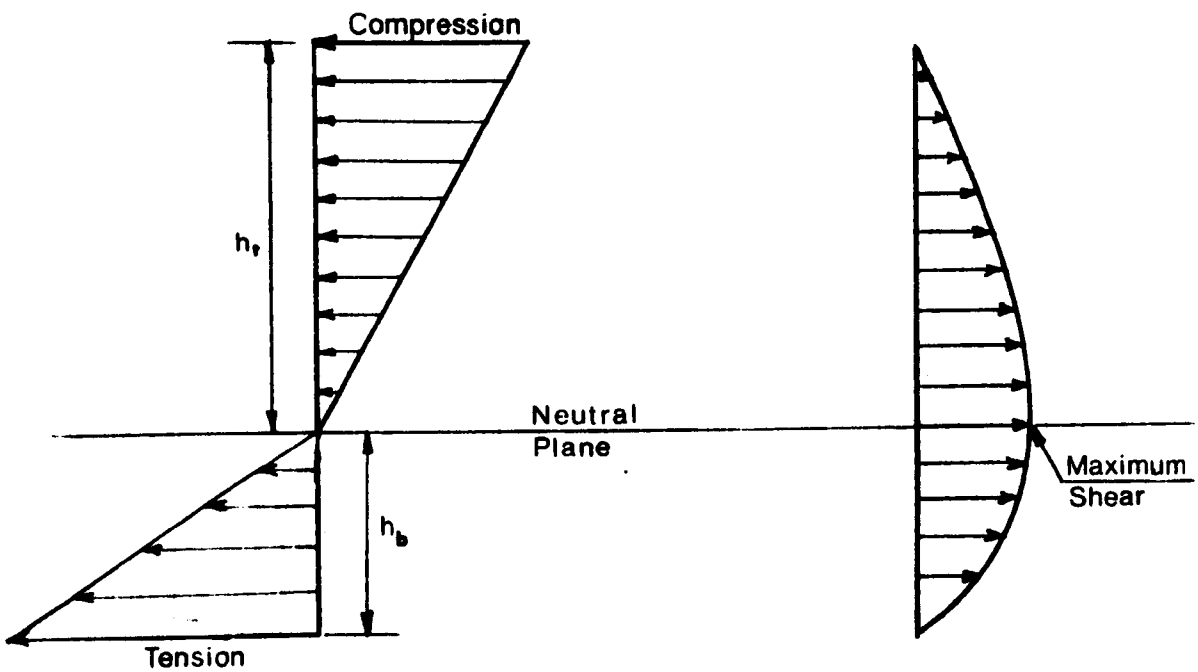

~STRESS VARIATION~ ~SHEAR VARIATION~

Only when $E_C = E_T$ can the neutral plane fall midway between the top and bottom of the specimen.

The maximum shear stress is independent of the modular ratio $\frac{E_T}{E_C}$. The reason for this is that the shear stress is zero at the top and bottom surfaces of the beam. Thus, the boundary conditions can only be satisfied by a parabolic variation of the shear stress through the beam. However, the plane at which maximum shear stress occurs does depend on the modular ratio.

Because $E_C < E_T$ for C.F.R.P., it follows that $h_b < h_t$ ie. $h_b < \frac{h}{2}$. In the equation given on Page 75, however, h_b is assumed equal to $\frac{h}{2}$. Hence, if

$$\sigma_{T_{max}} = \frac{3P}{4bh_b} \cdot \frac{L}{h}$$

for a given load, P, the resultant tensile stress is greater than that calculated by:-

$$\sigma_{T_{max}} = \frac{3PL}{2bh^2}$$

But, for a given load, P, the maximum shear stress $(\tau_{xy(max)})$ is $\frac{3P}{4bh}$. Thus, without raisung the shear stress for a given load, the tensile stress is greater for the case $E_C < E_T$ than for the case $E_C = E_T$. This endangers the case for failure in shear when

$$\sigma_{T_{max}} > \frac{2S_H L}{h}$$

because the failure stress may be prematurely reached.

If the limiting case is considered

$$\sigma_{fail} > \frac{S_H L}{h_b}$$

for shear failure, the normal failure stress of the composite must exceed the term on the right. The effect of lowering $\frac{h}{2}$ to h_b raises the value of this term and tends to level the imbalance.

Attention has been paid to the modes of failure in this work, but drastic changes in $\sigma_{C_{fail}}$ made certain assessments of shear impossible.

(B) The results for the model single fibre specimens require further explanation.

Clearly, stresses greater than σ_{fm} (matrix failure stress) cannot be applied. Thus, σ_r is always less than σ_{fm}. However, G_{11} may be so large for certain fibre-resin adhesions that the complex tensile-shear strength of the bond is not exceeded, ie. ignoring fibre-resin friction:-

$$G_{11} > \frac{\sigma_{fm}^2 E_f d}{8E_m^2}$$

This is the case for Types 111 and HTS fibres.

Although separate determinations of the compressive moduli E_m and E_f were not made, E_m is assumed to remain constant. Values for E_f are not to be found in the literature. Recent work by Hawthorne et al[292] suggests that the compressive behaviour of carbon fibres is quite different to tensile. Ultimate failure in compression goes from shear to micro-buckling with increasing anisotropy. It is suggested that this is caused by well-aligned but uncoupled microfibrils. Because these mechanisms of failure would undoubtably influence longitudinal compressive moduli, a simple relationship between fibre types cannot be assumed. Hence, although

$$\left[\sigma_{r_1}^2 E_f d\right]_{HT} : \left[\sigma_{r_2}^2 E_f d\right]_{HM} \quad \text{is} \quad G_{11(HT)} : G_{11(HM)}$$

the comparison of debonding energies cannot be accurately concluded.

3.3 CARBON FIBRE MICROSTRUCTURE.

Treatment of carbon fibres in glass ampoules at pressures reaching 25 atmospheres was considered to be too dangerous after several explosions in the ovens. Unfortunately, the corrosive nature of nitrogen dioxide at the temperatures and pressures used was too destructive for conventional metal 'bombs'. In addition, a fine layer of metal oxide was deposited on the fibre surfaces, making diameter measurements impossible. The porous nature of the oxide film in iron bombs also meant that the fibre: gas ratio was changing indeterminately during the treatment. Actually sticking fibres permanently to formers exposed to nitrogen dioxide at elevated temperatures and pressures was a problem. Silicone grease was tried with the results shown in Plate XI (a) and (b).

A solution was found which was not altogether satisfactory, but a necessary improvement from the safety aspect. Glass ampoules were sealed and placed in steel sleeves to prevent personal injury from flying glass. Secure aluminium 'stoppers' in the top and bottom allowed the ampoule to remain upright during its insertion and removal.

The intricacy of the method of treatment and high failure rate as measured by unsuccessful diameter reductions must satisfy any criticism aimed at the small number of fibres tested. The apparently impossible task of obtaining reproducibility in treatments with nitrogen dioxide on any type of carbon or graphite fibre cannot be satisfactorily explained.

When ten fibres of the same type are given simultaneously identical treatments, it was found that the remaining filaments had widely differing diameters. A typical breakdown of five attempts at identical treatments is given below:-

Volume of ampoules : 330ml
Volume of liquid N_2O_4/NO_2 : 5ml
No. of Type 11 fibres per treatment : 12-15
Time of Treatment : 2.5 hrs.
Temp. of Treatment : 500K.

		DIAMETER RANGES				
Sample No.	No. of Fibres.	8-5 µm	5-3 µm	3-2 µm	2-1 µm	Completely oxidised or not found.
1	12	2	7	1	2	0
2	12	4	4	2	1	1
3	14	1	3	4	2	4
4	15	2	3	1	1	8
5	14	2	5	1	2	4
TOTAL		11	22	9	8	17
Percentage		17%	33%	13%	12%	25%

Interest was strongest in fibres between 1.5 and 2.0 µm (anything below 1.5 µm was too difficult to test). This meant that if 60% of the fibres falling in this range of diameters were successfully tested, only three or four results would be obtained.

This was the case for the results shown.

Structure is discernable on untreated fibre types using polarised light spectroscopy. It was not possible, however, to get the magnification and illumination sufficiently high to examine treated fibres in a similar fashion.

Using a more powerful mercury vapour lamp source at R.A.E. (Farnborough) still failed to identify structure patterns on treated fibres less than 1.5 µm diameter.

Great difficulty was experienced in rapidly combusting samples for elemental analyses. This problem was also met by the analysts at the N.P.L., Teddington. They were sceptical about the validity of fibre elemental analysis from previous experiences and hence the results of this section may be ignored. Comment was made, however, regarding the difficulty with which certain treated samples combusted.

The thermal gravimetric analysis of carbon and graphite fibre tows was unsuccessful as already stated. The reason for this may have been because at any one time oxidation was not occuring at the same level in every fibre.

For example, if a simple sheath and core structure is assumed, ideally for T.G.A. methods to pick up discrete changes in oxidation rate, the oxidation 'front' should pass from sheath to core at the same time for all fibres. This, of course, is not the case. Several reasons may be responsible for this including carbon dioxide concentration gradients through the tow, different starting diameters for individual filaments and surface accessability.

This led directly to an optical method on single filaments.

CHAPTER FOUR

-DISCUSSION-

DISCUSSION.

4.1 INTRODUCTION.

It was intended that the experimental work described in Chapter Two should yield information in three distinct areas:-

A. The chemical reactivity of three types of carbon and graphite fibres,

B. The resistance to chemical attack of composites containing three types of carbon and graphite fibres reinforcing phenolic resins;

C. The changes conferred on the microstructure of carbon and graphite fibres by chemical treatment.

It must be stated here that the instigation of work on microstructure was a direct consequence of discoveries made during the progress of the first part of the programme.

A critique of the experimental work and results has already been given in Chapter Three, however, a useful wide ranging programme was completed.

Because the work on fibre exposures led directly to the work on fibre-NO_2 interactions, they will be discussed successively. For this reason, the work on composite exposures is discussed first (4.2). The fibre exposures are then dealt with (4.3), leading into the final discussion on fibre-NO_2 interactions (4.4).

4.2 EXPOSURE OF COMPOSITES TO VARIOUS FLUIDS.

It has been explained that where composites obey the law of mixtures mechanically, it is essential that fibre-resin adhesion be maintained. Loss of adhesion will have marked effects on shear values. This in turn will reflect in the tensile properties where shear modes of strain are introduced by stress transfer across adjacent fibre discontinuities.

Processes which affect the mechanical integrity of fibre reinforced resins may be listed as:

(1) Swelling of the resin matrix or fibre

(2) Actual solution of the resin by a solvent

(3) Chemical degradation of the resin by hydrolysis, oxidation, pyrolysis or radiation

(4) Chemical degradation of the fibre (Section 4.3)

(5) Destruction of the interfacial adhesion by chemical or physical means.

The results for this section of the work will be discussed in terms of these processes. Microscopical work will be discussed concurrently at relevant points with the main body of results, which will be dealt with in the following divisions:-

4.2.1 Weight, dimensional, flexural and inter-laminar shear strength changes after 100 days exposure period.

4.2.2 Monitored inter-laminar shear strength and flexural modulus changes.

4.2.3 Changes in torsional properties after 100 days exposure period.

4.2.4 Single fibre/resin model debonding.

Although initially treated separately, the trends in properties will be examined at the end of 4.2.3.

4.2.1 Weight, Dimensional, Flexural and Inter-Laminar Shear Strength (I.L.S.S.) Changes After 100 Days Exposure Period.

The information contained in the numerical results of Tables 20-21 can be favourably augmented by knowledge of the failure modes experienced in the I.L.S.S. tests. General comments on these failure modes have been made in Table 22 which require some explanation if their full value is to be realised. Work reported by Daniels et al [213] conveniently sums up the different types of failure mode in a diagram which is reproduced here for reference. (See Fig. 58).

The figure lacks mention of a multiple shear failure and also the possibility of more than one type operating at a time. For example, the 'tensile' mode might more accurately be called 'shear and tensile' in the case where 'clean tensile' has also been illustrated.

The specimen geometry for the limiting case when shear rather than tensile failure will occur has already been discussed (Section 2.2.2.). The problem arising here, however, is interpretation of change in failure modes brought about simply by exposing specimens to various reagents. All control specimens gave some form of simple shear failure and so it is conversion to a tensile, compressive or homogeneous mode of failure that is of interest here.

It was unlikely in well-cured specimens, which Fig. 44 shows these were, that a change to a tensile type of failure would occur. Such a change would require stiffening of the matrix and/or improvement in the resin-fibre adhesion. If a cure was not complete, it is possible that further loss of volatiles and advancement of cure may have occured. Hence, increased compressional stresses on fibres could improve the resin-fibre bond to such an extent that tensile failure occured. No evidence of this was found in the present work.

FIG. 58. [213]

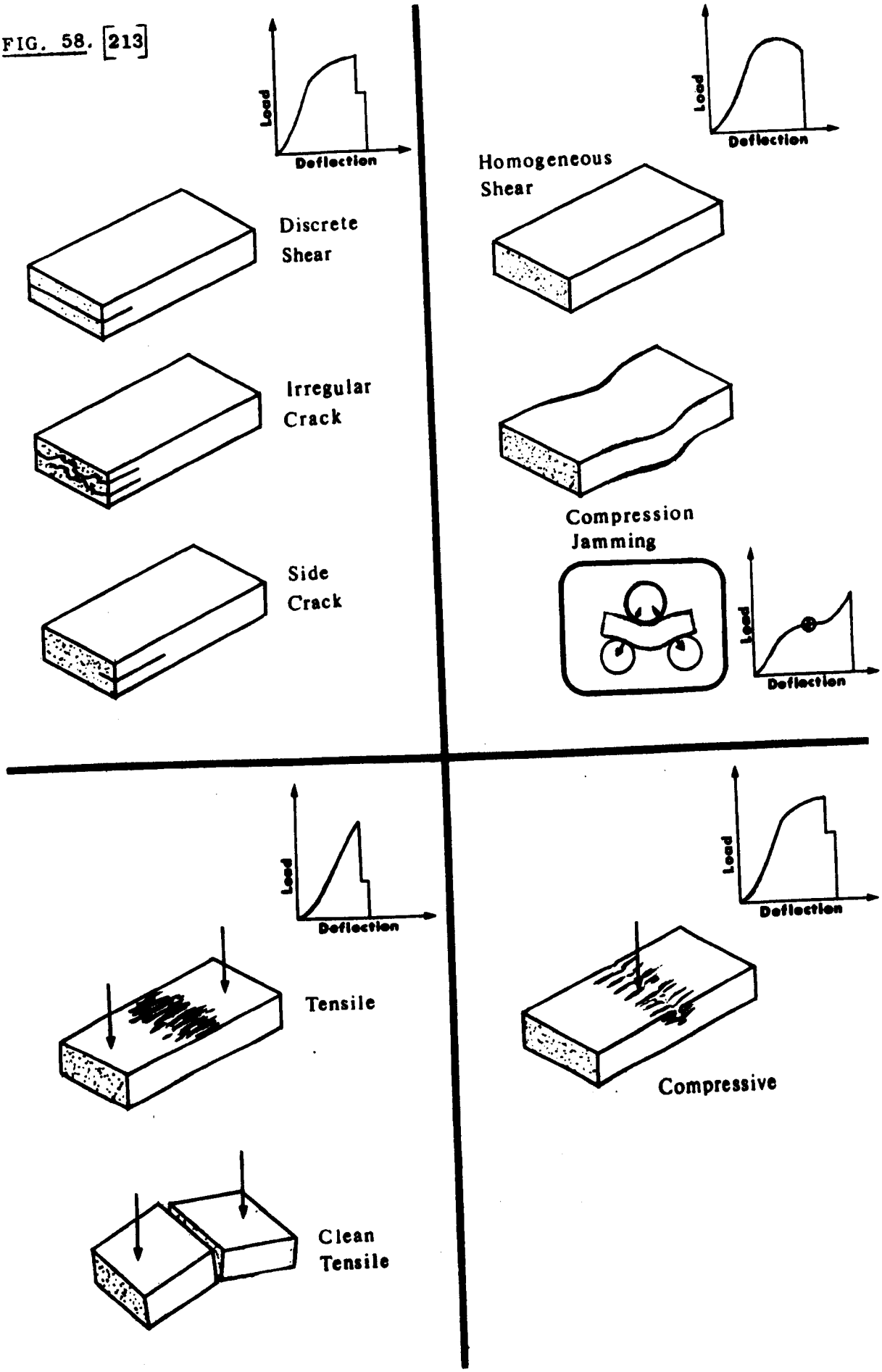
Load
Deflection
Discrete Shear
Irregular Crack
Side Crack
Load
Deflection
Homogeneous Shear
Compression Jamming
Load
Deflection
Load
Deflection
Tensile
Clean Tensile
Load
Deflection
Compressive

Conversion to compressive failure is a far more likely occurence and will accompany breakdown of the fibre-resin bond. This may be brought about by actual attack at the interface or relief of the compressional forces acting on the fibres through the matrix. Reagents attacking the interface or weakening the matrix, without destroying it, will result in compressive failure. The ability of the composite to still sustain a small transverse stress gradient is essential, otherwise homogeneous shear will occur.

Homogeneous shear is the result of complete mechanical failure. Matrix and/or interface are extensively attacked to the point where fibre-matrix-fibre interaction becomes negligible. Several reactions may cause this effect. Reagents which swell the matrix to the point of rupture or those which cause drastic debonding so that even friction from fibre pullout is eliminated are two examples.

Having looked at the mechanisms involved for changing failure modes, it must be pointed out that reagents were chosen, in most cases, for their known reactivity with carbon fibres (See Section 4.3) and phenolic resins (Section 1.4).

Results showed the following weakening processes to be operative.

(a) <u>Swelling of the Matrix</u> (Fig. (b) Plate V and Plate VII)

Alkalies have an affinity for phenolic groups within the resin matrix. The ingress of alkali swells the resin, causing mechanical failure of the composite. Comparing the results for the three types of fibre composites in sodium hydroxide supports the view that the mechanism is a simple matrix failure because we know that this reagent does not attack the fibres, and yet all three composite types approach the same low value for I.L.S.S. (Fig. 64).

More evidence for the swelling mechanism can be obtained from the homogeneous nature of the shear failure. Plate VII and Fig. 45 illustrate the disruption of matrix regions caused by swelling and subsequent drying of V.W.Phenolic specimens exposed to caustic alkali. Damage to fibres is not evident, which is the result anticipated from the previous studies on fibre chemical activity.

(b) Extraction of Soluble Matter from the Matrix.

Glacial acetic acid, methyl ethyl ketone and industrial methylated spirits, permeate through the composites and appear to leach out low molecular weight material and/or relieve compressive stresses at the fibre-resin interface. This mechanism would explain the relatively small weight, dimensional and visual changes accompanying a large fall in I.L.S.S.(Fig. 46 Micro-cracking upon removal of reagents supports a mechanism which involves leaching of material. (See Fig. 47).

The variation of the retention of I.L.S.S. between the three types of fibre indicates once again that the matrix is the object of corrosive attack (See (a)). The large I.L.S.S. loss for Type 111 fibres supports the mechanism of compressive stress relief at the fibre-resin interface.

Failure of the I.L.S.S. specimens in compression is a strong indication of attack on the matrix. Much stronger attack is seen by glacial acetic acid at 323K resulting in complete loss of mechanical integrity and homogeneous shear modes of failure in the I.L.S.S. test. Judging by the absence of any apparent attack by this reagent at 296K. one is led to assume either that the activation threshold falls discretely between the two temperatures, or that the reaction rate is extremely temperature sensitive. Another interesting feature of this reagent at 323K. is the gradual change in values for weight and volume increases

going from Type 1 to Type 111 fibre composites (See Table 38).

TABLE 38.

XYLOK COMPOSITES IN GLACIAL ACETIC ACID (100 days, 323K.).

Fibre Type	Weight Increase	Volume Increase
1	0	0
11	3%	5%
111	9%	16%

These results indicate that another mechanism may operate for this reagent at this temperature which is dependent on fibre type. The only satisfactory explanation is that the acid is chemically adsorbed onto the surface of the Type 111 fibres in large enough volumes to break down the resin-fibre bond, at the same time causing local swelling. The anomaly with regard to fibre type may be explained by reference to the number of available active sites on their surfaces. Surfaces containing large numbers of basal plane edges have already been shown [180] to be 'wetted' more easily by fluids containing polar groups. Watt [177] has already estimated these to be in the ratio of 600:1 for Types 11 and 1 respectively. This suggests that as glacial acetic acid does not attack fibre structure, an adsorption mechanism is most likely. This explanation gains support from the data regarding temperature dependence. This type of dependence is typical of chemical rate/diffusion controlled phenomena. If such a mechanism does operate, then the results are conveniently explained. If it does not, then an alternative explanation is not immediately available.

Fig. 48 shows the surface of a Type 111 Xylok composite after exposure to glacial acetic acid at 323K. The enlarged fibre tracks are noteworthy and not unlike those produced by oxidation with sodium hypochlorite (Fig. (a) Plate VI). Because a 'tunnelling' mechanism is believed to operate in the latter case, it is not unreasonable to gain some support for a similar mechanism operating for acetic acid.

Figs. 49 and 50 show degrees of attack by butanone and industrial methylated spirits at 296K. on Xylok and V.W. phenolic composites respectively, both made with Type 111 fibres. Both photographs are typical of 'leached' composites.

(c) Oxidation of Resin and/or Fibres.

Phenolic resins and carbon fibres are both susceptible to chemical attack by oxidising agents. Sodium hypochlorite, ferric chloride, nitric acid, air and steam at the temperatures used are representative of the oxidising conditions encountered within the working temperature ranges of the resin chosen.

Moderate oxidation (Figs. (a) and (b) Plate VI and Figs. 51 & 52) caused erosion of the composite surface, leaving partly oxidised fibres exposed and residual micro-cracked resin.

Vigorous oxidation removed most of the resin, leaving oxidised fibre bundles free on the composite surface. Unlike the cases discussed in Sections (a) and (b), there remains a composite core which is not substantially changed in composition from the original test bar (Fig. (c) Plate VI).

If the retention of I.L.S.S. of composites with different fibres are compared, for each oxidising agent, a decrease is observed from Type 111 to Type 1, that is, on increasing fibre heat treatment

temperature. The one exception is ferric chloride, which is the only good intercalating reagent amongst the milder oxidants used.

Type 1 composites are inherently weaker in shear than Type 111 and so an interesting disparity in I.L.S.S. between the three types results after oxidation. It was reported in Section 1.4.2 that highly graphitised fibres are least affected by oxidants, which leads to the conclusion that attack on the fibres alone could not have caused this phenomenon. Similarly, attack on the matrix alone would show effects similar to those exhibited by environments covered in Sections (a) and (b). The mechanism must, therefore, involve the interface.

The relatively good adhesion between Type 111 fibres and resin appears to render the composite less susceptible to oxidation than the poorer 11 and 1 fibre bonds. The implication here is that the oxidising reagents do not diffuse into the matrix, but enter composites through defects and along poorly bonded resin-fibre interfaces. Oxidation is essentially operative only at accessible surfaces. Good fibre-resin adhesion, therefore, makes the progress of an oxidant more difficult and the composite more resistant to this type of attack. This theory is supported by comparing the results for Types 1 and 11 surface treated and untreated fibres. The sole difference between these types is the strength of the fibre-resin bond and yet large differences exist for their resistance to oxidative attack (See Table 20 - Nitric acid).

Flexural strength data (Table 23) generally agrees well with the I.L.S.S. results. Where shear strength is low, one may anticipate that it will dominate as a failure mechanism over tensile modes even in flexural strength measurement. The comparatively low values for specimens exposed to air and steam at 498K. may be indicative of the surface cracks (See Fig. (a) Plate V) acting as stress concentrators which lead to premature failure.

4.2.2 Monitored Inter-Laminar Shear Strength and Flexural Modulus Changes.

Figs. 59 and 60 show graphically the changes occuring in Xylok/carbon fibre composites exposed to air and steam at 498K. with respect to flexural modulus and I.L.S.S. The graphs summarise the results of Table 24.

Figs. 61, 62 and 63 show changes occuring in I.L.S.S. at 323K. for each fibre type in Xylok resin exposed to nitric acid (S.G. 1.21), sodium hydroxide and glacial acetic acid. These graphs summarise the results of Table 25.

FIG. 59. Exposure of Xylok Composites to Air at 498K.

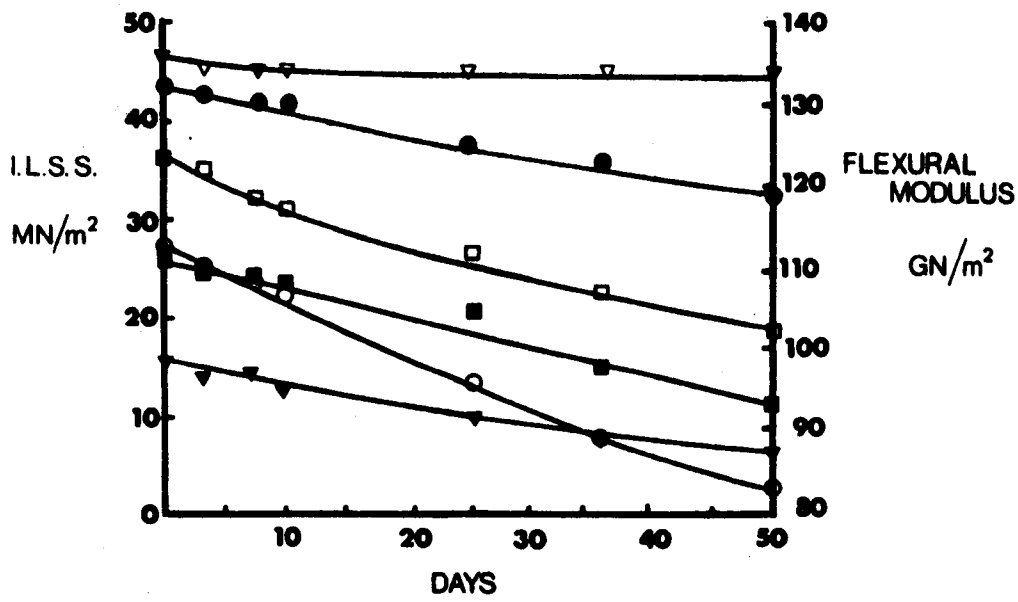

where, for Figs. 59 and 60 - I.L.S.S. { ○ Type I, □ Type II, ▽ Type III

Flexural Modulus. { ● Type I, ■ Type II, ▼ Type III

FIG. 60. Exposure of Xylok Composites to Steam at 498K.

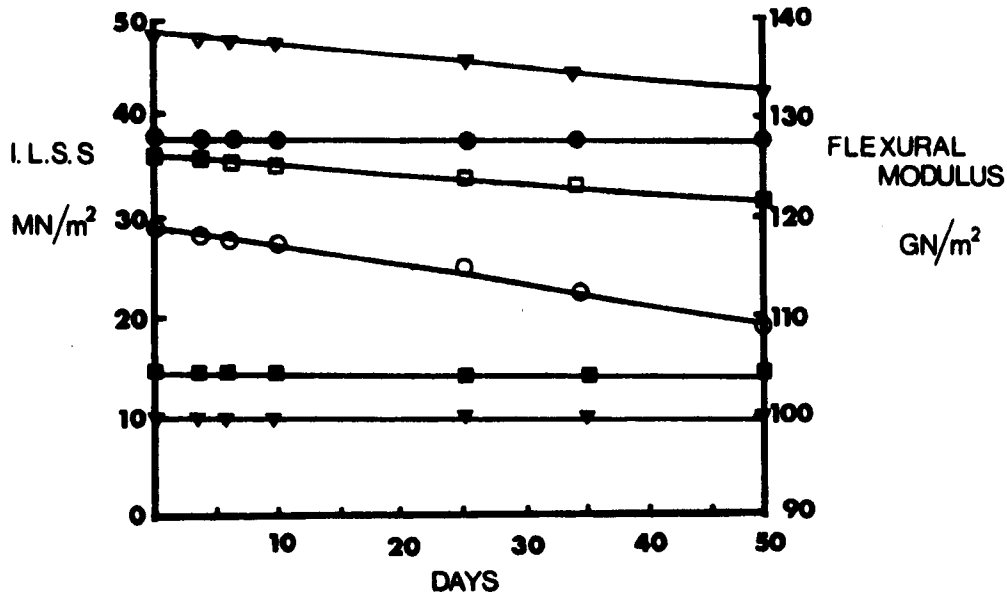

FIG. 61. Exposure of Xylok/Type III Composites at 323K.

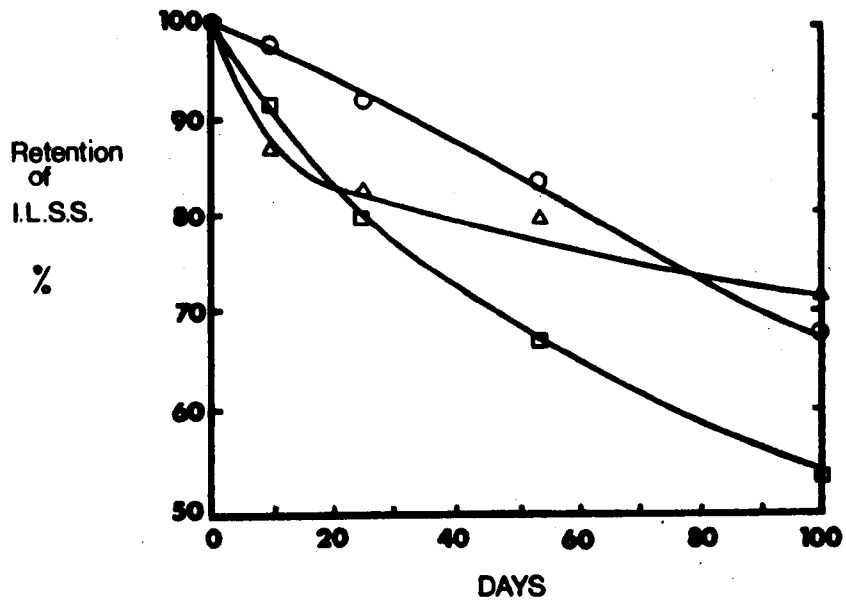

where, for Figs. 61,62 and 63 -

- ○ Nitric acid (S.G.1.21)
- △ Sodium hydroxide
- □ Acetic acid (glacial)

FIG. 62. Exposure of Xylok/Type II Composites at 323K.

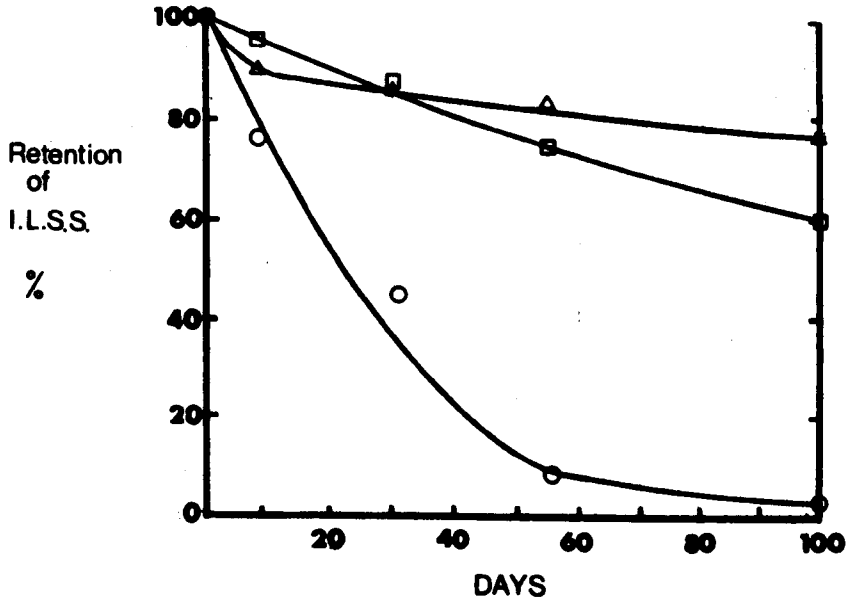

FIG. 63. Exposure of Xylok/Type I Composites at 323K.

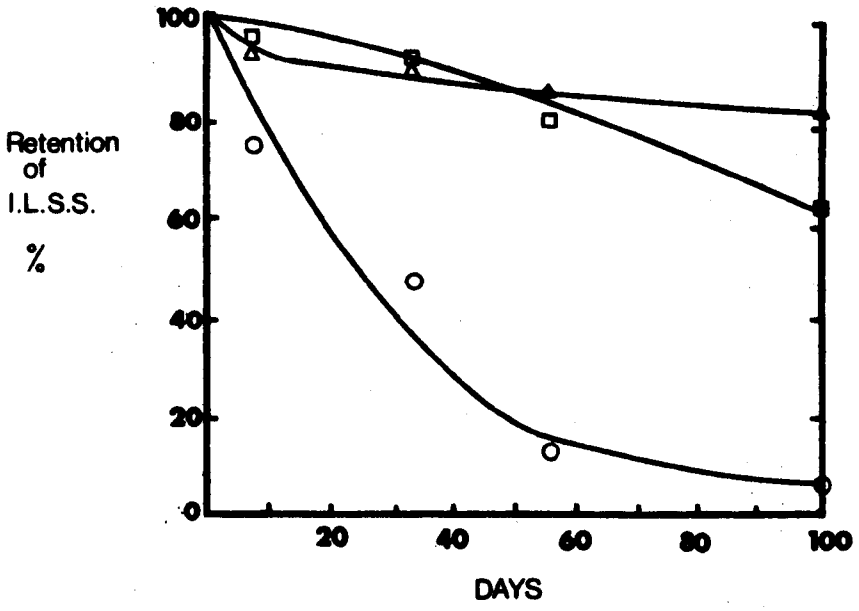

Figs. 59 and 60 serve to illustrate that the mechanical degradation of the composites has not reached a limiting extent. Oxidation is probably the main process of attack for both air and steam (containing air). It would appear from the graphs that the rate of attack is being maintained after 50 days, as measured by loss of I.L.S.S., even though it is slow.

Figs. 61, 62 and 63 show that whereas oxidation follows a fairly steady reaction rate, caustic alkali causes rapid degradation of I.L.S.S. followed by a cessation of extensive chemical activity. This suggests that diffusion of alkali into the matrix to sites with acid phenolic groups is fairly rapid and, in the case of Xylok, of finite duration. Further degradation does appear to go on but at a much diminished rate.

The attack of glacial acetic acid appears to follow a rate pattern between the two reagents previously mentioned. It exhibits a slight slowing down, but this is not as noticeable as for sodium hydroxide. If we assume a leaching process to operate, the rate of loss of mechanical strength would be expected to be slow and drawn out. If a mechanism of adsorption and fibre-matrix debonding were operative, however, this also would be expected to be slow and drawn out. The fact that the process of degradation is still continuing at a reasonable rate after 100 days suggests that with glacial acetic acid, the total damage and mode of attack is quite different from that experienced with caustic alkali. The rate of degradation resembles more in nature and extent that resulting from oxidation.

Certain trends in the rates of attack for the three fibre types are apparent. The inversion of rates for treatment of Types 1 and 11 with nitric and glacial acetic acids compared to Type 111 is noteworthy. The explanation for this clearly focuses on the large losses in I.L.S.S.

encountered with Types 1 and 11 fibre composites in oxidising media (See 4.2.1 (c)). Glacial acetic acid, however, exhibits a small counter trend which results in smaller losses in strength after 100 days for Types 1 and 11 fibres.

The results may be presented more demonstratively to show the matrix weakening mechanism involved. Taking the results for exposure of composites to sodium hydroxide (Figs. 61, 62, and 63), it appears that Type 111/Xylok composites are attacked most extensively. Plotting absolute values for I.L.S.S. shows, however, that all composite types approach the same low value, which is a function of the swollen matrix (Fig. 64).

FIG. 64 Exposure of Xylok Composites to 30% Sodium Hydroxide at 323K.

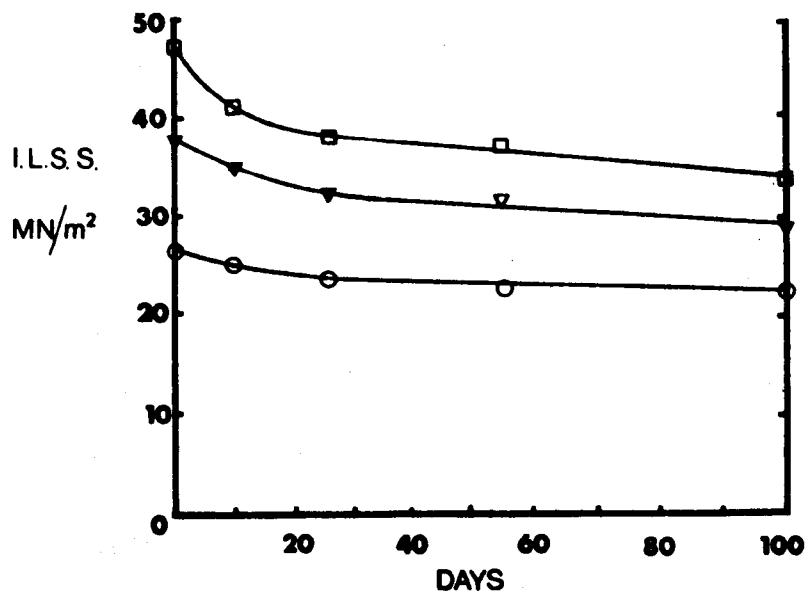

where - ○ Type I
▽ Type II
□ Type III

4.2.3 Changes in Torsional Properties After 100 Days Exposure Period.

All measurements on exposed specimens were carried out at ambient temperatures. To check that the resin matrix was in the glassy state, even at most exposure temperatures, a plot of shear modulus v's temperature is shown as Fig. 65 using the data of Table 26.

FIG. 65. Changes in Torsional Storage (Shear) Modulus with Temperature.

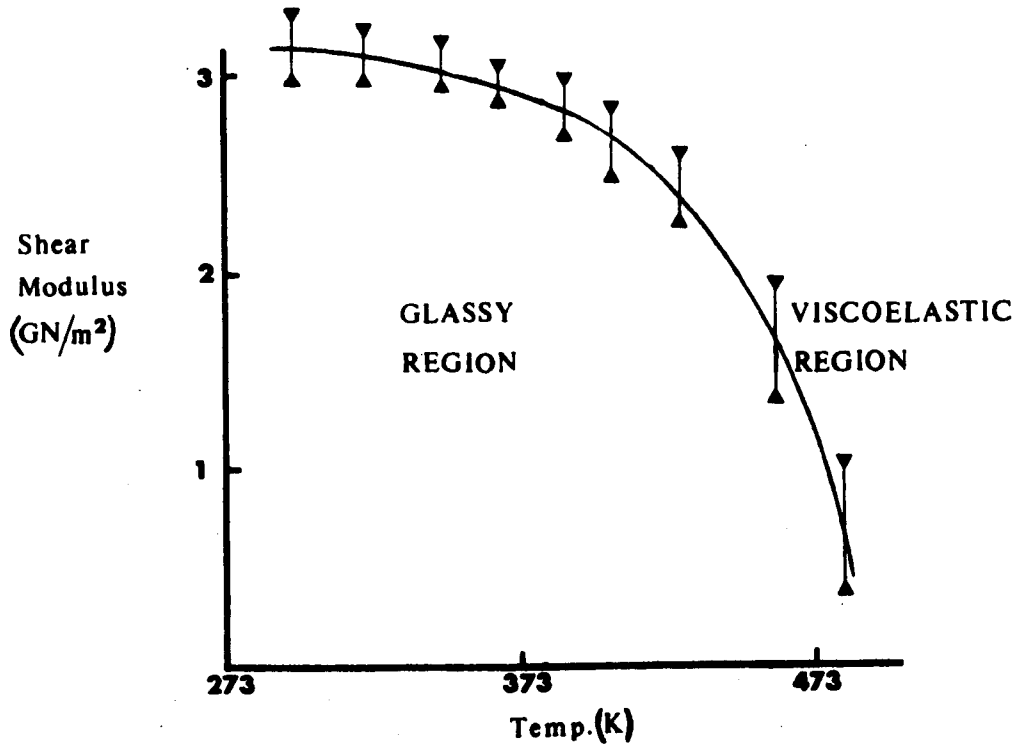

Interpretation of results does require a more detailed understanding of torsional properties than is given in Section 2.2.4.

The torsional shear modulus (storage modulus) is a measure of torsional rigidity. It is strongly dependent on the condition of the resin-fibre interface but also reflects the properties of the matrix and fibres. These facts are illustrated by the control values given in Table 27. The poor resin-fibre bond in Type 1, as compared to Type 111 fibre composites (Section 4.2.1 (c), dominates the opposing decrease in fibre modulus.

The logarithmic decay (Δ) and loss modulus (G'') are both measures of energy loss through matrix relaxation or internal friction. Large increases in logarithmic decay signify that these sources of energy losses are operative. Fibre debonding leading to internal friction is the most effective influence requiring only moderate visual damage.

The results of Table 27 mirror those for I.L.S.S. with regard to the degree of mechanical damage experienced in each environment. Quite different parameters are involved, however, for I.L.S.S. cannot be thought of as linked with shear modulus. At small strains, it is possible for very high shear modulus values to be reached by a specimen exhibiting a very weak shear strength. This is not a phenomenon likely to develop in a composite exposed to environmental attack, however, but more likely to exist in model systems devised specifically to illustrate it.

Two interesting features of the torsional pendulum results are the trends shown by glacial acetic acid at 323K. and 5% ferric chloride solution at 363K. (See Table 39).

The approach of the storage moduli to the same low value for the acetic acid environment is indicative of a matrix weakening process. This gains support from the fact that the loss modulus goes up for the well-bonded Type 111 composites, but significantly down for Type 1. This could be explained by considering three stages of debonding to exist which affect the loss modulus. These stages may be identified as bonded, partially debonded, and totally debonded fibre-resin interfaces. The loss modulus rises as the interfacial characteristics pass through the debonding phase. The composites under current examination largely comprise poorly bonded Types 1 and 11 fibres, which may be likened to a

TABLE 39. Trends in Torsional Results for Acetic Acid and Ferric Chloride.

CONTROL	G' (GN/m^2)	Δ	G'' ($MN/m^2 \times 10^{-1}$)	
111	3.2	0.04	4.074	INCREASING
11	2.4	0.09	6.875	
1	1.95	0.14	8.689	
GLACIAL ACETIC (323K.)				
111	0.60	0.221	5.98	DECREASING
11	0.60	0.223	6 17	
1	0.60	0.356	5.67	
FERRIC CHLORIDE (363K.)				
111	3.1	0.035	3.45	INCREASING
11	2.05	0.095	6.20	
1	1.85	0.167	7.71	

partly debonded system. Attack on the matrix (or interface) and consequent release of compressive forces at the interface result in Type 111-fibres entering the debonding phase and Types 1 and 11 entering the totally debonded phase. This data, therefore, supports a leaching

mechanism for attack by glacial acetic acid, but does not necessarily eliminate the possibility of other modes operating.

Ferric chloride solution at 363K. gives lower values of G'' which are, however, still increasing with respect to fibre type going from Type 111 to Type 1 fibre composites. The significance of this trend, when considered alongside the very small changes in Δ and G', could be the fibre swelling properties of the reagent by intercalation (Section 4.2.1 (c)). Damping is primarily a function of time dependent relaxations whereas the loss modulus is a measure of internal homogeneity with respect to structural faults. Improvement of the resin-fibre bond by compressibe stresses incurred during fibre swelling would explain the results without reservation. This mechanism may receive criticism from a standpoint that the reagent will not find the fibres easily accessible. The ingress of reagent as far as possible with subsequent fibre swelling will, however, prevent further degradation by oxidation. If a 'sealing' process operates, with oxidation limited to the outer surfaces of the specimen (See Fig.52), the small swelling effect could possibly cause the observed upward trend in shear modulus.

Before proceeding with 4.2.4., it is convenient to summarise the findings already discussed in this section.

By virtue of the fact that Type 111 fibres have more active sites for oxidation, they also bond more strongly to resin. The superior 'wetting' conferred by basal plane edges at the fibre surfaces give steadily poorer bonds to resin going from Type 111 to Type 1 fibres.

The shear properties of carbon fibre/phenolic resin composites approach the same low value regardless of the fibre type when exposed to environments that are known to attack the matrix but not the fibres.

Swelling of the composites by reagents capable of permeating through

the matrix readily causes stress relaxation at the fibre-resin interface and subsequent debonding.

Most oxidising reagents diffuse into the matrix relatively slowly and mainly enter composites through defects in the matrix and along poorly bonded resin-fibre interfaces. Oxidation is essentially operative only at accessible surfaces. A good fibre-resin bond, therefore, makes the progress of an oxidant more difficult and the composite more resistant to this type of attack.

The exception of glacial acetic acid to conform to just one type of attack suggests a more complicated process leading to the mechanical failure of composites exposed to this reagent. Several mechanisms have been proposed, but the exact nature of the attack cannot be confirmed with any degree of certainty using the data obtained.

4.2.4 Single Fibre/Resin Model Debonding.

Fig. 53 shows the stress pattern in polarised light of a specimen under axial compression. Since the light must pass through the whole thickness, interpretation of the fringe pattern is feasible only when the model is in a state of plane stress - the stress components then being very nearly uniform through the thickness. When this is not the case, as in this three dimensional stress distribution, the optical effect is an integral involving the stress at all points along the ray [28]. Allowing that the angle of incident light is not quite perpendicular to the vertical axis of the specimen, several points of interest may be made:-

(i) The stress distribution is symetrical:

(ii) Stress relief appears to be operating left and right of centre by bulging of the specimen sides;

(iii) The light band above and below the dark drill-hole signifies that this was a specimen previously boiled in water. Careful scrutiny shows that the lower portion of the specimen is 'boxed in' by a swollen layer of matrix.

(iv) The figure alone does not indicate whether fibre debonding has yet occured.

In support of this technique for the detection of debonding, it must be said that although point (iv) is accurate, it is still possible to observe vague changes in stress pattern around the fibre-matrix-hole region during compression.

Fig. 54 shows a failed specimen. The 'smokey' regions at 45° to the main crack are indicative of compressive stresses having imparted residual strain to this uncompressed specimen. These compressive stresses and the vertical crack (formed from horizontal tensile stresses) are

typical of stresses imposed by compression of this hole configuration. Savin[282] and, more specifically, Lekhnitskin[283,] show detailed analysis of two dimensional models containing holes using photoelastic techniques. The stress distribution of Fig. 54 is typical of their findings. It is also essential for the theory of failure for this model system.

For reasons given in 2.2.6., the sharp onset of debonding was measured by an optical method. Fig 35 shows the two stages of specimen failure in compression loading and illustrates the ease with which debonding may be observed Plate VIII shows catastrophic failure.

Preliminary investigations of the usefulness of this technique have shown that where fibre-resin adhesion is good, problems may occur. For example, Types III and HTS fibres did not debond before matrix failure at an axial load of 220 MN/m^2 . Therefore, a matrix of high compressive strength and toughness, free from microdefects is essential.

Type II fibre specimens gave clear debonding at axial loads of 135 MN/m^2 . They continued to debond smoothly in a direction away from the drill-hole as more load was applied. This indicated a poor resin-fibre adhesion because good bonding fails in a stick-slip fashion.

After boiling in water for one hour, the permeation of water into the specimens caused the matrix to swell and a light refractive layer was observed. Because of this swelling, the Type II fibres debonded even before compressing. Types III and HTS remained intact until matrix failure in compression.

4.3 EXPOSURE OF FIBRES TO VARIOUS FLUIDS.

Generally speaking the fibres behaved in a manner to be expected from the chemistry of bulk graphite. The relative degrees of graphitisation in the three fibre types were expected to give trends in behaviour from Type 111 to Type 1. It is the intention in this Section to first give a broad commentary on the results and then to analyse their specific nature.

The first example of a trend is shown in the effect of cold concentrated nitric acid (See Tables 4,5, and 6). The least ordered Type 111 fibres are most seriously affected, while Type 1 is least affected. The next most damaging reagent at room temperature is ferric chloride, where the same trend can be seen. The other reagent producing appreciable change at room temperature was sodium hypochlorite, which reduced the tensile strength of Type 111 but increased the strength of Types 11 and 1.

No other liquid reagent produced serious alterations in the mechanical properties at room temperature. Changes in modulus were generally similar to those in tensile strength. Organic reagents in particular had little effect.

Increasing the temperature of the reagents, first to 323K. and then to 363K., provided the expected acceleration in corrosion (See Tables 7 to 12). At 363K., both concentrated (sp. gr. 1.42) and relatively dilute (sp. gr. 1.21) nitric acid dissolved the Type 111 fibres at an early stage. The other two types resisted this drastic treatment well for the full 100 days and Type 1 was little affected. Sodium hydroxide had no effect on any of the filaments at 363K., but ferric chloride reduced the modulus values significantly at 323K.

The effect of halogen gases is quite small. Chlorine increased the

modulus slightly for 1 and 11 while reducing that of Type 111 (compare sodium hypochlorite). The very high strength and modulus of Type 11 fibres after nitrogen dioxide treatment is a phenomenon which will receive closer examination in Section 4.3.3.

None of the fibres appear to lose mechanical properties to any great extent at 523K. in air, although Type 111 is beginning to do so. At 573K. in air, Type 111 fibres are slowly oxidised away leaving a white residue of sodium carbonate (Pate 1V). This derives from the sodium compound originally used as an activator in the polymerisation of acrylonitrile, and is present at significant levels in Type 111, but in smaller quantities in Type 1. At 573K. in air, Type 11 fibres show a significant increase in strength and modulus, but Type 1 is unaffected after 100 days. Plate 1V (a) shows the formation of fissures in Type 111 fibre in air at 573K., which at one point have nearly joined to constitute a crack.

4.3.1 The Significance of Changes in Physical Properties.

(i) Diameter.

Apparent changes in diameter cannot be used as sound data for discussion because of the sampling size. The reason for this is that whereas they are necessary to calculate the fundamental properties of the material, they themselves vary enormously even within one fibre tow. In tow exposures one cannot ensure that the same fibre diameters have been measured before and after. The only reliable changes may be assigned to the several cases where fibres disintegrated altogether. These are clear cases of oxidation on Type 111 fibres of which air at 573K. and nitric acid at 363K. are examples.

(ii) Ultimate Tensile Stress.

Even from the simple relationship between heat treatment temperature and Young's Modulus, it is fair to assume that increasing the extent of graphitisation increases the modulus. The ultimate tensile stress is also sensitive to the degree and nature of graphitisation. However, another factor superimposes itself on this property, namely surface condition. In Fig. 4, the effect of internal and surface cracking is shown to have a drastic effect. Increases in this property after exposure may be explained as either an increase in extent of graphitisation or removal of surface flaws. The latter is likely to have the most marked effect and the former's contribution may be gauged from any increase in Young's Modulus.

(iii) Young's Modulus.

Although a simple relationship between the degree of graphitisation and Young's Modulus is acceptable for the present work, it may not describe the exact nature of the situation. For example, two separate

fibres may both contain the same proportion of graphitised carbon, but at the same time one may have its quota divided between many more sites. This being the case, then the latter would have quite different mechanical properties from that with fewer sites. In this work the concern has been with changes in properties and for this purpose both the fibres described above would show increases in modulus for increased graphitisation. It is safe to assume, therefore, that increases in modulus can be assigned as an increased proportion of graphitised to non-graphitised carbon. Decreases in Young's Modulus may be explained as plasticisation of the graphitic carbon by intercalating species or as a swelling effect from the same cause. This obviates the need to introduce an argument based on disordering of the system, which is not altogether clear for the case of intercalation.

4.3.2 Changes in Ultimate Tensile Stress.

Accepting that significant changes in ultimate tensile stress (U.T.S.) will be the influence of surface properties, it is convenient to discuss both U.T.S. and surface topography here.

Mild oxidative treatments, especially liquid reagents, appear to give 'smoothing' effects. Plates 1, 11 and 111 show losses in fluting, the Type 111 fibres being most affected.

Stronger oxidising conditions, especially gases, show extensive pitting as in Fig. (a) Plate 1V for Type 111 fibres.

If one assumes that mild oxidation occurs primarily in cases of low molecular or ionic mobility, it follows that diffusion of oxidant to the fibre surface is the rate controlling factor. This conclusion can be justified if the surface comprises a spectrum of sites of varying activity. This has been reported as the case for bulk graphite [141-2] and is even more likely to be true for less perfect graphitic structures. The chemical rate of oxidation at prime sites is controlled, therefore, by the slow rate of diffusion of oxidant to these sites. This mechanism will lead to the involvement of sites lower down the spectrum of relative activities by the proximity of oxidant on the surface. The involvement of all sites leads to general oxidation of the surface and notable 'smoothing'. Loss of flutings may be attributed to the presence of a higher proportion of active sites within them.

Vigorous oxidising conditions appear to give diffusion rates for oxidants that are large enough to give an adequate supply to the surface at all times. No restrictions are imposed on the prime active sites and in such cases high chemical rates are achieved. Local pitting is the result although general oxidation will also occur simultaneously.

Fibres that have been smoothed show appreciable increases in tensile strength, but those that become pitted are markedly weaker. Another mechanism leading to lower U.T.S. values involves initiation of a crack at an internal defect. This is illustrated in Fig. (a) Plate 1X and cannot be included as a consequence of post-manufacturing treatment.

Fig (c) Plate 111 shows a Type 111 fibre after exposure to ferric chloride solution. In the cold, a dross which probably consists of a precipitate of hydrated ferric oxide remains on the fibre surface. This is in marked contrast to the smooth surface of the filaments exposed at 363K., where surface oxidation predominates. This figure incidentally shows an inhomogeneity near the surafce of the fibre. Etching away of such inhomogeneities could increase tensile strength; this occurs with glass fibres.

4.3.3 Changes in Young's Modulus.

When the work began, improvement to Young's Modulus was considered unlikely. However, the results showed that in certain cases, notably with nitrogen dioxide, the Type 11 fibres gave significant increases which justified further examination. This discovery led to the work discussed in Section 4.4. The possible mechanism is discussed later, but the implication is of relevance here.

If the nature of the gases giving the most significant increases in modulus are listed, an interesting feature emerges. Nitrogen dioxide, bromine and chlorine, are all gaseous oxidants when damp. Bromine is known to intercalate graphite whereas uncertainty exists about the other two It has already been mentioned (1.3.2) that chlorine is thought to condense in the graphite pore system rather than intercalate. However, the exhaustive work of Hennig [127] may mean that in certain very special circumstances chlorine will intercalate. Moreover, Hooley [130] states that the system behave characteristically for condensation in a porous structure, but Jusa and Schmeckenberger [280] previously reported that the intercalating mechanism is not typical and requires the presence of HCl. It may be argued, therefore, that Hooley reported the adsorption isotherms were not characteristic of a typical intercalating mechanism and supported the findings of Jusa et al who also claimed to find the system unusual. Linked with the loss of diamagnetism in graphite after treatment with chlorine [129], which suggests intercalating, it is best to leave this question open.

Nitrogen dioxide will be discussed later in detail, but for the purpose of the immediate discussion it must be said that its intercalating powers are not known. Nitric acid strongly intercalates graphite, however, and it is therefore safe to assume a degree of intercalation

takes place for 'wet' nitrogen dioxide. The results of Table 8 are the product of damp conditions. All gases were introduced by displacement of air to unavoidably leave a trace of water vapour.

It emerges, therefore, that the gases are oxidants and most probably intercalating agents as well. This leads to a postulation that encompasses both properties in a mechanism of 'opening up' the fibre structure and preferentially removing amorphous graphite by oxidation. This is shown schematically in Fig. 66 with the structure 'condensing' upon removal from the attacking environment.

This mechanism is suggested with full consideration for accepted radial structure and the unlikelihood of new chemical bonds being inserted.

It is proposed that the gas diffuses into the porous structure intercalating the graphite regions. The resulting expansion of the fibre opens up non-graphitic sites for oxidation.

It is important to appreciate that both phenomena must operate. This gains support from the results for Type 1 and Type 111 fibres in the gases being discussed. The highly graphitic Type 1 fibres are subjected to intercalation, but oxidation is extremely slow. With Type 111 fibres, the dominance is reversed. Evidence for the oxidative properties of all three fibre types has been reported by Watt et al [177] who showed that the oxidation rates in air at the same temperature for Types 1 and 11 were about 1:600. This was attributed to the fact that Type 11 has many more reactive sites than Type 1.

The results show little change for Type 1 fibres in the three gases, but a slight downward trend, especially for chlorine, with Type 111 fibres.

This supports an argument proposing the importance of both properties acting simultaneously.

FIG. 66. Schematic Reorganisation of Ribbons.

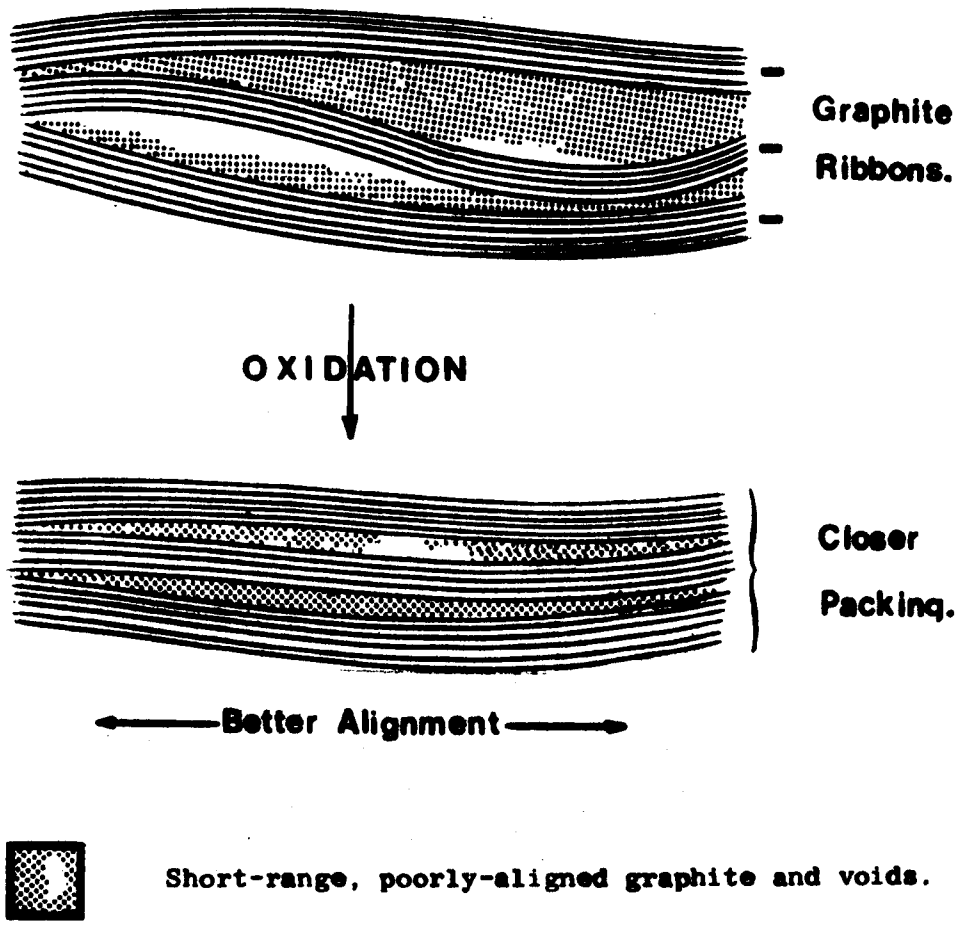

Several liquid reagents capable of intercalating graphite were amongst those used in the exposures, but it is interesting to note that none of these produced increases in Young's Modulus. Even with ferric chloride at 360K., which is strongly oxidising, no substantial increases in modulus were achieved. In fact, Type 11 fibres show small decreases. This suggests that accessibility is important and that the

hydrated ferric ions are unable to penetrate the intercalated system to reach active sites to oxidise them at an appreciable rate.

Air at 573K. has a marked effect on the modulus of Type 11 fibres after 100 days exposure. Increases in the region of 45% are recorded although Type 1 shows little change and Type 111 are destroyed at this temperature. The fact that oxygen (in air) does not intercalate graphite need not contradict the previous hypothesis for a mechanism giving modulus increases. Thorne and Price [168] reported that during gaseous oxidation an initial process of opening and widening capillary pores takes place. The oxidant, at high temperature, is then capable of diffusing into the fibre pore structure and oxidising material at active sites.

This phenomenon has been observed in the present work and is dealt with later. The failure of oxygen to intercalate but still be able to raise the modulus by selective oxidation suggests that chlorine may possibly use this mechanism also.

The postulation of selective removal of amorphous carbon to raise the Young's Modulus relies on subsequent 'collapse' of the resulting structure. Without a reduction of diameter, the stiff graphitic content, having remained constant, will give modulus values similar to those before treatment. It is only condensation of the graphitic zones that will give the observed effect. It is not proposed that graphitisation is occuring, but rather that the ratio of graphitic to non-graphitic carbon is being raised by preferential removal of the latter.

The need to examine this phenomenon further, including the anomalous behaviour with regard to present sheath and core theories, led directly to the work programme of Section 4.4.

4.4 CHANGES CONFERRED ON THE MICROSTRUCTURE OF CARBON AND GRAPHITE FIBRES BY CHEMICAL TREATMENT.

A suggestion has been made in Section 4.3.3 that the modulus of Type 11 fibres has been raised during chemical treatment by a mechanism involving selective removal of non-graphitic material.

There is no doubt that where a simple choice exists for oxidation of graphitic or amorphous carbon, the latter will be preferentially removed. The problems arising here, however, may be crystallised thus:-

(i) Can a simple argument be found which explains the facts based on existing knowledge of the radial structure of carbon fibres?

(ii) Can amorphous carbon be removed from deep within the fibre?

(iii) If carbon can be removed, then:-

(a) How does oxidant gain access?

and (b) Is it possible for the structure to condense afterwards?

The approach to the work has been, first of all, to confirm the applicability of existing theories of radial structure to the fibres under examination (4.4.1). With this established, the theoretical and experimental consequences of etching were compared (4.4.2 and 4.4.3).

Convinced that simple etching could not account for the observed modulus increases, attempts were subsequently made to identify physical changes either as they occured (4.4.4), or in the graphite fibre residues (4.4.5).

4.4.1 Confirmation of the Sheath and Core Theory.

Does the known radial structure for Type 11 fibres merit modulus rises from pure etching away of surface? If it does not, then a graphitic rearrangement within the fibre seems likely. Because the temperatures at which modulus increases have been achieved are well below those used for heat treatment, a conventional graphitisation process could not have taken place.

Recent theories on radial structure are detailed in Section 1.2.9. They are listed below:-

A. Outer orientated graphite sheath, inner less graphitic core [87, 120] [14, 121, 118, 115, 25, 47, 122, 123, 97, 108]

B. 'Spokes of wheel' structure [124-5, 108, 120, 123]

C. Third highly graphitic phase (location doubtful) [90, 93, 91, 114]

All three structures assume an outer core of well developed, aligned, graphitic crystallites, and an inner less ordered core.

The observations of Jones et al [115, 25] and Perry et al [121, 118] were confirmed by plotting Young's Modulus against diameter (Fig. 67) for untreated Type 11 fibres. A degree of orientation was also observed in transverse fracture surfaces which supports a sheath and core structure(Pl.1

Although it is appreciated that the sheath and core are not discrete regions, it was found informative to deal with them mathematically as such.

Assuming the outer and inner regions to be joined by an interphase, which, for the present argument is assumed to be infinitely thin, the curve (Fig. 67) may be solved by a 'best-fit' method. Thus:-

$$E_f A = E_{sh} A' + E_{co} A''$$

$$A = \frac{\pi d^2}{4}$$

$$A' = \pi s(d-s)$$

$$A'' = \pi\left(\frac{d}{2} - s\right)^2$$

E_{sh} = Modulus of sheath

E_{co} = Modulus of core

s = Sheath thickness

d - Fibre diameter

For the Type 11 fibre, this gives values of (See Appendix 2)

$$E_{sh} \approx 540 \ GN/m^2$$

$$E_{co} \approx 40 \ GN/m^2$$

$$s \approx 1.09 \ \mu m$$

Type 111 gives values of :-

$$E_{sh} \approx 300 \ GN/m^2$$

$$E_{co} \approx 150 \ GN/m^2$$

$$s \approx 1.1. \ \mu m$$

Although it is accepted that these values are not perfectly accurate, they may act as a rough guide. An interesting feature of the results is the apparent drop in core modulus. This may give some insight into the mechanism operating during graphitisation. We may assume from the slope of the Type 1 modulus - diameter curve, compared to the others below, that this downward trend is continued (ie. the disparity between sheath and core moduli increases from Type 111 to Type 1)(See Fig. 68).

One possible explanation of this phenomenon is the progressive 'shrinkage' of the sheath as graphitisation proceeds. Support for this is given by Mrozowski cracking in fibres produced at high heat treatment temperatures [93, 115]. The thermal shrinkage stresses result in surface cracking, but compressive stresses also undoubtably exist during heat treatment as compacting of the sheath by graphitisation occurs.

FIGURE 67. DIAMETER v's YOUNG'S MODULUS [Type II]

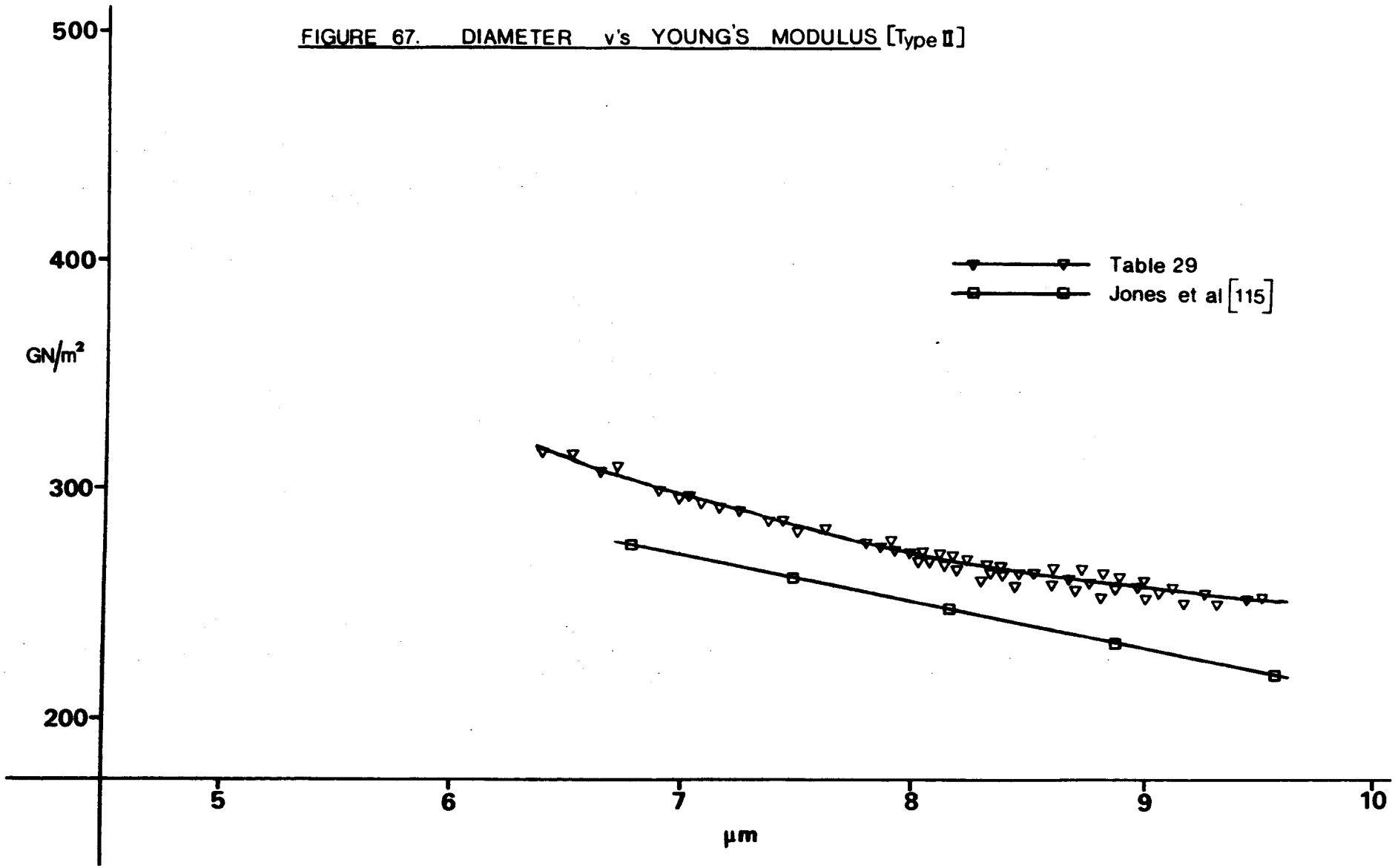

FIG. 68. Diameter-Modulus Relationships. [115].

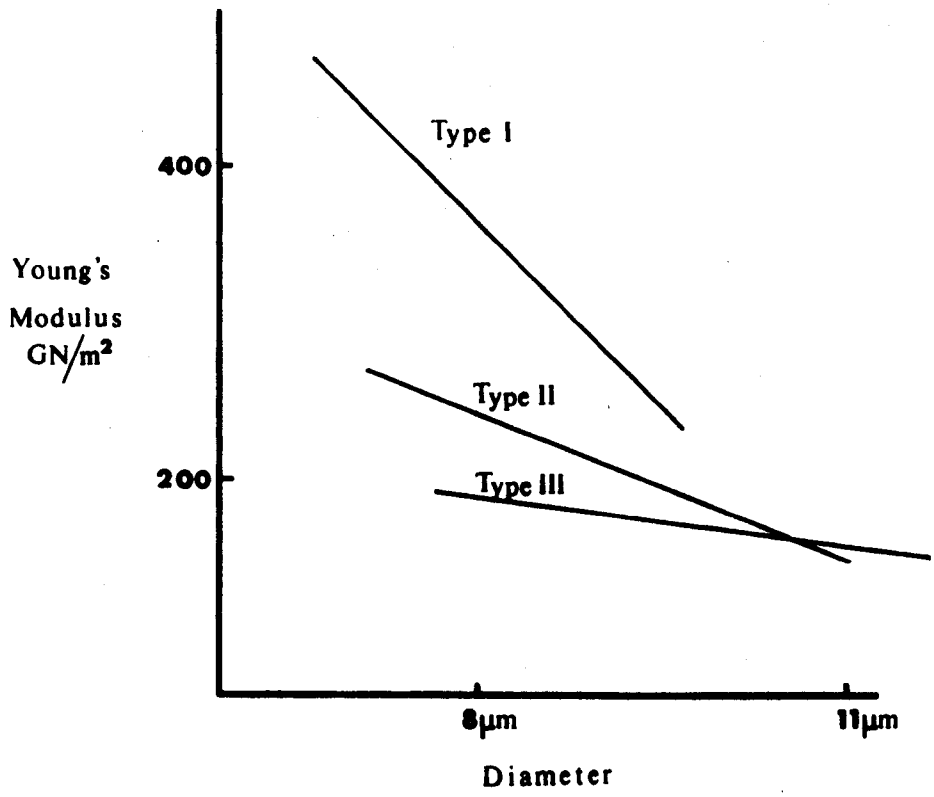

A residual axial compressive stress linked with the extent of graphitisation could explain why the core contributes less and less to the overall fibre modulus as H.T.T. increases.

4.4.2 The Theoretical Consequences of Etching.

Removing material from the outer surface of a fibre might explain modulus increases simply from radial structure considerations.

To test this hypothesis, it is necessary to plot a theoretical curve for diameter changes versus modulus during etching. The curve (Fig. 69) assumes that etching is solely the removal of the outer surface of a sheath and core structure. The values for sheath and core moduli are those of Type 11 fibres.

Clearly, unless a third phase of extremely highly graphitised material existed in the centre of the fibre, a simple etching of outer layers would not give modulus increases.

4.4.3 The Consequences of Etching with Nitrogen Dioxide.

To confirm the findings of Section 4.3 with regard to exposure to nitrogen dioxide, the experiments of 2.3 were begun. Typical results of Table 30 are plotted below and graphically illustrate modulus rises for exposures on adjacent fibre portions (Fig.70). Four 0.8 m. lengths of Type 11 fibre are represented. The values on the extreme left and right are for the untreated ends of the sample filaments. The inner portion has been divided into three parts and exposed to NO_2. Diameter changes are shown in the upper graph, modulus in the centre graph, and theoretical modulus (based on simple etching of sheath and core) in the bottom graph. Even assuming a radial structure of the 'spoked wheel' type would not explain the increases in modulus experienced after treatment with nitrogen dioxide.

More vigorous treatment with nitrogen dioxide has produced the results of Table 31 which are plotted in Fig. 71 showing the theoretical curve for reference.

With this evidence it is safe to conclude that the present

FIG. 69.

THEORETICAL PLOT OF MOD. v's ETCHED DIAM. – Schematic Sheath & Core (Type II)

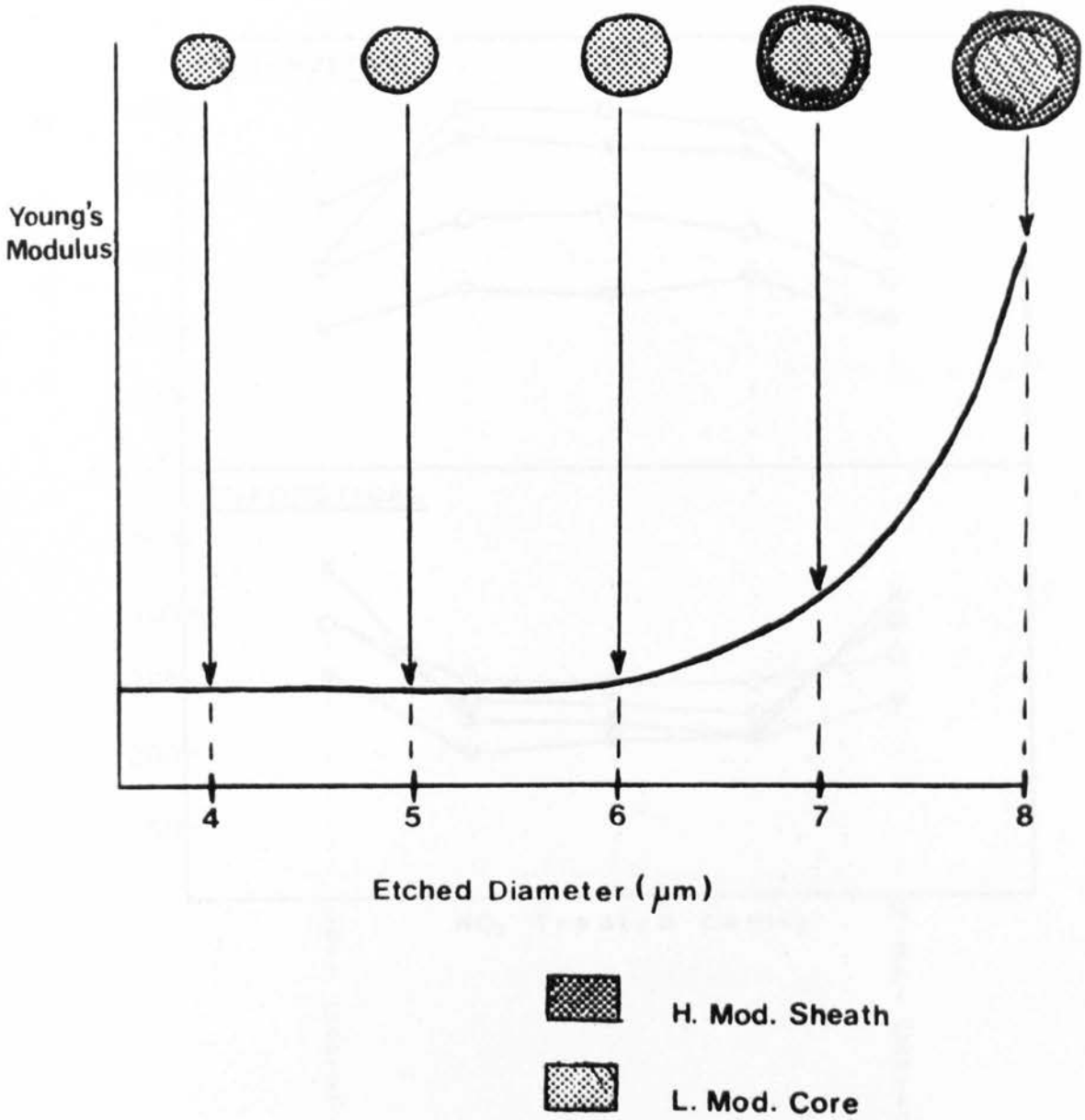

FIGURE 70 Table 30 v's simple etching of sheath & core.

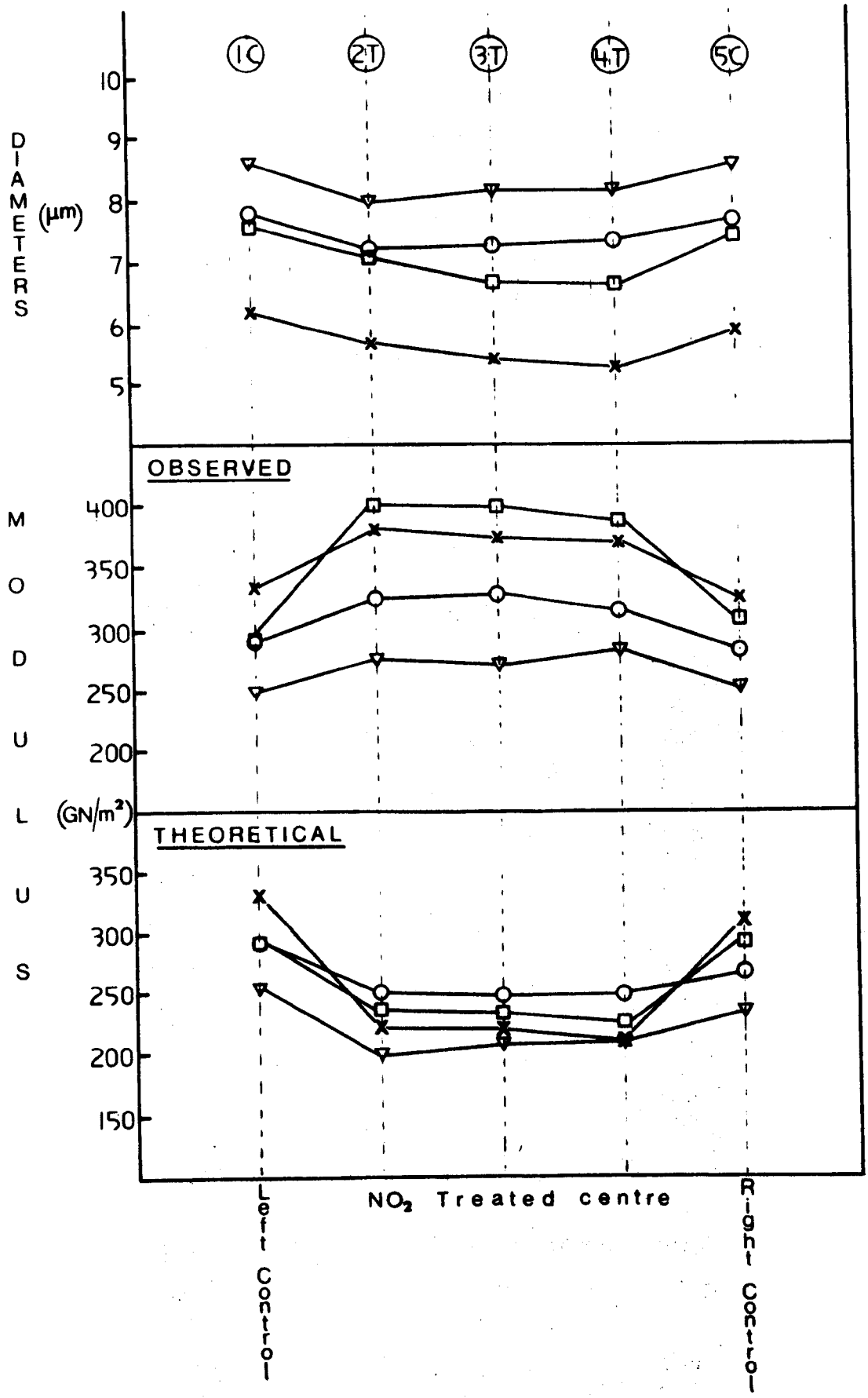

FIG. 71. Diameter/Modulus Curves for Type II Fibre NO_2 Treatments.

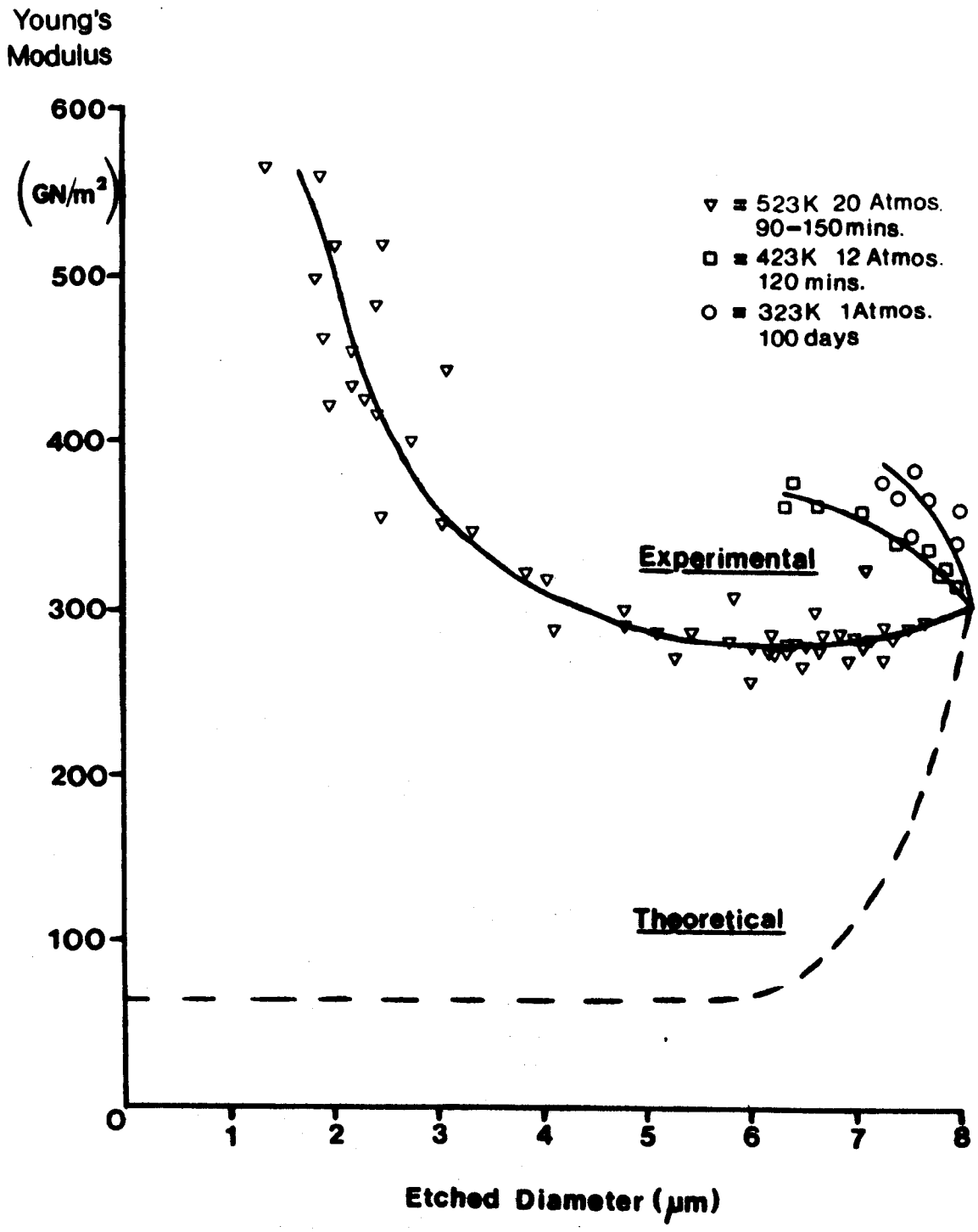

knowledge of radial structure cannot explain the observed effects. Unless the very basis of 'sheath and core' theory is attacked, it must be accepted that chemical modification of the fibre structure has taken place.

4.4.4 Physical Changes Observed During Oxidative Treatment.

Because a substitute for the 'sheath and core' theory does not exist, nor could one be readily contrived to satisfy both diameter and oxidation phenomena, the questions raised about removal of amorphous carbon from within fibres have been tested. The first requirement of such an investigation into the mode of attack by nitrogen dioxide on Type 11 graphite fibres is a better understanding of the gas.

(i) Chemistry of Nitrogen Dioxide.

Nitrogen dioxide exists in a strongly temperature dependent equilibrium with the dimer, dinitrogen tetroxide (N_2O_4). In the solid state the oxide is completely N_2O_4, at the boiling point (294.15K, 760 mm/Hg) 0.1% NO_2 exists. Dissociation is complete above 413K. Nitrogen dioxide is an odd electron molecule, thus accounting for its deep red-brown colour and ready dimerisation to diamagnetic N_2O_4. It can fairly readily lose its odd electron (ionisation potential 9.91 ev) to form the nitronium ion, NO_2^+. In the liquid state, most chemical evidence is consistent with NO^+ and NO_3^- being present or easily formed. The $NO^\bullet$ and $NO_3^\bullet$ radicals are also fairly easily formed and are almost certainly present in the gaseous phase.

Thermal decomposition of NO_2 begins at 423K. and is complete at 873K. to give oxygen and oxides of nitrogen.

This summary of the relevant chemistry of nitrogen dioxide shows that many reactive species are present in the conditions of treatment used so far. The complex equilibria may facilitate the action of one or more of the less predominant species without hindrance.

Very little has been published on the interactions between graphite and nitrogen dioxide. All oxides of nitrogen are known to be absorbed by graphite at 303K. [284-5]. Above 398K. graphite is oxidised by NO_2

to CO_2 . The amount of solid being oxidised is given by the expression $C = Ae^{b/T}$ where, in the range 373-423K.; A = 1.793 and b = -1370, and between 423 and 473K. A = 0.2433 and b = 494. At 423K. the reaction is first order with respect to NO_2, and the energy of activation is less than 3Kcal mol^{-1} [286] (cf. Air oxidation -46K. cal mol^{-1} [177]). Rate of reaction is inversely proportional to extent of graphitisation, and is initially rapid but quickly becomes diffusion controlled.

Clearly, nitrogen dioxide at 423K.+ is capable of extremely low energy oxidation of a selective nature. The rate and extent of oxidation by gaseous oxidants are governed by the following parameters:-

(i) Rate of diffusion of oxidant to the surface $<$ rate of chemical reaction and diffusion to interior.

(ii) Rate of chemical reaction and diffusion to interior $<$ rate of diffusion of oxidant to the surface.

(iii) Rate of chemical reaction and diffusion to interior $\approx$ rate of diffusion of oxidant to surface.

(iv) Rate of diffusion to interior $<$ rate of chemical reaction.

(v) Rate of diffusion to interior $>$ rate of chemical reaction.

It is unlikely that rate of diffusion to interior is $>$ rate of diffusion to the surface.

In the regimes of cases (i) and (ii), diffusion and then chemical rate are the dominating features of overall rate. For case (iii) small temperature variations may cause the reaction control to move either way.

The domains of these relationships are uncertain. At very low temperatures, chemical reaction rates are slow enough for (ii) to be applicable. For carbon fibres in tows at high temperatures case (i) is valid.

Of the five cases, (iv) and (v) are the most interesting and relevant in this discussion. The balance of these two interactions decides whether gross surface oxidation (iv) or extensive internal oxidation (v) will predominate.

The ideal conditions for the mechanism of selective carbon removal are:-

(a) Plentiful supply of oxidant to fibre ie. fast diffusion rate.

(b) Rapid diffusion to interior.

(c) Fast, selective oxidation of non-graphitic material. (These conditions ignore mechanical consequences for the moment).

Thus, ideally, rate of diffusion to surface $>$ to interior $>$ chemical reaction.

The rapid diffusion to the interior may be helped if the fibre structure is initially 'opened up' by oxidation or intercalation

Although nitrogen dioxide is not thought to intercalate graphite, it is safe to assume that when damp conditions prevail, nitrate ions will be present. Nixon et al [293] have shown that in very low concentrations of nitric acid vapour, the NO_3^+ ion intercalates to give order-disorder transformations in network stacking of synthetic graphites. These transformation are important when considering the proposed mechanism of 'reshuffling' for turbostratic to three-dimensional networks (See Fig.72).

At extremely low NO_3^+ concentrations sequence 4 predominates. Fibres immersed in nitric acid, however, give sequence 1. The failure of nitric acid to give modulus increases by the proposed mechanism might be ascribed to the immediate formation of sequence 1 and the low diffusion rates of hydrated ions within expanded graphite.

(ii) Air Oxidation.

The results for oxidation in air (Table 13) and the need to identify

FIG. 72. Intercalation Sequences for NO_3^+ in Graphite. [293]

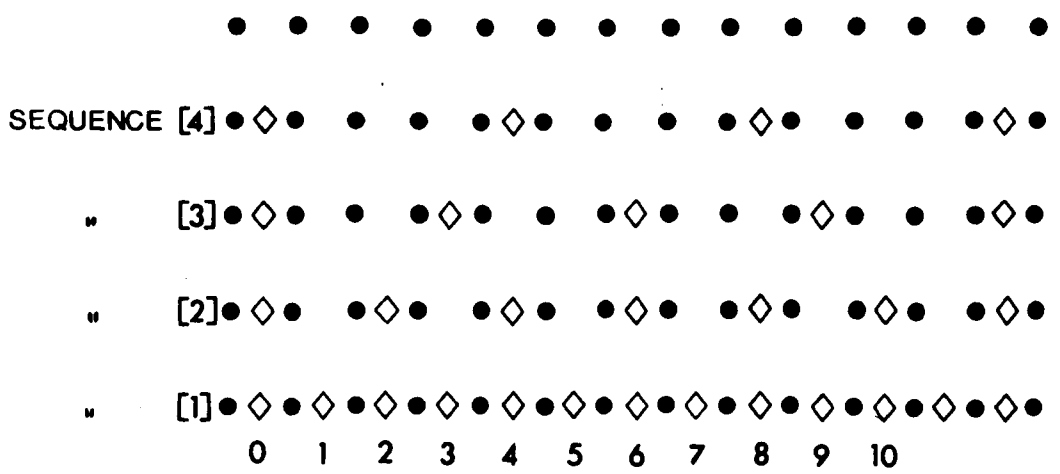

◇ = Nitrate ions

● = Graphite planes

the 'opening-up' of the fibre structure led to the experiments of 2.3.9 (Tables 32-4)It was hoped to identify different rates of diameter loss for sheath and core at the same time. The results are plotted in Figs. 73, 74 and 75. The graphs indicate that either a very thin sheath exists, of the order of 0.4 μm, or an initially slow oxidation rate during an 'opening-up' process can be expected with Types 1 and 11 graphite fibres. Both these possibilities are supported strongly in the literature. Johnson, D.J. et al[287]recently claimed the sheath on high modulus fibres to be only 0.1 μm thick. The evidence for 'opening-up' the porous structure has already been discussed in Chapter Two. The important points

FIG.73 OXIDATION – Type I

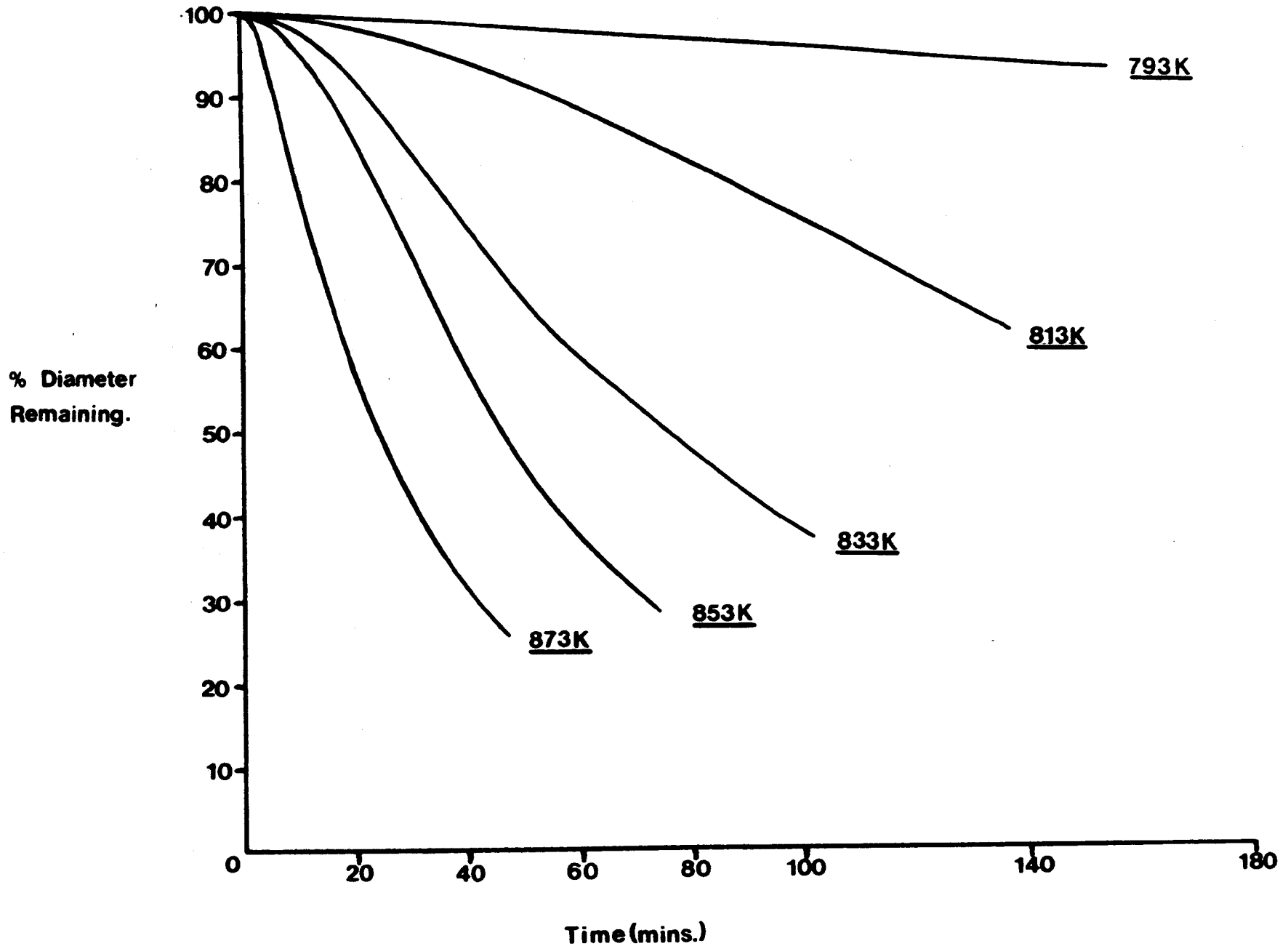

FIG. 74

OXIDATION – Type II

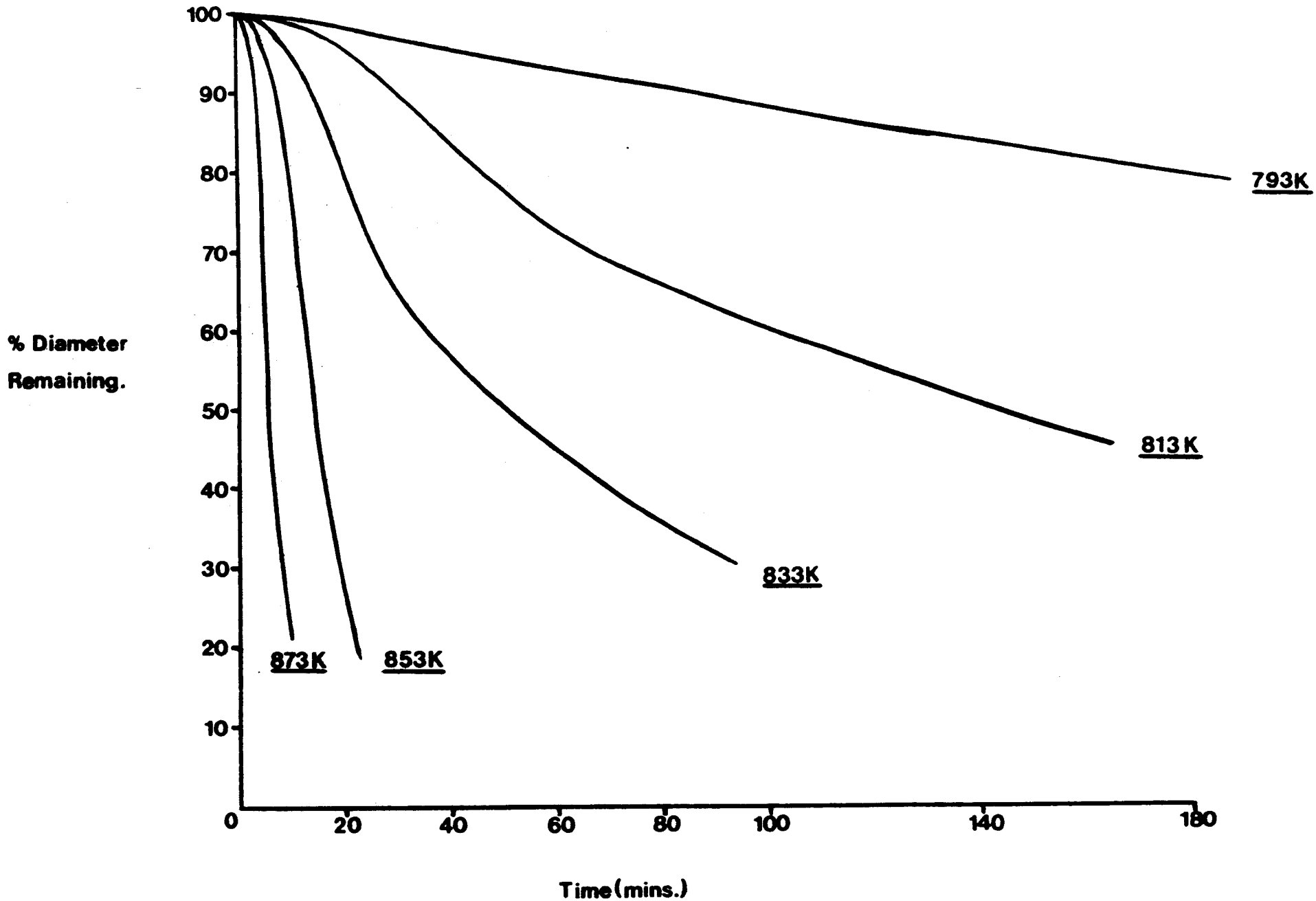

FIG. 75

OXIDATION —Type III

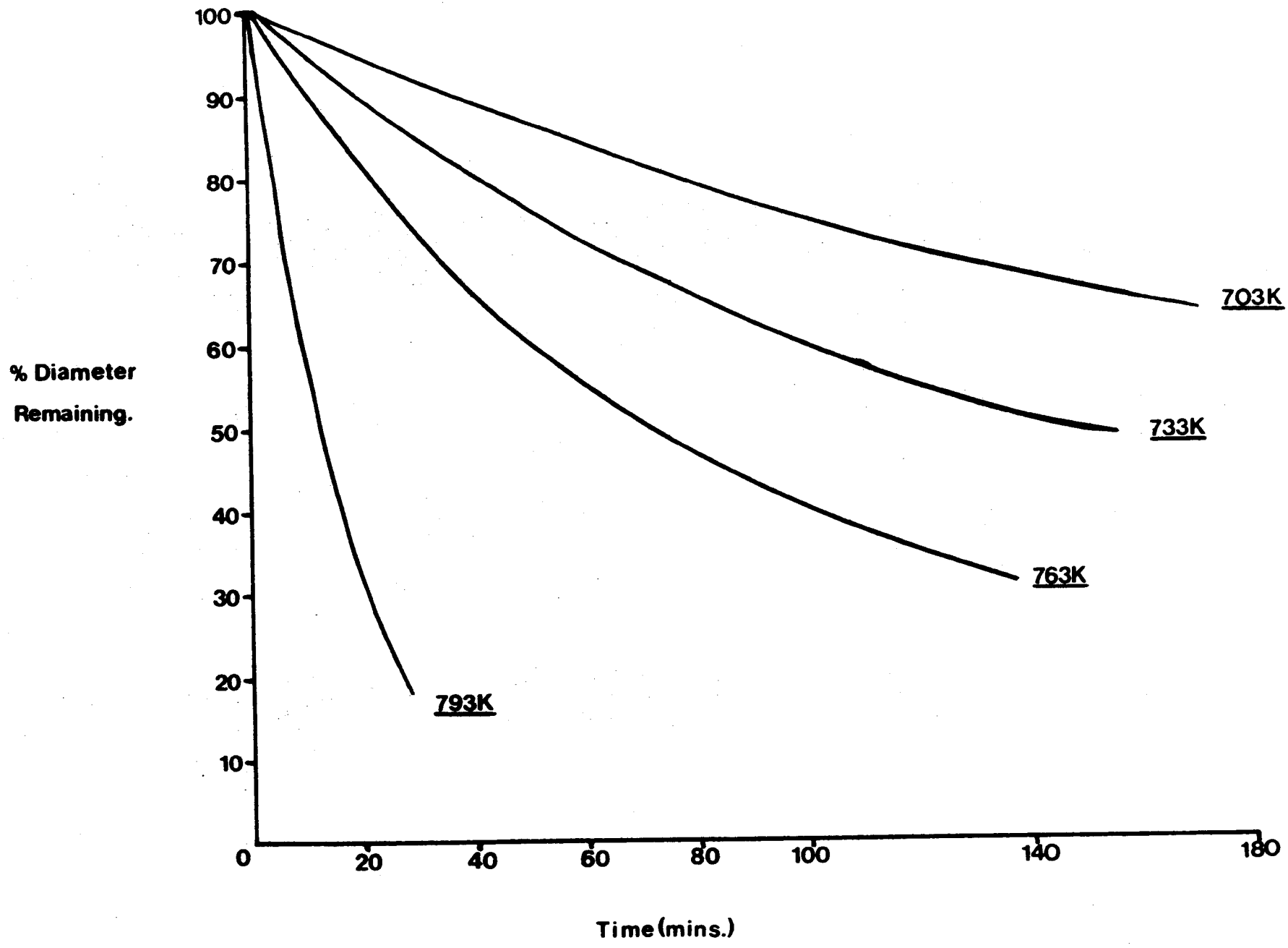

to be made, however, are the obvious temperature dependency of oxidation and the gradual decrease of the rate of diameter loss with fibres experiencing moderate conditions. The best examples of this are shown by Type 11 fibres at 833K. and 813K.; Type 1 fibres at 833K. and Type 111 fibres at 703K., 733K. and 763K.

All these treatments failed to give smooth surfaces, but the results, linked with the brief study made on T.G.A., show an interesting point. Rate of diameter loss need not necessarily reflect rate of loss of material if the deep oxidation is occuring. Examination of the rate of material loss, using T.G.A. results, shows that whereas the rate of diameter loss decreases, the rate of material loss does not (at least it does not at the values for diameter loss experienced here). This very strongly supports a mechanism involving removal of material from the interior of the fibre. Air treatment appears to be even more uncertain with regard to raising the modulus of Type 11 fibres than treatment with nitrogen dioxide. All the fibre types showed the well-known behaviour of removal of flutings, pitting and local thinning (Fig. (c) Plate X1) followed by premature fracture. It was felt, however, that the elimination of a carbon dioxide gradient through fibre tows by using single filaments was not sufficient precaution to prevent the oxidation from being diffusion controlled. By lowering the temperature of oxidation, a truly chemical rate controlled oxidation gave smoothing effects with Types 1 and 11 but not with 111.

These facts led to the conclusion that under moderate oxidising conditions with the interior of the fibre accessible, preferential removal of amorphous carbon by air seems likely. Pitting from vigorous oxidation in this diameter monitoring technique is shown in Figs. (a)

and (b) (Plate X).

(iii) Nitrogen Dioxide Oxidation.

The work described above was carried out in air essentially for convenience. To have spent this time overcoming the difficulties that precluded the use of nitrogen dioxide in the hot stage of the microscope would have been unjustifiable. The more successful treatments with nitrogen dioxide, however, gave convenient fibres for the subsequent examinations of structural changes. Unbroken residues with diameters in the range 1.8 to 3.0 μm were characteristically smooth (Plate XIII). They were also of highly uniform diameter, in contrast to the controls, and possessed considerably higher Young's Modulus. No substantial increases in modulus were found in fibres etched by this method until the diameters were less than 4 μm. No increases in modulus were found on examining the residues from Type III (low HTT) fibres. It was not found practicable to thin Type III fibres to very small diameters without fracture, although perseverance might eventually result in the selection of suitable conditions.

All subsequent examinations were exclusively on Type II fibres.

4.4.5 Physical Changes Observed in Treated Fibre Residues.

Experimental support has already been given for the 'sheath-core' theory, which is, therefore, acceptable in principle. It has also been shown that diameter-loss data agrees with simple removal of outer layers during oxidation. The remainder of this discussion centres around the possible structural rearrangements and the evidence obtained to support them.

The remaining question posed at the beginning of Section 4.4. may now be reworded. If a modulus increase is to be achieved without new graphitic regions being formed, does 'condensation' of the remaining graphitic 'skeleton' follow removal of amorphous carbon?

The answer must clearly be 'yes' to explain the modulus rises. There are many methods by which structural alteration may be detected, of which several have been tried (2.3.4., 2.3.5., 2.3.6., 2.3.7., and 2.3.8.).

(i) Polarised light microscopy failed to identify structural changes (Plates XIV and XV).

(ii) The better alignment, higher proportion of graphitic carbon and denser packing which should result from the proposed oxidation mechanism were investigated by electrical resistivity and specific gravity measurements (See Tables 35 and 36). Using the curve of Watt for resistivity plotted against heat treatment temperature, the treated fibres with substantial diameter reductions show that considerable effective graphitisation has occured (Appendix 3).

Treated fibres were found to have apparent densities of up to 3.5% higher than those of the controls. This denser packing cannot be attributed to any other cause but condensation of the fibre structure. It is equivalent to a rise from 2073K. to 2373K. in H.T.T.

(iii) The examination of the degree of crystallinity using high resolution transmission microscopy and electron diffraction proved to be the most useful technique employed.

Initial studies on fibres treated singly, and already tested to show significant modulus rises, gave promising results.

Powdered fragments of control and exposed single fibres with diameters in the region of 2 μm were examined. Plate XVI is a high resolution micrograph of the most perfectly graphitised phase in control Type II fibres. This is similar to previously reported [93] micrographs with perhaps a larger amount of disorientation.

Plates XVII and XIX (Fig. (a)) are of an extremely well graphitised phase which would be expected to result from normal graphitisation during heat treatment of the material in Plate XVI. The circular turbostratic crystallites are most unusual in that they are not normally seen in P.A.N.-based fibres and that they have a much smaller diameter than inclusions seen in pitch and lignin-based fibres. Polygonal inclusions indicate three-dimensional graphite; this is borne out by electron diffraction observations. These structures are extremely interesting and there is considerable interlinking of the crystallites, especially in the specimen of Plate XVIII.

In an effort to locate the regions of highly graphitised material, a transmission electron microscope study of sections was subsequently attempted. Several fibre tows were treated in nitrogen dioxide for 2½ hours at 503K. Single filaments were not exposed because it was thought, possibly erroneously, that risking unpredictable treatments was not necessary and the sectioning of single fibres would be more difficult in any case.

Initial confusion over the appearance of the treated tows is demonstrated in Fig. (a) (Plate XII). The oxidised tow has fused together to give one 'fibre' of about 8.0 μm diameter. The fact that this is truly a bundle of fibres with drastically reduced diameters is only apparent from subsequent pictures (Figs. (b) and (c) Plate XII).

The fusing of the tow might be responsible for the disappointing results obtained. Fig. (b) (Plate XIX) is an electron diffraction pattern of oxidised fibres showing only moderate preferred orientation which can readily be found in Type II control fibres. Fig. (c) (Plate XIX) shows a degree of preferred circumferential orientation with a random graphitic layer apparently deposited on the surface. This 'nodule' like graphite appears to be the 'glue' in the fused tows resulting from nitrogen dioxide treatment. Diffusion, and hence successful fibre treatment, would clearly be hindered in the fused tow. It has already been shown that the carbon dioxide gradient formed during oxidation of fibre tows, has a deleterious effect on diffusion of oxidant to the centre. It would appear that the higher temperature of this treatment (which was employed to ensure complete treatment) and the use of tows, has achieved an effect opposite to that desired. The oxidation appears to have become very markedly diffusion controlled which has resulted in surface oxidation prevailing (see earlier discussion). This is not only referring to oxidation being confined to the outer layers of the individual fibres, but also to the outer regions of the tows. The evidence of Figs. (a) and (b) (Plate XIX) shows that the fibres contained in the residual fused tow have probably only just been exposed to extensive oxidising conditions. These conditions are not even conducive to exceptionally 'deep' oxidation, judging by the temperature sensitivity found with oxidation in air. If this explanation

is correct, then as little as 10% of the fibres' structures have been modified. This accounts for the electron diffraction pattern and 'typical' transmission picture (Figs. (b) and (c) Plate XIX) recorded for the sample.

It is just possible that the fibrillar 'dross' on the specimens shown in (b) and (c) (Plate XII) are the extremely fine (<0.1 μm) residues of fibres previously on the outer edge of the tow.

4.4.6 The Proposed Mechanism Giving Modulus Increases.

The crucial factor involved in the proposed 'deep' oxidation mechanism is access of oxidant to the inner regions.

Donnet and co-workers [288] concluded, by examination of the residue left after oxidising away 96% by weight of a fibre bundle in nitric acid, that the process if graphitisation can begin in fibres which had never been heat treated above 1373K. In the light of existing knowledge of the action of hot strong acids on bulk graphite [22] (See 1.3.2) this may be a hasty conclusion because some rearrangement may have occured.

The NO_3^+ ion is known to be a strong intercalating agent, and the presence of it in moist NO_2 and the experiments of Donnet [288] and Nixon [293] may not be coincidental. The strong dependence of successful fibre treatments upon pressure and temperature may indicate the involvement of an intercalation process. Intercalation may produce the extensive 'opening-up' of the fibre interior to oxidation, especially in the locality of existing graphitic refions. A 'reshuffling' of layers may occur as the intercalating molecules are inserted and withdrawn. (See 'chemical working' 1.3.7). The rearrangement of layer planes will be influenced by residual stresses in the fibres. Because these tend to be compressive stresses, the suggestion that 'condensation' of the structure ensues seems acceptable. The discovery of extensive regions of three dimensional graphite in treated fibre must confirm the mechanism for rearrangement

The proposed mechanism, for which substantial evidence has been given, is summarised schematically in Figs. 76 and 77.

FIGURE 76

SCHEMATIC X-SECTION

graphitic carbon

amorphous "

intercalated graphite

voids

Turbostratic graphite ribbons with voids and amorphous carbon. Residual compressive stress tending to collapse the structure inwards.

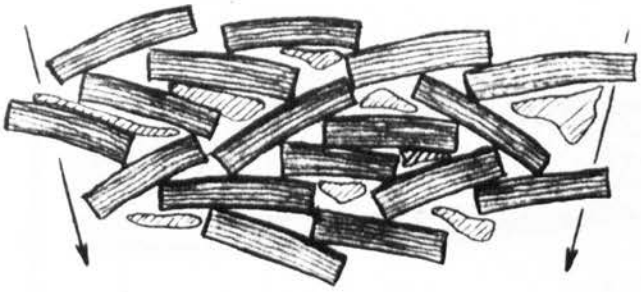

Intercalation of graphite phase.
'Opening-up' of structure.

Oxidative removal of amorphous graphite.

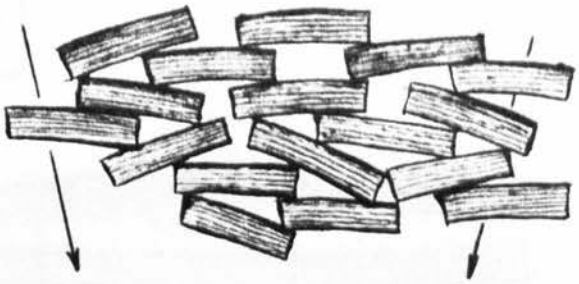

Removal of intercalation agent. Collapse and rearrangement of structure. Also basal plane stacking sequence changes.

FIGURE 77

SCHEMATIC LONGITUDINAL SECTION

graphitic carbon

amorphous "

intercalated graphite

voids

Turbostratic graphite ribbons with voids and amorphous carbon. Residual compressive stress tending to collapse the structure inwards.

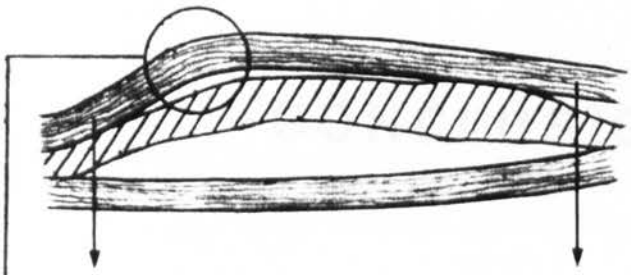

Intercalation of graphite phase.
'Opening-up' of structure.

Gradual rearrangement of stacking sequences towards ABABA....

Oxidative removal of amorphous graphite.

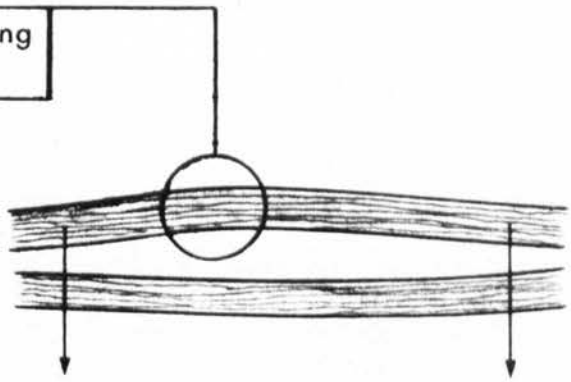

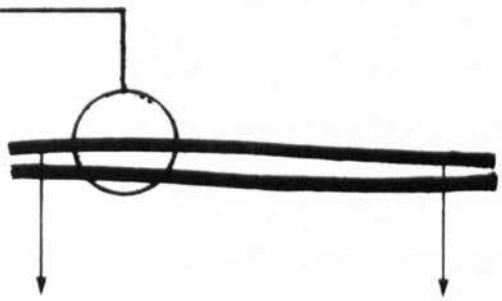

Removal of intercalation agent. Collapse and rearrangement of structure.

CHAPTER FIVE

-CONCLUSIONS-

CONCLUSION.

The aim of the work was to elucidate the mechanisms that are involved in the chemical attack by gases and liquid reagents on carbon fibres and their phenolic composites. As the result of changes in Young's modulus conferred on Type 11 fibres by certain gases, a further examination of changes in these fibre's microstructure was instigated. The conclusions of these three areas of the work programme are dealt with below.

5.1 Three primary modes of attack by reagents on phenolic composites have been identified which are:- matrix swelling; leaching out of low molecular weight material; and oxidation.

(a) Caustic alkali swells the matrix thus relieving compressive forces at the fibre-resin interfaces. Loss of overall mechanical integrity, as measured by shear and flexural properties, results from weakening of both the matrix and the matrix-fibre interfacial-bond.

(b) Butanone and industrial methylated spirits leach out low molecular weight material to relieve compressive stresses at the fibre-resin interfaces. Matrix weakening and matrix-fibre interfacial bond failure are the result.

(c) Oxidation appears to be controlled by the chemical reaction rate and hence, it is a surface phenomenon. Oxidising agents appear to attack accessible surfaces, both internal and external, rather than diffuse through the matrix.

Acetic acid and ferric chloride appear to give anomalous results. Glacial acetic acid has been suggested to give mild swelling and leaching

with perhaps some specific attack at the fibre matrix interface. Ferric chloride results have been explained by invoking a mechanism of fibre intercalation.

Highly graphitised fibres bond weakly to resins and so give poorer shear properties than lesser graphitised types. The effects of (a) and (b) are to bring all shear properties down to the same low value. The effect of (c) is that the accessibility of internal surface conferred on Type 1 fibre composites by poor resin-fibre adhesion leads to more extensive attack. Better bonded fibre types give composites correspondingly more resistant to oxidation.

5.2 Two types of reagent attack carbon and graphite fibres.

(a) OXIDISING AGENTS.

These attack the least graphitised (Type 111) fibres most vigorously. The attack becomes less pronounced going through the three types to the most graphitised (Type 1).

(b) INTERCALATING AGENTS.

These attack the most graphitised fibre type to give 'swelling effects' on mechanical measurements for cases where the intercalated graphite is stable at room temperature and pressure (the conditions of test).

When both (a) and (b) operate together, or possibly to a limited extent, just (a), substantial increases in Young's modulus are obtained. The mechanisms of fibre modification giving these increases was investigated in the third part of the work programme.

5.3 Type 11 graphite fibres undergo an interaction with nitrogen dioxide which is extremely temperature and pressure sensitive. The

results of this interaction are increases in Young's modulus, diameter reductions and surface smoothing.

It is proposed that preferential removal of non-graphitic carbon has occured to a fixed depth below the fibre surface. The depth and extent of carbon removal are governed by temperature, pressure and time.

It is also proposed that graphitic rearrangements occur, both in the stacking sequences and ribbon conformations. These are best induced by insertion and removal of an intercalating species, which is most probably NO_3^+.

RECOMMENDATIONS FOR FURTHER WORK.

Two areas of the work herein presented require further examination.

1. The mechanism by which glacial acetic acid at 323K. attacks composites of carbon fibre and Xylok resin is by no means clear from the data collected. Detailed surface examinations to detect adsorbed layers after immersion of the three fibre types in acetic acid may lead to a better understanding of this system. Further work observing the ingress of 'labelled' acid molecules into the composite system might be informative.

2. The need to repeat electron microscopic studies of the residues left after NO_2 treatment of single filaments is vital. High resolution electron transmission examination of sections of such residues should prove conclusive evidence in support of the hypothesis in 5.3.

Higher resolution in polarised light of treated samples or moderate resolution of less vigorously treated specimens, may indicate that structural changes have occured.

APPENDIX I.

STATISTICAL CALCULATIONS.

The arithmetic mean $= \frac{\sum X}{n} = \bar{X}$

where X = observation

n = Number of observations

Since deviations are always positive then

Mean deviation $= \left[\bar{X} - X\right]$, or $\left[X - \bar{X}\right]$

Variance: is the sum of the squares of the mean deviations divided by one less than the total number of observations

ie. variance $(\sigma^2) = \sum X - \bar{X}$

The square root of the variance is termed the standard deviation (σ)

Confidence Limits.

Confidence limits define, for a given degree of confidence, the limits within which the true value of the arithmetic mean lies

Confidence limits $= \pm \frac{t\,\sigma}{\sqrt{n}}$

where t = Student's t

n = number of results

For 95% Confidence limits (ie. 0.05 Probability Level) the value of $\frac{t}{\sqrt{n}}$ is

n	$\frac{t}{\sqrt{n}}$
3	2.483
5	1.243
10	0.6723
15	0.5325

APPENDIX 2.

The equation

$$E_f A = E_{sh}A' + E_{co}A''$$

is based on the relative cross-sectional areas of sheath and core. Thus, the overall modulus of the fibre comprises a sheath area of high modulus material and a core of lower modulus.

The curve of Fig. 67 gives values of E_f and d. Substituting three pairs of values into the equation above will give solutions for the three unknowns; E_{sh}, E_{co} and s. The quadratic in 's' does not allow quick computation of answers, however, and so a more convenient method was adopted

This method involves a trial and error procedure which rapidly gives accurate values for E_{sh}, E_{co} and s.

Logically, because the sheath is of a fixed thickness and its modulus is considerably greater than that of the core, the actual slope of the graph and its curvature gives strong indication of the sheath dimensions.

Using the values: E_{sh} = 540 GN/m

E_{co} = 40 GN/m

s = 1.09 um

we have:—

when d = 10 μm, E_f (Calculated) = 244GN/m^2 (c.f. Exptl. ≃ 245)

d = 8 μm, E_f (") = 276GN/m^2 (c.f. Exptl. ≃ 275)

d = 6 μm, E_f (") = 338GN/m^2 (c.f. Exptl. ≃ 340)

No other values for E_{sh}, E_{co} and 's' fulfil the equation as precisely as these do for Type II fibres.

APPENDIX 3.

The Resistivity - H.T.T. Curve of Watt [294] Showing Experimental Values of Table 35.

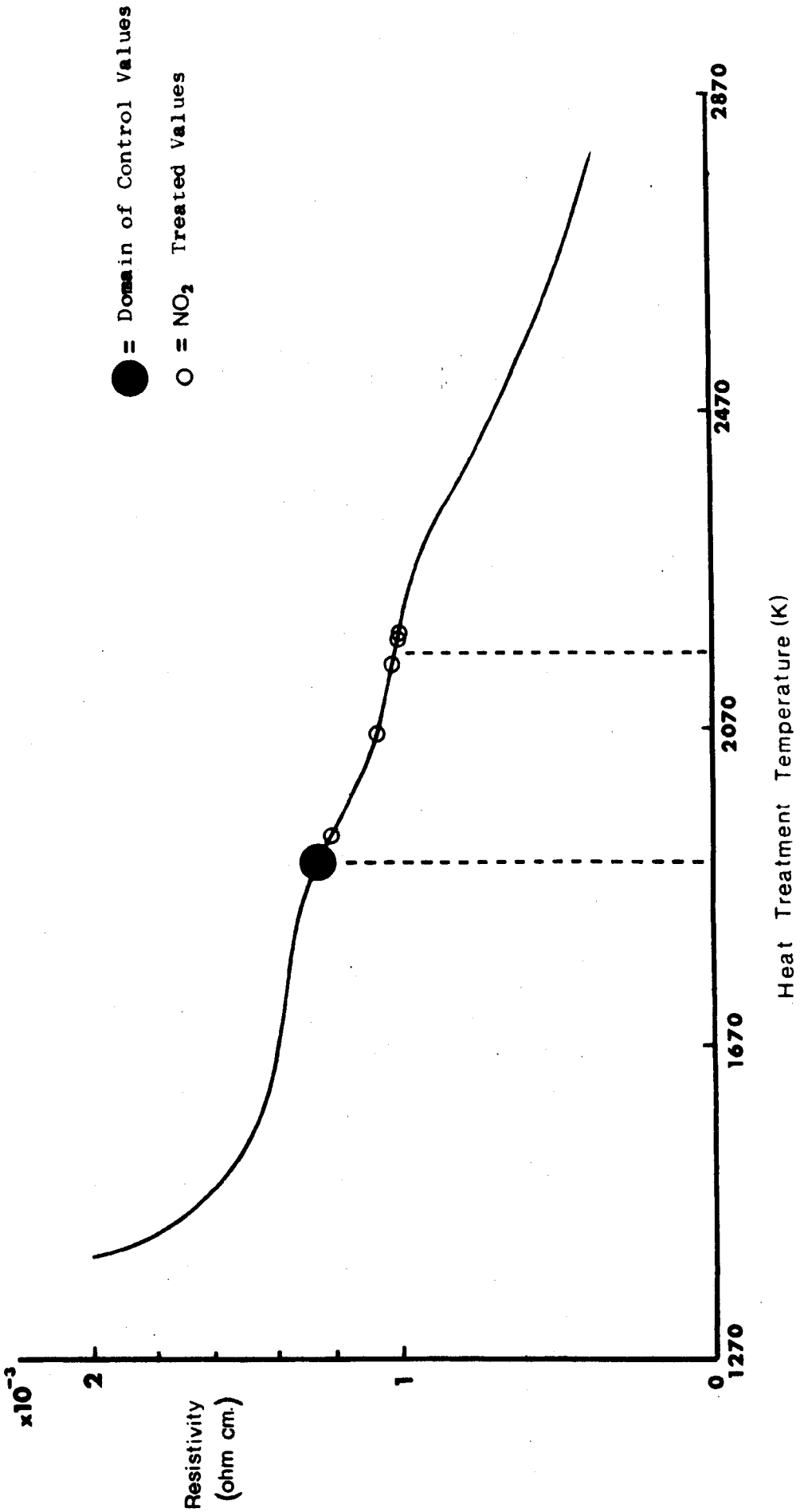

APPENDIX 4.- List of Symbols.

A_n - Amplitude of nth swing

A_{n+k} - Amplitude of n + kth swing

A - Cross-sectional area of fibre

A' - Cross-sectional area of fibre sheath

A'' - Cross-sectional area of fibre core

b - Breadth of specimen

C_o - Vertical unit cell dimension

δ - Deflection

Δ - Logarithmic decrement of decay

e - Distance between inner zones in diffraction pattern

E_{sh}- Young's modulus of sheath

E_{co}- Young's modulus of core

E_c - Young's modulus of composite

E_f - Young's modulus of fibre (Tensile & compressive)

E_m- Young's modulus of matrix (Tensile & compressive)

f - Focal length; frequency of oscillation

G - Three dimensional ordering in graphite fibres

G' - Shear modulus (Storage)

G'' - Loss modulus

G^* - Complex modulus

G_{II} - Strain energy released by fibre debonding

h - Depth of specimen

h_t - Distance of neutral shear plane from specimen top

h_b- Distance of neutral shear plane from specimen bottom

I - Moment of inertia

L - Distance between supports, grips or electrical contacts

λ - Wavelength

L_a - Crystallite size in a-axis direction

L_c - Crystallite size in c-axis direction

μ - Shape factor

Ω - Ohms

P - Load

p - Degree of disorientation in graphitised structure

$|q|$ - Degree of order in graphitised structure

R_F - Filament resistance

R_1, R_2 & R_3 - Resistances in Wheatstone bridge

r_c - Contact resistance

ρ - Electrical resistivity

S_H - Short beam shear strength

s - Sheath thickness

σ - Stress

σ_{ut} - Ultimate tensile stress

σ_{fm} - Tensile strength of fibre-matrix adhesion

σ_m - Matrix failure stress

σ_r - Applied stress

$\sigma_{T_{max}}$ - Maximum tensile stress

$\sigma_{C_{fail}}$ - Compressive stress at failure

t - Embedded fibre length

T_I - Well-ordered turbostratic phase in graphite fibres

T_{II} - Poorly ordered turbostratic phase in graphite fibres

τ_{fm} - Shear strength of fibre-matrix adhesion

τ_{xy} - Shear stress in xy plane

τ_m - Matrix shear failure stress

τ_d - Resin-fibre friction

V_f - Fibre volume fraction

V_m - Matrix volume fraction

x - Debonded length of fibre

APPENDIX 5.

REFERENCES.

1. Judd, N.C.W.
   Proc. Int. Carbon Fibre Conf.,Paper 32, (1971)

2. Fourdeux, A., Perret, R and Ruland, W.
   Proc. Int. Carbon Fibre Conf., Paper 9, (1971)

3. Johnson, J.W., Rose, P.G., & Scott, G.
   Third Conf. on Ind. Carbons and Graphite, Session 7, 443-7, (1970)

4. Grassie, N.
   Proc. 1st. Carbon Fibre Conf., Discussion on Papers 1-6, (1971)

5. Grassie, N., Hay, J.
   Journal of Polym. Sci., 56, 189, (1962)

6. Clarke, A.J., Bailey, J.
   Nature, 243, 146, (1973)

7. Potter, W.D. & Scott, G.
   Nature, 236, 30, (1972)

8. Shindo, A.
   Proc. Int. Carbon Fibre Conf., Paper 3, (1971)

9. Bell, F., Lehrle, R., & Robb, J.
   Polymer, 12, (9), 579-99, (1971)

10. Johnson, W.
    Third Conf. on Ind. Carbons and Graphite, Session 7, 447-52, (1970)

11. Watt, W., Johnson, W.
    Nature, 257, 211

12. Houtz, R.C.
    Tex Res. J., 20, 786, (1950)

13. Watt, D., Johnson, D.J., Parker, F.
    Proc. 2nd. Carbon Fibre Conf., Paper 1, (1974)

14. Watt, W.
    Carbon 10,(2),121-43, (1972)

15. Watt, W., Green, J.
    Int. Conf. on Carbon Fibres, Paper 4, (1971)

16. Strong, S.L.
    J. Matls. Sci., 9, (6), 993-1003, (1974)

17. Watt, W., Johnson, W.
    Interscience NY,'High Temp. Res. Fib.', 215, (1969)

18. Moreton, R.
    Proc. Int. Carbon Fibre Conf., Paper 12, (1971)

19. Bacon, R.
Interscience NY, 'High Temp. Res. Fib from Org. Polymers', 213, (1969)

20. Donnet, J.B., Voet, A., Dauksch, H., Ehrburger,P., Marsh, P.
Carbon 11,(4),430.

21. Moreton, R., Watt, W.
Nature, 247, 5400, 390, (Feb 1974)

22. Laidler, D., & Taylor, A.
Nature, 146, 130, (1940)

23. Moreton, R.
Nature, 213, 690, (1967)

24 Shindo, A.
Studies on Graphite Fibre, Rep. 317, (Gout. Osaka), (1961)

25 Jones, B.F.
J. Matls. Sci., 6, (9), 1225-7, (1971)

26 Mrozowski, S.
Proc. 1st & 2nd Conf. Carb., 31, (1954)

27 Gobin, P., Merlin, J., Rouby, D., Jouquet, G., & Rappeneau, J.
Third Conf. on Ind. Carbons and Graphite, Session 6, 349-72, (1970)

28 Sharp, J.V., Burnay, S.G.
Proc. Int. Carbon Fibre Conf., Paper 10, (1971)

29. Cooper, G.A., Mayer, R.M.
J. Matls. Sci., 6, (1), 60-67,(1971)

30. Murphy, F.V. & Jones, B.F.
Carbon, 9, 1, 91, (1971)

31. Moreton, R., Watt, W.
Carbon, 12, 274, 543, (1974)

32. Kelly, A.
Proc. Roy. Soc., Ser. A., 319, 95, (1970)

33. Judd, N.C.W.
Proc. Int. Carbon Fibre Conf., Paper 32, (1971)

34. Rogers, K.F., Kingston-Lee, D.M.
Third Conf. on Ind. Carbons and Graphite, Session 7, 503-7, (1970)

35. Jones, I.P.
Chem Process Eng., 51, (2),63-4, (1970)

36 Clayton W.E.
FRP in Chem. Proc. Equip., Matls. Protect., 9,(2), 34-6, (1970)

37. Phillips, L.N., Judd, N.C.W.
Process Engineering, 61-63, (Dec. 1969)

38. Gallant, P.E., Jones, M.W.
Plastics & Polym., 37, 127, 27, (1967)

39. Giltrow, J.P., Lancaster, J.K.
Proc. Int. Carbon Fibre Conf., Paper 31, (1971)

40. Giltrow, J.P., Lancaster, J.K.
3rd. Conf. on Ind. Carbons and Graphite, Session 7, 483-90, (1970)

41. Harris, C.L., Wyn-Roberts, D.
Inst. Mech. Eng., Symp. Lubric. in Hostile Environments, Paper 7, London, (1969)

42. Ubbelohde, A.P.
'The Chem. of Carb. & Graphite', Brit. Coal Util. Res. Ass. Gazette, 51, 1 (1964)

43. McMahon, P.E.
ASTM STP, 521, 367, (1973)

44. Bacon, R., Schalamon
Appl. Polym. Symp. 9, 285, (1969)

45. Aoki, K., Yajima, S
J. Matl. Sci., 6, (11), 1338-44, (1971)

46. Kupperman, D.S. , Chau, C.K., Weinstock, H.
Carbon 11, (2), 171, (1973)

47. McLintock, I.S. & Orr, J.C.
Chem. & Phys. of Carbon, 11, 243, (1973)

48. McLintock, I.S. & Orr, J.C.
Carbon, 12, (1974)

49. Delhaes, P.
Chem. & Phys. of Carbon, 7, ch. 4. , (1971)

50. Reynolds, W.N.
Chem. & Phys. of Carbon, 11, ch. 6. , (1973)

51. Owston, C.N.
Brit. J. Appl. Phys. D, 3, 1615, (1970)

52. Berg. C.A., Cumpston, G.H. & Rinsky, A.
Fib. Sci. & Tech, 4, 153, (1971)

53. Trostyanskaya et al
Mosk. Tekhnol. Inst. Moscow Mekh. Polim. 7, 5, 846-50, (1971)

54. Miyauchi, K., Takahashi, Y., Mikaibo, T.
Carbon, 9,(6),807, (1971)

55. Aoki, K., Yajima, S
J. Matls. Sci., 6,(11), 1338-44, (1971)

56. Rogers, K.F. and Kingston-Lee, D.M.
R.A.E. Tech. Mem., MAT 158, (Dec. 1972)

57. Trezbiatowski, W.
Roczniki Chem., 17, 73, (1937)

58. Walker, P.L. & Imperial, G
Nature, 180, 1185, (1957)

59. Matuyama, E.
Nature, 183, 670, (1959)

60. Franklin, R.E.
Acta Cryst., 4, 253, (1951)

61. El Goresy, A., Donnay, G.
Science, 161, 363-4, (July, 1968)

62. Laidler, D. & Taylor, A.
Nature, 146, 130, (1940)

63. Lipson, H. & Stokes, A.R.
Nature, 146,130. (1942)

64. Lipson, H. & Stokes, A.R.
Proc. Roy. Soc A181, 101

65 Bacon, G.E.
Nature, 166, 794, (1950)

66. Franklin, R.E.
Acta Cryst. 3, 107, (1950)

67. Franklin, R.E.
Proc. Roy. Soc., A209, 196, (1951)

68. Franklin, R.E.
Acta Cryst., 4, 253, (1951)

69. Ruland , W.
Proc. Int. Carbon Fibre Conf., Paper 9, (1971)

70. Laves, F. & Baskin, Y.
Z. Krist, 107, 22, (1956)

71. Ubbelohde, A.R.
Nature, 180, 380, (1957). Quart. Rev. Chem. Soc. 11, 246

72. Freise, E.J. & Kelly, A.
Phil. Mag., 8, 1519, (1963)

73. Tsuzuku, T.
Proc. 3rd, Carbon Conf., 433, (1957)

74. Amelinckx, S., Delavignette, P., & Heerschap, M.
Chem. & Phys. of Carbon, 1, Ch. 1., (1965)

75. Fitzer, E., Fritz, W., Overhoff, D.
Proc. 2nd. Ind. Carb. & Graph Conf., London, Session 3-4, 144-58, (1966)

76. Dresel, E.M. & Roberts, L.E.J.
Nature. 171, 170, (1953)

77. Turkdogan, E.T., Olsson, R.G., & Vinters, J.V.
Carbon, 8, (4), 545-64, (1970)

78. Craievich, A., Perpinal de Dujouny, E.
J. Matls, Sci., 8, (8), 1165-70, (1973)

79. Johnson, D.J. & Tyson, C.N.
J. Phys. D: Appl. Phys., 2, 789, (1969)

80. Reynolds, W.N.
Phys. Props. of Graphites, Elsevier, (1968)

81. Noda, T., Inagaky, M.
Bull Chem. Soc., Japan, 37, 153, (1964)

82. Frank, F.C.
Advances in Physics, 1, 91, (1952)

83. Feldman, M.H., Goeddel, W.V., Dienes, G.J. & Gossen, W.
J. Appl. Physics, 23, 1200, (1952)

84. Dienes, G.J.
J. Appl. Phys., 23, 1194, (1952)

85 Kanter, M.A.
Phys. Rev., 107, 655, (1957)

86. Johnson, W., Watt, W.
Nature, 215, 384, (1967)

87. Badami, D.V., Joiner & Jones, G.A.
Nat. 215, 5099, 386-7, (1967)

88. Jackson, P.W. & Marjoram J.R.
Nature, 218, 83, (1968)

89. Beaumont. P W.R., Fitz-Randolph, J., Phillips, D.C., Tetelman, A.S.
J. Matls. Sci., 7, (3), 289-94, (1972)

90. Johnson, D.J., Tyson, C.N.
Brit. J. Appl. Phys., 2, 787, (1969)

91. Johnson, J.W., Rose, P.G., Scott, G.
3rd. Conf. Ind. Carb. & Graph., Session 7, 443-7, (1970)

92. Robson, D., Assabghy, F.Y.I., Ingram, D.J.E., Rose, P.G.
Third Conf. on Ind. Carbons and Graphite, Session 7, 453-5, (1970)

93 Johnson, D.J., Crawford, D., Jones, B.F.
J. Matls. Sci. 8, (2), 286-90, (1973)

94 Hérinckx, C. & Perret, R. & Ruland, W.
Nature, 220, 63, (1968)

95. Bobeth, W., Müller, U.
Furserforschung und Textiltechnik, 16, (9), 290, (1965)

96. Lieberman, M.L. & Noles, G.T.
J. Matls. Sci. 7,(6),654-62, (1972)

97. Hugo, J.A., Phillips, V.A., & Roberts, B.W.
Nature, 226, 144, (1970)

98. Stewart, M., Zubzanda, O , Feughelmen, M.
Nat. Phys. Sci., 242, 42-3, (1973)

99. Ergun, S.
10th Biennial Conf on Carb., 155, (1971)

100. Ergun, S.
Nat. Phys. Sci., 238, 137, (1972)

101. Johnson, D.J.
Proc. 1st Carbon Fibre Conf., Paper 8, (1971)

102. Tang, M.M., Bacon, R.
Carbon, 2, 211- 221, (1964)

103. Bacon, R. & Silvaggi, A.F.
Carbon, 9,(3),321, (1971)

104. Fourdeux, A., Perret, R., & Ruland, W.
9th Conf Carbon, Boston, Paper SS-23, (1969)

105. Ruland, W.
9th Conf. Carbon, Boston, Paper MP-24, (1969)

106. Perret, R. & Ruland, W.
9th Conf. Carbon, Boston, Paper SS-22, (1969)

107. Ergun, S.
9th Conf. Carbon, Boston, Paper SS-21, (1969)

108. Barnet, F.R., Norr, M.K.
N.O.L.T.R., 72-32, (1972)

109. Wicks, B.J.
J. Matls. Sci., 6,(2),173-5, (1971)

110. Johnson, D.J.
Proc. Int. Carb. Fibre Conf., Paper 8, (1971)

111. Firalker, A.S. et al.
Mekh Polim. 5. 925-6, (1972)

112. Hawthorne, H.M.
Proc. Int. Carbon Fibre Conf., Paper 13, (1971)

113. Thorne, D.J.
Third Conf. on Ind. Carbons and Graphite, Session 7, 463-5, (1970)

114. Layden, G.K.
Carbon, 10,(1),59-63, (1972)

115. Jones, B.F. & Duncan, R.G.
J. Matls. Sci., 6, (4), 289-93, (1971)

116.
117. Moreton, R.
Fib. Sci. & Tech., 1, 273, (1969).

118. Nicoll, A.R., Perry, A.J.
Fib. Sci. & Tech., 6, 135-9, (1973)

119. Cooper, G.A., Mayer, R.M.
J. Matls. Sci., 6, (1), 60, (1971)

120. Diefendorf, R.J., Butler, B.L.
9th Biennial Conf. on Carbon, 161, (1969)

121. De Lamotte, E., & Perry, A.J.
Fib. Sci. & Tech., 3,(2),157, (1970)

122. Donnet, J.B., & Dankisch
Proc. Int. Carb. Fib. Conf, Paper 7, (1971)

123. Butler, B.L., LeMaistre, C.W., Diefendorf, R.J.
28th SPI, Paper 21-C, (1973)

124. Knibbs, R.H.
UKAEA - R6768, (1972)

125. Knibbs, R.H.
J. Microscopy, 94, (3),273-81, (1971)

126. Ubbelohde, A R., Lewis, F.A.
'Graphite & Its Crystal Comps', Clarendon (1960)

127. Hennig, G.R.
J. Chem. Phys., 20, 1443, (1952)

128. Jusa, R., and Schmeckenberger, A.
Z. Anorg. Chem., 292, 46, (1957)

129. Jusa, R.,Jonck, P., Schmeckenberger, A.
Z. Anorg. Chem., 292, 34, (1957)

130. Hooley, J.G.
Carbon, 8,(3),333, (1970)

131. Rudorff, W., Schulze, E , & Rubisch, O.
2 Anorg. Chem., 282, 232, (1955)

132. Fredenhagen, K., & Suck, H.
2 Anorg. Chem., 178, 353, (1929)

133. Croft, R.C.
J. Appl. Chem., 2, 557, (1952)

134. Croft, R.C.
Nature, 172,725, (1953)

135. Croft, R.C.
Austr J. Chem., 9, 184, (1956)

136. Lukesh, J.S.
J. Chem. Phys., 19, 1203, (1951)

137. Platzer, N.
C.R. Acad. Sci. Paris, 244, 2932, (1957)

138. Platzer - Rideau, N.
Ann. Chim., 805, (1960)

139. Métrot, A., Hérold, A.
C.R. Acad. Sci., 264, 883, (1967)

140. Hewitt, G.F.
Chem. & Phys. of Carbon, 1, ch. 2, (1965)

141. Watt, J.D., & Franklin, R.E.
Nature, 180, 1190, (1957)

142. Watt, J.D., & Franklin, R.E.
Ind. Carbon and Graphite Conf., 321, (1958)

143. Roscoe, C., Thomas, J.M.
Proc. Roy. Soc., A297, 397, (1967)

144. Thomas, J.M.
Carbon, 8, (4), 413-21, (1970)

145. Kosika, W.L., & Dienes, G.J.
Advances in Catalysts, Academic Press,New York, 9,398, (1957)

146. Boehm, H.P.
Angew. Chem. Intern. 5, 533, (1966)

147. Boehm, H.P. & Voll, M.
Carbon, 8, (1), 7-17, (1970)

148. Epstein, B.D., Dalle Molle, E., & Mattson, J.S.
Carbon, 9,(5),609-15, (1971)

149. McKee, D.W.
Carbon, 8, (5), 623-35, (1970)

150. McKee, D.W.
Carbon, 8, (2), 131-39, (1970)

151. Maire, J., Mering, J.
Proc. Third Carb. Conf., (3), 337, (1957)

152. Rudorff, W.
2. Anorg. Allg. Chem., 245, 383, (1941)

153. Heerschap, M., Delavignette, P., & Amelinckx, S.
Carbon, 1, (3), 235., (1964)

154. Eeles, W.T. & Turbull, S.A.
Proc. Roy. Soc., A 283, 179, (1965)

155. Brocklehurst, J.E. & Weeks, J.C.
J. Nucl. Matl., 9, 197, (1963)

156. Brocklehurst, J.E. & Bishop, R.A.
Carbon, 2, 27, (1964)

157. Brocklehurst. J.E. & Martin, W.H.
Carbon, 1, (2), 133, (1963)

158. Blackman, L.C., Mathews, J.F., Ubbelohde, A.R.
Proc. Roy. Soc., A 256, 15, (1960)

159. Tsuzuku, T., Saito, M.
J. Appl. Phys., Japan, 6, 54, (1967)

160. Dietz, Y.R., Vaughan, W.H.
29th SPI, Paper 21-A, (1974)

161. Warner, S.B., Peebles, L.H., Uhlman, D.R.
Proc. Int. Carbon Fibre Conf., Paper 3, (1974)

162. McCarroll, B. & Mckee, D.W.
Nature, 225, 723, (1970)

163 Tomita, A., Sato, N., Tanai, Y.
Carbon, 12,(2),143, (1974)

164. McCarroll, B. & McKee, D.W.
Carbon, 9,(3),301-11, (1971)

165. Hérinckx, C. & Perret, R. & Ruland, W.
Nature, 220, 63, (1968)

166. Salzano F.J., Aronson, S.
J Chem. Phys , 47, 2978, (1967)

167 Mrozowski, S.
Proc. 1st. Conf. on Carb., 31-45, (1955)

168 Watt, W., Green, J.
Proc. Int. Carbon Fibre Conf., Paper 4, (1971)

169. Byrne, G.A., & Jeffries
Chem & Ind., 17, (1971)

170. Mimeault, V.J.
Fib. Sci. & Tech., 3, (4),273, (1971)

171. Johnson, J.W., Thorne, D.J.
Carbon, 7, (6),659, (1969)

172. McKee, D.W. & Mimeault, V.J.
Chem & Phys. of Carbon, 8, ch. 3, (1973)

173. Galasso, F.S., Pinto, J.
Fib Sci. & Tech., 2, 303, (1970)

174. Murphy, F.V. & Jones, B.F.
Carbon, 9, (1),91, (1971)

175. Simon, R.A., Prosen, S.P. and Duffy, J.V.
Nat. 213, 1113, (1967)

176. Thomas, J.M.
Chem. & Phys. of Carbon, 1, ch. 3, (1963)

177. Clark, D., Wadsworth, N.J., Watt, W.
Proc. 2nd. Carbon Fibre Conf., Paper 7, (1974)

178. Watt, W., Paddon, J., Edwards, P.
RAE TECH. REP. 69087

179. Herrick, J.W.
23rd SPI., Paper, 16-A. (1968)

180. Butler, B.L., LeMaistre, C.W., Diefendorf, R.J.
28th. SPI., Paper 21-C, (1973)

181. Johnson, J.W.
'High Temperature Resistant Fibres from Organic Polymers',
Interscience, N.Y., 229, (1969)

182. Novak, R.C.
'Composite Materials: Testing and Design',
ASTM, Special Tech. Publ. No. 460, 540, (1969)

183. Bobka, R.J., & Lowell, L.P.
'Integrated Research on Carbon Composite Materials',
AFML-TR-66-310, Part 1, Air Force Materials Laboratory, 145-152, (1966).

184. Goan, J.C., & Prosen, S.P.
'Interfaces in Composites', ASTM Special Tech Publ. No. 452, 3.

185. Wadsworth, N.J. & Watt, W.
U.S. Pat. 3,476,703 (1969)

186. Brydson, J
'Plastics Materials', Iliffe Books Ltd. chs. 1-9, (1966)

187. Friedel, C. & Crafts, J.M.
Bull. Soc. Chim. Fr., 43, 53, (1885)

188. U.S. Pat. 2,870,098

189. Doebens, J.D., & Cordts, H.P.
Ind. Engng. Chem., 53, 59, (1961)

190. Phillips, L.N.
Trans. Plast. Inst., 298, (1964)

191. US Pat.3,405,091

192. Phillips, L.N.
B.P. 1,094,181

193. Harris, G.I.
B.P. 1,099,123

194. B.P. 1,127,122

195. Harris, G.I.
Brit Poly J., 2, 270, (1970)

196 Simon, R.A., Prosen, S.P.
23rd. SPI. Paper 16-B, (1968)

197. Outwater, J.O. & Murphy, M.C.
24th. SPI, Paper 11-C/25th SPI, Paper 16-D, (1969-70)

198. Harris, B., Beaumont, P. & Rosen, A.
J. Matls. Sci., 4, (5), 432-8, (1969)

199. Mimeault, V.J. & McKee, D.W.
Nature, 224, 793, (1969)

200. Cooper, G.A., Kelly, A.
'Interfaces in Composites', ASTM STP 452, 90-106, (1969)

201. Broutman, B.J.
'Interfaces in Composites' ASTM STP 452, 27-41, (1969)

202. Greszcuk. L.B.
'Interfaces in Composites' ASTM STP 452, 27-41, (1969)

203. Marston, T.U., Atkins, A.G. Felbeck, D.K.
J. Matls. Sci., 9, (3), 447-55, (1974)

204. Reynolds, W.N., Hancox, N.L.
J. Phys. D. Appl. Phys., 3, 1747-53

205. Herrick, J.W. Gruber, P.E., Mansur, F.T.
Avco. Tech. Rep., AFML-TR-66-178, 1, (1966)

206. Scola, D.A. & Brooks, C.S.
25th Soc. Plastics Ind. Meeting, Washington, D.C., (1970)

207. Herrick, J.W.
12th Nat. Symp. Soc. Aerosp. Mater. Process Eng., Anaheim, Calif., Paper AC-8, (October 1967)

208 Schmidt, D.L. & Hawkins, H.T.
'Filamentous Carbon and Graphite',
AFML-TR-65-160, Air Force Materials Laboratory, (August, 1965)

209. Harris, B., Beaumont, P., & Rosen, A.
J. Matls. Sci., 4, (5), 432-8, (1969)

210. Prosen, S.P., Duffy, J.V., Erickson, P.W. & Kinna, M.A.
21st. Soc. Plastics Ind Ann. Tech. Conf., 8-D, (1966)

211. Friedericy, J.A., Davis, J.W., Pentch, B.W.
'Testing Techniques for F.R.P.', AFML-TR-66-274, (Sept. 1966)

212. Chamis, C.C.
29th. SPI., Paper 16-D, (1974)

213. Daniels, B.K., Harakas, N.K., & Jackson, R.C.
Fib. Sci & Tech., 3,(3),187

214. Griffith, A.A.
Phil. Trans. Roy. Soc., 221A., 163, (1920)

215. Heaton, M.D.
Brit. J. Phys. D. Series 2, 1, 1039, (1968); 3, 672, (1970)

216. Cook, J.,Gordon, J.E.
Proc. Roy. Soc., A282, 508, (1964)

217. Piggott, M.
J. Matls. Sci., 5, (8), 669-75, (1970)

218. Fitz-Randolph, J., Phillips, D.C., Beaumont, P.W.R., Tetelman, A.S.
J. Matls. Sci., 7, (3), 289-94, (1972)

219. Outwater, J.O., & Murphy, M.C.
Conf on Failure of F.R.C., Surrey Univ., Paper 2., (July, 1972)

220. Broutman, L.J.
Polymer Eng. & Sci., 6, 3, (1966)

221. McGarry, F.J., Marshall, D.W.
ASTM STP 327, 133-45, (1963)

222. Favre, J.P. & Perrin, J.
J. Matls. Sci., 7, (10), 1113-8, (1972)

223. Wyatt, R.C. & Ashbee, K.H.
Fib. Sci. & Tech., 2,(1),29, (1969)

224. Judd, N.C.W., & Judge C.H.
R.A.E. Tech. Mem. MAT 142, (June 1972)

225. Walters, B.J.
Newsletter on N.D.T. of Composite Matls. and Adhesive Bonded Joints, R.A.E. No. 1., (June, 1973)

226. Stone, D.E.W.
Proc. 2nd. Carbon Fibre Conf., Paper 28, (1974)

227. Fairbairn, G., Dominic, C.J., Garnish, E.W.
Carbon Fibre Conf., Paper 24, (1971)

228. Chamis, C.C.
Private Communication, (1974)

229. Kalnin, I.L.
29th. SPI., Paper 21-C, (1974)

230. Judd, N.C.W.
First Int. Conf. on Carbon Fibres, Paper 32, (1971)

231. Hancox, N.L.
J. Matls. Sci., 7, (9), 1030-6, (1972)

232. Koedam, M.
Phillips Tech. Rund., 27, 182, (1966)

233. Cauville, K.J. et al.
24th SPI., Paper 14-C, (1969)

234. Watt, W., Johnson, W.
Design Engineering, 119, (June 1971)

235. Nicoll, A.R., Perry, A.J.
J. Fib. Sci. & Tech , 6, 135-9, (1973)

236.
Grafil 'Test Methods', Carbon Fibres Unit, Coventry, (1969)

237. Watt, W., Phillips, L.N., Johnson, W.
Engineer,Lond., 221, (1966)

238. Gill, R.M.
Carbon Fibres in Composite Matls., Plastics Monograph, 60, (1972)

239. Moreton, R.
Fib. Sci. & Tech., 1, 273, (1969)

240. Thorne, D.J.
Third Conf. on Ind. Carbons and Graphite, Session 7, 463-6, (1970)

241. Dietz, R., Peover, M.E.
J. Matls, Sci., 6,(12),1441-6, (1971)

242. Wagner, C.
J. Electrochem. Soc , 97, 3, 71-4, (1950)

243. Parsons, R.
Modern Aspects of Electrochemistry, 1, 103, (1954)
Ed. Bockris Butterworths, London.

244. Bird, J., Feng, H., Gimer, J., Turchan, M.
Proc. 23rd. Ann. Power Sources Conf.

245. Reynolds, W.N.
Physical Properties of Graphite, Elsevier Materials Science Series, 80, (1968)

246. Prof Mitsou Takehana
N.D.T. Symp., Paper 15.

247. Reynolds, W.N.
Proc. 2nd. Carbon Fibre Conf.,Paper 27, (1974)

248. Speake, J.H., Curtis, G.J.
Proc. 2nd. Carbon Fibre Conf , Paper 29, (1974)

249. Learmonth, G.S., Pritchard, G., Reinhardt, J.
J. Appl. Pol. Sci , 12, 3, 403, (1968)

250. Nederveen, C.J. & van der Wal, C.W.
Rheol. Acta., 6, 316, (1967)

251. Nonius Torsional Pendulum Manual, T.N.O. Labs., Delft, Holland, (1960)

252. Brydson, J
'Plastics Materials', Iliffe Books Ltd., p.423, (1966)

253. Brydson, J
'Plastics Materials', Iliffe Books Ltd., p.146, (1966)

254. Bader, M.G., Johnson, M.
Composites, 58-62, (March, 1974)

255. Kelly , A.
Strong Solids, Oxford University Press, (1973)

256 Collings, T.A.
Composites, 108-116, (May 1974)

257. Friedericy, J.A., Davis, J.W., Rentch, B.W.
'A Test Method for the Determination of Shear Properties of Reinforced Epoxy Structures', AFML-TR-66-274 (Sept. 1966)

258. ASTM., 'Tentative Method of Test for Dynamic Mech. Props. of Plastics by Means of a Torsional Pendulum', D. 2236-67T.

259. Nielson, L.E.
'Mech Props. of Polymers', Reinhold, NY., (1963)

260. McCrum, N.G.
J. Polym. Sci., 34, 355, (1959)

261. Learmonth, G.S., Pritchard, G., Reinhardt, J.
J. Appl. Pol. Sci., 12, 3, 403, (1968)

262. Pritchard, G.P.
PhD. Thesis., (1968)

263. Puck, A., Schneider, W.
Plastics Inst. Conf., 'Research Projects in R.P.', (March, 1968)

264. Shiriajeva, G.V., Andeevskaya, G.D.
Sov Plast., 4, 40, (1962)

265. Broutman, L.J.
Mod. Comp. Matls., ed. Broutman & Krock, Addison-Wesley, Mass., (1967)

266. Mooney, R.D. & McGarry, F.J.
14th. SPI., 'Resin-Glass Bond Study', Paper 12 E, (1959)

267. Anderson & Healy
13th. SPI., Paper 3-B, (1958)

268. Arrington, M.K.
PhD. Thesis, Sussex Univ , (1970)

269 Rothwell, R. & Arrington, M.K.
NAT. (Phys. Sci.), 233, 43, 163-4 , (1971)

270. Outwater, J.O. & Murphy, M.C.
25th. SPI., Paper 16-D, (1970)

271 Woodrow, J., Mott, B.W., Haines, H.R.
Proc. Phys. Soc., B, 65, 603, (1952)

272. Ezekiel, H.E.
J. Appl. Phys., 41, 5351, (1970)

273. Connor, P.N. & Owston, C.N.
Nature, 223, 1146, (1969)

274. Watt , W.
Phys Bull., 20, 508, (1969)

275. Andrews, K.W., Dyson, D.J., Keown, S.R.
'Interpretations of Electron Diffraction Patterns', Adam Hilger Ltd., (1971)

276. Haine, M.E.
'Advances in Electronics and Electron Physics', 6, 295-369, (1954)

277. Heidenreich, R.D.
J. Appl. Phys., 20, 993, (1949)

278. Van Dorsten, A.C., & Van Den Broek, S.L.
Proc. 4th. Int. Conf on Electron Microscopy, Berlin, 171, (1958)

279. Kay, D.H.
'Techniques for Electron Microscopy', Blackwell Scientific Publications, 2nd. Edition, (1965)

280. Jusa, R. & Schmeckenberger, A.
2, Anorg. Chem., 292, 46, (1957)

281. Drucker, D.C.
'Handbook of Experimental Stress Analysis', Ed. M. Hetenyi, J. Wiley & Sons, Inc., N.Y., (1950)

282. Savin, G.N.
'Stress Concentration around Holes', N.Y., (1961)
(trans. from Russian original of 1951)

283. Lekhnitskii, S.G.
Anisotropic Plastics - Moscow, Gostekhisdat, (1957)

284. Reyerson, L.H., Wertz, J.E.
22nd. Nat. Coll. Symp., (1948)

285. Okhramovich, A.E., Baranov, A.V., Nauchn, T
Dhepropetr. Khim. Tekhnol. Inst., No. 12, 2, 189-96, (1961)

286. Masakyn Sakeguchi (univ. Toyami)
Bull. Chem. Soc., Japan, 35, 486-91, (1962)

287. Bennett, S.C., Johnson, D.J.
Conf. on Study of Carbon & Graphite by Electron Microscopic Techniques, Paper 13, (1975)

288. Donnet, J.B., Voet, A., Danksch, H., Ehrburger, P., Marsh, P.
Carbon, 2, 4, 430, (1973)

289. Watt, W.
Proc. 1st Carbon Fibre Conf., Introduction to Section B. (1970)

290. LeMaistre, C.W.
PhD. Thesis, 'The Origin of Structure in Carbon Fibres', Rensselaer Polytechnic Inst Troy, N.Y., (Sept. 1971)

291. Fourdeux, A., Hérinckx, C., Perret, R., Ruland, W.
Compt. Rend., 269, 1597, (1967)

292. Hawthorne, H.M. & Teghtsoonian, E.
J. Matls. Sci., 10, 41-51, (1975)

293. Nixon, D.E., Parry, G.S., Ubbelohde, A.R.
Proc. Roy. Soc., A., 291, 324-9, (1966)

294. Watt, W.
Private Communication, (1975)